



Durham E-Theses

Resonance observations in cubic laves phase rare earth compounds

Issa, M.A.A.

How to cite:

Issa, M.A.A. (1973) *Resonance observations in cubic laves phase rare earth compounds*, Durham theses, Durham University. Available at Durham E-Theses Online: <http://etheses.dur.ac.uk/8688/>

Use policy

The full-text may be used and/or reproduced, and given to third parties in any format or medium, without prior permission or charge, for personal research or study, educational, or not-for-profit purposes provided that:

- a full bibliographic reference is made to the original source
- a [link](#) is made to the metadata record in Durham E-Theses
- the full-text is not changed in any way

The full-text must not be sold in any format or medium without the formal permission of the copyright holders.

Please consult the [full Durham E-Theses policy](#) for further details.

RESONANCE OBSERVATIONS IN CUBIC LAVES PHASE
RARE EARTH COMPOUNDS

by

M.A.A. Issa, B.Sc.

Presented in candidature for degree of
Doctor of Philosophy

June 1973



TO MY FATHER

ABSTRACT

N.M.R. Spin Echo spectra of $Gd_{1-x}Y_xAl_2$ and $Gd_{1-x}La_xAl_2$ ($0 \leq x \leq 0.4$) were studied in the ferromagnetically ordered state at 4.2 K. The Al resonance line profiles were analysed under the assumption of various models for the spatial extent of the conduction electron polarization and general confirmation of RKKY like oscillatory polarization was found. Slowly decreasing nonoscillatory polarization functions were shown to be unable to explain the observed spectra. The line shape has been shown to depend rather critically on the value of the Fermi wave vector K_f . The effect of the conduction electron mean free path on the line shape is similar to the K_f .

E.S.R. of Gd in YAl_2 was measured in the temperature range from 65 K to 340°K. The experimental results are discussed using Hasegawa's theory. The dependence of line width on temperature and Gd - concentration indicates the existence of a "bottleneck" in the relaxation between the conduction electrons and the lattice. The behaviour of the line width with temperature in the ferromagnetic region makes it possible to study the Curie temperature for these compounds.

The hyperfine field at the ^{59}Co nucleus have been observed for some of $A Co_2$ (A - rare earth metal) compounds. The field strength has essentially the same value of about 60 kOe for all the compounds studied.

The results can be interpreted in terms of contributions to the hyperfine field arising from the transition metal

sublattice and from the rare earth sublattice. The former appears to be proportional to the magnetic moment associated with the transition metal ion while the rare earth contribution is taken to arise predominantly from conduction electron polarization.

Acknowledgements

I would first like to thank sincerely Dr. K.N.R. Taylor for his guidance, help, encouragement and interest throughout the course of this work, which was carried out under his supervision. I am also grateful to Dr. G. Brown for teaching me how to use the present apparatus and for reading my thesis. I would like to thank Mr. I. Osman from the computer unit for his help in writing the computer program.

My appreciation goes to the entire physics department of Durham University, particularly to professor G.D. Rochester the Head of the Department, and to my colleagues in the solid state group.

I am indebted to the University of Riyadh, Saudi Arabia, for the financial support.

Finally, I would like to thank Mrs. J. Lincoln for typing the thesis and my wife for putting up with me whilst the thesis was being written.

CONTENTS

	Page
Abstract	i
Acknowledgements	iii
CHAPTER 1 - INTRODUCTION	1
1.1 Rare earth metals	2
1.2 Laves Phase intermetallic compounds	9
1.3 Indirect exchange interaction	12
1.3.1 The exchange interaction	12
1.3.2 The RKKY interaction	14
1.4 Hyperfine interaction	20
1.4.1 Magnetic hyperfine interaction	21
1.4.2 Core polarization and conduction electron polarization	23
1.4.3 Experimental methods and Results	25
CHAPTER 2 - A REVIEW OF THE MAGNETIC PROPERTIES IN RARE EARTH INTERMETALLIC COMPOUNDS.	33
2.1 Brief theory	33
2.2 (Rare earth)Al ₂	36
2.3 Rare earth 3d transition metal AB ₂ 's	44
CHAPTER 3 - N.M.R. SPIN ECHO AND THE BASIC THEORY OF E.S.R.	54
3.1 Magnetic resonance phenomenon	54
3.1.1 Pulse methods	57
3.1.2 Free induction decay	57
3.2 The Bloch equations	58
3.3 N.M.R. Spin Echo	60
3.3.1 Primary Spin Echo	62
3.3.2 Stimulated echoes	65
3.4 The basic theory of E.S.R.	66
3.4.1 Dispersion and absorption line shape	66
3.4.2 g - shift	68

	Page
3.4.3 Linewidth consideration	71
3.4.3.1 Korringa relation	71
3.4.3.2 Linewidth for Bottlenecked E.S.R.	72
3.4.3.3 Review of experimental results of E.S.R in metallic alloys	77
 CHAPTER 4 - EXPERIMENTAL TECHNIQUES	 85
4.1 N.M.R. Spin echo instrumentation	85
4.1.1 The sample probe	85
4.1.2 Pulse generator	87
4.1.3 The transmitter and the receiver	87
4.1.3.1 The transmitter	87
4.1.3.2 The receiver	88
4.2 E.S.R. Spectrometer	89
4.3 Specimen Preparation	90
4.3.1 Rare earth Co_2	90
4.3.2 Rare earth Al_2	91
4.4 Curie and Neel temperature determination	92
4.5 Temperature Control	93
4.5.1 The Cryostat	93
4.5.2 Temperature measurements	93
 CHAPTER 5 - EXPERIMENTAL RESULTS	 95
5.1 Lattice parameters	95
5.2 Curie Temperature	96
5.3 Spin echo observation	96
5.3.1 Gd-A'Al_2 (A = Y, La, Dy)	100
5.3.2 ACo_2	103
5.3.3 $\text{Gd}(\text{Co}_{1-x}\text{Al}_x)_2$	103
5.3.4 GdFe_2	105
5.4 Relaxation measurements	105
5.5 E.S.R. results	107
 CHAPTER 6 - DISCUSSION OF RESULTS	 108
6.1 $\text{Gd}_{1-x}\text{Y}_x\text{Al}_2$ and $\text{Gd}_{1-x}\text{La}_x\text{Al}_2$ compounds	108
6.1.1 The lattice parameter and the Curie temperature	108
6.1.2 N.M.R. Line shapes	110
6.1.3 E.S.R. of $\text{Gd}_{1-x}\text{Y}_x\text{Al}_2$	125

	Page
6.2 N.M.R. of $GdDyAl_2$	130
6.3 N.M.R. of ACo_2 (A is a rare earth)	130
6.3.1 The temperature dependent hyperfine fields in $GdCo_2$	137
6.4 N.M.R. of $Gd(Co_{1-x}Al_x)_2$	139
6.5 Conclusion	143
References	146
Appendix 1	163

CHAPTER 1

Introduction

The rare earth elements, alloys and compounds form a group of materials with widely diverse magnetic and electrical properties (refs: 1.1, 1.2, 1.3, 1.4, 1.5, 1.6, 1.7, 1.8). The magnetic ordering observed in the rare earth metals arises from an indirect exchange mechanism involving a polarization of conduction electrons by the local 4f moments. In intermetallic compounds with stoichiometry AB_2 (A = rare earth element and B = Co, Fe, Ni, Al...,) the presence of the rare earth elements has been of value in understanding the complexities of the electronic behaviour and may be of value in solving the problem of the properties of the transition metals themselves. The measurement of hyperfine fields and g-shifts are known to be capable of providing useful information on the mechanisms involved in the magnetic properties of these compounds.

This thesis describes an experimental investigation using:

1. nuclear magnetic resonance to study the hyperfine field at the ^{27}Al nuclei in GdAl_2 and in $\text{Gd}_{1-x}\text{A}'_x\text{Al}_2$, where A' is Y, Dy, La, and at ^{59}Co nuclei in some of ACo_2 compounds; the measurements were made in zero field at a temperature of 4.2 K (GdCo_2 between 4.2 K and 275 K) and at frequencies between 35 MHz and 70 MHz, using a nuclear magnetic resonance (NMR) spin echo spectrometer which is described in chapter four;
2. electron spin resonance to study the g-shift and the line width of the resonance at Gd in $\text{Gd}_{1-x}\text{Y}_x\text{Al}_2$ ($x = 0$ to 0.9); these measurements were made in the paramagnetic region, in fields



between 0 and 6 kOe, using an X-band reflection spectrometer operating at 9 GHz. This system is described in chapter four. The results of these measurements are presented in tables and graphs in chapter five. In chapter six the results are discussed and accounted for.

Chapter three is confined to some basic theory of spin echo and electron spin resonance. The magnetic properties of AB_2 compounds and a brief theory of the observable effects of conduction electron polarization which apply to these compounds are given in chapter two.

In this chapter (one), the structure and the magnetic properties of rare earth metals, and the RKKY and hyperfine fields will be discussed.

1.1. Rare earth metals

The fourteen 4f transition series elements form a sub group in the periodic table and are all chemically and structurally quite similar. They have electron configurations of the general form $(Xe) 4f^n 5d^1 6s^2$, in which the $4f^n$ shell is progressively filled from $n = 0$ for La to $n = 14$ for Lu. The 4f-shell is embedded in the Xenon-core (Xe) and is well screened against perturbations from the environment by electrons in the $5s^2$ and $5p^6$ shells. The three valence electrons, corresponding to $5d^1$ and $6s^2$ atomic states, form the conduction band. The series may be divided at the point of the half filled 4f shell into light (La - Eu) and heavy (Gd - Lu) rare earth metals.

The f-electrons behave, to a first approximation, like those in a free ion. Hund's rules apply well in describing the ground state electronic behaviour of most the tripositive rare earth

ions. Spin and orbital angular momentum are strongly coupled yielding J as a good quantum number equal to $L-S$ for the light group and $J = L + S$ for the heavy rare earth group.

The heavy rare earth metals (Gd to Tm) and Y crystallize in the hexagonal close-packed structure (hcp) which has an AB...AB stacking pattern. The c/a ratios are almost the same, varying between 1.57 and 1.59. The light rare earth metals have a more complex double-hexagonal structure in which the stacking sequence of the layers is ABAC...ABAC. The face-centred cubic structure may also be written in this form by stacking layers in the form ABC ABC. Thus in the double structure the layers have alternatively hexagonal and cubic environments. Sm has a more complex structure regarded as rhombohedral with the stacking sequence ABABCBCACA consisting of nine layers. The c/a ratios for the light rare earths are 1.61. The basic information about the crystal structures of the rare earth metals is summarized in table (1.1), together with similar data on Y and Sc.

Because the work described in this thesis is only concerned with the elements of the second half of the series, we shall concentrate on the heavy rare earths. The reader is referred to review articles (refs. 1.1, 1.2, 1.3, 1.4, 1.5, 1.6) for a more complete discussion of the physical and magnetic properties of all the rare metals.

The heavy rare earth metals with 7 or more $4f$ electrons are strongly magnetic members of the series exhibiting magnetic states with ordering temperatures ranging from 57 K (Tm) to 293 K (Gd). The exceptions are divalent ytterbium, which is non-magnetic, and lutecium both having a filled $4f$ shell. For the heavy series only the lowest level of the J angular momentum manifold is

Table 1.1 Crystal structure of rare earth metals.

		T 25°C		
	Structure	a	c	c/a
Sc	h.c.p.	3.309	5.268	1.592
Y	h.c.p.	3.650	5.741	1.573
La	d-hex	3.772	12.144	1.610
Ce	d-hex	3.673	11.802	1.607
Pr	d-hex	3.672	11.833	1.611
Nd	d-hex	3.659	11.799	1.612
Pm	d-hex	3.65	11.65	1.600
Sm	rhomb hex	3.626	26.18	1.605
Eu	b.c.c.	4.580		
Gd	h.c.p.	3.634	5.781	1.591
Tb	h.c.p.	3.604	5.698	1.581
Dy	h.c.p.	3.593	5.655	1.574
Ho	h.c.p.	3.578	5.626	1.572
Er	h.c.p.	3.560	5.595	1.572
Tm	h.c.p.	3.537	5.558	1.571
Yb	f.c.c.	5.483		
Lu	h.c.p.	3.505	5.553	1.584

The c/a ratios of the d-hex and Sm structures are given as c/2a and c/4.5a respectively (ref. 1.1).

	g_f^J	expt. M_{set}	T_N	T_C	θ_{H1}	θ_L	theor. $M_{eff}(a)$	expt. M_{eff}	$G(b)$
	(μ_B)	(μ_B)	(K)	(K)	(K)	(K)	(μ_B)	(μ_B)	(μ_g)
Gd	7.0	7.55		292.7	317	317	7.94	7.98	15.75
Tb	9.0	9.34	230.2	219.6	195	239	9.72	9.77	10.50
Dy	10.0	10.33	176.0	88.3	121	169	10.64	10.64	7.08
Ho	10.0	10.34	130.0	19.0	73	88	10.60	11.20	4.50
Er	9.0	8.00	85.0	19.5	61.7	32.5	9.60	9.9	2.55
Tm	7.0	7.14	57.2	32.0	41	17	7.56	7.61	1.17

(a) $g \sqrt{J(J+1)}$

(b) $G = (g-1)^2 J(J+1)$

References to original investigations are given in (ref.1.8).

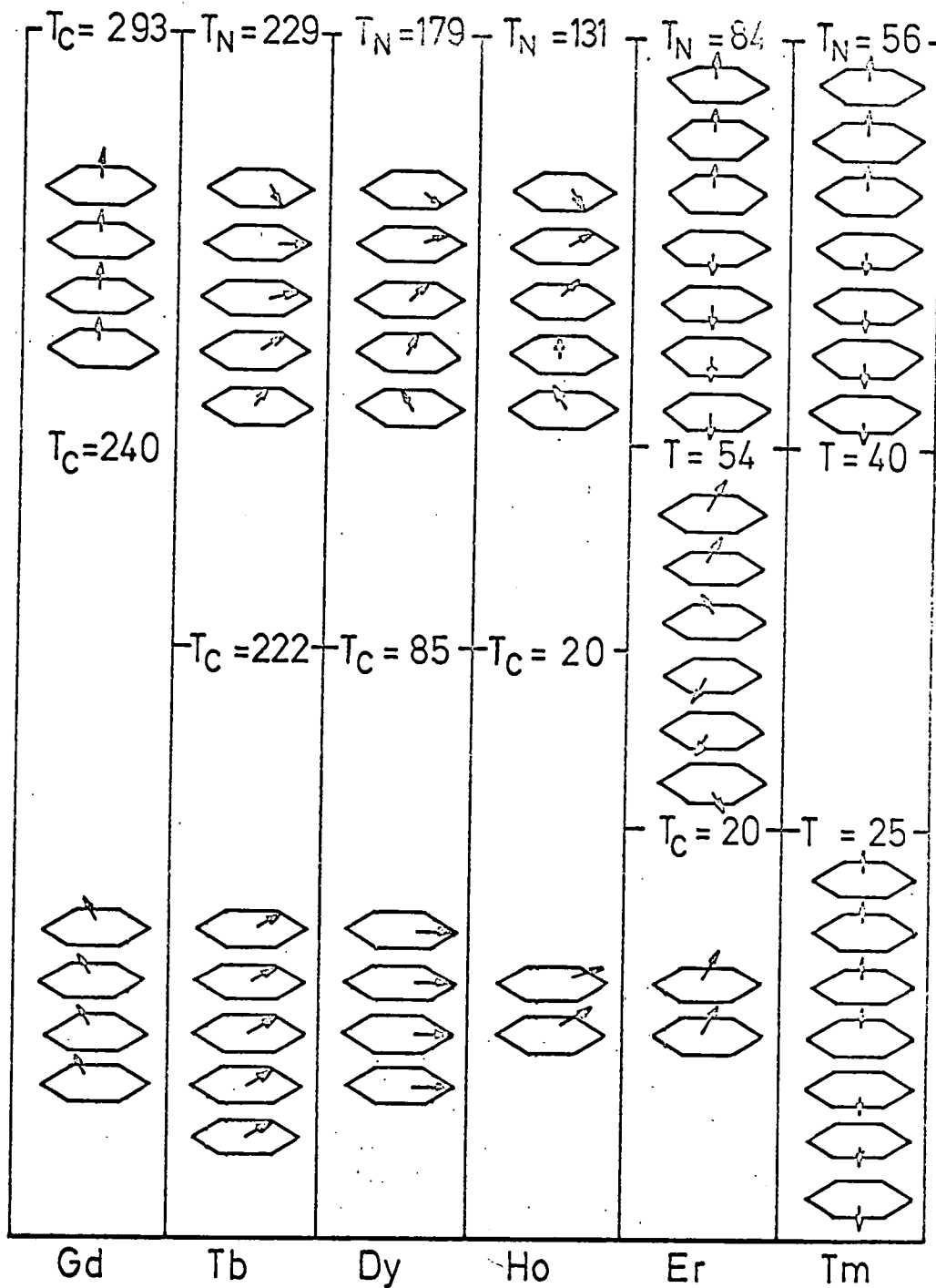
Table 1.2 Some physical properties of the heavy rare earths.

excited, and thus the $4f$ moment is given by $\mu = g_j J$, where g_j is the Lande' g -factor. The experimental value of the 0 K saturation moment exceeds slightly the value predicted from $g_j J$. The excess is attributed to the polarization of the conduction electrons in the vicinity of the ions caused by the interaction of the ionic moment with the electrons. Some pertinent physical properties of these heavy rare earth metals are summarized in table (1.2). T_N (Neel temperature) refers to the transition temperature from paramagnetism to a periodic moment antiferromagnetism state, while T_C (Curie temperature) marks the onset of ferromagnetic order. Also given in the table are values of the theoretical and experimental paramagnetic moments from susceptibility data and the values of θ_{para} for fields applied parallel ($\theta_{||}$) and perpendicular (θ_{\perp}) to the C crystal direction. The basic magnetic structure observed in the heavy rare earths is shown in fig. (1.1).

Gadolinium is truly ferromagnetic over the whole temperature range but nevertheless provides a variety of spin orientations as indicated by the magnetocrystalline anisotropy observations. These changes in easy direction have now been confirmed by various neutron diffraction studies (refs. 1.9, 1.10, 1.11) and show that between 294 and 232 K the moments lie parallel to the crystallographic c -axis, but below 232 K the moments move away from this axis to a maximum deviation of 75° near 180 K and then back to within 32° of the c -axis at 4.2 K. This is in remarkably good agreement with results of Corner et al. (ref. 1.12) obtained using torque measurements. The remaining elements show various changes in the type of order, with correspondingly complex magnetization-temperature behaviour.

Fig. 1.1 The observed magnetic structure of the rare earth metals in zero applied field. The detail discussion is given in (ref. 1.1)

all temperatures in K.



Dysprosium, for example, initially orders as an helical antiferromagnet and has low-temperature basal plane ferromagnetic states. The transition from helix to ferromagnet, which occurs spontaneously at T_c , can be forced to occur at a higher temperature by an applied field (ref. 1.13). For $T > T_c = 88$ K the magnetization is initially small up to a critical field required for the first order collapse of the helix to a ferromagnetic configuration. At higher temperatures ($T \geq 130$ K) where these influences are minimal the antiferro-ferromagnetic transition is thought to proceed by a series of intermediate "fan-like" moment states. The initial critical field for the transition shows an almost linear variation with temperature as shown in fig. (1.2). Below T_c the magnetization curve is like those of a conventional anisotropic ferromagnet. The antiferromagnetic helical spin system is shown in fig. (1.3). In this ordered state in Dy, the magnetic moments of the ions in any one plane of the h.c.p. structure are aligned ferromagnetically (i.e. parallel to one another). However, the direction of these moments with respect to the crystal lattice changes from one plane to the next with a constant angle between the spins in successive planes. This so-called "turn-angle" is temperature-dependent and decreases with increase in temperature (ref. 1.3).

In metallic alloys, the heavy rare earth metals (except Yb) form continuous solid solutions among themselves and with non-magnetic yttrium. Yttrium's lattice constants are nearly identical to those of Gd at room temperature. Since Y is non-magnetic it serves as a nearly ideal diluent for the rare earths. The solid solutions of the heavy rare earths with each other and with Y retain the hexagonal close-packed structure of the metals.

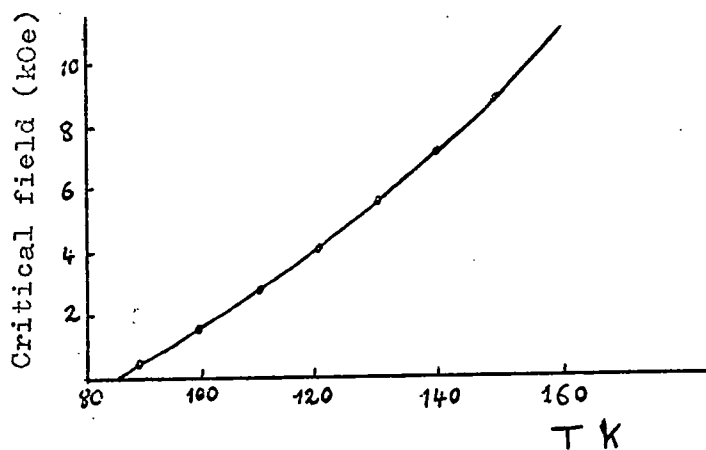
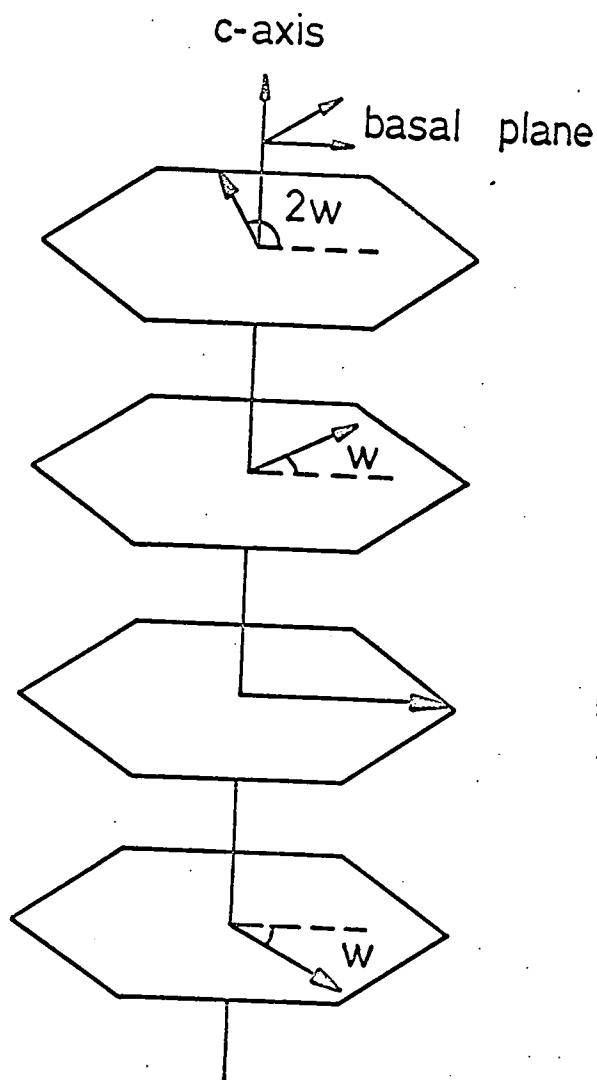
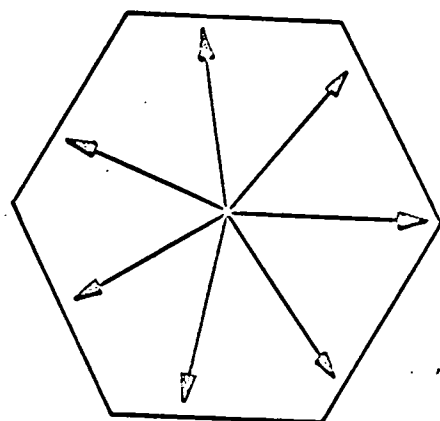


Fig. 1.2 Critical fields and corresponding temperatures for the helical to ferromagnetic spin transitions in dysprosium (after ref. 1.13).



(a) Oblique view of hexagonal planes showing moment directions.



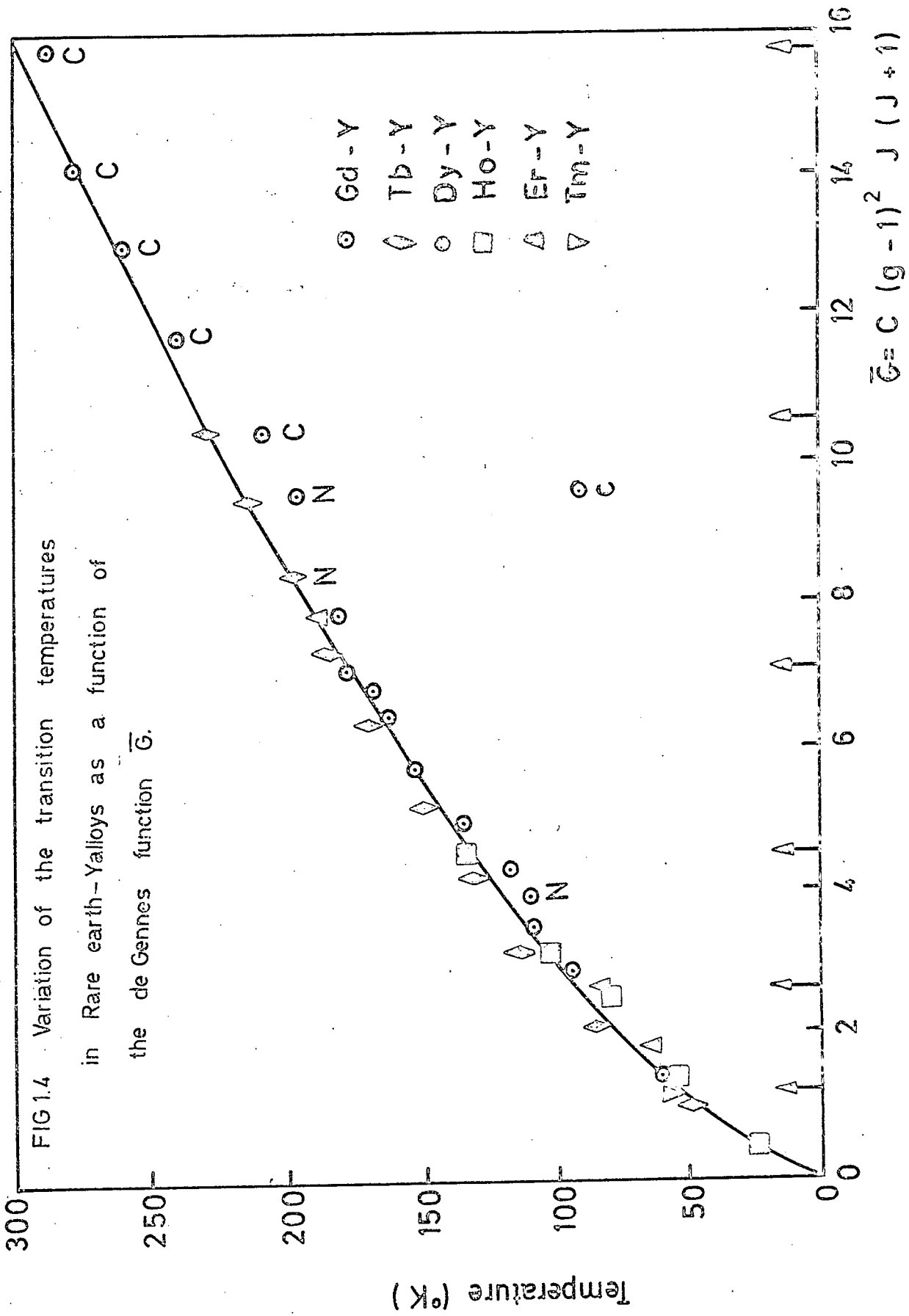
(b) View along c-axis

Fig.1.3 A simplified view of the helical spin structure, in which the ordering in any plane is ferromagnetic but the moment direction from plane to plane changes through a constant 'turn angle' ω resulting in overall antiferromagnetic behaviour. (after ref.1.3)

Their magnetic properties have been discussed in several review articles (see, for example refs. 1.1, 1.2). Studies of the Gd-Y system (ref. 1.17) showed that anti-ferromagnetic ordering occurred at 40 % Y concentration. Neutron diffraction studies (ref. 1.18) have shown that in the anti-ferromagnetic phase the spins have a helical configuration similar to that in Dy metal. The ferromagnetic Curie temperatures and the Neel points (refs. 1.17, 1.19, 1.20, 1.21) are given in fig. (1.4) as a function of the average of the de Gennes factor, $\bar{G} = CG$, where C is the rare earth concentration, and $G = (g_J - 1)^2 J(J+1)$ is the de Gennes factor (see chapter two). In addition the turn angle ω for the alloys is shown in fig. (1.5). ω shows only a small dependence on temperature for small G of value about 50° per layer, but with increasing G the variation becomes more marked, and for G greater than about 7, ω can show a sudden decrease to zero at some finite temperature (ref. 1.21).

Finally the existence of the helical spin structure can be interpreted very simply in terms of an exchange interaction whose magnitude is an oscillating function of distance. An exchange mechanism which satisfies these requirements is the indirect exchange interaction (see section 1.3, and chapter two) of Ruderman, Kittel, Kasuya and Yosida (RKKY). This mechanism has been remarkably successful in accounting for the basic magnetic properties of the rare earth metals, alloys and compounds. Many of the properties can be understood in terms of a Hamiltonian consisting of the three terms for localized rare earth ion moments (ref. 1.6).

$$\mathcal{H} = \mathcal{H}_{ex} + \mathcal{H}_{cf} + \mathcal{H}_{me} \quad (1.1)$$



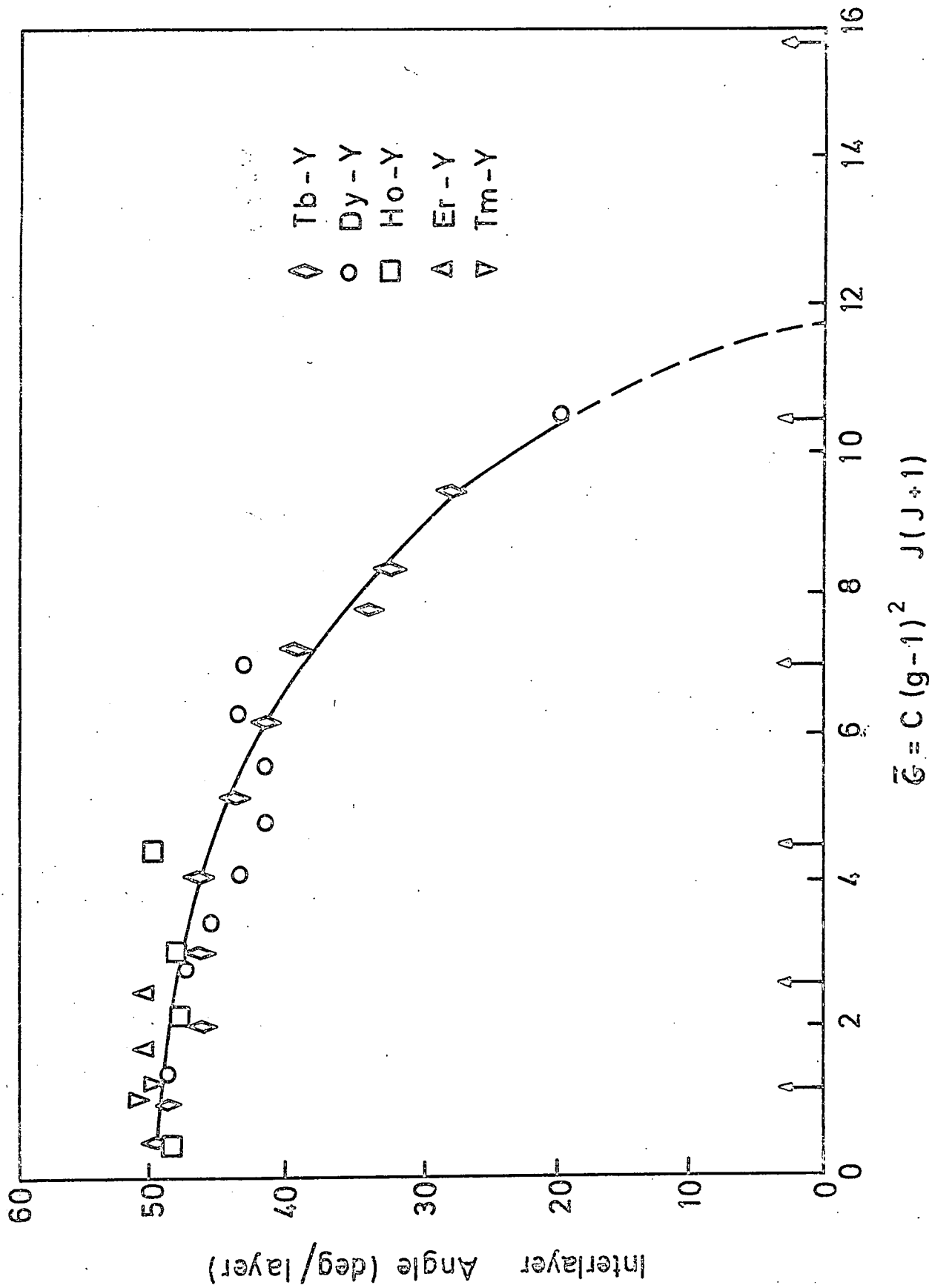


FIG. 1.5 The initial turn angle of the rare earth - yttrium as a function of the deGennes function \bar{G} .

The first contribution arises from a long-range oscillatory exchange interaction of the RKKY type via polarization of the conduction electrons (section 1.3). The second term is a single-ion anisotropy energy resulting from crystalline electrostatic field interactions on the distribution of the 4f electrons, and the third term is the magnetostriction contribution. For the heavy rare earth metals, especially the ferromagnetic metal Gd, the dominant term in the Hamiltonian is the first term. The other terms are usually assumed to be small.

1.2 Laves Phase Intermetallic Compounds

The Laves phase denotes a large group of related intermetallic compounds of stoichiometry AB_2 , having one of the three following structures:

1. C15 (cubic $MgCu_2$ -type)
2. C14 (hexagonal $MgZn_2$ -type)
3. C36 (hexagonal $MgNi_2$ -type)

The differences in the three arise from the stacking of the close-packed layers. The stacking sequences of the $MgZn_2$, $MgCu_2$, and $MgNi_2$ structures are ABAB..., ABCABC..., and ABACABAC..., respectively. The C15 structure is face-centred-cubic, the A atoms lying on a diamond-cubic lattice with B atoms stacked as tetrahedra. This structure has twenty four atoms (8 formula units) per unit cell (fig. 1.6) and belongs to the space group $Fd\bar{3}m-O_h^7$. Each A atom is surrounded by twelve nearest-neighbour B atoms at a distance $(a\sqrt{11}/8)$ and four next-nearest-neighbour A atoms at $(a\sqrt{3}/4)$. Each of the B atoms have six other B atoms as neighbours at $(a\sqrt{2}/4)$, and six A atoms at $(a\sqrt{11}/8)$. Appendix 1 gives the radii and the multiplicities of

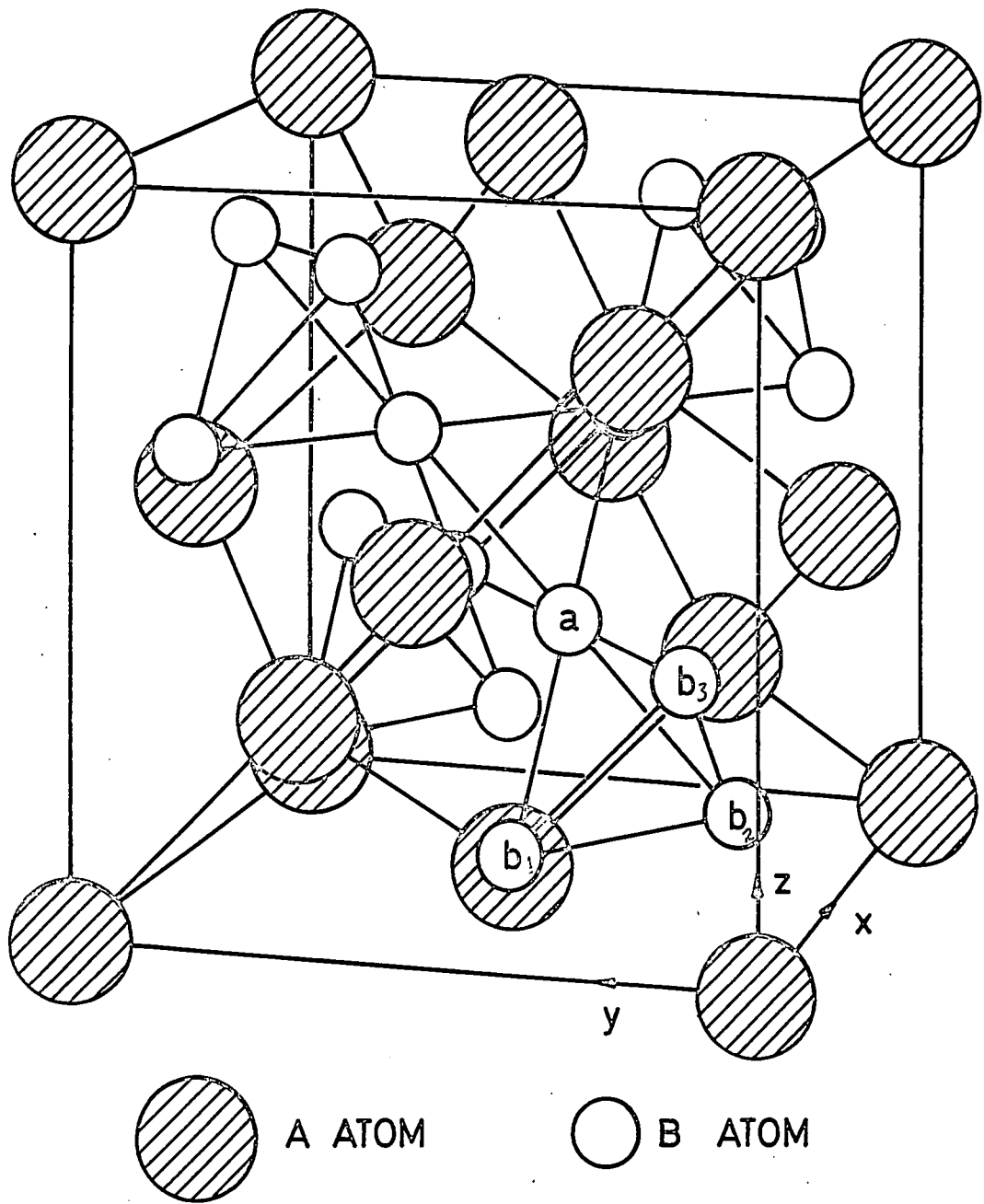


FIG.(1.6) C15 Laves Phase Structure.

the first 40 shells centred on A and B atoms. The C14 hexagonal phase contains 4 formula units per unit cell (twelve atoms per unit cell). The C36 hexagonal phase contains twenty-four atoms per unit cell (8 formula units).

The pioneer work on the three structures was performed by Laves (refs. 1.22, 1.23) who extended the ideas of Goldschmidt (ref. 1.24) on the importance of ionic radius ratios on the basis of a hard sphere model with A atoms in mutual contact, the ideal Laves structure required the ratio of atomic diameters d_A/d_B to be equal to 1.225. Taking the Goldschmidt radii of pure elements as indicative of the "size" of the A and B atoms, it is found that in practice the ratio R_A/R_B can vary from 1.05 to 1.68 (ref. 1.25) in the formation of stable Laves phase compounds. When the compounds are formed with the Laves structure it appears that the ionic radii either "expand" or "contract" in order to approach the ideal ratio 1.225. The importance of the size factor in the formation of Laves compounds can be summarized as follows (ref. 1.26):

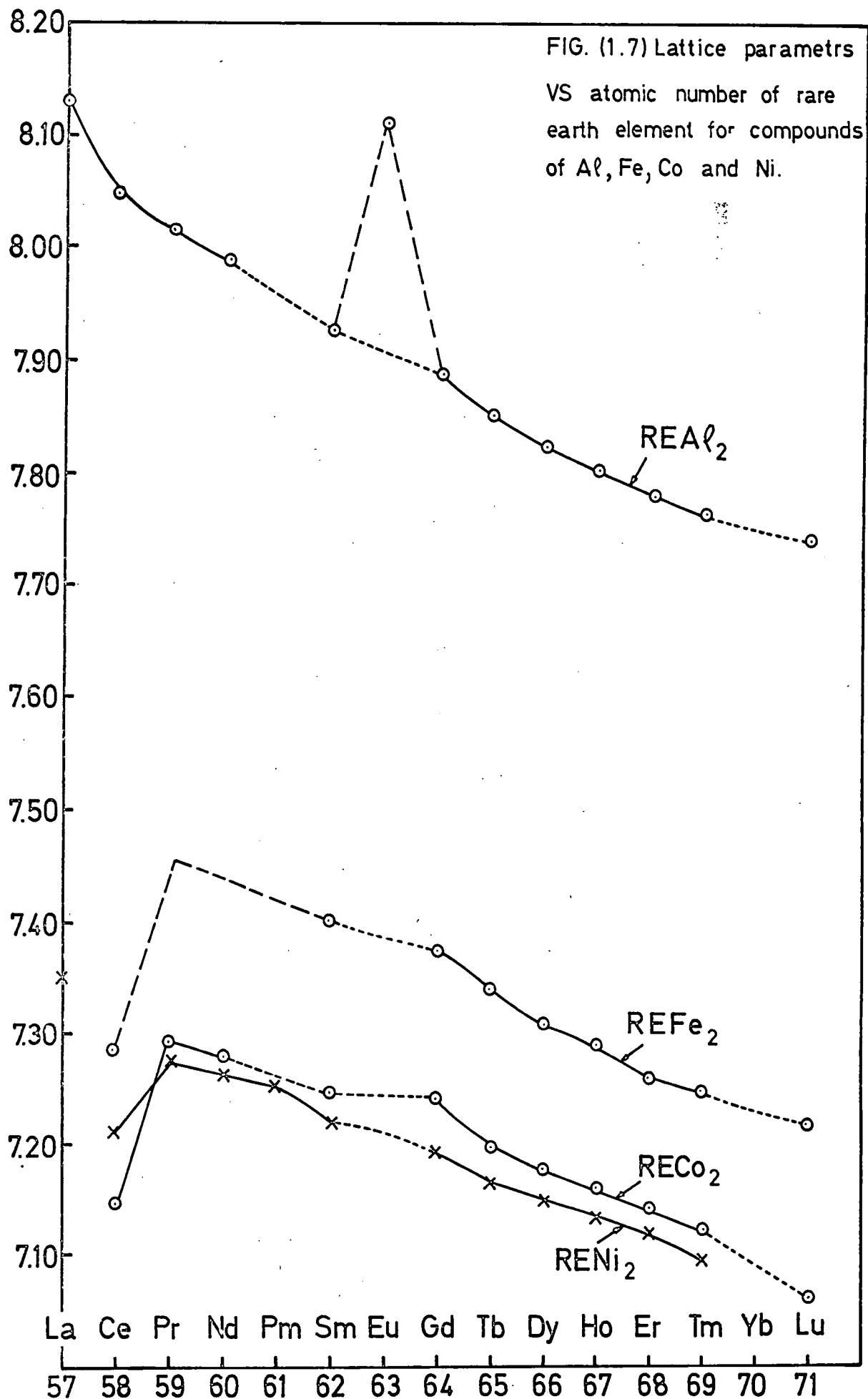
1. The atomic radius of the A element has to be larger than the radius of the B element,
2. The two elements must be able to accommodate their radii to approach $d_A/d_B = 1.225$.

It is generally thought (ref. 1.25) that while the radius ratio is critical to the formation of the Laves phase it is not effective in determining which of the phases will be preferentially formed. Rather it is the electrons-per-atom ratio which is the dominant factor in this respect. This ratio is known better perhaps as the valence electron concentration and refers to the average number of valence electrons per atom in the

structure. For example the $\text{MgCu}_2\text{-MgAl}_2$ system has the MgCu_2 type structure for concentrations of 1.33 - 1.73 valence electrons per atom, the MgNi_2 type for 1.84 - 1.95, and the MgZn_2 type for 2.03 - 2.05. Such results clearly show that the type of Laves phase formed is dependent on the valence electron concentration.

Binary intermetallic compounds existing between rare-earth metals and Co, Ni, Fe, and Al having the MgCu_2 type of structure have been studied by several authors. The radius ratio of the constituent atoms of AB_2 (with Fe, Co, Ni, and Al) is greater than the ideal value. Thus it would seem that the rare earth atoms contact and the B atoms expand. The lattice parameters of these compounds are shown in fig. (1.7) (refs. 1.26, 1.27, 1.28, 1.29, 1.30, 1.31). This figure shows the same systematic decrease with increasing rare earth atomic number as that found in the rare earth elements themselves. The cerium compounds show a large negative deviation from the expected value and this is associated with the loss of the one 4f electron of cerium to the conduction band leaving the ion quadripesitive (ref. 1.29). The lattice parameter of EuAl_2 is large, (ref. 1.26) as expected from the large atomic diameter of divalent europium.

A pseudo-binary compound of the form $(\text{AA}')\text{B}_2$ or $\text{A}(\text{BB}')_2$ can crystallize as a Laves phase, and can maintain the same structure over quite a wide concentration range. The pseudo-binary compounds of the form $\text{AB}_2\text{-AAl}_2$ (A = rare earth and B transition metal) show the effect of the changing valence electron concentration on the structure, where the structure changes from cubic C15 (MgCu_2) to hexagonal C14 (MgZn_2) and back again to the C15 structure with increasing Al content (or in other



words the number of free electrons (refs. 1.32, 1.33, 1.34). We have seen the same effect in $\text{Gd}(\text{CoAl})_2$ as described in chapters 5 and 6.

1.3 Indirect exchange interaction

The 4f electron of a rare earth atom in the metallic state can not undergo an exchange interaction directly with the 4f electrons of a neighbouring atom. Because of the high degree of localization of the 4f electrons, there is essentially no overlap between the neighbouring ion cores, the mean radius of the 4f shell being small compared with the interionic spacing. The principal mechanism responsible for magnetic ordering is believed to be the indirect exchange interaction in which the conduction electrons play a key role in allowing the neighbouring ions to interact with each other. In this interaction each 4f shell moment polarizes the spins of the conduction electrons in the neighbourhood of the ion through a Heisenberg exchange interaction.

The theory of indirect exchange interaction was first developed by Rudermann and Kittel (ref. 1.35) for the case of nuclei interacting via the hyperfine interaction with the conduction electrons. Kasuya (ref. 1.36) and Yosida (ref. 1.37) extended these ideas and obtained the so-called Rudermann, Kittel, Kasuya, Yosida (RKKY) exchange interaction for materials such as the rare earths.

1.3.1 The exchange interaction

The Hamiltonian of the exchange interaction between the localized and conduction electrons has been treated by a number

of authors (refs. 1.38, 1.39, 1.40, 1.41, 1.42, 1.43, 1.44), following the work of Kasuya (ref. 1.14) and may be written as:

$$H_{sf} = -\frac{1}{N} \sum J_{sf}(K, K') e^{i(K-K')R_n} \times \\ ((C_{K\uparrow}^* C_{K'\uparrow} - C_{K\downarrow}^* C_{K'\downarrow}) S_n^z + C_{K\uparrow}^* C_{K'\downarrow} S_n^- + C_{K\downarrow}^* C_{K'\uparrow} S_n^+) \quad (1.2)$$

where

$$J_{sf}(K, K') = N \int e^{-i(K-K')R_n} \mathcal{U}_{K'}^*(r_2) \Psi^*(r_1 - R_n) \frac{e^2}{r_{12}} \times \\ \mathcal{U}_K(r_1) \Psi(r_2 - R_n) dr_1 dr_2 \quad (1.3)$$

where $\mathcal{U}_K(r) e^{iKr}$ is a normalized Bloch function, C_K, C_K^* are the creation and annihilation operators of the electron with wave vector K , S_n denotes the spin operator of the localized shell electrons located at R_n with S^+ the step-up and S^- the step-down operator $J_{sf}(K, K')$ is the exchange integral between the 4f electrons of an ion and a conduction electron, known as the sf exchange interaction constant. From the various approximations the exchange interaction is usually assumed to be isotropic and a function of $K-K' = q$ only. In many applications it is assumed to be independent of K and K' and is replaced by a constant term J_{sf} .

The $J_{sf}(q)$ approximation allows equations (1.2, 1.3) to be written as:

$$H_{sf} = -\sum J_{sf}(|r-R_n|) S_n S_i \quad (1.4)$$

$$\text{and } J_{sf}(|r-R_n|) = \frac{1}{N} \sum_q J_{sf}(q) e^{i(r_i - R_n) \cdot q} \quad (1.5)$$

where r_i and S_i are respectively the co-ordinate and spin

operator of the i -th electron.

1.3.2 The RKKY Interaction

Rudermann and Kittel (ref. 1.35) first considered the indirect coupling of nuclear spins by calculating the second-order perturbation of the energy using the hyperfine interaction analogue of the H_{sf} interaction. Kasuya (ref. 1.36) proposed that it was the important interaction for the case of the rare earths and Yosida (ref. 1.37) used it for the electron spin coupling in transition metal alloy systems. The relation between the R-K and K-Y types of calculations was given by Van Vleck (ref. 1.45). A detailed discussion of the exchange coupling parameter was given first by Liu (ref. 1.46) and by Watson and Freeman (refs. 1.47, 1.48, 1.49) who also investigated the long-range conduction electron spin polarization induced by the sf interaction. The $4f$ electrons overlap the conduction electrons strongly and the net $4f$ spin polarizes the conduction electrons via the sf interaction. This polarization has an oscillatory component due to the Fermi distribution which restricts the wave vector of the conduction electron sea that carries the polarization. This resultant polarization is carried over to the vicinity of other ions and then interacts with the moment of their $4f$ shells to produce an alignment of the moments.

Let us consider the effect of the interactions of the localized spin moments S_n and S_m located at sites R_n and R_m and the conduction electrons. Using second order perturbation theory, the effective exchange interaction between the two spins is

$$H_{nm} = - \sum_{K, K'} | \langle K' | H_{sf} | K \rangle |^2 \left\{ \frac{f(K) - f(K')}{E(K) - E(K')} \right\} \quad (1.6)$$

Substituting H_{sf} from equation (1.2), using the properties of closure on the intermediate states and retaining only terms dependent on the spin orientation yields, in operator form:

$$H_{nm} = - \frac{1}{N^2} \sum_{K, K'} | J_{sf}(K, K') |^2 \frac{f(K) - f(K')}{E(K) - E(K')} e^{i(K-K')(R_n - R_m)} \\ \times (2S_n^z S_m^z + S_n^- S_m^+ + S_n^+ S_m^-) \quad (1.7)$$

where $f(K)$ is the fermi occupation function. This expression was derived for the interaction of two localized sites. For many lattice sites with localized spins we may write:

$$H_{nm} = - \sum J(R_n - R_m) S_n S_m \quad (1.8)$$

where the indirect exchange coupling constant is given by,

$$J(R_n - R_m) = \frac{1}{N^2} \sum_{K, K'} | J_{sf}(K, K') |^2 \frac{f(K) - f(K')}{E(K) - E(K')} e^{i(K-K')(R_n - R_m)} \quad (1.9)$$

It is convenient to define a wave-vector-dependent susceptibility of the conduction electron system $\chi(q)$, which yields the response of the electron gas to the exchange field of the localized spin. $\chi(q)$ is usually defined by the equation:

$$\chi(q) = \frac{1}{N} \sum \frac{f(K) - f(K')}{E(K) - E(K')} \quad (1.10)$$

By substituting this equation in equation (1.7) and replacing $J_{sf}(K, K')$ by $J_{sf}(q)$ for convenience and simplification gives:

$$H_{nm} = \frac{-1}{N} \sum_{n, m, q} J_{sf}(q)^2 \chi(q) e^{iq(R_n - R_m)} S_n S_m \quad (1.11)$$

and

$$J(R_n - R_m) = \sum_q J_{sf}(q)^2 \chi(q) e^{iq(R_n - R_m)} \quad (1.12)$$

For a free electron gas in three dimensions (refs. 1.4, 1.50)

$\chi(q)$ is given by the well known function,

$$\chi(q) = \frac{mK_f}{2\pi^2 \hbar^2} \left\{ 1 + \frac{4K_f^2 - q^2}{4K_f q} \operatorname{Ln} \left| \frac{q + 2K_f}{q - 2K_f} \right| \right\} \quad (1.13)$$

where K_f is the radius of the conduction-electron Fermi surface, which is taken to be spherical. This function is shown in fig. (1.8). $\chi(q)$ slowly decreases from the value 1.0 to $\frac{1}{2}$ as q changes from 0 to $2K_f$. At $q = 2K_f$, the slope is infinite and for $q > 2K_f$, $\chi(q)$ falls rapidly to zero.

Substituting for $\chi(q)$ from (1.13) in (1.12) and using the RKKY approximation for $J_{sf}(q)$ to be constant (say Γ), the summation in Eqn (1.12) has been calculated by Kittel (ref.1.50) to be the following,

$$J(R_n - R_m) = \frac{q \pi z^2 \Gamma^2}{2E_F} \sum F(2K_f (R_n - R_m)) \quad (1.14)$$

where

$$F(x) = \frac{\sin x - x \cos x}{x^4} \quad (1.15)$$

$$x = 2K_f R_{nm}$$

This function is often referred to as the RKKY function. The interaction is thus of long range, decreasing as R^{-3} for large R so that it is closely centred about the ion site and oscillates with the period $(2K_f)^{-1}$. The lattice sum $F(x)$ varies for the different crystallographic structures and has been evaluated by several authors in connection with the

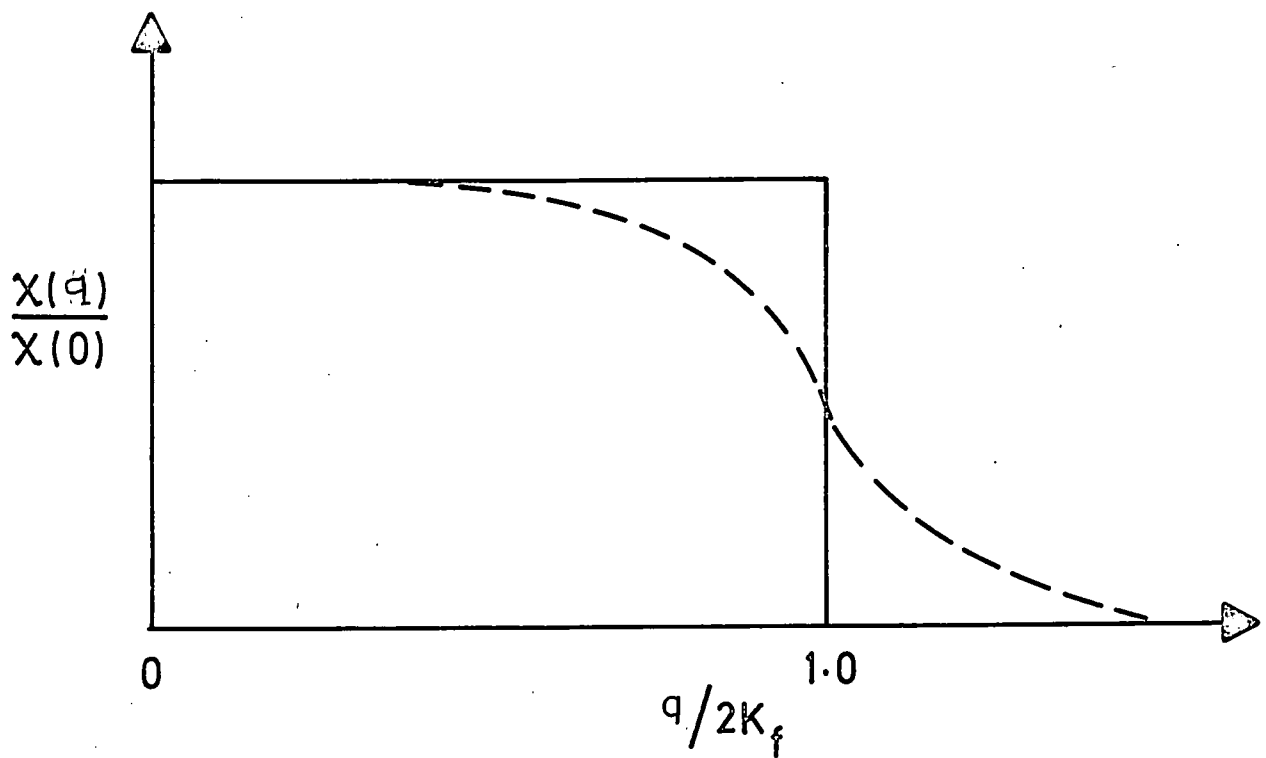


FIG. (1.8) Normalized $X(q)$ versus q (-----) and the model proposed by Yosida (——)

interpretation of magnetic properties (see chapter 2).

Yosida (ref. 1.37) considered the applicability of the expression (1.14) to the magnetic problem of the ion cores interacting with the conduction electrons. He pointed out that this expression does not adequately take into account the decrease in $J(q)$ with increasing q . He also gave the formula for $J(R_n - R_m)$ which is obtained by taking $J_{sf}(q)^2 \chi(q)$ constant for $q \leq 2K_f$ and zero for $q > 2K_f$ Fig. (1.8). One then obtains:

$$J(R_n - R_m) = \frac{q \pi z^2 \Gamma^2}{2 E_F} \sum 2K_f(R_n - R_m) F(2K_f(R_n - R_m)) \quad (1.16)$$

It is seen that the exchange interaction decreases with R^{-2} rather than with R^{-3} . The analysis above assumes that the conduction electrons have an infinite mean free path.

De Gennes (ref. 1.52) and recently Buschow (ref. 1.51) attempted to take this into account by introducing an exponential decay which is written as $\exp(-R/\lambda)$ where λ is the conduction electron mean free path. This may be introduced as a multiplying factor in the equations above.

The assumption that $J_{sf}(K, K')$ is defined solely over the electrostatic exchange integral, as in equation (1.3), means that the exchange energy is positive and this immediately implies that the net induced moment is parallel to that of the local moment. However, anti-parallel net spin polarizations are observed (see chapter 2). This necessitates the existence of other exchange effects which give negative contributions to a total effective exchange coupling. Such an effective exchange interaction can arise out of the mechanism of interband or covalent mixing between the conduction and the

local moment electrons. Watson and Freeman approximated the total exchange integral for the s-f exchange interaction as:

$$\begin{aligned} J_{\text{tot}}(K, K') &= J_0(K, K') + J_{\text{abs}}(K, K') + J_{\text{em}}(K, K') \\ &= J_0(K, K') + J_{\text{inter}}(K, K') \end{aligned}$$

where $J_0(K, K')$ is the conventional electrostatic exchange interaction, $J_{\text{em}}(K, K')$ arises from a process in which an electron in an occupied local moment level (with energy $\epsilon_{4f} \uparrow$) is emitted into a Bloch state K' and the created hole absorbs a Bloch electron K , and $J_{\text{abs}}(K, K')$ is the absorption process. Shaltiel et al. (ref. 1.53) suggested that the mixing between the f-electron and d-band of the host may be the most significant contribution to a negative total exchange.

Recently, Campbell (ref. 1.54) has suggested a further possibility. He argues that the f-electron spin of the rare earth may create a positive local d-moment through f-d exchange and that d-d interactions with other d-moments are then important.

All the calculations up till now have assumed a susceptibility appropriate to a non-interacting free electron gas. Wolff (ref. 1.55), Overhauser (ref. 1.56) and Herring (ref. 1.57) emphasized that the Coulomb interactions between the conduction electrons play an essential role in determining the wave-vector-dependence of the spin susceptibility, $\chi(q)$. The various calculations (ref. 1.55) indicate that the electron-electron interaction greatly enhances the spin susceptibility of the non-interacting electrons. The electron gas is perturbed with a magnetic field H giving the response (refs. 1.47, 1.50)

$$M(q) = \chi(q) H(q) \tag{1.16}$$

Now suppose the response induces an effective exchange field proportional to $M(q)$, say $\nu M(q)$, where ν is a constant which may depend on q . Then eqn. (1.16) is replaced by,

$$M(q) = \chi(q) \left[H(q) + \nu M(q) \right] \quad (1.17)$$

solving for $M(q)$ gives

$$M(q) = H(q) \left[\chi(q) / (1 - \nu \chi(q)) \right] \quad (1.18)$$

where the exchange-enhanced susceptibility is given by,

$$\chi_\nu(q) = \chi(q) / (1 - \nu \chi(q)) \quad (1.19)$$

The susceptibility is enhanced in value when ν is positive. As we have seen from fig. (1.8), $\chi(q)$ in three dimensions decreases monotonically as q increases, so that $\chi(q)$ at low values of q is enhanced more than $\chi(q)$ at high values of q .

Giovannini et al. (ref.1.58) considered the effect of the enhanced susceptibility on the spin polarization for various values of the factor, ν , above. They obtained an increase in both the amplitude and the range of the spin polarization over the free-electron RKKY form and used their results to account for the g-shift and line-broadening due to the rare-earth impurity in a Pd-Gd host.

Generalizations of the RKKY interaction for nonspherical Fermi surfaces have been considered by several workers (refs. 1.59, 1.60, 1.61, 1.62). The theoretical work of Roth et al. (ref. 1.59) shows the following general features. For spheroidal or ellipsoidal surfaces the interaction falls off with distance as R^{-3} , and the period of oscillation is anisotropic, depending upon the length of the wave-vector which calipers the Fermi surface in the direction of R . There may be several such periods, corresponding to different parts of the

Fermi surface. For cylindrical regions, and for flat regions of the surface, the range of the interaction may be considerably increased, falling off as R^{-2} and R^{-1} respectively.

More details about the RKKY interaction are given in refs.

1.1, 1.2.

Finally, the polarization of conduction electrons manifests itself in other ways. For example it produces a shift in the g -value of the magnetic ions which can be determined by esr measurement and it gives rise to a hyperfine field which may be measured by nmr or Mossbauer techniques. For these and other observable effects of the electron polarization see chapter 2.

1.4 Hyperfine Interaction

Hyperfine interactions have been studied for many years, and are defined as those interactions which take place between the atomic electrons and the nuclear charge and moment distributions. The hyperfine interaction is divided into two classes.

a. The magnetic hyperfine interaction. This interaction arises from the effect on the electronic magnetic moment of the magnetic field of the nucleus. This field may be given by

$$\mathcal{H}_n^{\text{mag}} = -(\mu_I \cdot H_e) \quad (1.20a)$$

where μ_I is nuclear magnetic moment, and H_e is the magnetic field at the nucleus generated by the magnetic electrons (ref. 1.65). For a free ion we can write $\mu_I = g_n \beta_n I$, and $H_e = -(A/g_n \beta_n) J$, so that equation (1.20a) becomes.

$$\mathcal{H}_n^{\text{mag}} = A(J \cdot I) \quad (1.20b)$$

b. The electric interaction. This interaction represents the electrostatic interaction between the charge distribution of a nucleus and that of the surrounding electrons; for the present work, only the magnetic interaction is considered in detail.

1.4.1 Magnetic Hyperfine Interaction

In magnetically ordered systems such as ferromagnets, four types of interaction can be distinguished which may contribute to the hyperfine field at the nucleus. These are:

a. The electronic orbital contribution which comes from the orbital part of the electronic angular momentum. For the lanthanides the main contribution comes from this term except for those S-state ions like Gd. This is due to the fact that the angular momentum is not quenched. In the 3d transition series, where the orbital angular momentum is "quenched" by the crystal field, this term is usually small i.e. 10^4 Gauss for iron. This field has the form:

$$\mathcal{H}_l = \sum_i \frac{g \beta \gamma \mu_n}{\hbar^2} \frac{1}{r_i^3} l_i \cdot I \quad (1.21)$$

b. The electronic dipole contribution from surrounding ions. This may be written as

$$\mathcal{H}_d = \frac{g \beta \gamma \mu_n}{\hbar^2} \sum_i \frac{1}{r_i^3} \left[S_i \cdot I - \frac{3(S_i \cdot r_i)(I \cdot r_i)}{r_i^3} \right] \quad (1.22)$$

It is generally relatively small (of the order of 10^4 Gauss) and in cubic symmetry drops out entirely.

c. The "local" field contribution which consists of the

external, demagnetizing, and Lorentz fields, and is given by:

$$\mathcal{H}_{loc} = H_{ext} + \frac{4}{3} \pi M - DM \quad (1.23)$$

where D is the demagnetization factor and depends upon the shape of the sample and has a value $4\pi/3$ for a sphere and 2π for an infinite cylinder. M is the magnetization.

d. The Fermi contact contribution, which comes from the spin density at the nucleus. This is the dominant term for most systems where a transition or nonmagnetic impurity is dissolved in a ferromagnetic host. The interaction is between the nuclear magnetic moment and the electronic spin density at the nucleus, this field is given by

$$\mathcal{H}_c = \frac{8\pi}{3\hbar^2} \gamma g \beta \mu_n |\psi(0)|^2 I \cdot S \quad (1.24)$$

where $|\psi(0)|^2$ is the square of the amplitude of the probability density of the s-electron within the nuclear volume.

It is clear that only the s electrons have non-vanishing values at $|\psi(0)|^2$. The Fermi contact contribution can be subdivided into three components, which are cited below.

a. Core Polarization (CP) (in closed shells), which results from the contact interaction with the unbalanced spin density of the ion core s electrons at the nucleus.

b. Conduction Electron Polarization (CEP) can contribute to the effective magnetic field at a nucleus by a direct contact interaction of the nuclear spin with the s-like part of the spin polarization.

c. Contributions from the admixture of s-character into the magnetic shell (e.g. 3d, 4f etc.)

The total hyperfine interaction can then be written

$$\mathcal{H} = \frac{g\beta\gamma\mu_n}{2} I \cdot \left\{ |\psi(0)|^2 S + \sum_{r_i} \frac{1}{r_i^3} \left[l_i - S_i + \frac{r_i}{r_i^2} (S_i r_i) \right] \right\} + H_{loc} \quad (1.25)$$

In the absence of an external magnetic field, and assuming spherical domains, H_{loc} will be zero. We may write the expression in curly brackets in (1.25) simply as a vector N so that (1.25) becomes:

$$\mathcal{H} = 2\beta\gamma\hbar (N \cdot I) \quad (1.26)$$

This is equivalent to an interaction

$$-\gamma_n \hbar (H_e \cdot I) \quad (1.27)$$

1.4.2 Core Polarization and Conduction Electron Polarization

The contact interaction is generally the dominant mechanism producing hyperfine fields at the impurity nuclei. There has long been known to be competition between core polarization (CP) and conduction electron polarization (CEP) at the impurities in ferromagnets. For nonmagnetic impurities, it is generally accepted that CEP is the dominant, and in some cases the only, mechanism. The CP field which results from the contact interaction with the unbalanced spin density of the ion core s-electrons at the nucleus can be written as

$$H_{cp} = - \frac{8\pi}{3} g_s \beta (|\psi_{\uparrow}|^2 - |\psi_{\downarrow}|^2) S \quad (1.28)$$

where the spin densities are evaluated at the nucleus, and S is the total spin for the ion under consideration. The effect

of the exchange interaction is to attract the core electrons with spin parallel to the net spin of the magnetic shell (spin \uparrow), whilst repelling those of antiparallel spin. This means that for inner closed shells, there will be a net contribution to the hyperfine field, whilst the contribution from outer shells will be positive. The CEP can contribute to the effective magnetic field at the nucleus by a direct contact interaction of the nuclear spin with the s-like part of the spin polarization. The field due to the direct contact of s-like conduction electrons can be written as:

$$H_{\text{CEP}} = \frac{8}{3} \pi Z g \beta |\psi_{\text{CE}}(0)|^2 \langle s \rangle \quad (1.29)$$

Where Z is the number of conduction electrons per ion.

In order to explain the occurrence of hyperfine fields at the nuclei of nonmagnetic impurities in ferromagnets it is necessary to have a mechanism whereby the CEP of the host can be carried over to the region of the impurity. The work of Rudermann, Kittel, Kasuya and Yosida has shown that the conduction electron polarization CEP interacting with the nuclear spin via the contact term, gives a hyperfine field.

$$H_{\text{hf}}^{\text{c}} = \frac{1}{g_n \beta_n} \frac{3n}{8E_{\text{FN}}} \sum_{\mathbf{q}} A(\mathbf{q}) J(\mathbf{q}) f(\mathbf{q}) e^{i\mathbf{q}\cdot\mathbf{r}} S \quad (1.30)$$

$$= - \frac{q \pi Z^2}{g_n \beta_n E_{\text{FN}}} A(0) \left[\sum_{\mathbf{K}_f} F(2\mathbf{K}_f) R_{\text{nm}} \right] \langle S \rangle \quad (1.31)$$

For more details see chapter 2 and chapter 6.

1.4.3 Experimental methods and results

The conventional methods for observing hyperfine interactions have been described in the literature. The experimental methods which are important for measuring hyperfine fields in magnetic materials are, specific heat, Mossbauer effect, angular correlation of X-rays and resonance methods (which include nuclear magnetic resonance and electron paramagnetic resonance). In this thesis we discuss nuclear magnetic resonance spin echo (see chapter three) in detail. The other methods have been discussed extensively by several authors. For details and references see refs. 1.67, 1.68.

The magnetic hyperfine field contribution (section 1.4) in the rare earth metals, alloys and compounds has been the subject of several authors. (In the specific case of the intermetallic compounds of the form AB_2 the hyperfine field at the B nucleus will be discussed in chapter two and six).

In general the magnetic hyperfine field acting on a rare earth nucleus can be written as

$$H_{hf} = H_{4f} + H_{CP} + H_{CEP} + H_m \quad (1.1)$$

where H_{4f} is the hyperfine field produced by the 4f electrons in their direct interaction with the nucleus, H_{core} is the hyperfine field produced by the closed shells which are deformed and polarized through the interaction with the 4f electrons and H_m is the hyperfine field due to the polarization of conduction electrons, covalency effects, and direct overlap of the 4f wave function. When J is a good quantum number, the ionic H_{4f} contribution can be given by (ref. 1.63),

$$H_{4f} = 2 \mu_B \langle r^{-3} \rangle \langle J || N || J \rangle J \quad (1.2)$$

where $\langle r^{-3} \rangle$ is measure of the radial distribution of the 4f electrons and has been calculated for free ions (ref. 1.64) $\langle J || N || J \rangle$ is the conversion factor in the operator equivalent technique developed by Elliot and Stevens (ref.1.65) who also tabulated the values for the rare earths.

The contribution from core polarization was estimated by Freeman and Watson to be $-(g_J - 1) J = 90$ kOe (ref.1.66) or $-(g_J - 1) J = 100$ kOe by Bleaney (ref. 1.64). This term is the important term for Gd and Er, and is negligible compared with the observed fields for the other elements.

Bleaney first discussed and calculated the free-ion hyperfine interaction for the tripositive lanthanides in detail (ref. 1.69). The measurement of the hyperfine interactions in rare earth metals gives results which are very close to the free-ion values in the case of the heavy rare earths as may be seen from table (1.3). This indicates that the crystal-field interaction is much smaller than the exchange interaction, and also that the orbital hyperfine field is much larger than the contribution from the conduction electron polarization. In Gd and Eu metals the conduction electron polarization field is relatively large.

Using the Mossbauer effect, Hufner and Wernick (ref.1.74) studied the hyperfine field of Eu metal as a function of dilution with Yb and obtained the results listed in table (1.4).

Zmora et al. (ref. 1.75) have determined the various contributions to the magnetic hyperfine field in Gd metal from measurements of the hyperfine fields acting on Gd and

Lu nuclei in $Gd_x Lu_{1-x}$ alloys, using the perturbed angular correlation technique. They found that the effective field varies linearly with concentration, and at the same rate, at both the Gd and the Lu nuclei. This variation with concentration was attributed to the effects caused by the polarization of the conduction electrons by the surrounding ions. The Gd effective field for $x = 0$ is equal to (-90 ± 20) kOe, and may be attributed to the sum of the core polarization and of the conduction electron polarization by the ion itself. This value is in agreement with that obtained by Hufner (ref. 1.76) see table 1.4.

Itoh et al. (ref. 1.77) have used spin echo measurements to observe the resonance in ^{159}Tb and ^{163}Dy in Tb-Gd, Tb-Dy and Dy-Gd alloys. They found that the hyperfine fields at the Tb and Dy nuclei vary by roughly the same amount per unit variation of the average spin S of the alloy while the resonance line width was nearly the same throughout all concentrations of the alloys. They attributed this result to an almost uniform polarization of the conduction electrons. The hyperfine fields of ^{165}Ho at different concentrations in Gd, Tb and Dy have been extensively studied by McCausland et al using spin echo measurements and have been discussed by Bleaney (ref. 1.78) and Taylor (ref. 1.1) and Guimaraes et al (ref.1.79). The results provide further evidence of a linear shift of the hyperfine field with concentration as shown in figure (1.9), and have shown that the NMR frequency can be represented by the formula;

$$\omega_0 = 6602 - 73 (g_j - 1) J + 1.1 g_j J$$

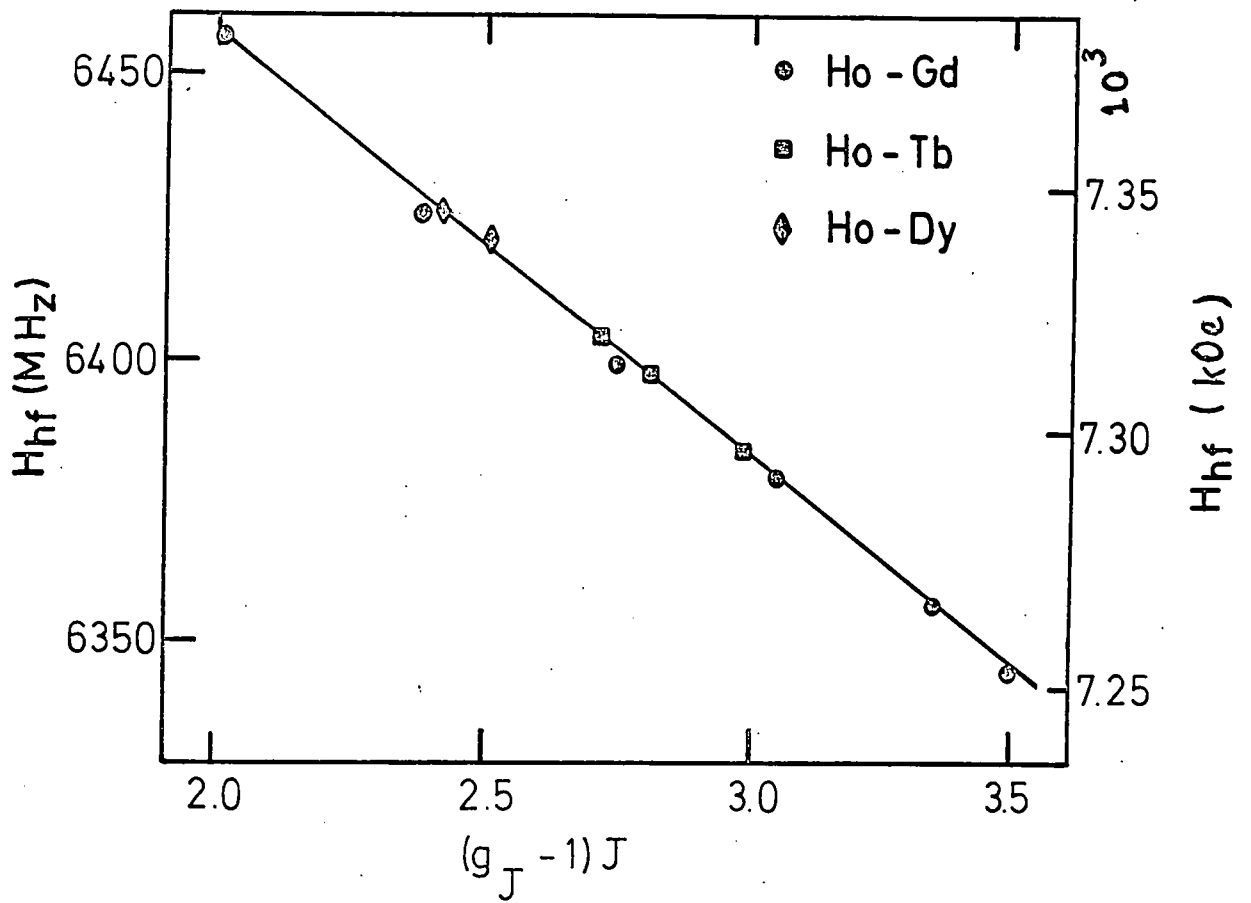


Fig. (1.9) N.M.R. measurement of the Ho resonance frequency at liquid helium temperature in various alloys

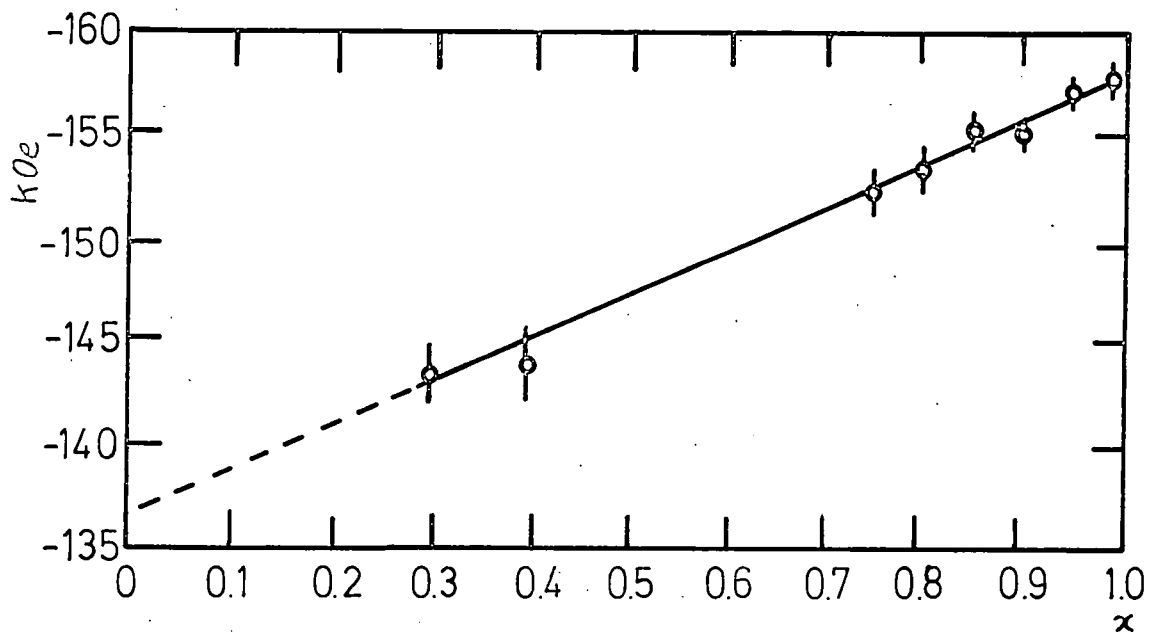


Fig.(1.10) Effective magnetic field at Gd site in $Gd_xAl_{1-x}_2$ as function of concentration at 4.2K. The points at $x = 0.4$ and $x = 0.3$ were achieved at about $2.5^{\circ}K$.

Table 1.3 The hyperfine field in rare earth metals

Ln	Free Ion (kOe)	Reference	Metals (kOe)	Reference
Sm	3390 ± 30	1.70	3430 ± 170	1.70
Gd	316 ± 3	1.70	371 ± 20 374 ± 9	1.71 1.92
Tb	3139 ± 31	1.70	3068	1.72
Dy	5700 ± 21	1.70	5768	1.73
Ho	7404 ± 9	1.70	7344 ± 6	1.78
Er	7640 ± 80	1.70	7730 ± 24	1.70
Tm	6705 ± 85	1.70	6420 ± 280	1.70

Table 1.4 Estimated contributions to the hyperfine field in Er, Gd and Ho metals

	Eu (ref.1.74)	Gd (ref.1.76)	Ho (ref.1.1)
Core polarization,(kOe)	-340	-340	7430
Conduction electron polarization by 4f electron.(kOe)	190	250	120
Neighbour effects: Conduction overlap + covalency (kOe)	-115	-260	-170
Experimental value for metal	-265	-350	7380

The last term is the contribution from the Lorentz field, while the second term is proportional to the mean value of $(g_j - 1)J$ averaged over the relative concentrations. In their measurements, they obtained the value $a = 6450$ MHz (ref. 1.79). The hyperfine contributions for Ho are shown in table (1.9). Finally Bailey (ref. 1.80) observed from spin echo measurements that the magnetic hyperfine parameter a_0 of holmium changes linearly with the average value of $(g_j - 1)J$ in the ferromagnetic $H_{0.01} Gd_{0.99-x} Lu_x$ alloy system. This relation is thought to be due to the polarization of the conduction electrons by the localized 4f electrons.

The hyperfine field at the rare earth nuclei in inter-metallic compounds in the AB_2 Laves phase are of approximately the same magnitude as in the metal whenever B is non-magnetic. On the other hand, when the element B carries a magnetic moment the effective fields are substantially different, and show an increase of several hundred kilo-oersteds in relation to those in metals. This increase has been observed using the Mossbauer effect on $SmFe_2$ (ref. 1.81), $TbFe_2$ (ref. 1.82), $DyFe_2$ (ref. 1.83), $ErFe_2$ (ref. 1.84), and nuclear magnetic resonance measurements have been reported on $GdFe_2$ (ref. 1.85), and $HoFe_2$ (ref. 1.86). The large positive value for the Gd hyperfine field in $GdFe_2$ is about 800 kOe larger than the value in pure Gd metal (ref. 1.85). Gegenwarth et al. (ref. 1.87) measured the hyperfine field in several gadolinium compounds using the spin echo technique with the results shown in table (1.5). The different values of the effective fields at the Ln nucleus in cubic Laves phase $LnFe_2$ compounds may be due to the polarization of the conduction electrons by 3d ions, or to overlap

Table 1.5 Gd hyperfine fields in various compounds

Compounds	Hyperfine field (kOe)
GdAl ₂	-170
GdRh ₂	-103
GdPt ₂	180
GdFe ₂	453
GdMn ₂	385 ± 30
GdN	370

Table 1.6 Contribution to the magnetic hyperfine field at Gd nucleus in GdAl₂

Core polarization	-320 ± 20 kOe
Self CE polarization	186 ± 20 kOe
Neighbour effects (due to A atoms)	- 22 ± 2 kOe
Neighbour effects (due to B atoms)	0 kOe
Total Experimental	-158 ± 0.3 kOe

and covalency effects, or to a mixture of the two (ref. 1.78).

N.M.R. spin echo measurements have been used on ^{165}Ho in intermetallic compounds of the form $(\text{Ho}_x \text{Gd}_{1-x})\text{X}_2$, where $x = \text{Fe, Co, Al}$ (ref. 1.88). In the Fe_2 compounds the hyperfine field is about 650 kOe higher than in Al_2 compounds and about 500 kOe higher than in pure Ho. Bailey has investigated three samples of the series $\text{Ho}_{0.03} \text{Gd}_{0.97} (\text{Fe}_x \text{Co}_{1-x})$, with $x = 0.1, 0.3, \text{ and } 0.99$, by using spin echo measurements (ref. 1.80). Satellite structure was clearly visible in each sample indicating that the transferred hyperfine interaction from 3d ions is essentially a nearest-neighbour effect.

Recently, the hyperfine specific heat measurements of Bloch et al. (ref. 1.93) for the Ho nucleus in HoCo_2 yield the value of the hyperfine field equal to $(0.316 \pm 0.005)\text{K}$.

Dintelmann and Buschow (ref. 1.89) investigated the hyperfine field at the Gd nuclei in $(\text{Gd}_x \text{Y}_{1-x})\text{Al}_2$ and found that the hyperfine field changes linearly with concentration, figure (1.10) giving a value at $x = 0$ of:

$$H_{\text{hf}} (x = 0 \text{ Gd}) = - (140.4 \pm 6.7) \text{ kOe}$$

However the Gd hyperfine field in pure $\text{GdAl}_2 = -(162.4 \pm 4.7) \text{ kOe}$, consequently the contribution of neighbouring Gd ions to the Gd hyperfine field is $-(22 \pm 2) \text{ kOe}$. A summary of the various contributions to H_{hf} on GdAl_2 is given in table (1.6).

Finally, Mossbauer studies (refs. 1.90, 1.91) of the hyperfine field at the ^{193}Ir nucleus in LnIr_2 show that it is approximately proportional to $(g_j - 1)J$ as predicted by the Kasuya, Yosida model of conduction electron polarization.

The variation is shown in figure (1.11), from which it can be seen that the results extrapolate to a hyperfine field strength of -170kOe at $(g_j - 1)J = 0$. This can be interpreted in terms of other contributions to the total field, which are nearly independent of the ionic moment, or to the variation of the exchange constant Γ describing the exchange interaction. Atzmony et al. (ref. 1.90) attempted to fit the experimental data by allowing for a change in Γ using the relation for the paramagnetic Curie temperature (chapter two, equation 2.3). Eliminating Γ from the Curie equation and using the expression

$$P(r) = \frac{9\pi Z}{E_F} \Gamma (g_j - 1) \sum (F(2K_f |R_i - R_j|) J_Z$$

for the conduction electron polarization leads to the relation:

$$P(r) = \text{constant} \left[\theta_J / (J - 1) \right]^{1/2}$$

This was considered to represent the data more satisfactorily than did the simpler relation indicating a proportionality to $(g_j - 1)$, and assuming a constant Γ .

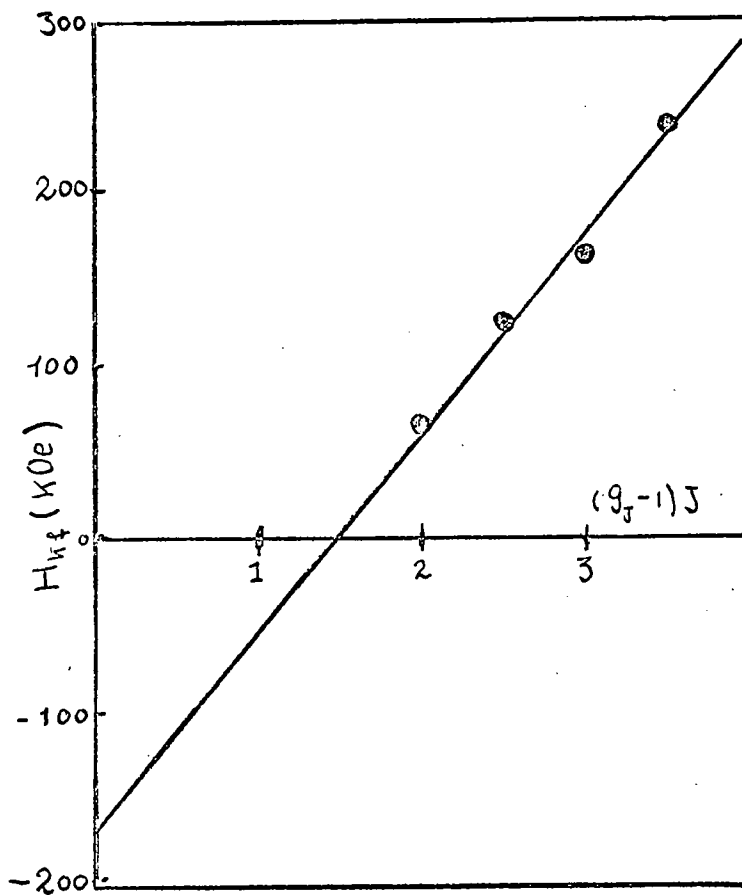


FIG. 7.11 The hyperfine field as a function of $(g_J - 1)J$ in the Alr_2 compounds.

CHAPTER 2

A REVIEW OF THE MAGNETIC PROPERTIES IN RARE EARTH
INTERMETALLIC COMPOUNDS

This chapter is divided into three sections, the first deals briefly with a simple theory which will then be applied to the interpretation of the magnetic properties of the rare earth- Aluminium compounds in the second section, and to the rare earth - 3d compounds in the third section.

2.1 Brief Theory:-

In rare earth metals and intermetallic compounds, the indirect exchange interaction between rare earth spins via the conduction electrons is believed to be an important mechanism for providing the necessary coupling required for magnetic ordering (see chapter 1). This may be written

$$H_{ex} = -\sqrt{s} \cdot S \quad 2.1$$

where s is the conduction - electron spin and S is the localized 4f. - electron spin.

As we have seen, under the assumption of a spherical Fermi surface, the RKKY interaction generates a conduction - electron spin polarization which falls off and oscillates with the distance R from the polarizing rare - earth ion. This polarization is proportional to,

$$F(x) = (x \cos x - \sin x) / x^4 \quad 2.2$$
$$x = 2 K_f R_{nm}$$

where K_f is the wave vector of the conduction electrons at the

Fermi surface. The conduction electron polarization produces a long-range indirect coupling between the spins of the rare earth ions. In terms of the molecular field theory, de Gennes (ref. 2.1) and Rocher (ref. 2.2) have shown that for compounds of the same crystal structure and having the same number of free electrons per magnetic ion, the paramagnetic Curie temperatures vary as $(g_j - 1)^2 J(J + 1)$. The paramagnetic Curie temperature is, according to de Gennes:

$$\theta_p = \frac{-3 \pi Z^2 \Gamma}{4kE_F} (g_j - 1)^2 J(J + 1) \sum_{n \neq m} F(2K_f R_{nm}) \quad 2.3$$

where Z is the number of conduction electrons per atom, E_F is the Fermi energy, R_{nm} is the distance between the rare - earth ions and k is Boltzmann's constant.

Another effect of the conduction electron polarization is to produce an excess Knight shift because the polarization of the electron cloud is seen by the nucleus. The Knight shift $K(T)$ consists of a sum of two terms, the non - $4f$ (K_0) and $4f$ ($K_f(T)$) contributions.

$$K(T) = K_0 + K_f(T) \quad 2.4$$

K_0 is the Knight shift associated with only the conduction - electron bands, which arises from the Fermi contact hyperfine interaction with S - like conduction electrons (eqn. 1.29). The term $K_f(T)$, due to the presence of the $4f$ electrons, arises from an interaction of the form $AI \cdot \langle S \rangle$ where A is a hyperfine interaction constant, I is the nuclear spin and $\langle S \rangle$ is the time-averaged value of the rare earth $4f$ spin component of the angular momentum $\langle J \rangle$. Since J is a good quantum number, S must be projected on to J , giving

$$AI \cdot S = \frac{AI \cdot J \langle S \cdot J \rangle}{J(J+1)}$$

and in terms of the Lande factor g_j we have (ref.2.4)

$$A I \cdot S = (g_j - 1) AI \cdot J$$

The most general expression for $K(T)$

is given by:-

$$K(T) = K_0 + (g_j - 1) H_{hf} \chi_f(T) / N g_j \mu_B \quad 2.6$$

where H_{hf} ($=A/\gamma h$) is the hyperfine field per unit spin, S

γ is the nuclear gyromagnetic ratio, N is Avogadro's number,

μ_B is the Bohr magneton, and $\chi_f(T)$ is the f electron susceptibility per rare earth ion. In terms of the uniform conduction electron spin polarization (refs. 2.5 and 2.6), the resulting Knight shift is given by,

$$K(T) = K_0 \left(1 + \frac{J_{sf}(g_j - 1) \chi_f(T)}{2g_j \mu_B^2} \right) \quad 2.7$$

Since K_0 is, to a good approximation, independent of temperature whereas χ obeys a Curie Weiss law, measurements of $K(T)$ together with $\chi_f(T)$ permit an estimate of J_{sf} from a plot of $K(T)$ versus $\chi_f(T)$ with T as an implicit parameter. The linearity of $K(T)$ versus $\chi_f(T)$ behaviour is well verified experimentally (ref.2.3, 2.6). For a model in which the conduction electron polarization is non-uniform we may write

$$J_{sf} = 6\pi\Gamma Z \sum_n F(2K_f R_{nm}) \quad 2.8$$

where R_{nm} represents the distance between a rare - earth ion and a non-magnetic ion at the origin.

A similar shift occurs in the electronic g value due to the conduction electron polarization which was shown by Yosida (ref. 2.7) to be given by

$$\frac{\Delta g}{g} = 3n J_{sf}/2 n_f g_j E_F = \frac{3}{4} \frac{Z J_{sf}}{g_j E_F} \quad 2.9$$

The existence of the exchange interaction equation 2.1 leads to a spin-dependent, electron - scattering mechanism which results in a spin - disorder contribution to the total resistivity. The form of this contribution has been examined by several authors (refs. 2.1, 2.2, 2.8) and it is generally accepted that the spin disorder resistivity (ρ_s) in the paramagnetic region of the conduction electrons is given by:-

$$\rho_s = (3 \pi N M^2 / 8 \hbar e^2 E_F) \Gamma^2 (g_j - 1)^2 J(J + 1) \quad 2.10$$

Finally, the exchange interaction between the localized rare earth spin S and the conduction electron spin s (eqn. 2.1) leads to a conduction electron polarization which interacts with the nuclear spin via the Fermi contact term, giving a hyperfine field contribution (refs. 2.1, 2.7),

$$H_{hf} = \frac{9 \pi Z^2 A(0)}{4 E_F g_N \mu_N} \langle s \rangle \Gamma \sum F(2K_f R_{nm}) \quad 2.11$$

and for ^{27}Al in intermetallic compounds this equation becomes (refs. 2.9, 2.10)

$$H_{hf} = (\text{Const}) \frac{A^{27}(0)}{E_f} \Gamma (g_j - 1) \langle J \rangle \quad 2.12$$

2.2 (Rare Earth) Al_2 Compounds

Magnetic properties of the AAl_2 (A = rare earth) inter-

metallic compounds have been studied extensively during the last fifteen years. These investigations have included nuclear magnetic resonance (NMR), Knight shift and Electron spin resonance (ESR) studies (refs. 2.5, 2.6 and from 2.11 - 2.15), studies of magnetic transition temperature (refs. 2.16 - 2.20), susceptibility (refs. 2.11, 2.22), and resistivity (refs. 2.1, 2.7, 2.3). This work has been conducted in an attempt to illuminate various aspects of the interactions between the presumably localized rare earth spins and the electronic conduction band. Magnetization (refs. 2.16 - 2.18) and neutron - diffraction (refs. 2.19, 2.20) measurements verified that most of the compounds order ferromagnetically below a transition temperature T_C . Several groups (refs. 2.10, 2.24 - 2.26) have studied the ^{27}Al hyperfine interactions in ferromagnetic the phase of GdAl_2 . Kaplan (ref. 2.9) describes an extension of the ^{27}Al hyperfine field study to the ferromagnetic phase of compounds with non - S - state ions, ranging from PrAl_2 up to HoAl_2 , with the exception of EuAl_2 .

This thesis describes the hyperfine field of the ^{27}Al in GdAl_2 , $\text{Gd}_{1-x}\text{Y}_x\text{Al}_2$ and $\text{Gd}_{1-x}\text{La}_x\text{Al}_2$ ($x = 0.1, 0.2, 0.3, 0.4$) by using NMR spin echo, and the e.s.r. g - shift in $\text{Gd}_{1-x}\text{Y}_x\text{Al}_2$.

The AAl_2 compounds all possess the cubic laves phase (C15) structure (chapter one). These compounds have been shown to be ferromagnetic by Williams et al (ref. 2.16), with the exception of those of La, Lu, Yb which do not order in YbAl_2 (the Yb is divalent and hence its 4f - shell is full). They found from susceptibility measurements that the Curie temperature has a maximum value 176°K for GdAl_2 , and that the variation of the Curie temperature across the series is proportional to the de Gennes function $G = (g_J - 1)^2 J(J + 1)$ (cf. eqn. 2.3) for

the compounds with heavy rare earth elements (fig. 2.1). The ordering temperatures of the compounds with the light elements do not fit so well into this general pattern. CeAl_2 has been shown to be antiferromagnetic with a Neel temperature (T_N) below 4°K (ref. 2.27). The recent measurement of Niculescu et al (ref. 2.22) for CeAl_x indicate that in CeAl_2 $\theta_p = -7\text{ K}$ and the molecular moment = $2.64\mu_B$. Mader and Wallace (ref. 2.28) deduce from susceptibility measurements that Eu in EuAl_2 is divalent and found $T_N = 15\text{ K}$ and $\theta_p = 0\text{ K}$.

Stalinski and Pokrzywnicki (ref. 2.29) studied the susceptibility of GdAl_2 above liquid nitrogen temperatures and reported a moment of $7.88\mu_B$, $\theta_p = 171.5\text{ K}$, and $T_C = 171\text{ K}$. Hacker et al (ref. 2.30) found that $T_C = 167.8\text{ K}$ from plots of σ^2 vs T . The magnetic studies of Buschow et al (ref. 2.21) yielded values of θ_p , T_C and μ_{eff} , all of which are higher than those of Stalinski and Hacker. The measurements of Deenadas et al (ref. 2.31) indicate that an unusually broad magnetic contribution to the heat capacity exists in GdAl_2 . Their data shows a peak at 153 K with essential completion of the magnetic transition at 170 K . On the basis of resistivity and thermoelectric power measurements, Mydosh et al (refs. 2.32, 2.33) reported $T_C = 151\text{ K}$, which was in agreement with that inferred from the Knight shift by Jones and Budnick (ref. 2.12). Van Daal and Buschow (ref. 2.23) also studied the resistivity of GdAl_2 and reported $T_C = 173\text{ K}$.

The magnetization results of these compounds suggest that the values of the molecular magnetic moment are generally less than those corresponding to the free trivalent ions the reduction normally being attributed to crystal field effects.

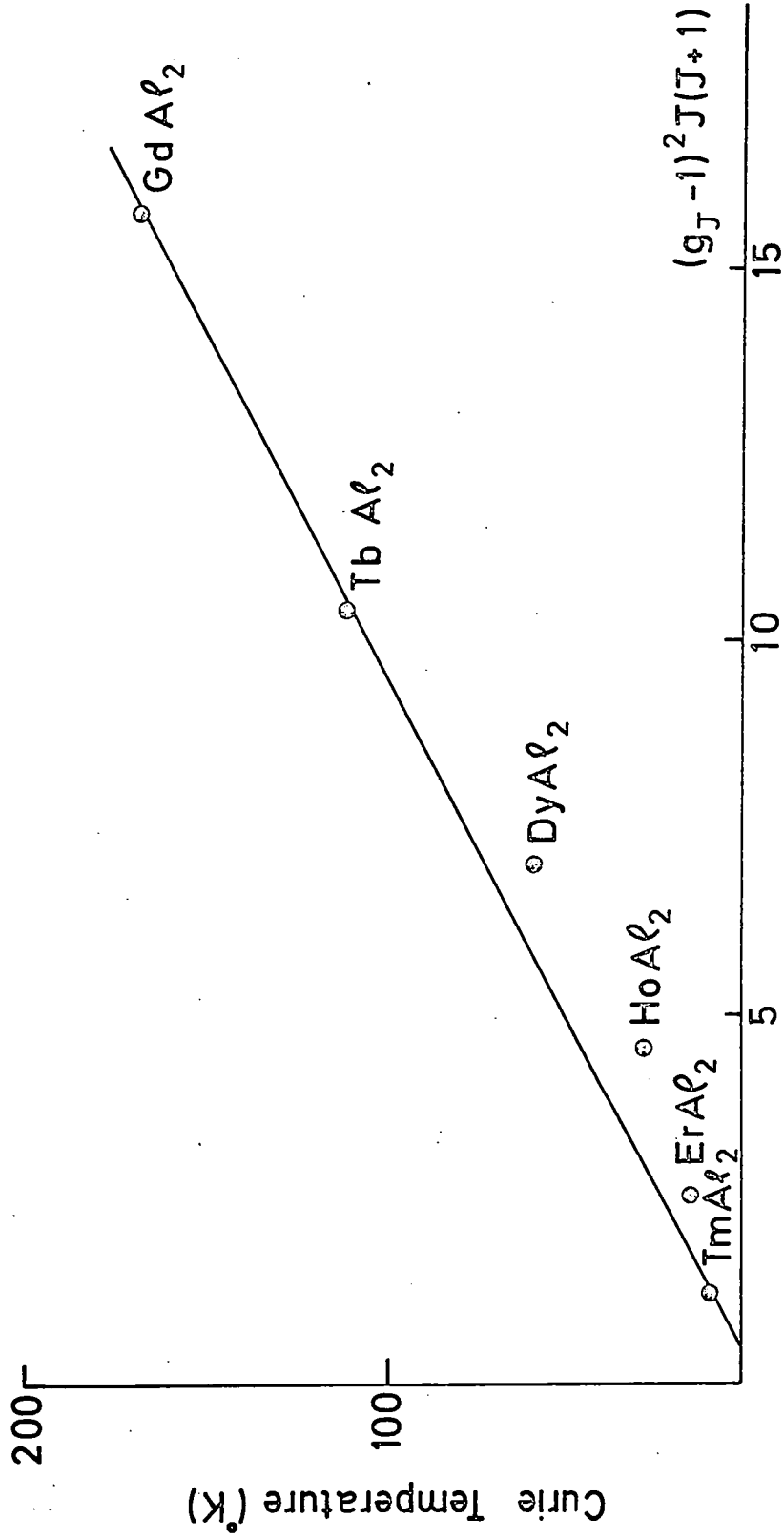


FIG. 2.1 The Curie Temperature of the RAl₂ as a function of de Gennes function.

Nereson, Olsen and Arnold (refs. 2.19, 2.20) studied the Dy, Nd, and Pr compounds by neutron diffraction and confirmed the ferromagnetic behaviour at low temperatures. In DyAl_2 they observed extra peaks at temperatures below 24 K and suggested that the compound showed weak helical antiferromagnetism in addition to ferromagnetism. The ordered moment of $9.1\mu_B$, indicated by this work, is within 10% of the free ion value and it is concluded that crystal field effects play little part in determining the dysprosium moment in DyAl_2 .

Magnetostatic measurement on pseudobinary compounds of formula $\text{AA}'\text{Al}_2$ show that the moments of the lanthanide ions A and A' are anti-parallel when A is a heavy rare - earth and A' is a light rare - earth (ref. 2.16). These alignments have confirmed that the rare - earth ions interact via a ferromagnetic spin coupling since the observed magnetization for compounds such as $(\text{Gd}, \text{Nd})\text{Al}_2$ corresponds to a ferromagnetic coupling of the two types of moment. This follows directly since the ionic moment is proportional to the total angular momentum J and this in turn is given by $J = L - S$ and $J = L + S$ for the light and heavy elements respectively. Pseudobinary work on the compounds GdAl_2 , TbAl_2 and ErAl_2 with the rare earth partially substituted by Y, La have been used to identify the exchange coupling with RKKY theory (ref. 2.21). Fig.(2.2) shows the variation of the Curie temperature in the series $(\text{Gd} - \text{Y})\text{Al}_2$, $(\text{Gd}, \text{La})\text{Al}_2$. The Curie temperature shows a linear decrease to zero with increasing Y or La content as may be expected on the basis of simple dilution effects in eqn. (2.3).

In an evaluation of the rare - earth conduction-electron exchange interaction, Jaccarino et al (refs. 2.5, 2.6) seems

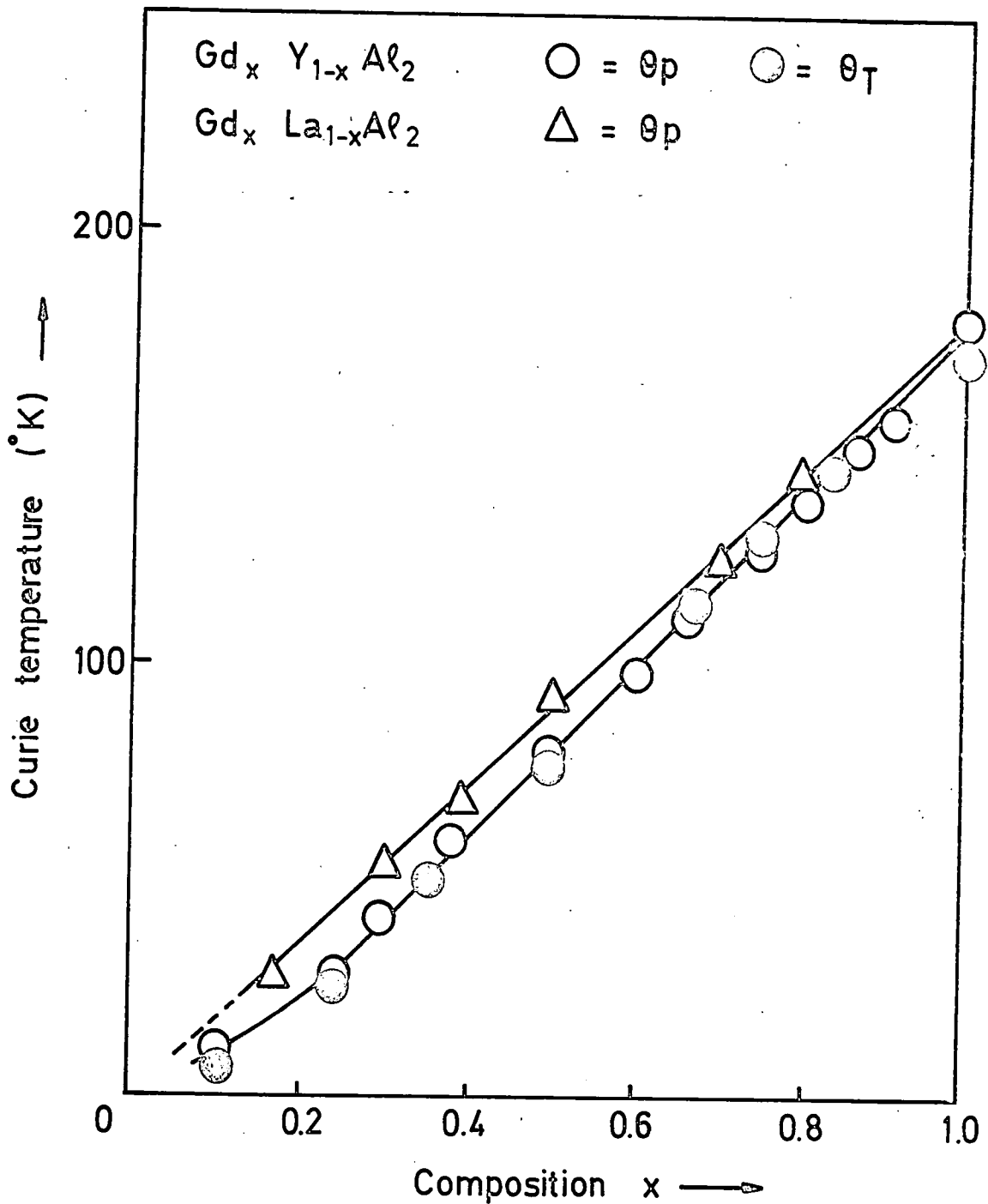


Fig.(2.2) Curie Temperatures for the Y, La substituted $Gd Al_2$ compounds.

to be the pioneer in this field. He was able to determine the sign and magnitude of the conduction electron polarization arising from the exchange interaction between localized f electrons and the conduction electrons (s - f interaction), by using the Knight shift of the ^{27}Al nucleus at the Al site and using the g - shift in ESR at the rare earth site. These results of ESR and NMR experiments have shown that the s - f interaction is negative, and that the amplitude of the spin polarization at the aluminium site is also negative. Several workers confirm this negative interaction using Knight shift measurements. The values of Δg for all the dialuminides have been collected by Jones (ref.2.3) and are given in table (2.1). The fractional change in g value provides direct evidence for the sign and magnitude of J_{sf} . In contrast to the observations of most workers using pure compounds, Coles et al (ref. 2.34) have recently reported positive Δg values, and hence positive J_{sf} in gadolinium - doped LaAl_2 (see chapter three for more detail).

Other evidence for the relative magnitude of J_{sf} arises from the results of spin disorder resistivity, eqn. 2.10, and the reduction of the superconducting transition temperature in LaAl_2 by addition of the magnetic rare earth elements. Since the exchange constant appears as the square in both methods, no indication of the sign of the conduction electron polarization is found. Van Daal and Buschow (refs. 2.23) have measured the electrical resistivity of all the AAAl_2 compounds. Using the values of ρ_s obtained from this investigation, along with the known Curie temperatures, the value of m^* and Γ were obtained and found to be in close agreement with those of other workers. Similarly the depression of the superconducting transition

	CeAl ₂	PrAl ₂	NdAl ₂	SmAl ₂	GdAl ₂	TbAl ₂	DyAl ₂	HoAl ₂	ErAl ₂	TmAl ₂	YbAl ₂
J _{sf} ^a	0.63	0.48	- 0.38		- 0.31	- 0.28	- 0.25	- 0.38	- 0.30	- 0.29	
b		1.688	1.337	1.353	1.0	0.885	0.747	0.512			

a - from Knight Shift

b - from N.M.R. Spin Echo

Table 2.1 The exchange constants J_{sf} and (✓) for rare earth Al₂ compounds.

temperature by the addition of rare - earth impurities (ref. 2.35) indicates a variation of the exchange constant across the series which is consistent with that obtained using the other techniques.

Finally Kaplan et al (ref. 2.9) have recently calculated for most of the series (Table 2.1) from the conventional relation between the hyperfine field and Γ , eqn. 2.12.

Although the magnetic results have shown that an RKKY type of interaction is responsible for the observed properties, it should be pointed out that a negative value for J_{sf} (and hence Γ), the exchange integral, is incompatible with simple RKKY theory since this integral is, by nature, positive, (see chapter one). This problem has received attention in the theoretical calculations by Watson et al. (ref. 2.36) who considered the considerable mixing between the conduction - electron states near the Fermi surface and the 4f states below and above the Fermi level. The result of this interband mixing is a raising and lowering in energy for the conduction electrons having their spin parallel and anti-parallel to the localized moment spin, respectively. In this way, a negative conduction electron polarization is produced which gives rise to an s. s interaction opposite in sign to the exchange integral. The relative strength of both contributions determines the magnitude and sign of the effective exchange interaction. Watson et al. carried out numerical calculations of Γ as a function of the Fermi wave vector K_f . They found that for large K_f the contributions from interband mixing dominate over the exchange integral. In the present case of the rare earth dialuminides, the indication is that the interband mixing contribution is dominant (ref. 2.37).

In addition to the determination of J_{sf} , the ^{27}Al Knight

shift observations may be used in conjunction with the paramagnetic susceptibility data to derive the strength of the ^{27}Al hyperfine field below the Curie temperature. Jones and Budnick (ref. 2.12) obtained a value for the ^{27}Al hyperfine field at 4.2 K of - 46 kOe, by using the measured values of $K(T)$, K_0 and $\chi(T)$, for ^{27}Al in (GdAl_2) . Budnick et al (ref. 2.38) have reported the observation of the ^{27}Al resonance in (GdAl_2) at 49.2 MHz and 4.2 K by using a spin echo system. These results agreed very well with the recent results reported by Dintelmann et al (refs. 2.24, 2.26) and Shamir et al (ref. 2.25) both of whom observed two ^{27}Al resonances at 4.2 K, with frequencies of 49.5 and 60.6 MHz respectively. The appearance of two lines was interpreted in terms of two inequivalent sites for the Al ions in (GdAl_2) , with the Gd spin aligned along the (111) direction. This approach was first introduced to account for the Mossbauer effect observations in ZrFe_2 and TmFe_2 (ref. 2.39), the difference in hyperfine field strength arising because of the spatial distribution of B atoms in the AB_2 cubic laves phase compounds.

Kaplan et al (ref. 2.9) studied the ^{27}Al hyperfine field in AAl_2 (A = Ho, Dy, Tb, Gd, Sm, Nd, Pr). They found that these fields are proportional with $(g_j - 1) J$. They were able to determine the easy direction for each compound according to the number of lines in the spectrum and the intensity ratio of these lines. The intensity ratio is predicted from a consideration of the number of atoms occupying the equivalent sites. The derived values being (fig. 2.3), (111) easy, two sites with three atoms in one and one in the other, intensity ratio 3 : 1. (110) easy, two pairs of inequivalent sites and consequently

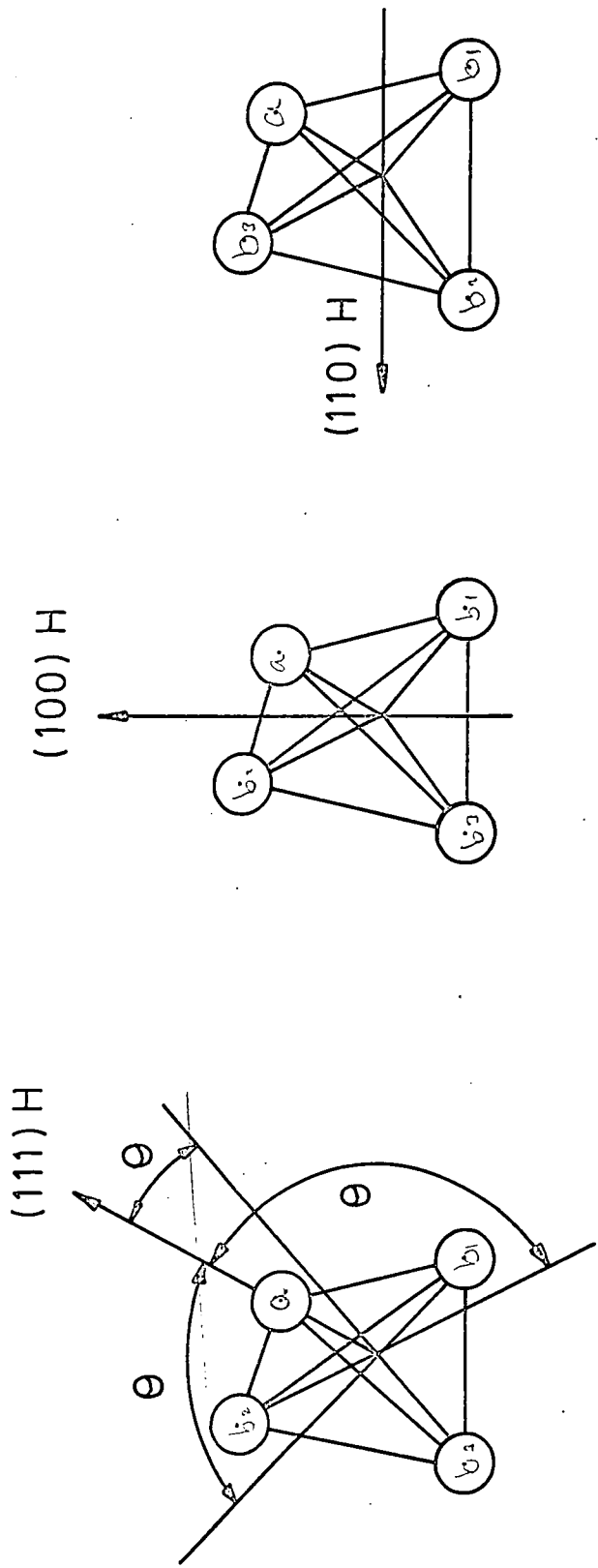


FIG. 2.3 The Orientation of Al atoms about $[1\bar{1}1]$, $[100]$, $[110]$, axial directions.

the spectral intensity ratio 1 : 1.

(100) easy, all sites are equivalent and only one resonance line is found.

Table (2.2) shows the easy directions for AA_2 .

Similar effects have been observed in Mossbauer effect measurements by Nevitt et al (ref. 2.40) and Bowden et al (ref. 2.41) on AFe_2 compounds.

2.3 Rare Earth - 3d transition metals AB_2 S:-

In the preceding part (Section 2.2) we have discussed the magnetic properties of AA_2 . In this section we shall consider the magnetic properties of the ANi_2 , ACo_2 and AFe_2 compounds.

The study of the magnetic behaviour of these compounds has been a subject of great interest from both a theoretical and a practical point of view. Magnetic studies of ANi_2 compounds (refs. 2.42, 2.43) show that in the paramagnetic state the susceptibility exhibits a Curie - Weiss behaviour for all the materials except $CeNi_2$, $LuNi_2$ and $SmNi_2$. The first two of these three compounds are Pauli paramagnets, the cerium in $CeNi_2$ being quadrivalent, having lost its 4f electron to the conduction band. The non-linear variation of the inverse susceptibility with temperature for $SmNi_2$ is similar to that observed in other samarium compounds and is probably due to electron excitation into the first excited $J = 7/2$ multiplet of the ion. YNi_2 and $LuNi_2$ present a temperature-independent paramagnetism, for which the 4f shell is either empty or full. This behaviour suggests that there is no magnetic moment associated with the nickel ions in these compounds. The saturation magnetic moment

Table 2.2 Hyperfine field of $AA\text{Al}_2$ Compounds.

Compounds	Easy Direction	H_{kf} at 4.2 K (a) site MHz	H_{kf} at 4.2 K (b) site MHz
PrAl_2	(100)	20.4	-
NdAl_2	(100)	24.7	-
SmAl_2	(111)	35.1	36.4
GdAl_2	(111)	61.15	49.5
TbAl_2	(111)	53.00	34.10
DyAl_2	(100)	29.8	-
HoAl_2	(111), (110)	25.5	12.8

of GdNi_2 further supports the idea of zero nickel moment since the measured molecular moment is very close to the Gd free ion value ($g_j J = 7$). Neutron diffraction studies (ref. 2.44 on TbNi_2 have been unable to detect any nickel moment so that it is generally assumed that the nickel is in the non-magnetic $3d^{10}$ state by electron transfer from the conduction band. Assuming that the nickel moment of the rest of the ANi_2 's is also zero, both Bleaney (ref. 2.45) and Wallace and Skrabek (ref. 2.46) have attributed the difference between the observed moments and the free ion $g_j J$ value to the crystal-field quenching of the orbital contribution to the total moment. This assumes that the easy axis of magnetization is the (111) axis.

The variation of the Curie temperatures T_C obey approximately a "de Gennes" relation. Normalizing this relation to the Curie temperature (GdNi_2 , a good agreement is observed for the $(g_j - 1)^2 J(J + 1)$ variation in the case of the heavy rare - earth compounds whereas fig. (2.4), for the light ones this approaches an $S(S + 1)$ dependence. The T_C values obtained recently by Burzo (ref. 2.43) are different from those previously reported (ref. 2.42) and give a better fit to the de Gennes function.

From g - shift measurements EPR, Burzo was able to determine the sign and the magnitude of the effective exchange parameter J_{sf} . He found that $J_{sf} = 0.022$ eV. The negative exchange parameter shows that the mean density of the conduction electron polarization is antiparallel to the local moment direction. The negative sign of J_{sf} probably appears as a result of interband mixing as discussed previously (section 2.2, chapter two). The values of J_{sf} observed from the paramagnetic Curie temperature

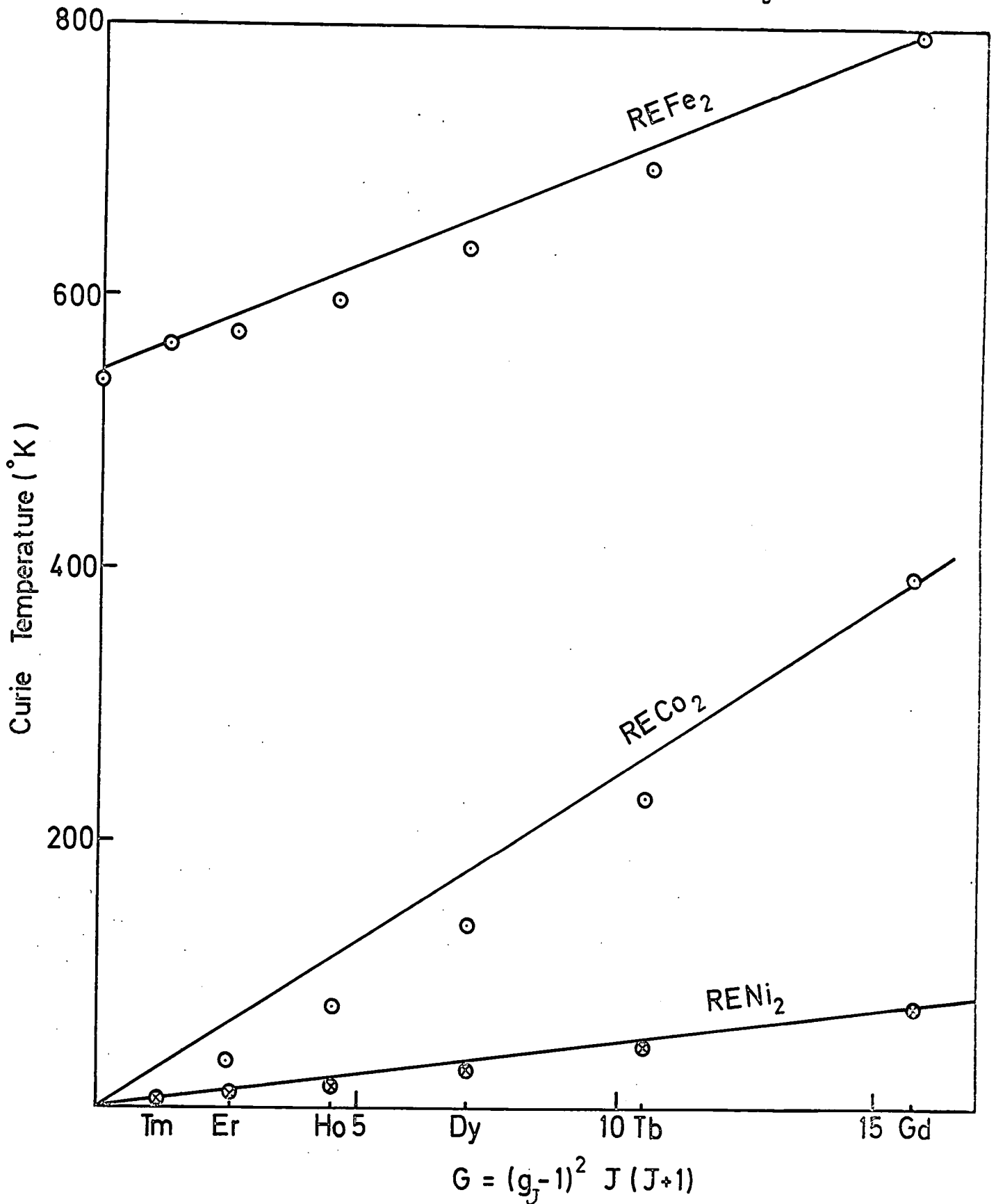
gives $J_{sf} = \pm 0.34$ eV, which is an order of magnitude greater than determined from Δg_s . This could be justified by taking into account the simplification used in the R.K.K.Y. model.

The magnetic properties of ACo_2 and AFe_2 have been studied by various authors (refs. 2.42, 2.46, 2.47, 2.48, 2.49, 2.50, 2.51, 2.52, 2.53, 2.54). The saturation magnetic moments of the cobalt and iron compounds with Gadolinium have values of $5.09 \mu_B$ (ref. 2.55) and $3.35 \mu_B$ respectively. Since Gadolinium is an S state ion, its moment is little influenced by the crystalline field, and by accepting the magnetic moment of the Gd ion as $7 \mu_B$, the magnetization data suggest that the transition metal moments must be antiparallel to the Gd (heavy rare earths) moments and have magnitudes of $1.0 \mu_B$ for cobalt and $1.8 \mu_B$ for iron. The compounds PrCo_2 , NdCo_2 and SmCo_2 appear to be ferromagnetic, however, with parallel moment alignment. The resultant structures arise immediately from the fact that the net J in the light rare earths is given by $J = L - S$, whereas in the heavy rare earths $J = L + S$. From neutron diffraction studies on HoFe_2 . The magnetic moment of Fe has been determined to be $1.7 \mu_B$ (ref. 2.56). Burzo (ref. 2.57) found that the magnetic moment of Fe in AFe_2 (A = Gd, Yb, Dy, Ho, Er, Tm) compounds is $(1.6 \sim 1.7) \mu_B$ and $1.44 \mu_B$ in YFe_2 . The Curie temperatures of the cobalt compounds follow approximately a "de Gennes" relation being proportional to $(g_J - 1)^2 J(J + 1)$ for heavy rare earth, whereas, for the light ones, these again approach an $S(S + 1)$ relation. The main contribution to the magnetic ordering seems to be the R.K.K.Y. interaction. The presence of the magnetic cobalt ions results in higher values of T_c than those of rare earth metals through the additional Co - RE

exchange. The Curie temperatures of the iron compounds have the same behaviour. Fig. (2.4) shows the variation of the Curie temperature with de Gennes function for ANi_2 , ACo_2 , AFe_2 , where A is the heavy rare earth. This graph shows that for the iron compounds in the limiting case of $G = 0$ (YFe_2 and LuFe_2) there is a positive intercept on the temperature axis, while for both YNi_2 and YCo_2 the Curie temperatures are zero. Since the transition metal moment is not zero in YFe_2 , the intercept must be representative of the transition metal exchange interaction in these compounds. The experimental value of 550 K indicates that these interactions are greater than those between the rare - earth ions. When both types of ion carry a moment, then the Curie temperature will be further affected by A - B interaction. The YCo_2 has zero as the intercept and indeed the prevailing evidence is that YCo_2 is non-magnetic.

Pseudobinary study on the systems $(\text{Dy}, \text{Y})\text{Fe}_2$ and $\text{Gd}(\text{Co}, \text{Ni})_2$ (refs. 2.60, 2.61) indicate a non-linear variation of the transition metal moment with composition. The observed behaviour was explained on a model in which the 3d electrons form a band giving rise to an itinerant electron moment. Piercy and Taylor (ref. 2.62) carried out a series of experiments on the system $\text{Y}(\text{Fe}_{1-x}\text{Co}_x)_2$. The magnetization results, shown in fig.(2.5), can be interpreted in terms of the gradual filling of the 3d band as cobalt is added to the system. The sudden collapse at a composition of about 20% iron may be attributed to the disappearance of the splitting of the 3d sub-bands in association with the increased 3d - electron concentration and the inter-transition metal exchange interaction. Slanicka (ref. 2.63) observed a rapid decrease in the total moment of the heavy rare

FIG. 2.4 The dependence of the Curie temperature of REFe_2 , RECo_2 and RENi_2 compounds on $(g_J - 1)^2 J(J + 1)$



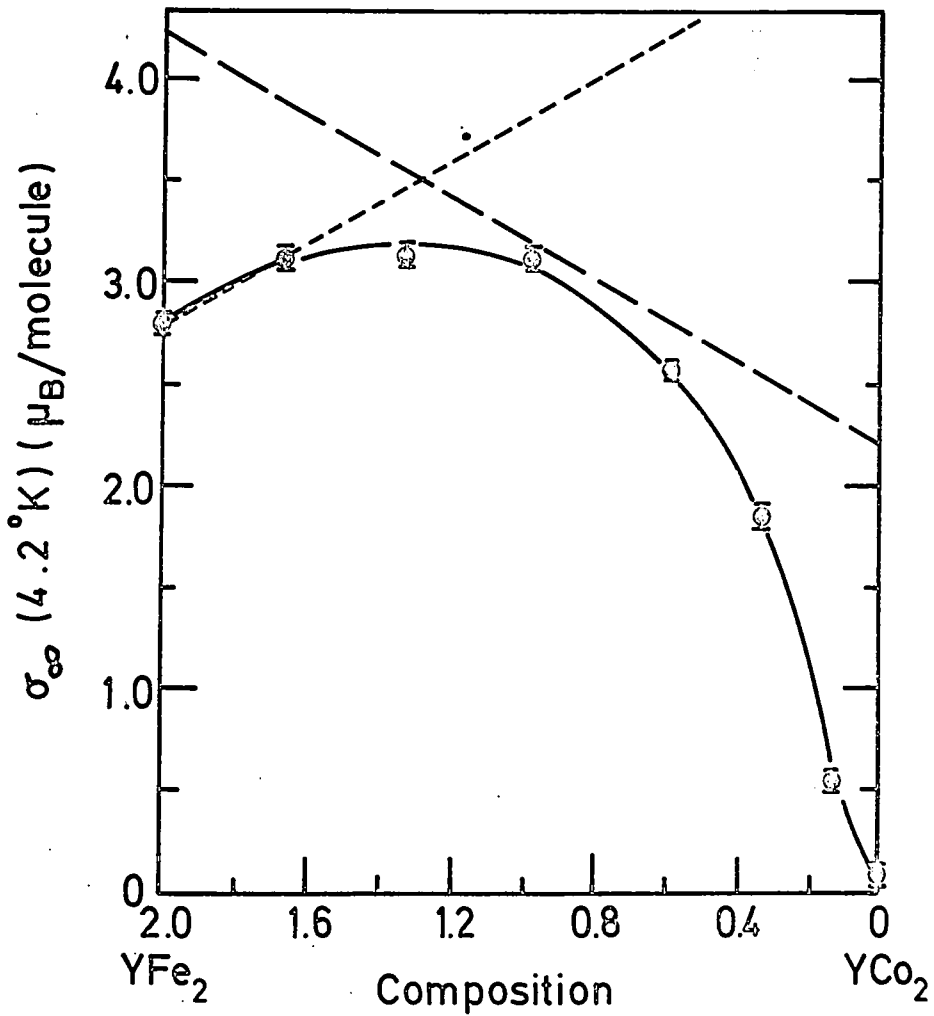


FIG. 2.5 The change in the transition metal moment in the Y(Fe,Co) series of pseudobinaries, with increasing 3d electron concentration.

earth pseudobinary compounds formed with iron, cobalt and nickel, in the vicinity of the pure ACo_2 composition. This occurred for decreasing 3d electron concentration and was accompanied by a sudden rise in the Curie temperature (see fig. 2.6). The observed changes were interpreted in terms of the development of a 3d moment associated with the detailed band structure of the compound, and with the exchange field at the rare earth ions in the lattice.

The absence of a nickel moment in these compounds and the reduced moment values associated with the cobalt and iron atoms were originally attributed (refs. 2.46, 2.58, 2.59) to electron transfer from the rare - earth ions, resulting in the filling of localized 3d states.

Mossbauer investigations on the AFe_2 compounds have been carried out by several authors. From the work of Wertheim et al (ref. 2.64) and Wallace (ref. 2.46) it can be seen that, to a good approximation, the hyperfine fields at the ^{57}Fe nuclei are independent of their lanthanide partners. It appears therefore that the iron electron configuration is substantially the same in all the AFe_2 compounds.

The hyperfine field observations have allowed the magnetic easy direction of the AFe_2 compounds to be determined (Sec.2.2). Wertheim et al (ref. 2.39) made a special study of the iron site in the two TmFe_2 and ZrFe_2 compounds. From the presence of two superimposed ^{57}Fe hyperfine spectra at the iron site, they were able to deduce that the magnetization of the iron sub-lattice pointed along (111) direction. Observations by Nevitt et al (ref. 2.40) and Bowden et al (ref. 2.65, 2.66) showed that both (111) and (100) direction could be observed as the easy axis in

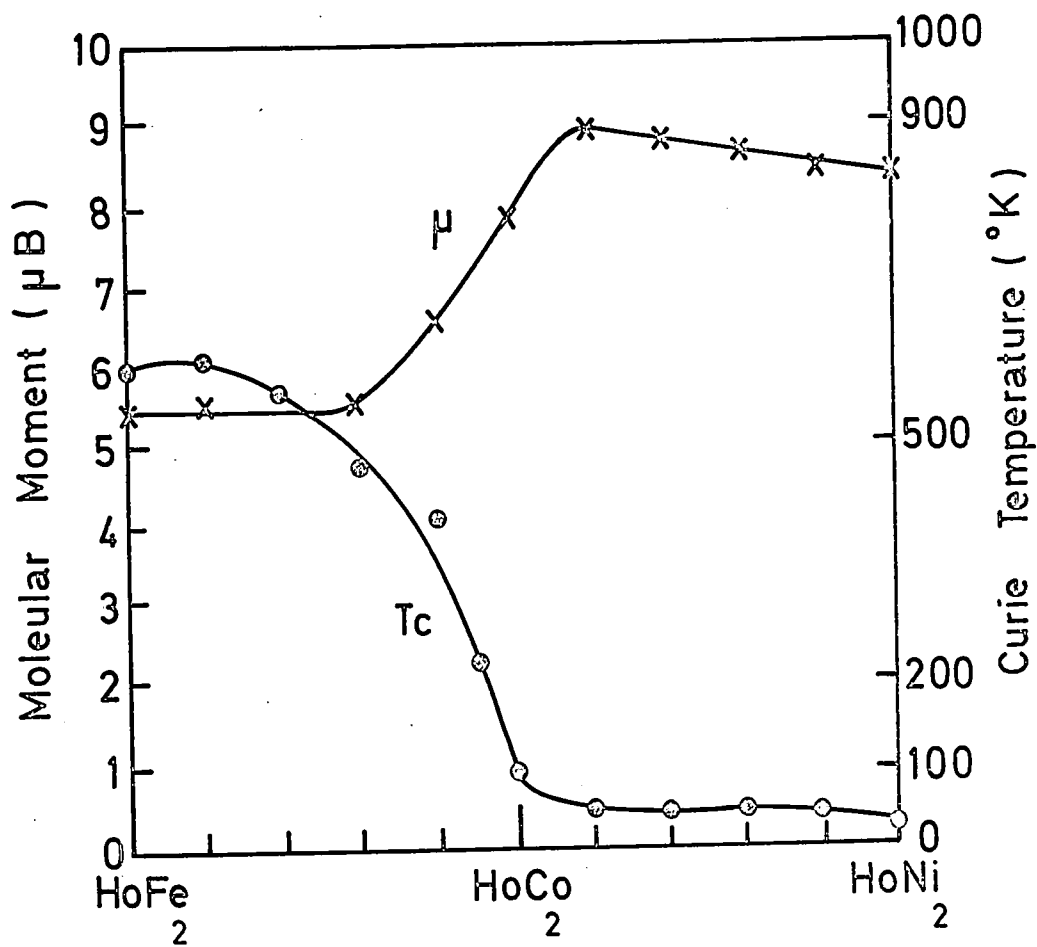


FIG. 2.6 The composition dependence of the molecular moment and Curie temperature of the holmium in the $\text{Ho}(\text{Fe},\text{Co})_2$ $\text{Ho}(\text{Co},\text{Ni})_2$

Table 2.3 Hyperfine field parameters of AFe₂ compounds

Compounds	Theoretical easy direction	Experiment easy dir- ection	H _{hf} at 78°K k(Oe)	Second Site kOe
CeFe ₂	(111)	(001)	156	-
SmFe ₂	(111)	(1.01)	216	190
GdFe	(111)	Complex	238	224
TbFe ₂	(111)	(111)	226	197
DyFe	(001)	(001)	224	-
HoFe ₂	(001)	(001)	221	-
ErFe ₂	(111)	(111)	228	204
TmFe ₂	(111)	(111)	216	209
ErFe ₂	(111)	(101)	207	203
YFe	(111)	(111)	221	211

the AFe_2 series and Bowden (ref. 2.41) used a simple crystal field approach to show that these easy directions were primarily controlled by crystal field effects. The agreement between this simple theory and experiment are listed in table (2.3). The hyperfine field values at the ^{57}Fe nucleus, obtained from these measurements are also listed.

The decomposition of the total hyperfine field at the ^{57}Fe nucleus is a difficult task, although it has been shown that the field direction is antiparallel to that of the magnetization (refs. 2.67, 2.68 and 2.69) as it is in metallic iron (ref. 2.70). The variation of the total field with $(g_j - 1) J$ departs appreciably from linearity and it is not possible to give any reasonable estimate of the contribution arising from the rare earth sublattice. From spin echo observations of ^{59}Co in $GdCo_2$ and on pseudobinary compounds based on $GdCo_2$, Taylor and Christopher (ref. 2.71) have proposed a detailed balancing of the various contributions to the net hyperfine field. This has been done on the assumption that the field due to the cobalt ions can be taken as proportional to the cobalt moment in the compounds under investigation, the absolute value being scaled from the known ^{59}Co field in pure cobalt for which the ionic moment is also known. On this basis the contribution to the field from the rare earth ions is assumed to arise from conduction electron polarization. The ^{59}Co hyperfine field was found to be 60 kOe for $GdCo_2$. In the present work the spin echo observation in the ACo_2 compounds show that the hyperfine field at the ^{59}Co nucleus is almost independent of the rare earth partner, the field being approximately 61 kOe for all compounds measured. Recently Mossbauer measurements have been done of ^{57}Fe hyperfine

interaction in $Y(Fe_{1-x}Co_x)_2$ and $Ho(Fe_{1-x}Co_x)_2$ systems by Guimaraes and Bunbury (ref. 2.72). They found that the ^{57}Fe hyperfine field in these compounds changes with concentration x and has a maximum value at $x = 0.4$ as shown in the fig. (2.7). In the $Ho(Fe_{1-x}Co_x)_2$ compounds the magnetization remained parallel to an (001) direction at every concentration examined ($x = 0, 0.2, 0.4, 0.6, 0.8$) since the holmium anisotropy dominates that associated with the transition metal. The direction of magnetization of the $Y(Fe_{1-x}Co_x)_2$ series, however, changed with the addition of cobalt: YFe_2 magnetizes along a (111) direction but the other solid solutions with $x \geq 0.17$ all magnetize along a (101). This conclusion was reached from the intensities of resonance lines.

E.P.R. measurements have been carried out by Burzo (ref. 2.51). He found that the g - values changed with temperature, the g - values being smaller than those of the Gd^{3+} ion indicating in this case a negative conduction electron polarization, (see chapter three), for $GdCo_2$.

From the above discussion it is evident that the interactions within the Fe and Co compounds are more complex than for those of the Ni (and Al) compounds, since the transition metal has a moment. The possible interactions are:

- a) the rare earth - rare earth interaction
- b) the transition metal - transition metal interaction
- c) the rare - earth - transition metal interaction

The first interaction is due to the localized character of the 4f moments; it is an indirect interaction proceeding via the conduction electron spin polarization. This polarization

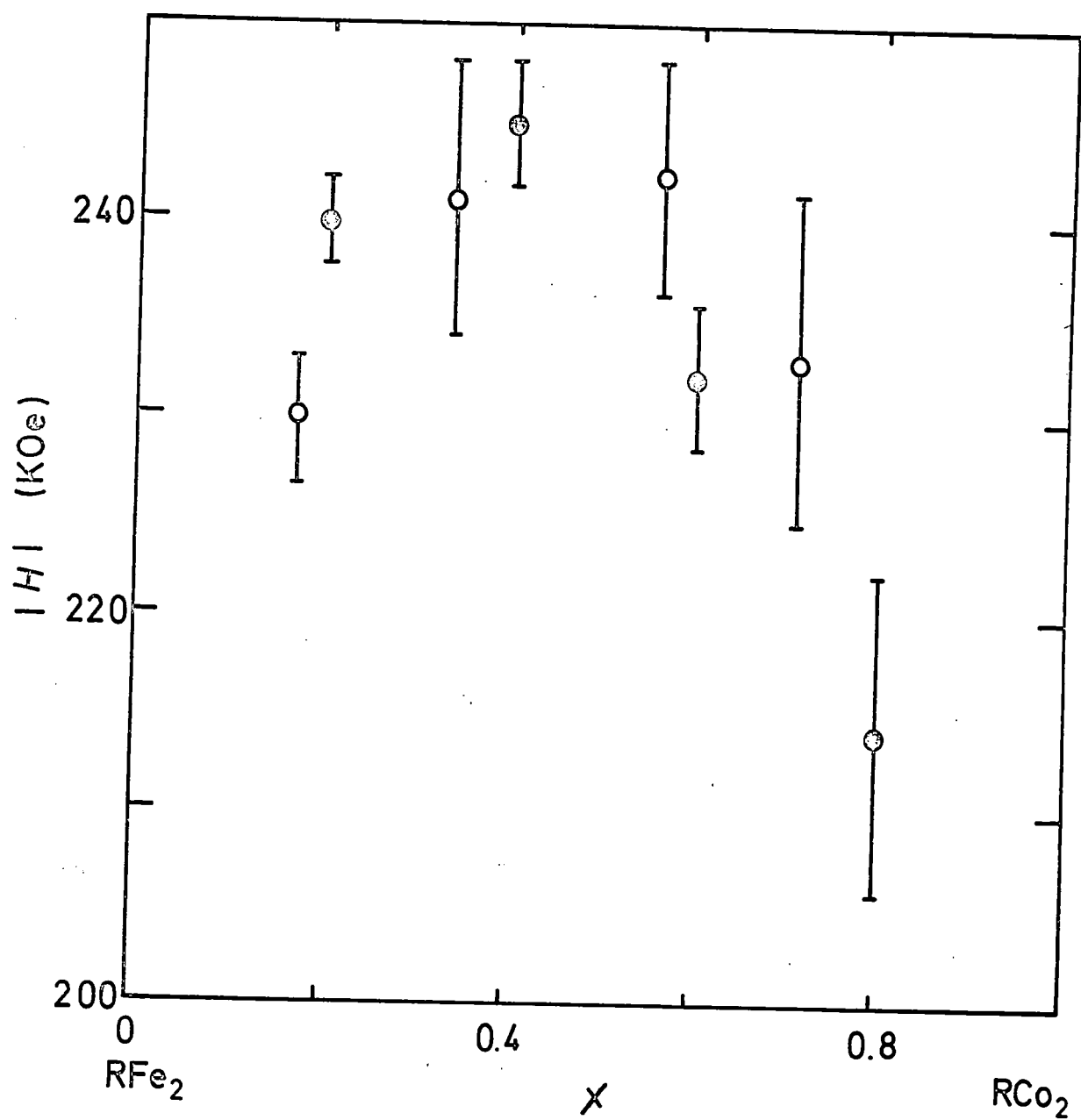


FIG. 2.7 Variation of the iron hyperfine fields in $Y(Fe_{1-x}Co_x)_2$, \circ , and $Ho(Fe_{1-x}Co_x)_2$, \odot , with cobalt concentration ($T=78K$)

is not uniform and can lead to ferromagnetic as well as anti-ferromagnetic coupling between the 4f moments. This case applies very well to the AA_2 and AN_2 compounds.

The second interaction can be studied in compounds in which the rare earth component is non-magnetic, ie. for compounds in which A at AB_2 represents La, Lu or Y. Finally, the order of magnitude of the rare earth - transition interaction appears to be between the first and the second interactions. It is thought to proceed indirectly via the conduction electrons (ref. 2.54).

CHAPTER 3

N.M.R. SPIN ECHO AND THE BASIC THEORY OF E.S.R.

The nuclear magnetic resonance of magnetic impurities in metals is similar in many aspects to electron spin resonance. In this chapter we shall first introduce the magnetic resonance phenomenon in a general way which is common to both N.M.R. and E.S.R. In section 3.2 we discuss the N.M.R. Spin Echo and some of its applications. In section 3.4 the basic theory of E.S.R. is discussed.

3.1 Magnetic Resonance Phenomenon

Magnetic resonance is a phenomenon found in magnetic systems that possess both magnetic moments and angular momentum. A system such as a nucleus may consist of many particles coupled together so that in any given state, the nucleus possesses a total magnetic moment μ and a total angular momentum I , and the two are related by the equation.

$$\mu = \gamma \hbar I \quad (3.1)$$

where γ is the gyromagnetic ratio, which is of order (e/mc) for electrons and (e/Mc) for nuclei.

When such a moment is subjected to a magnetic field H , the Hamiltonian which describes the Zeeman interaction between μ and the magnetic field H is

$$\mathcal{H} = -\gamma \hbar I \cdot H \quad (3.2)$$

H will produce a torque on the magnetic moment μ given by $\mu \wedge H$ and the equation of motion is found by equating the torque

with the rate of change of angular momentum I. That is:

$$dI/dt = \frac{1}{\hbar} (\mu \wedge H) \quad (3.3)$$

which may be combined with equation 3.2 to give

$$d\mu/dt = \gamma \mu \wedge H \quad (3.4)$$

The motion of the vectors I and μ consists of a uniform precession about H with angular velocity $\omega_L = -\gamma H$ (assuming H lies along the Z axis of a system of cartesian coordinates).

If M is the vector sum of the μ 'S, then by summing equation (3.4) vectorially over μ we obtain the following relation for the macroscopic magnetization:

$$dM/dt = \gamma M \wedge H \quad (3.5)$$

In this treatment it is very helpful to refer the motion to a coordinate system that rotates about H in the same direction as that in which the magnetic moment precesses. This coordinate system is often called the rotating frame, a technique that has proved of great assistance in the description of magnetic resonance (ref. 3.1).

The equation of the motion of the magnetization M in the rotating coordinate system (x' , y' , z') is related to eqn. 3.4, in the laboratory system (x, y, z), by the equation:

$$(dM/dt)_{\text{fixed}} = (dM/dt)_{\text{rot}} + \omega \wedge M \quad (3.6)$$

where ω is the frequency of rotation vector which is directed along the $z = z'$ axis.

From equation 3.5 and equation 3.6

$$\begin{aligned} (dM/dt)_{\text{rot}} &= \gamma M \wedge H - \omega \wedge M \\ &= \gamma M \wedge H + \gamma M \wedge \omega / \gamma \\ &= \gamma M \wedge (H + \omega / \gamma) \end{aligned} \quad (3.7)$$

This has the same form as eqn. 3.5 provided the magnetic field H is replaced by an effective field $H^* = H + \omega / \gamma$. Thus the motion relative to the rotating system will again be a precession with angular velocity:

$$= -\gamma (H + \omega / \gamma) = \omega_L - \omega \quad (3.8)$$

This result enables us to derive simply the motion of the magnetization M under the combined action of a steady field H , along the z axis of the cartesian coordinate system, and a field H_1 , rotating about the z -axis with frequency ω , where $H_1 = |H_1| (i \cos \omega t_\omega + j \sin \omega t_\omega)$, and i and j are unit vectors along the x and y axis respectively as shown in fig.(3.1).

Under this condition the couple acting on the magnetization M is now:

$$\begin{aligned} (dM/dt)_{\text{rot}} &= \gamma M \wedge [(H + \omega / \gamma) k + H_1 i] \\ &= \gamma M \wedge H_{\text{eff}} \end{aligned} \quad (3.9)$$

The magnitude of the effective field H_{eff} is:

$$H_{\text{eff}} = \left[(H + \omega / \gamma)^2 + H_1^2 \right]^{1/2} \quad (3.10)$$

The angle α is found to be (fig.(3.1))

$$\cos \alpha = \cos^2 \theta + \sin^2 \theta \cos(\gamma |H_{\text{eff}}| t_\omega) \quad (3.11)$$

When the frequency of rotation of H_1 is not equal to the natural precession frequency ω_L , the magnetization M precesses about the field H_{eff} which makes an angle θ with H where

$$\tan \theta = H_1 / (H + \omega / \gamma). \quad (3.12)$$

If the resonance condition is fulfilled exactly ($\omega = \omega_L$), the effective field is then simply $i H_1$. The macroscopic moment M that was assumed to be initially parallel to the static field

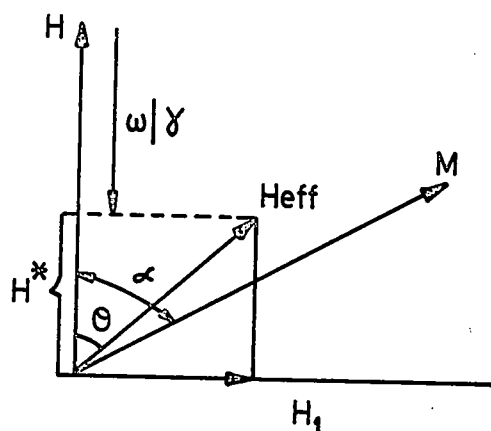


FIG. 3.1 Effective field in the rotating frame.

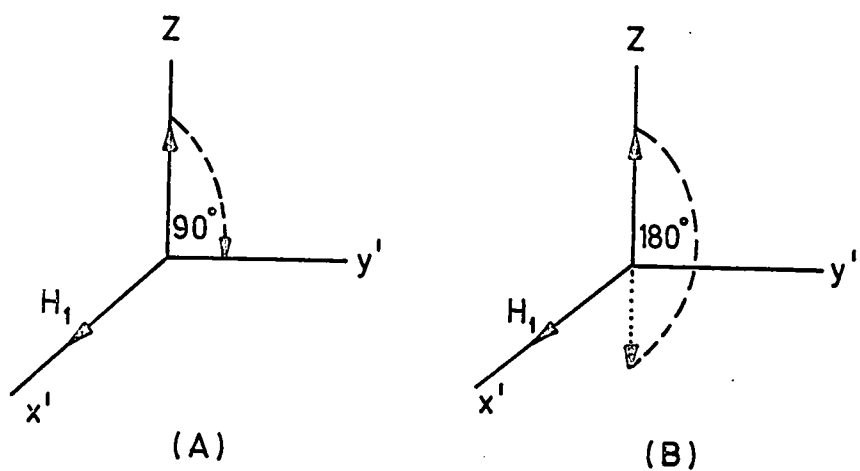


FIG. 3.2 Precession of M about H_1 in the rotating frame by 90° (A) or 180° (B).

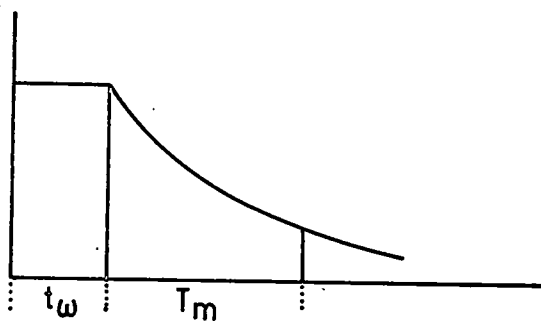


FIG. 3.3 The application of a single pulse of width t_w and F.I.D. with the time T_m

H will then precess in the y-x plane. In this condition the angle θ in equation (3.12) equals 90° , and hence the equation (3.11) becomes:

$$\cos \alpha = \cos (\gamma H_1 t \omega)$$

where $\alpha = \gamma H_1 t \omega$ (3.13)

The result of this treatment is discussed extensively by Abragam and Bleaney (ref. 3.2), Abragam (ref. 3.3) and Slichter (ref. 3.4).

3.1.1 Pulse Methods

An alternative way of obtaining magnetic resonance data is to apply a short pulse of radio frequency (RF) power to the sample and observing the reaction of the sample, to examine the behaviour of the nuclear spin system as a function of time.

Suppose the macroscopic magnetization, M , is at equilibrium in a magnetic field H , directed entirely along the z-axis, with no component in the x-y plane. Then by applying the R.F. field H_1 along the x-axis in the rotating frame, when the RF and Larmor frequencies coincide, a resonance interaction occurs, and the macroscopic magnetization is tipped through an angle α , where defined in equation (3.13).

By choosing the strength of the R.F. field and the time t for which it is applied, the magnetization M will tip either into the x-y plane (a 90° pulse) fig. 3.2a, or into the negative z-axis (a 180° pulse) fig. 3.2b

3.1.2 Free Induction Decay (FID)

In FID the decay of precessing nuclear moments is observed immediately after the application of a short pulse of RF (90° pulse).

FID has the form indicated in fig. 3.3. Bloch (section 3.2) showed that M_{xy} (the component of M in the x-y plane) decays by a first order process with a characteristic time T_2 , known as the spin-spin, or transverse, relaxation time. Thus, provided there are no effects of magnetic field in-homogeneity, the FID signal decays exponentially with a decay time T_2 . However, since the magnetic field is never perfectly homogeneous, nuclei in different parts of the sample experience slightly different values of the applied field and hence resonate at slightly different frequencies. In practical, then, a FID signal usually decays in a time T_m , where

$$\frac{1}{T_m} = \frac{1}{T_2} + \frac{1}{T_2^*} \quad (3.14)$$

where T_2^* is the contribution from magnetic field in-homogeneities. In other words, M_x and M_y decay with time as $\exp(-t/T_m)$.

3.2 The Bloch Equations

Bloch (refs. 3.5, 3.6) showed that the motion of the macroscopic magnetization in the presence of an applied magnetic field could be explained in terms of phenomenological differential equations. When the sample is placed in a static magnetic field, M aligns itself along the field over a time equal to the spin-lattice relaxation time T_1 . The mechanisms responsible for T_1 are processes by which a perturbed nuclear spin system in a higher energy state can transfer its energy to the surroundings (the lattice) and thus return to the equilibrium (ref. 3.7) condition. If a radio frequency (RF) field H_1 is applied at right angles to the static field H , then the magnetization will

tend to follow the rapid variations in the direction of H_1 . A natural resonant frequency $\omega_L = \gamma H$ exists wherein the magnetization will absorb energy from the oscillating field. The halfwidth ΔH_1 of this resonant absorption is inversely proportional to the spin-spin relaxation time T_2 of the sample. This relaxation time T_2 is a measure of the time that it takes to establish equilibrium between the magnetic moment components perpendicular to the applied magnetic field H .

In a static magnetic field $H = H_0$, the trend of the magnetization towards its equilibrium value $M = M_0 = \chi_0 H_0$ can be described by the equation:

$$dM/dt = (M_0 - M_z)/T_1$$

From $H = 0$ at $t = 0$ to $H = H_0$ at $t = \tau$, M will increase in accordance with the exponential relation

$$M_z = M_0 (1 - e^{-\tau/T_1})$$

If the relaxation mechanisms are added to eqn. (3.4), then its three components constitute the following equations,

$$dM_x/dt = \gamma (M \wedge H)_x - M_x/T_2 \quad (3.15a)$$

$$dM_y/dt = \gamma (M \wedge H)_y - M_y/T_2 \quad (3.15b)$$

$$dM_z/dt = \gamma (M \wedge H)_z - (M_z - M_0)/T_1 \quad (3.15c)$$

In the rotating frame, restricting H_1 to the x' direction, eqn. (3.9) and the eqns. (3.15) assume the simplified form:

$$dM_{x'}/dt = \gamma M_{y'} H_1 - M_{x'}/T_2 \quad (3.16a)$$

$$dM_{y'}/dt = \gamma (M_{z'} H_1 - M_{x'} H) - M_{y'}/T_2 \quad (3.16b)$$

$$dM_{z'}/dt = -\gamma (M_{y'} H_1) - (M_{z'} - M_0)/T_1 \quad (3.16c)$$

The set of equations (3.15) and (3.16) are called the Bloch equations.

These equations give a quantitative description of the behaviour of the macroscopic spin system and its relaxation behaviour.

In this thesis, the solution of these equations will be used in section 3.4.

3.3 N.M.R. Spin Echo

In 1950, Hahn (ref. 3.8) invented a pulse technique called spin echo, based upon a sequence of pulses. Hahn used two successive 90° pulses separated by a time interval τ and observed an echo pulse at a time equal to 2τ . The echo appears as a consequence of the constructive interference of the magnetization vectors under the influence of the second pulse. An oscilloscope trace of an echo pattern is shown in fig. 3.4.

The principles of the spin echo are illustrated in fig. 3.5. The magnetization vectors are initially in the direction z of the static magnetic field as shown in fig. 3.5a. The spin echo experiment is begun by applying a 90° radio frequency (RF) pulse which means that equation (3.13) becomes $\gamma H_1 t = \omega = \pi/2$. This pulse causes the magnetization vectors to rotate through 90° about H_1 until they are aligned along the y -axis as shown in figs. 3.5b. The pulse is turned off at $t = t_\omega$ and the magnetization vectors of nuclei in different parts of the sample begin to fan out or lose phase coherence, because of magnetic field inhomogeneity (fig. 3.5.c). Eqn. (3.9) contains the effective field $H^* = H + \omega/\gamma$ in the z -direction in the

Fig. 3.4b Stimulated echoes

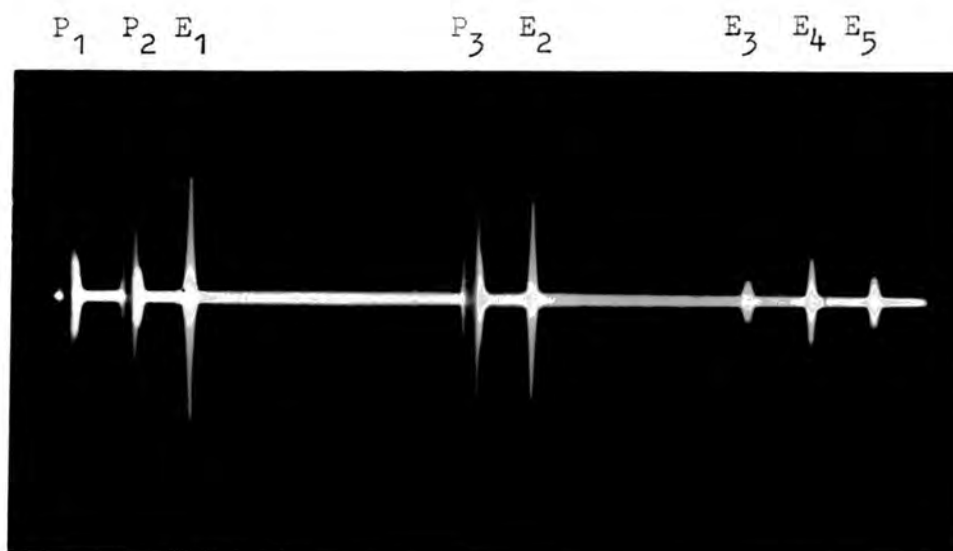
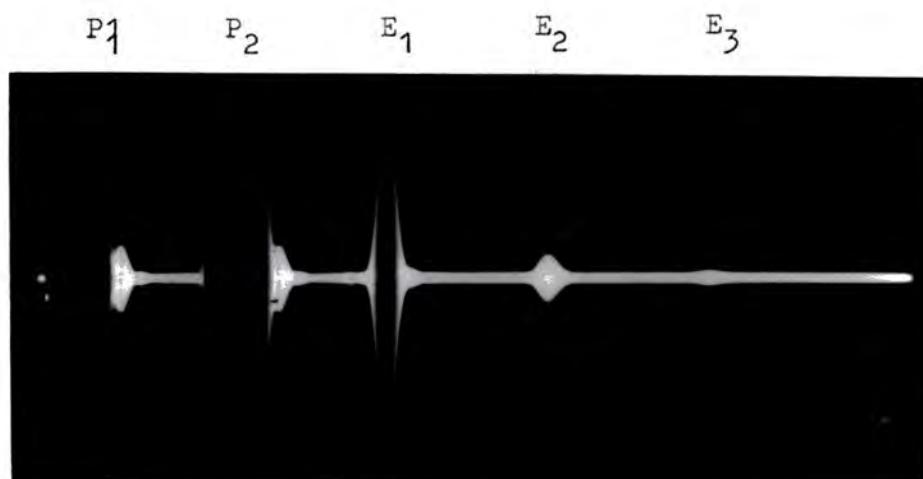


Fig. 3.4a Primary echoes



rotating frame. This vanishes for $\omega = \omega_L = \gamma H$, and is positive or negative depending upon whether or not ω is less or greater than $\omega_L = \gamma H$. At a time τ after the beginning of the first pulse a second pulse is applied, identical with the first. This causes all the magnetization vectors to flip through 90° about H_1 (fig. 3.5d). The precession illustrated in fig. 3.5e shows that all magnetization vectors interfere destructively with one another and distribute themselves isotropically until the time $\approx 2\tau$ when they interfere constructively to produce the echo signal as shown in fig. 3.5f.

In 1954, Carr and Purcell (ref. 3.9) demonstrated the existence of spin echo by using a pulse programme consisting of a 90° pulse followed by successive 180° pulses. This pulse sequence produces echoes at $2\tau, 4\tau, \dots, 2n\tau$. Meiboom and Gill (1958) (ref. 3.10) modified the Carr and Purcell method by applying successive coherent pulses and shifting the phase of the 90° pulse by 90° relative to the phase of 180° pulse. These modifications eliminated the adjustment of the 180° pulses.

Many different pulse sequence techniques have been developed since 1950. These techniques have been used to study paramagnetic impurity effects, magnetic alloys, hyperfine fields, nuclear quadrupole resonance, T_1 and T_2 . A brief review of the application of pulse NMR can be found in the literature distributed by manufacturers of pulse equipment (ref. 3.11) and in the book by Farral and Becker (ref. 3.12).

In this work we have used the spin echo phenomenon to study mainly the hyperfine field and the relaxation times T_2 and T_1 .

3.3.1 Primary Spin Echo

The above discussion of the spin echo model has been derived mathematically by Hahn (ref. 3.8) and by Das and Saha (ref. 3.13), Jaynes (ref. 3.14) and Bloom (ref. 3.15) and by Abragam (ref. 3.3). The primary echo is produced as illustrated in fig. 3.5.

By using the basic Bloch equations and their solution (section 3.2), together with eqn. (3.9), and using the normalized Gaussian distribution to represent the distribution in $\Delta\omega$ among the spins (the homogeneity of the magnetic field causes distribution in the Larmor frequency ω_L and hence in $\Delta\omega = \omega_L - \omega_1$ among the groups), Das and Saha obtained the total echo amplitude in the following equation:

$$\begin{aligned}
 V(E) = & \sin\omega_1 t_\omega \sin^2\omega_1 t_\omega / 2 \exp \left[\frac{t}{T_2} - \frac{(t - 2\tau)^2}{2 T_2^2} \right] \\
 & \times \exp \left[- \frac{k}{3} \{ (t - \tau)^3 + \tau^3 + 3\tau(t - \tau)^2 \} \right] \\
 & - \sin\omega_1 t_\omega \cos^2\omega_1 t_\omega / 2 \exp \left[- \frac{t}{T_2} - \frac{t^2}{2 T_2^{*2}} \right] \\
 & + \exp \left[- \frac{k}{3} \{ (t - \tau)^3 + \tau^3 + 3\tau(t - \tau)^2 \} \right] \\
 & - W(C) \sin\omega_1 t_\omega \left[- \frac{t - \tau}{T_2} - \frac{(t - \tau)^2}{2 T_2^{*2}} \right] \\
 & \times \exp \left[- \frac{k}{3} \{ (t - \tau)^3 + 3(t - \tau)^2 \} \right] \quad (3.17)
 \end{aligned}$$

where $k = (\gamma G)^2 D$, G is the field gradient constant, D is the self-diffusion coefficient of the nuclei and T_2^2 is the net transverse relaxation time and may be given by the equation

$$T_2^{*2} = (2 \ln 2)^{\frac{1}{2}} / (\Delta\omega)_1^{\frac{1}{2}}$$

The first and third terms of equation (3.17) give, respectively, the primary echo at $t = 2\tau$, and the free induction signal following the second pulse. The middle term is a continuation of the free-induction signal following the first pulse. By substituting $t = 2\tau$ in equation and rewriting the first term, we get:

$$V(E) = V(E)_0 \exp \left(- \frac{2\tau}{T_2} - \frac{5}{3} k\tau^3 \right)$$

If $\frac{5}{3} k\tau^3 \ll 2\tau/T_2$ (ref. 3.8) then the equation becomes

$$V(E) = V(E)_0 \exp \left(- \frac{2\tau}{T_2} \right) \quad (3.18)$$

This equation implies that the echo amplitude decays exponentially with time T_2 , the spin-spin relaxation time, can be measured directly by plotting the logarithm of the echo amplitude versus arbitrary values of 2τ (τ is the pulse spacing).

Mackenzie has found experimentally that the decay of the echo amplitude fits the equation (3.18) (within experimental error (ref. 3.16)). However in some pulsed N.M.R. and E.S.R. experiments, the spin echo amplitude was observed to have an oscillatory behaviour as a function of τ (refs. 3.17 - 3.21). This modulation has been reported to be due to the effect of the nuclear-quadrupole-interaction in which a magnetically induced electric field gradient (EFG) was observed at the nuclear site of magnetic ions in solids. For an axially symmetric EFG, the explicit expression given in (ref. 3.17) for the echo amplitude, for nuclei with $I = 5/2$, is

$$V(E) = e^{-2\tau/T_2} \sum_{n=0}^4 c_n \cos(2n\tau + \phi_n) \quad (3.19)$$

where a is the frequency of the superimposed echo oscillation and is given by

$$a = \left[\frac{3e^2 Qq}{4I} (2I - 1) \right] (3\cos^2 \theta - 1) \quad (3.20)$$

C_n and δ_n are constants depending on the initial conditions and the shape and width of the r-f pulses and θ is the angle between the axis and the local magnetic field. Recently it has been found that the higher harmonic terms in eqn. (3.19) (ref. 3.21) can be neglected and the equation may be written as

$$V(E) = e^{-2t/T_2} [C_0 + C_1 \cos(2a\tau + \delta_1)] \quad (3.21)$$

This equation verifies that the echo decay is modulated at a frequency proportional to the quadrupole interaction eQq .

Recently, the oscillation was observed in $GdAl_2$, $HoAl_2$, and $NdAl_2$ (ref. 3.20). In the present work we have observed this oscillation clearly in $GdAl_2$ (see chapter 5).

In some pulsed N.M.R. experiments on ferromagnetic material, multiple spin echoes were observed (refs. 3.17, 3.22) at 2τ , 3τ , 4τ , ... The observation of these multiple echoes was explained as follows; the first echo, which appears at a time 2τ after the first pulse, acts as a refocusing pulse for the second r-f pulse and produces the second echo at 3τ and so on: fig. (3.4a). This photograph was taken for the ^{59}Co resonance in $GdCo_2$.

In addition to the measurement of T_2 , the primary echo has been used to study the hyperfine field in magnetic materials by several authors (see chapters one and two). The line shape can be obtained by plotting the amplitude of the observed echo as a function of frequency. The centre of the peak represents the hyperfine field multiplied by the gyromagnetic ratio of the

nucleus under investigation.

3.3.2 Stimulated Echoes

Stimulated, or secondary, echoes are produced by a third pulse, applied at a time T with respect to $t = 0$. Under these conditions another echo will be obtained at $(T + \tau)$ and also at $(2T - 2\tau)$, $(2T - \tau)$ and $2T$. A typical pulse and echo pattern is shown in fig. (3.4b). The principal characteristic of all these echoes is that the time intervals between the echoes and the incident pulses, and between the echoes themselves, always correspond to the original intervals among the incident pulses, or combinations of these. In the figure, the stimulated echo is produced by the combination of the three pulses (P_1, P_2, P_3). From the primary echo and the three pulses, the other echoes are produced as follows:

1. The third echo is produced by the first echo and the third pulse,
2. The fourth echo is produced by the second and the third pulses,
3. The fifth echo is produced by the first and the third pulses.

Hahn, and Das and Saha, discussed the existence of these echoes mathematically; we will consider here only the equation for the stimulated echo, which may be written as

$$V(SE) = \frac{1}{2} \sin^3 \omega t \omega \exp \left[- (T - \tau) \left(\frac{1}{T_1} - \frac{1}{T_2} \right) - \frac{t}{T_2} \right] \\ \times \exp \left[\frac{(t - (T + \tau))^2}{2T_2} \right] \exp \left(- \frac{1}{3} k \{ (t - T)^3 \right. \\ \left. + \tau^3 + 3T(t - \tau)^2 + 3(T - \tau)(t - T)^2 \} \right).$$

For $t = T + \tau$ this equation becomes

$$V(SE) = V_0(SE) \exp\left(\frac{\tau - T}{T_1} - \frac{2\tau}{T_2}\right) \exp\left(-\frac{1}{3}k(3\tau^2 T_2 + 2\tau^3)\right)$$

If the condition $k\tau^2 T_2 \ll T/T_1$ is satisfied and $\tau \ll T$ this equation becomes:

$$V(SE) = V_0(SE) \exp\left(-\frac{T}{T_1}\right) \quad (3.22)$$

In this case T_1 can be measured by plotting the logarithm of stimulated echo amplitude versus arbitrary values of T .

3.4 The basic theory of E.S.R.

3.4.1 Dispersion and Absorption Line Shape

When a paramagnetic sample in a resonance cavity is subjected to the resonance condition $\hbar\omega = g\beta H$, the spins interact with the r.f. field $2H_1 \cos \omega t$ and the magnetization can be written

$$M_x = 2H_1 (\chi' \cos \omega t + \chi'' \sin \omega t) \quad (3.23)$$

Where χ' and χ'' are the so-called real and imaginary parts of r.f. susceptibility $\chi = \chi' - i\chi''$, defined by the relations

$$H_x = 2H_1 \text{RE}(e^{i\omega t}), \quad M_x = 2H_1 \text{RE}(\chi e^{i\omega t})$$

The solution of the Bloch equations (section 3.2) is

$$M_x' = \frac{\chi_0 \omega_0 T_2 H_1 (\omega - \omega_0) T_2}{1 + (\omega - \omega_0)^2 T_2^2 + \tau^2 H_1^2 T_1 T_2} \quad (3.24a)$$

$$M_y' = \frac{\chi_0 \omega_0 T_2 H_1}{1 + (\omega - \omega_0)^2 T_2^2 + \tau^2 H_1^2 T_1 T_2} \quad (3.24b)$$

The magnetization M_x which may be assumed to be along direction (x) in the laboratory frame is

$$M_x = M_x' \cos \omega t + M_y' \sin \omega t \quad (3.25)$$

and hence from the comparison of equations (3.23), (3.24),

(3.25), we can get:

$$\chi' = \frac{1}{2} \chi_0 \omega_0 T_2 \frac{(\omega - \omega_0) T_2}{1 + (\omega - \omega_0)^2 T_2^2 + \gamma^2 H_1^2 T_1 T_2} \quad (3.27a)$$

$$\chi'' = \frac{1}{2} \chi_0 \omega_0 T_2 \frac{1}{1 + (\omega - \omega_0)^2 T_2^2 + \gamma^2 H_1^2 T_1 T_2} \quad (3.27b)$$

χ' is the dispersion mode and χ'' is the absorption mode.

The signal that appears on the recorder may be either dispersion, absorption, or a mixture of the two. The mixture of χ' and χ'' in the signal was discussed by Peter, Shaltiel, Wernick, Williams, Mock, and Sherwood (1962) (ref. 3.23) and is similar to the situation involved in this work.

By using the transformation

$$\omega = \gamma H, \omega_0 = \gamma H_0, T_2 = 2/\gamma \Delta H_1/2$$

and by assuming $\gamma^2 H_1^2 T_1 T_2 \ll 1$, the equations (3.25) may be transformed to the form that is used when magnetic field scanning is employed ie.

$$\chi' = \left[\frac{\chi_0 H_0}{\Delta H_1/2} \right] \frac{x}{1 + x^2} \quad (3.28a)$$

$$\chi'' = \left[\frac{\chi_0 H_0}{\Delta H_1/2} \right] \frac{1}{1 + x^2} \quad (3.28b)$$

where $x = (H - H_0) / (1/2 \Delta H_{1/2})$

The first derivatives have the explicit analytical values

$$\frac{d\chi'}{dH} = \frac{(2\chi_0 H_0)}{(\Delta H_{1/2})^2} \frac{1 - x^2}{(1 + x^2)^2} \quad (3.29a)$$

$$\frac{d\chi''}{dH} = \frac{(4\chi_0 H_0)}{(\Delta H_{1/2})^2} \frac{x}{(1 + x^2)^2} \quad (3.29b)$$

The lineshapes of equations (3.28, (3.29) are shown in fig. 3.6 and 3.7.

The experimentally observed quantity is

$$\frac{dP}{dH} = \frac{d\chi'}{dH} + \frac{d\chi''}{dH}$$

In 1955, the theory of E.S.R. line shapes obtained from conduction electrons in metals was worked out by Dyson (ref.3.24). He showed that the line shape depends upon the time T_d that it takes an electron to diffuse through the skin depth, the time T_t that it takes for an electron to traverse the sample, the electron spin lattice relaxation time T_1 and the electron spin-spin relaxation time T_2 . Feher and Kip (ref. 3.25) found satisfactory agreement between Dyson's theory and their experimental result.

3.4.2. g-shift

In the presence of an external magnetic field H in the z -direction the ionic energy levels are given by

$$E = - g_s \beta H_z S_z \quad (3.30)$$

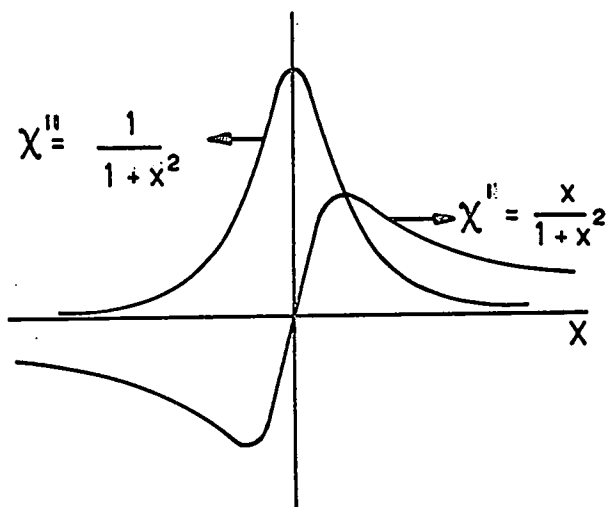


FIG. 3.6 Lorentzian dispersion χ' and absorption χ''

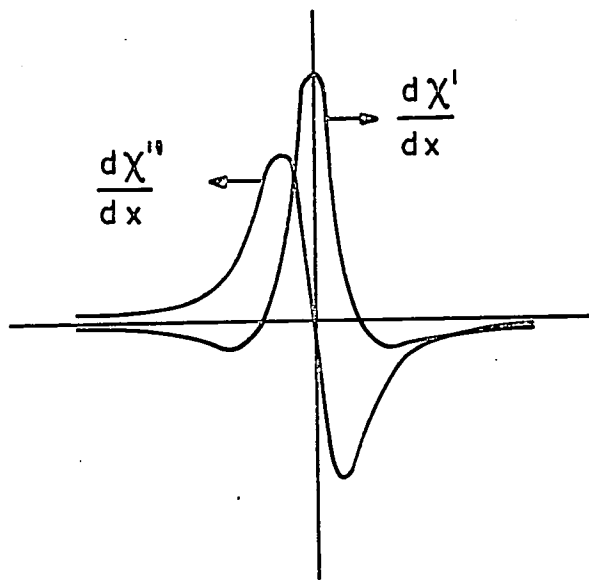


FIG. 3.7 Lorentzian dispersion ($d\chi''/dx$) and absorption ($d\chi'/dx$).

which represent the Zeeman energy. In intermetallic compounds containing rare earth ions, it is generally assumed that the conduction electrons interact with the localized 4f-electron (see chapters one and two). This interaction produces an additional term to the equation (3.30), which may shift the E.S.R. line to lower or higher magnetic field according to the sign of the exchange interaction. The allowed energy levels are now (ref. 3.26),

$$E = - S_z (g_s \beta H_z + \frac{J}{n_0} \sigma_z) \quad (3.31)$$

where n_0 is the number of lattice sites per unit volume and σ_z is the electronic spin density and may be given by

$$\sigma_z = \chi_z H_z / g_e \quad (3.32)$$

χ_z is the conduction electron volume susceptibility. By substituting from equation (3.32) to (3.31) we get

$$E = - S_z \beta H_z (g_s + \chi_z \frac{J}{n_0 g_e \beta^2}) \quad (3.33)$$

Hence we find a shift in the effective g value away from g_s , given by

$$g_s = \frac{J \chi_z}{n_0 g_e \beta^2} \quad (3.34)$$

This g-shift is analogous to the Knight shift in NMR. (ref. 3.23). If the metallic electrons can be represented by a free electron gas we get

$$\chi_z = \frac{1}{2} g_e^2 \beta^2 N(E_F) \quad (3.35)$$

where $N(E_F)$ is the density of state and equal to $3n/4E_F$

(n , is the number of conduction electrons per unit volume).

Hence

$$\Delta g_s = \frac{3Jn}{2g_e E_F n_0} = \frac{3}{4} \frac{Z J}{g_e E_F} \quad (3.36)$$

In this equation $E_F \Delta g_s$ is a measure of the exchange parameter J only in the case of a free electron gas. In certain cases, χ_z is enhanced by interelectronic exchange. If this exchange interaction is taken to be strongly localized, it can be characterized by a parameter \bar{v} and the enhanced susceptibility is then given by (refs. 3.26, 3.27, 3.28) (also see chapter one).

$$\chi_z = \chi_z^0 \frac{1}{1 - N(E_F) \bar{v}} \quad (3.37)$$

This equation may be written as

$$\chi_z = \chi_z^0 (1 - \alpha)^{-1} \quad (3.38)$$

where χ_z^0 is the Pauli spin susceptibility and is given by equation (3.35). The enhancement factor α is given by

$$\alpha = v \chi_z^0$$

where v is the Fourier coefficient of the potential (ref.3.29) from this equation and equation (3.37) we can get

$$v = \frac{2 \bar{v}}{g_e^2 \beta^2}$$

From (3.37 and (3.34) we get

$$\Delta g_s = \frac{J \chi_z^0}{n_0 g \beta^2} (1 - \alpha)^{-1} \quad (3.39)$$

This equation represents the enhanced g-shift.

3.4.3 Linewidth Considerations

3.4.3.1 Korringa Relation

The relaxation mechanisms for nuclear spins in metals are mainly due to their interactions with the conduction electrons. This mechanism is represented by a process of inelastic scattering of an electron due to the Fermi interaction in which a flip of the nuclear spin occurs. The relaxation rate is proportional to the square of the Fermi interaction constant and to the square of the electronic state density at the Fermi level. The relaxation rate, therefore, is proportional to the square of the Knight shift. Korringa obtained a relation between the relaxation time T_1 and the Knight shift k , (ref. 3.30) given by

$$k^2 T_1 T = (\gamma_e / \gamma_n)^2 (\hbar / 4 \pi K_B) \quad (3.40)$$

where γ_e and γ_n the gyromagnetic ratios of the electrons and the nucleus. By analogy with g-shift, this equation may be written as (ref. 3.31)

$$\frac{1}{T_1} = \frac{(4 \pi K_B)}{\hbar} J^2 N (E_F)^2 T \quad (3.41)$$

The Korringa relation, equation (3.40), is useful for providing an estimate of the relaxation rate knowing the value of the Knight shift. Obviously this relation is only an approximation. In several transition metals the Knight shift is found to be larger than the value calculated using the Korringa relation (ref. 3.32). This may be explained by the fact that as several contributions are present in K and $1/T_1$ the Korringa relation has no meaning. Narath (refs. 3.29, 3.33) and Bose (ref. 3.34)

have discussed extensively the various contributions to the Knight shift K and to the relaxation time T_1 .

Moriya (ref. 3.35) has considered the effect of electron-electron interaction on the nuclear spin relaxation in metals. The magnetic susceptibility enhancement factor for the relaxation is an average of $(1 - v \chi_2(f(q)))^{-1}$ over all q values which span the Fermi surface. For a spherical Fermi surface, $f(q)$ is defined in chapter one eqn. (1.13). Narath and Weaver (ref. 3.36) have given a complete discussion of various possible explanations for the remaining discrepancy between theory and experiment. They show that the correct form of the Korringa relation for an enhanced host is

$$\frac{1}{T_1} = \frac{1}{T_{1K}} \times K(\alpha) \quad (3.42)$$

where

$$K(\alpha) = \left(\frac{1 - \alpha}{1 - \alpha f(q)} \right)^2$$

$K(\alpha)$ and α have been defined and tabulated by Narath and Weaver (ref. 2.36), Moriya (ref. 3.35) and recently by Shaw and Warren (ref. 3.37). The Korringa relation may also be affected by considering the Bottleneck effect as is shown in the next section.

3.4.3 • 2 Linewidths for Bottlenecked E.S.R.

The bottleneck phenomenon can be derived from phenomenological macroscopic equations of motion for the various magnetizations, and one finds that the conditions for bottlenecking are:

1. The g-value of the impurity should be near that of the conduction electron spin i.e. near 2.
2. The spin-lattice relaxation rate of the impurity must be sufficiently small.

Hasegawa (ref. 3.38) studied the problem in dilute systems and obtained expressions for the g-shift and linewidth in terms of the strength of the thermal contact between local moments, conduction electrons and the lattice as illustrated in fig.(3.8). He described the physical situation shown in this figure, by considering the phenomenological equations of the Bloch form:

$$\dot{M}_e = \gamma M_e \wedge (H_0 + \lambda M_i) - \frac{1}{T_{eL}} (M_e - M_e^0) - \frac{1}{T_{ei}} M_e + \frac{1}{T_{ie}} M_i \quad (3.43a)$$

and

$$\dot{M}_i = \gamma M_i \wedge (H_0 + \lambda M_e) + \frac{1}{T_{ei}} M_e - \frac{1}{T_{ie}} M_i \quad (3.43b)$$

The parameter λ is proportional to the value of the exchange coupling of the form:

$$\lambda = J/N q^2 \beta^2 \quad (3.44)$$

T_{ei} and T_{ie} are the relaxation times from the conduction electrons to the local ions and vice versa. T_{eL} is the relaxation time from electron to the lattice, M_e and M_i are the total magnetization vectors of the conduction electron spin and local moment spin respectively. He assumed that in an equilibrium situation the magnetizations M_e and M_i are constant and have a definite value M_e^0 and M_i^0 satisfying a law of detailed balance:

$$\frac{M_e^0}{M_i^0} = \frac{T_{ei}}{T_{ie}} = \frac{\chi_e}{\chi_i} \quad (3.45)$$

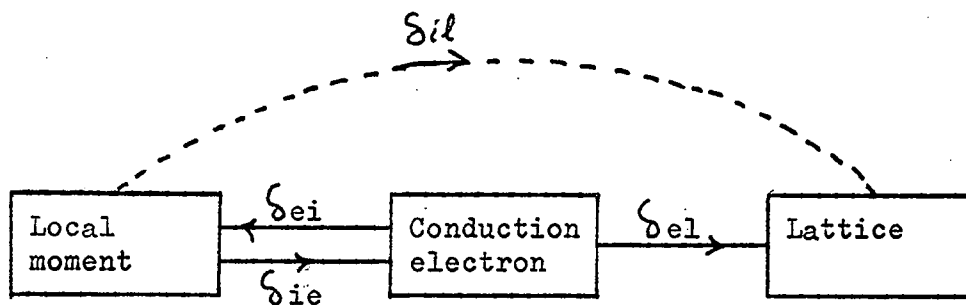


Fig. 3.8 Schematic diagram of the relaxation for the local moments in metals.

Hasegawa solved this coupled set of equations to obtain expressions for both the line width of the resonance and the g-shift. These relations can be written as follows.

$$\Delta g = \frac{x^2}{(1+x^2) + (\gamma\lambda\chi_{iH}/\delta_{ei})^2} \Delta g_0 \quad (3.46a)$$

$$\sigma\Delta H_1 = \frac{(1+x) + (\gamma\lambda\chi_{iH}/\delta_{ei})^2}{(1+x)^2 + (\gamma\lambda\chi_{iH}/\delta_{ei})^2} x \delta_{ie} \quad (3.46b)$$

$$x = \delta_{el} / \delta_{ei}, \quad \delta_{el} = \frac{1}{T_e}, \quad \delta_{ei} = \frac{1}{T_{ei}}, \quad \delta_{ie} = \frac{1}{T_{ie}}, \quad \chi_i \text{ and}$$

χ_e are the susceptibilities of the magnetic ions and the conduction electrons. By neglecting the dynamic term $(\gamma\lambda\chi_{iH}/\delta_{ei})$ from the equations (3.46) we can get

$$\Delta g = B^2 \Delta g_0 \quad (3.47a)$$

$$\text{and } \sigma\Delta H_1 = B \delta_{ie} \quad (3.47b)$$

where $B (= \frac{x}{1+x})$, is termed the bottleneck factor.

The effective line width in this equation differs from the simple Korringa result of equation (3.41) by the bottleneck factor B. T_{ei} is given by Overhauser (ref. 3.39) for the relaxation rate from conduction electrons to the ionic system and may be written as:

$$\delta_{ei} = \frac{1}{T_{ei}} = \left(\frac{8\pi}{3h} \right) N(E_F) J^2 S(S+1) C \quad (3.48)$$

where C is the concentration of magnetic ions. δ_{el} can be

separated into two parts, one of which is independent of the ionic concentration and gives the relaxation rate δ_{el}° characteristic of the undisturbed host-lattice. The other is proportional to the ionic concentration, and arises from spin-flip-scattering at the impurity due to the spin-orbit interaction (ref. 3.40) and may be written as

$$\delta_{el} = \delta_{el}^{\circ} + \frac{d\delta_{el}}{dc} c \quad (3.49)$$

The expressions above (3.47a and 3.47b) may be evaluated for two limiting cases:

1. $T_{el} \ll T_{ei}$

This is known as the unbottlenecked limit in which the full g-shift should be observed and the linewidth becomes

$$\tau \Delta H_1 = \delta_{ie} \quad (3.50)$$

which yields the simple Korringa result of equation (3.41) as explained in section (3.4.3.1)

2. $T_{el} \gg T_{ei}$

In this case the conduction electrons relax to the ions faster than to the lattice and the relaxation of the ions is said to be bottlenecked. The g-shift is then reduced from the full value by a factor $(\delta_{el}/\delta_{ei})^2$, and in the limit the linewidth is given by

$$\begin{aligned} \tau \Delta H &= \frac{\delta_{el}}{\delta_{ei}} \times \delta_{ie} \\ &= (3K T N(E_F) / 2S(S+1) C) \delta_{el} \end{aligned} \quad (3.51)$$

This formula describes the dependence of the linewidth on

both the temperature and the concentration of the magnetic impurities, and provides a useful means of identifying bottlenecking in a solid solution alloy system.

The existence of the bottleneck has been verified by studying the dependence of the E.S.R. linewidth on impurity concentration, C , and conduction electron relaxation time T_{el} by several authors (ref. 3.41, 3.49), as shown in fig.(3.9).

The Hasegawa equations have been generalized by many authors. Cottet et al. (ref. 3.50) and Davidov and Shaltiel (ref. 3.51) have considered the effect of the dynamic parameter $(\sigma\lambda_{iH}/\delta_{ei})$ in equation (3.46a). They found that when δ_{ei} is of the same order of magnitude as δ_{el} , the g-shift is reduced from its full unbottlenecked value, for either a reduction in temperature or an increase in the concentration. Schultz et al. (ref. 3.52, 3.53) have extended the Hasegawa theory to include a direct relaxation path T_{il} from the local moments to the lattice (i.e. in addition to the Korringa process) and show that the observed linewidth may then be given by

$$\tau\Delta H = \delta_{el} \frac{1}{1+x_r} \delta_{il} \frac{x_r}{i+x_r} \quad (3.52)$$

where $x_r = \delta_{ei}/\delta_{ie}$

Nakamura (ref. 3.42) modified the equation (3.47b) by adding directly the relaxation T_{il} which represent the residual linewidth and obtained.

$$\tau\Delta H = B\delta_{ie} + \delta_{il} \quad (3.53)$$

Giovannini (ref. 3.54) has shown that Hasegawa's equation (3.43) does not satisfy the requirement that the energy absorp-

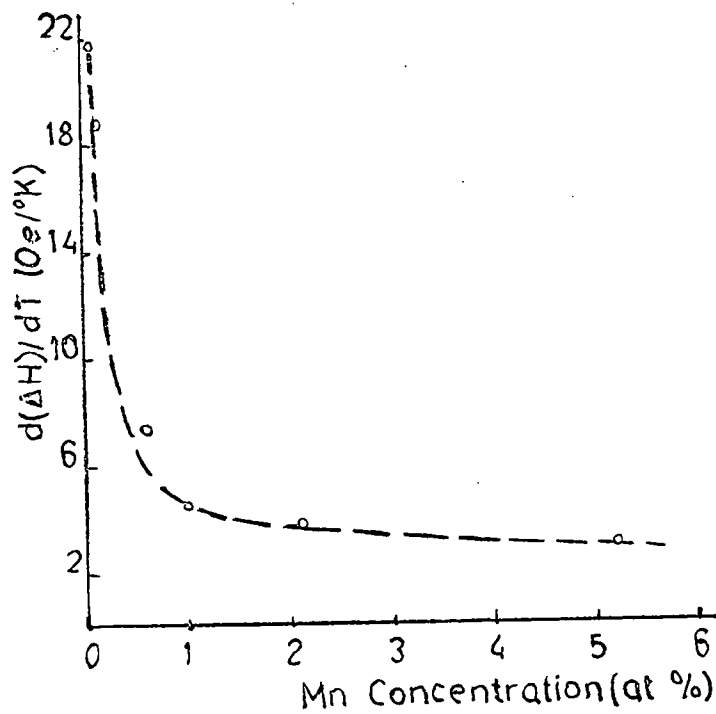


FIG. 3.9 Concentration dependence of the slope (with respect to temperature) of the ESR linewidth in CuMn. The dashed curve is a plot of eqn.(3.51). (ref.3.42).

tion is always positive definite, and has proposed other relaxation terms,

$$\begin{aligned} \dot{M}_i &= \gamma_i [M_i \wedge (H + \lambda M_e) - \delta_{ie} (M_i - \chi_i (H + \lambda M_e)) + \delta_{ei} (M_e - \chi_e (H + \lambda M_i))] \\ \dot{M}_e &= \gamma_e (M_e \wedge (H + \lambda M_i) - (\delta_{ee} + \delta_{ei}) [M_e - \chi_e (H + \lambda M_i)] \\ &\quad + \delta_{ie} [(M_i - \chi_i (H + \lambda M_e))] \end{aligned} \quad (3.54)$$

where $H + \lambda M_e$ and $H + \lambda M_i$ are effective fields on the local ions and the conduction electrons, respectively. $\chi_e (H + \lambda M_e)$ and $\chi_i (H + \lambda M_e)$ represent the equilibrium electronic and ionic magnetization.

3.4.3.3 Review of the experimental results of E.S.R in metallic ions.

We have mentioned some of these results in chapter two to compare the values of the exchange parameters J obtained from E.S.R. measurements with the results from other techniques such as N.M.R. In this section, an attempt has been made to review the experimental work on the E.S.R. of inter-metallic compounds.

Jaccarino et al. (ref. 3.55) observed electron spin resonances in the intermetallic compounds EuAl_2 and GdAl_2 between 100 K and 300 K. They found $\Delta H = 900 \pm 30$ Gauss for the half power width of the line and $g = 1.982 \pm 0.003$ in the case of GdAl_2 . For EuAl_2 they found $g = 1.994 \pm 0.003$ at 300 K which is close to the Eu free ion value.

Shaltiel et al. (ref. 3.56) measured the g value and linewidth of GdNi_5 and GdCu_5 at 78 K and 65 K respectively. They found a g -value of 1.942 ± 0.007 and $\Delta H = 905 \pm 90$ Gauss

for the Ni compound and $g = 2.009 \pm 0.007$, $\Delta H = 875$ Gauss for Cu compound. They interpreted the positive g-shift in $GdCu_5$ and the negative g-shift in $GdNi_5$ to be due to true exchange and due to the high density of states in the almost full d-band, respectively.

Wernick et al. (ref. 3.57) investigated $EuAl_4$ between 1.8 K and 295 K and obtained a high temperature g-value of 1.995 ± 0.04 with half width at half power of 430 Gauss.

Davidov and Shaltiel (ref. 3.58) measured the g-value of the compounds $GdAl_2$, $GdRh_2$, $GdMn_2$ and $GdIr_2$ finding negative g-shifts for all these, the value for $GdAl_2$ agreeing well with the previous measurement (ref. 3.55).

Hacker et al. (ref. 3.59) have obtained a value of $g = 1.984 \pm 0.003$ for $GdAl_2$ at room temperature, in excellent agreement with the results above.

Very recently Taylor (ref. 3.60) investigated the temperature dependence of the g-value and linewidth in $GdAl_2$ compound between 80 K and 300 K. He found g-value of 1.989 ± 0.005 in agreement with above in paramagnetic regime and the linewidth has a slope of 2.1 G.K^{-1} . He found the absolute value of the linewidth at 295 K to be 517 ± 25 Gauss, and 445 ± 2 Gauss at 260 K. Below 200 K the linewidth broadens rapidly with decreasing temperature.

The temperature dependence of the g-value and linewidth in the compounds $GdNi$, $GdNi_2$ and $GdNi_5$ has been investigated by Ursu and Burzo (ref. 3.61) between 100 K and 300 K. These results are tabulated in table (3.1). The g-value for $GdNi_5$ is in good agreement with Shaltiel et al. (ref. 3.55). They found that the g-value was constant over all temperatures.

Table 3.1

	Δs	$\Delta H/T$	$\Delta H/T$ calculated
GdNi	- 0.014	2.90	3.00
GdNi ₂	- 0.012	2.45	2.20
GdNi ₅	- 0.048	6.40	5.50

The line-width data were linear with temperature with the slope shown in table (3.1). A value of $K(\alpha)$, equal 0.1, in equation (3.13), was assumed to bring the measured values of g and $d\Delta H/dT$ into good agreement. E.S.R. measurements on the $RECo_2$ (RE, Gd, Tb, Dy, Ho and Er) compounds were performed by Burzo (ref. 3.62). He found the following:

1. $GdCo_2$ showed an appreciable narrowing of the line width as the temperature is increased up to approximately 405 K. Above this temperature the line width broadens rapidly. This measurement was carried out between 380 - 426 K fig. (3.10), the g -value changing with temperature as shown in the figure. He found that the g -values are smaller than those of the Gd^{3+} ion, indicating in this case a negative polarization. He claimed that the cause of this effect is associated with the presence of magnetic cobalt atoms which determines complex interactions in the compound and consequently the magnetic behaviour cannot be described by the simple Hamiltonian of the form $J.S_s$ characteristic of RKKY interactions.
2. $TbCo_2$ shows a resonance signal in the temperature range 223 - 245 K. He found that the g -values could not be determined because of the wide line ($\Delta H > 3500$ Oe).
3. $DyCo_2$ gives a minimum of the line width at 141 K ($\Delta H = 2200$ Oe, $g = 3.40 \pm 0.20$). The line rapidly broadens as the temperature increases. No resonance signals were observed for $HoCo_2$ and $ErCo_2$ between 103 and 300 K.

Shaltiel et al. (ref. 3.56) have measured the Gd g -shift in $LaNi_5$ for a few samples of relatively high Gd concentrations at the temperatures 20 and 60 K. They found a large Gd g -shift

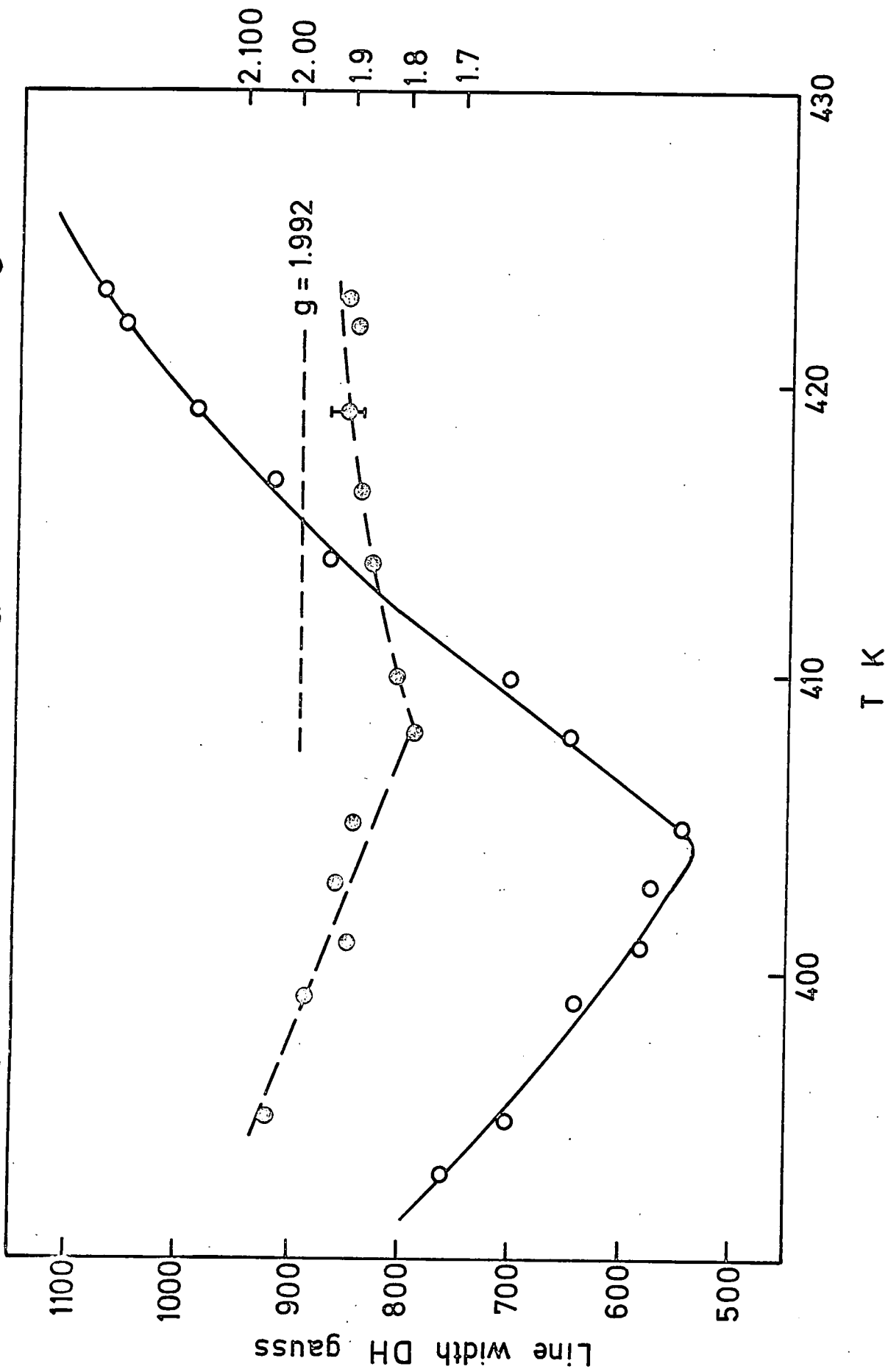


FIG. 3.10 The temperature dependence of line width and g values for $GdCo_2$ (after ref. 3.44)

which depends both on temperature and on concentration. They explained this behaviour in terms of dynamic effects, equation 3.46. Davidov et al. (ref. 3.63) also investigated the same system with varying Gd concentration between 0.005 and 0.1, and found the following:

1. For Gd concentrations above 1% in $Gd_x La_{1-x} Ni_5$, the g-shift varies appreciably with temperature, whereas for lower Gd concentrations ($x < 0.01$), the shift was found to be almost temperature-independent.
2. At 4.1 K both the g-shift and the line width are concentration-dependent.

They emphasized that the variation of the ionic g-shift as a function of temperature and concentration is mainly due to the variation of the ratio $\sigma \lambda \chi_1 H / \delta_{el}$, with these parameters, the effect due to the bottleneck is much smaller as can be verified by equation (3.46). However, the increase in line width with concentration was not explained by the above theory; instead it was assumed that local clusters of Gd ions resulted in inhomogeneous broadening, with exchange narrowing at higher concentration.

Davidov et al. (ref. 3.64) also investigated the system $Gd_x Zr_{1-x} Zn_2$ ($x = 0.06, 0.05$ and 0.03). They found that the line width varies with temperature and has a maximum at approximately 40 K. Above 40 K it decreases sharply up to 60 K and then increases moderately at the rate of approximately 3 Oe per degree at higher temperatures. The g-shift is always negative: it varies with temperature, and has a maximum at 30 K, a shallow minimum at 50 K, and decreases asymptotically at

higher temperatures. They claim that a fairly good fit to the data above 20 K may be obtained by consideration of dynamic effects, equation 3.46.

The measurements by Debray and Ryba (ref. 3.65) on GdZn_2 by E.S.R. show the g-value to be independent of temperature and equal to 2.029 ± 0.005 . The line width increases linearly with temperature with a slope of ≈ 4.4 Gauss/K. The observation of a positive g-shift indicates the dominance of the exchange parameter.

Schäfer et al. (ref. 3.48) observed the resonance in $\text{Gd}_x\text{Y}_{1-x}\text{Al}_2$ for ($x = 0.003, 0.005, 0.007, 0.01, 0.02, 0.05$). They found the line width changes linearly with temperature, the slopes being concentration-dependent, decreasing with increasing Gd concentration. They observed no measurable g-shift. These observations were taken as a strong indication that the system was well bottlenecked. By adding Th to the compounds they observed that the slope of the line width increases with increasing Th concentration, but at fairly high Th concentrations the slope becomes nearly independent of the Th concentration and approaches an upper limit of about 40G/K, and the observed line width corresponds to the Korringa rate. They claimed that the relaxation can be changed continuously from the bottlenecked region to the isothermal limit, where the conduction electrons are in thermal equilibrium with the lattice.

Recently, Koopmann et al. (ref. 3.46) observed the resonance in $\text{Gd}_x\text{La}_{1-x}\text{Al}_2$ and $\text{Eu}_x\text{La}_{1-x}\text{Al}_2$ (x between 4% and 0.08%) for Eu and ($x = 1\%$ and 0.02%) for Gd at temperatures 1.7 - 25 K. The line width was found to be 300 Gauss for Eu and 100 Gauss for Gd at 1.7 K. A positive g-shift was obtained of value 0.05

for Eu and 0.1 for Gd.

More recently, Davidov et al. (3.66) have reported E.S.R. measurements on the compounds $Gd_x La_{1-x} Al_2$ which may indicate the existence of a bottleneck effect. Their results can be summarized as follows.

1. The g-value and line width ΔH change appreciably from one sample to another. Any increase in the slope of the line width is always associated with an appropriate increase in the effective g-value. This indicates the presence of bottleneck effects in the magnetic resonance.
2. The lowest value obtained for g is 1.988 ± 0.003 which is in agreement with the g-value of $GdAl_2$. The smallest observed value of $\Delta H / \Delta T$ was 20 G/K.
3. Substitution of $ThAl_2$ in place of $LaAl_2$ in $Gd_x La_{1-x} Al_2$ increases both Δg and $\Delta H / \Delta T$. The maximum value of Δg and $\Delta H / \Delta T$ is 0.11 ± 0.01 and 70 G/K, respectively. These values are independent of further increase in Th concentration, and are identified as the fully-unbottlenecked g-shift and line width.
4. The g value was slightly temperature-dependent, increasing by 0.01 ± 0.01 in the high temperature limit. This effect, as well as low and high field measurements, indicates that the dynamic effect, though small at high temperature, cannot be completely neglected here.

From these results they proposed a two band model of the following character. (1) J_{f-s} between the Gd 4f electrons and the s-band conduction electron is positive. (2) J_{f-d} between Gd 4f-electrons and the d-band conduction electrons

is negative.

These assumptions lead to the following equations.

$$\Delta g = \Delta g_d + \Delta g_s \frac{x^2}{(1+x)^2 + (\gamma \lambda \chi_i H / \delta_{ei})^2}$$

$$\Delta H = \frac{\pi K_B}{g \mu_B} T \left[(\Delta g_d)^2 F_d K_d (\alpha_d) + (\Delta g_s)^2 K_s (\alpha_s) \left(\frac{x(1+x) + (\gamma \lambda \chi_i H / \delta_{ei})^2 x}{(1+x)^2 + (\gamma \lambda \chi_i H / \delta_{ei})^2} \right) \right]$$

where the s-band relaxes weakly to the lattice and is therefore bottlenecked, and the d-band relaxes rapidly to the lattice and is therefore unbottlenecked.

CHAPTER 4

EXPERIMENTAL TECHNIQUES

4.1 NMR Spin Echo Instrumentation:-

The pulsed Nuclear Magnetic Resonance Spectrometer requires a pulse generator to provide a suitable pulse train, a transmitter for generating the radio frequency (RF) field, a pre-amplifier - receiver unit for processing the signal, and a probe to couple the sample to the transmitter and to the receiver.

A block diagram of the NMR Spin Echo system is shown in fig. (4.1), where the radio frequency (RF) power is derived from the pulse generator - transmitter combination. The RF power was coupled into the sample by means of a coil surrounding the specimen tube. The signal detected by the same coil was amplified and then mixed with a continuous wave (CW) signal from the local oscillator, thus producing a 30 MHz intermediate frequency (IF) signal displayed directly on an oscilloscope having a vertical band-width of 33 MHz, synchronized from the pulse generator.

4.1.1 The Sample Probe

The power requirements of the RF transmitter used in an NMR experiment depend not only on the gyromagnetic ratio of the nucleus being studied, but also on the sample coil geometry.

It has been shown (ref. 4.1) that the RF power H_1 in the sample coil is given by:-

$$H_1 = 3(PQ / \nu_0 V)^{1/2} \quad (1)$$

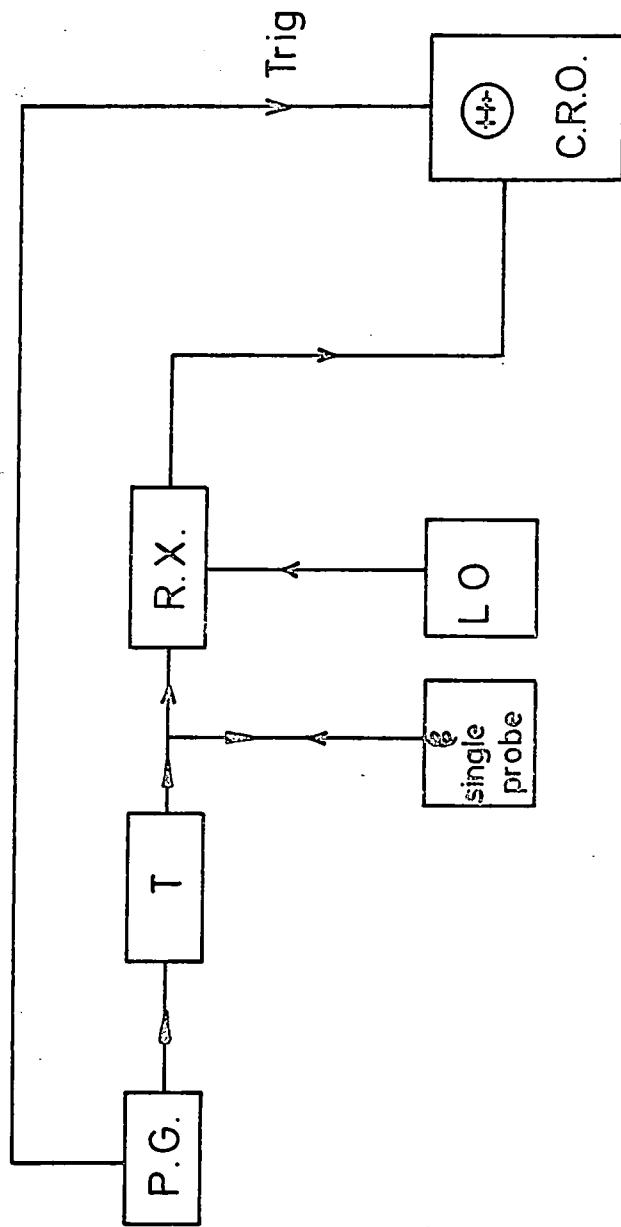
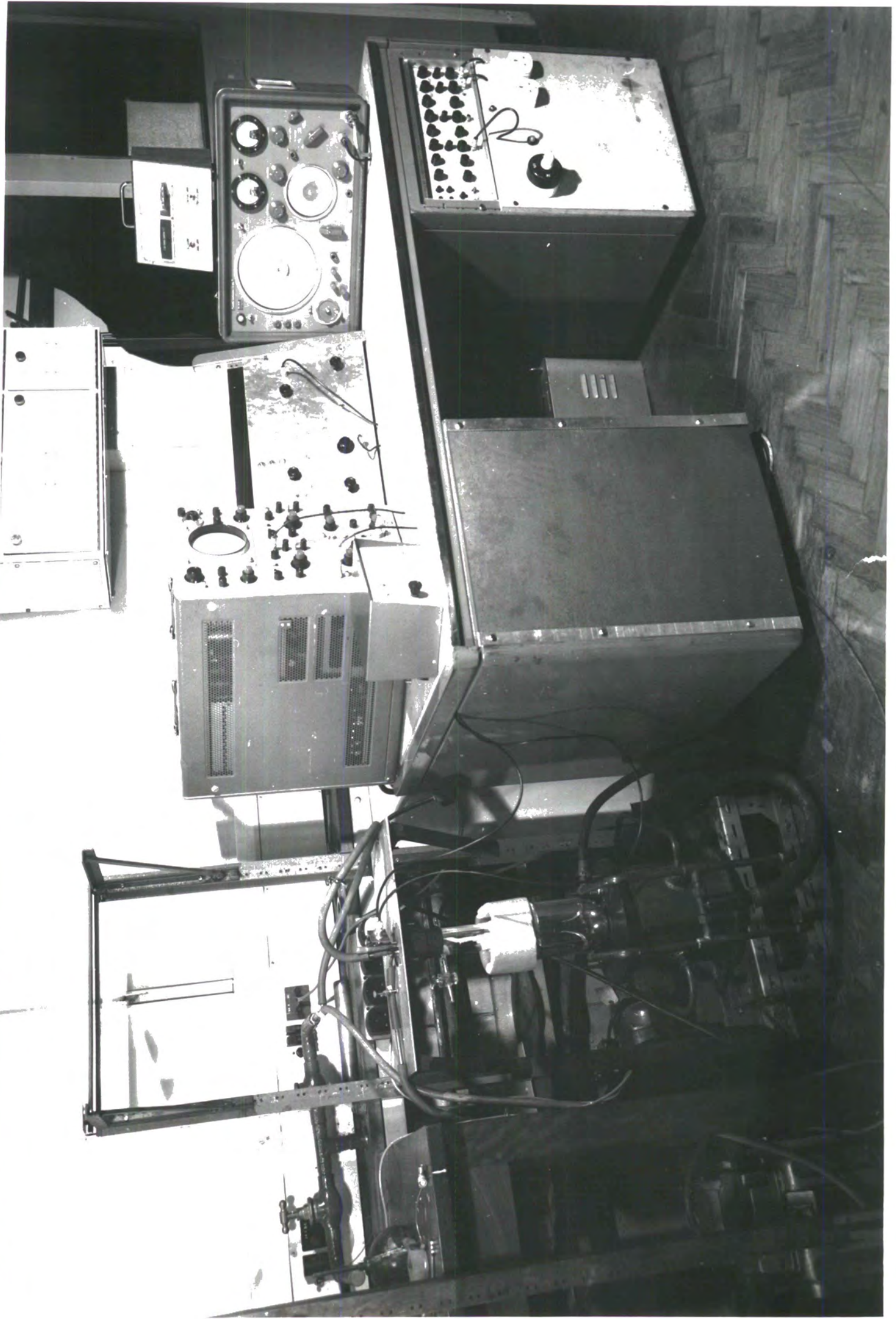


FIG.4.1 BLOCK DIAGRAM OF NMR SPIN ECHO.



or alternatively

$$H_1 = 3.7 (PT_r / V)^{1/2} \quad (2)$$

with

$$Q = 1.5 \nu_0 T_r$$

where P is the transmitter power in watts, Q is the quality factor, ν_0 is the resonance frequency in MHz, T_r is the rise and fall time of the envelope of the RF pulse in microseconds, $2H_1$ is the RF field in gauss and V is the volume of the sample coil in cubic centimetres. To obtain the largest output signal from the probe coil, the "filling factor" (the ratio of the sample volume to the volume of the coil) must be kept as large as possible. This is achieved by using a thin-walled quartz tube to contain the specimen.

The sample probe that has been used is shown in fig.(4.2). The quartz tube with its powdered sample is placed in L_1 , the probe coil, which is tuned with the capacitance C_1 to obtain the maximum RF field H_1 and to recover a nuclear signal with the greatest sensitivity. The probe coil acts as both the transmitter load and the signal source for the receiver.

The sample coil is a single-layer helix \sim 1.1 cm long and 1.2 cm in diameter, small enough to fit easily inside the tail of the helium dewar. It can be mounted vertically or horizontally to allow the direction of H_1 to be varied for use in an external magnetic field. The number of turns on the coil depends upon the range of frequency being used. The feeder lengths shown in fig. 4.2 were determined empirically to give a satisfactory compromise between maximum power at the sample and maximum signal at the receiver input.

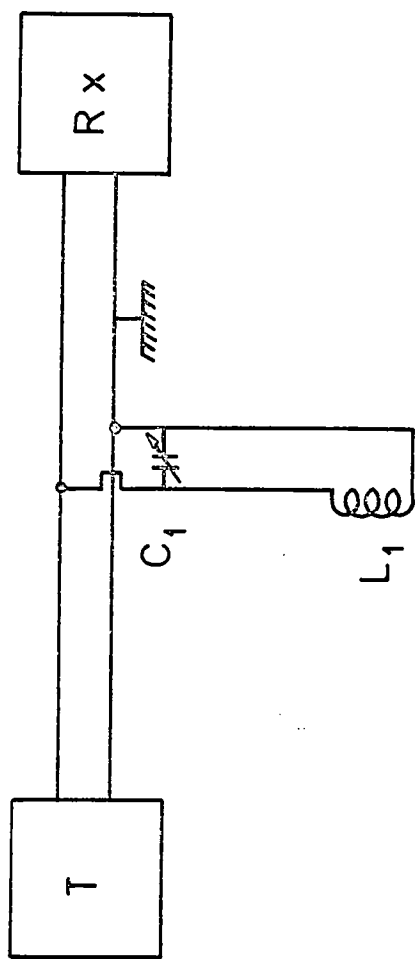


FIG. 4.2 THE SAMPLE PROBE. THE TUNED SAMPLE CIRCUIT CONSISTS OF L_1 AND C_1

4.1.2 Pulse Generator:-

This unit was a commercial system (Farnell Instruments) and allowed the Pulse Repetition Frequency (PRF), Pulse width, Pulse Delay (the time between the two pulses) and the output pulse amplitude to be controlled independently.

A maximum of three, positive or negative-going pulses could be obtained with a PRF varying from 1 Hz to 10 MHz in seven ranges. The delay is adjustable from 0.1 μ s. to 1.0 s in seven decade ranges. The pulse width can be adjusted over a range from 0.1 μ s. to 1.0 s also in seven decade ranges. The output pulse amplitude can be varied from 10V down to 30mV in stepped ranges of 10dB. A continuous level control enables the output amplitude to be varied between these steps.

4.1.3 The Transmitter and the Receiver:-

These units were designed and built by Dr. G. Brown for this particular research work, but for completeness some details of the circuitry will be included here.

4.1.3. 1 The Transmitter - fig(4.3)

This is basically a high-power double - tetrode oscillator with capacitive positive feedback, the output of which is inductively coupled into the feeder leading to the probe coil. The grids are normally biased to - 150 volts, so that oscillation is only possible when the cathode approaches this value. Under normal conditions, the cathode is at earth potential and the valve is cut off.

The triode modulator controls the cathode bias and operates

on a negative rail of - 150 volts. The quiescent current through the 2.7 K and 33 K resistors cut off this valve. When a 20 volts positive pulse is applied through a DC blocking condenser to the grid, the valve is biased heavily "on" and the anode is brought down almost to the cathode potential (\sim - 141 volts). Direct coupling from this anode to the oscillator cathode brings the power valve into oscillation, and it will remain oscillating until the pulse is removed and the cathode assumes earth potential again. The diodes prevent overshoot of this transient, ensuring a clean edge to the RF pulse.

The power supply for the transmitter, shown in fig.4.4 is conventional. Each valve has a separate heater supply to minimise RF coupling.

4.1.3 2 The Receiver - Figs.(4.5) & (4.6)

The signal from the probe coil is fed directly to a transistor amplifier with a crossed-diode limiter at its input. This amplifier has a gain of \sim 10dB and its output is again limited before being fed to the integrated circuit (I.C) mixer (Texas Instruments type 76514N).

The output of an external local oscillator (Marconi TF 801/B) is fed into the double-balanced mixer which rejects both the input frequencies, leaving at the output, only the sum and difference frequencies, and some harmonics. Pins 3 + 13 are anti-phase outputs and the resulting signals are applied to a push-pull tuned filter operating at 30 MHz. The capacitive centre-tap provides good matching to the 600Ω output of the mixer.

The I.F. amplifier consists of two linear (i.c.) amplifiers

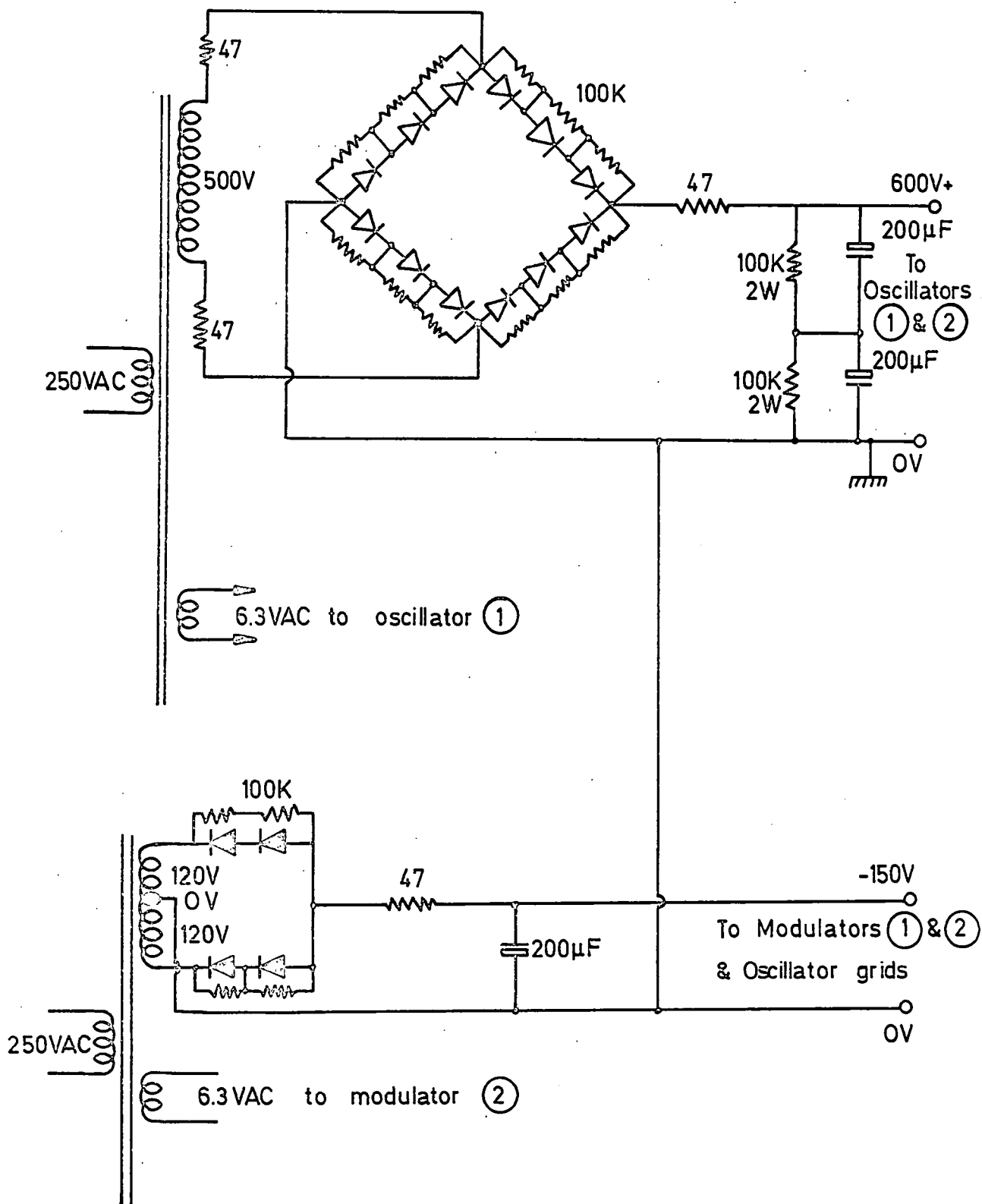
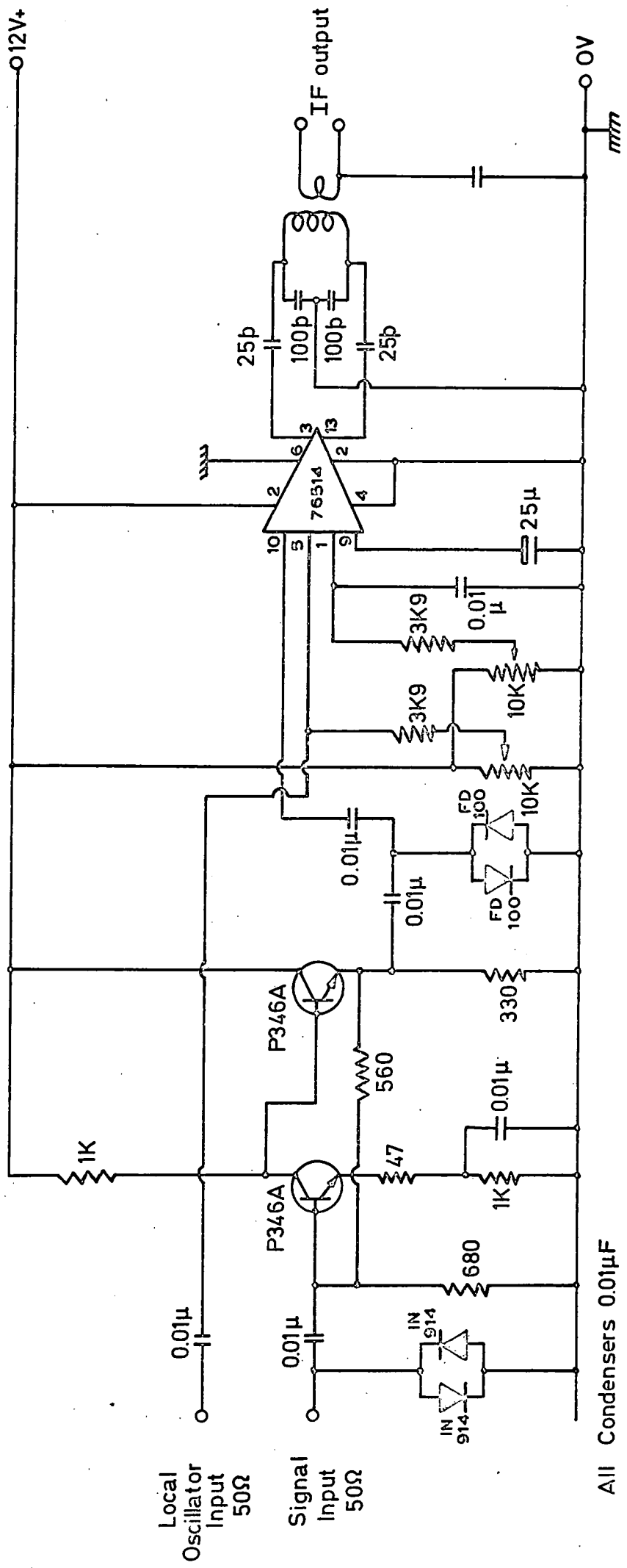


FIG.4.4 TRANSMITTERS' POWER
SUPPLY



Local
Oscillator
Input
50Ω

Signal
Input
50Ω

All Condensers 0.01μF
Unless Stated Otherwise

FIG. 4.5 MIXER CIRCUIT.

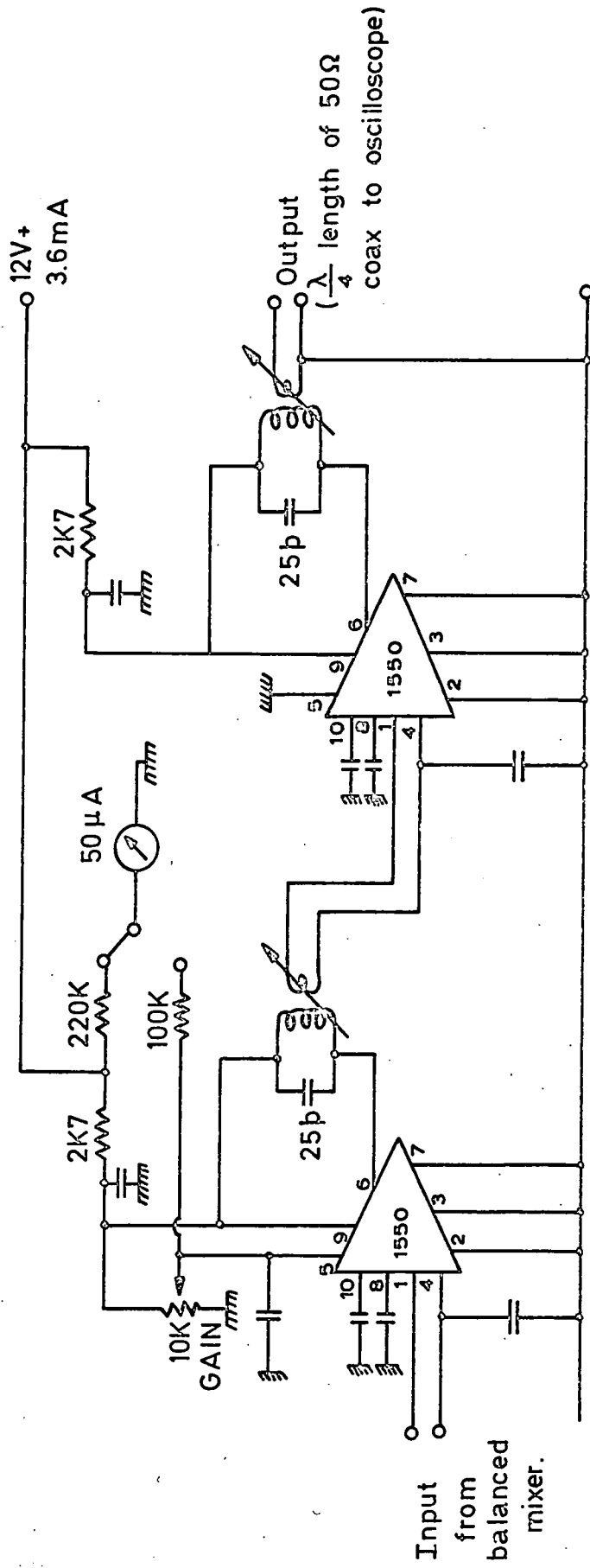


FIG.4.6 30Mc/s IF AMPLIFIER.

with single-tuned 30MHz transformers in the outputs. The low-impedance output of the final stage is transformed by a $\lambda/4$ feeder to match the high-impedance oscilloscope input.

4.2 E.S.R. Spectrometer:-

Electron spin resonance measurements were made on a conventional X - band reflection spectrometer. Microwave power is fed from a 9 GHz Klystron to a "magic T" which splits the power between a "sample" arm and a "balancing" arm. The "balancing" arm contains a phase shifter and an attenuator, followed by a short circuit. It can be shown that the impedance of the cavity in the "sample" arm, as seen at the magic T junction, can be matched exactly by the impedance of the "balancing" arm components, when correctly adjusted. Two identical signals thus reach the series junction of the magic T when the balancing is correct. The symmetry properties of a series junction (ref. 4.2) make it impossible for two identical signals in the opposite arms to be propagated in the adjacent arm. When the external conditions are correct for a sample resonance to occur, the cavity Q, and hence its impedance, changes. The bridge is now unbalanced and microwave power then passes equally

- (a) into the detector arm
- (b) back towards the Klystron.

Part (a) is mixed with CW power from a local oscillator Klystron in the first detector of a conventional superheterodyne receiver. The L.O. klystron is frequency - locked 30 MHz from the monitor klystron frequency which, in turn, is frequency - locked to the sample cavity. For recording sample resonances, the signal to noise ratio is increased by measuring the differ-

ential absorption signal produced by small - amplitude modulation of the magnetic field at 180 Hz, and by subsequent phase sensitive detection. The overall block diagram is shown in Fig. (4.7) and is discussed by R.P. Hunt (ref. 4.3).

4.3 Specimen Preparation

Specimens were prepared in the form of buttons of approximately three grams weight by melting the compounds in an arc furnace and in an induction furnace. The rare earth of Yttrium elements were obtained with a purity of 99.9% and the transition metals (irons, cobalt, aluminium) were obtained with a purity of 99.998% from Koch - Light Laboratories Ltd.

4.3.1 Rare Earth - Co₂

The melting took place on a water-cooled copper hearth under an argon atmosphere at a pressure of about 400 torr. The argon was obtained as 'Puragon' with an oxygen content of no more than 3 p.p.m. The arc furnace was pumped down to 10^{-3} torr then flushed with 'Puragon' to 700 torr, pumped down to 10^{-3} torr again and then filled to 400 torr with 'Puragon'. This procedure ensured that the oxygen content of the atmosphere in the furnace was down to the same order of magnitude as that of the Puragon. A tantalum getter was heated for a minute before melting the sample components together in order to purify further the atmosphere in the furnace.

The sample melting was done at as low a temperature as possible to minimize loss of material by evaporation. The lower face of the melted button is in contact with the cold copper so that it is necessary to turn the specimen over and

remelt it several times to obtain a homogeneous mixture. The weight loss was usually no greater than 1%.

4.3.2 Rare Earth - Al₂

Samples of (GdAl_2) , $(\text{Gd,Y})\text{Al}_2$, $(\text{Gd, Dy})\text{Al}_2$ and $\text{Gd}(\text{Co,Al})_2$ were prepared by melting the components in the arc furnace as above for the first melting. The resulting ingots were exceedingly brittle and shattered on re-melting, thus it is impossible to re-melt these compounds using the arc furnace. Instead we have used an induction furnace for the second melting of the specimens. The induction field is set up by a high RF current which flows through a coil which is driven from a 25 kW generator, working at a frequency of 465 kHz. The melting has been done inside a water-cooled enclosure, which is placed in the coil, at a pressure of about 10^{-3} torr. Quartz crucibles were used as the containing vessels.

Annealing of samples was done on half - buttons wrapped in molybdenum or tantalum foil and placed in a quartz tube. Several samples were placed in one annealing tube and each was spaced from its neighbour by a short length of quartz tube closed at one end which fitted freely inside the annealing tube. The annealing tube was filled with 'Puragon' and gettered by the same procedure as described above for preparing a sample button. The argon was then pumped out to 10^{-3} torr and the samples isolated from each other and the atmosphere by collapsing the quartz tube onto the spacers. The samples were then ready for annealing. The annealing time was seven days at a temperature of 800°C .

Powdered samples from the specimens were examined by X-ray

diffraction. X-ray photographs were obtained from a rotating powder sample using a Philips 360 mm circumference Debye - Scherrer X-ray camera and cobalt K_{α} - radiation. The results will be discussed in chapter 5.

4.4 Curie and Neel temperature determination (A.C. Susceptibility Technique.)

The principle of this technique is described here briefly. A detailed description can be obtained from (ref. 4.4). A small transformer is powered by a 500 Hz sinusoidal voltage which induces an A.C. field of less than 1 Oe in the core of the transformer. The core of the transformer consists of the sample in powder form. Thus the secondary of the transformer gives an output voltage which is proportional to the permeability of the core. Since the filling factor of the measuring coils is significantly less than unity, they are connected in series - opposition with a small adjustable ferrite-cored transformer to form a Hartshorn bridge. The total output of the two transformers may thus be nulled in the absence of a sample. The output in the presence of a sample is then proportional to χ_{AC} , the initial susceptibility of the sample in an A.C. field. This output is amplified and detected by a phase - sensitive detector. The resulting signal is applied to the Y - input of an X - Y pen recorder. The temperature of the sample is obtained from a thermocouple whose sensing junction is placed in the powder sample. The output voltage of the thermocouple is applied to the X input of the X - Y recorder. Thus, as the temperature varies the χ_{AC} vs T plot is traced out. Typical output shown in fig. (4.8).

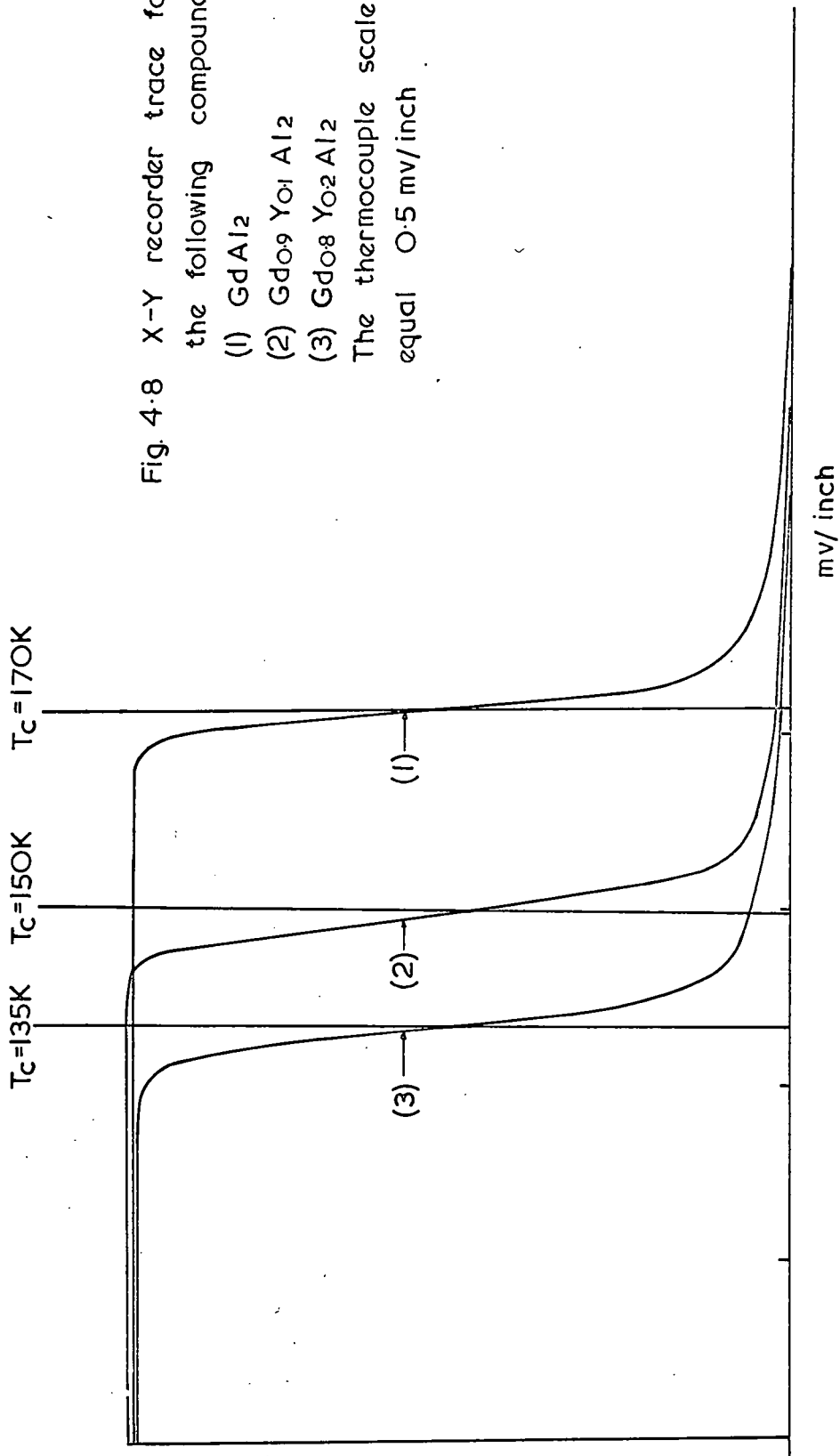


Fig. 4.8 X-Y recorder trace for X_{AC} vs T for the following compounds :-

- (1) $GdAl_2$
- (2) $Gd_{0.9}Y_{0.1}Al_2$
- (3) $Gd_{0.8}Y_{0.2}Al_2$

The thermocouple scale on X input equal 0.5 mv/inch

From the form of the χ_{AC} vs T plot and from what was known about the magnetic properties of the material it was possible to decide whether the sample ordered antiferromagnetically or ferromagnetically. In the case of antiferromagnetic samples a sharp peak is expected, the temperature corresponding to the peak being the ordering temperature of Neel point T_N . In the case of ferromagnetic sample the ordering temperature T_C of ferromagnetic is the temperature above which spontaneous magnetization just disappears.

4.5 Temperature Control

4.5.1 The Cryostat:-

The cryostat was designed for containing liquid helium in order to measure the hyperfine field of a sample from 4.2 K up to room temperature. The dewars are made of pyrex glass and are tailed as shown in the diagram, Fig. (4.9). The dimensions are listed in the table (4.1). The nitrogen dewar was evacuated and sealed permanently, but the inner helium dewar is flushed with air and pumped on each occasion it is used to remove any helium gas, which can diffuse through the inner wall.

4.5.2 Temperature measurement

This was done by means of thermocouples. Two thermocouples were available. One was of standard thermocouple quality copper and constantan wires, insulated with PTFE sleeving, and the junction made in a normal bunsen flame, for use at temperatures above 77 K. The other was of gold - copper: copper for use between 4.2 K and liquid nitrogen and the thermoe.m.f. was measured by a Pye Portable Potentiometer in conjunction

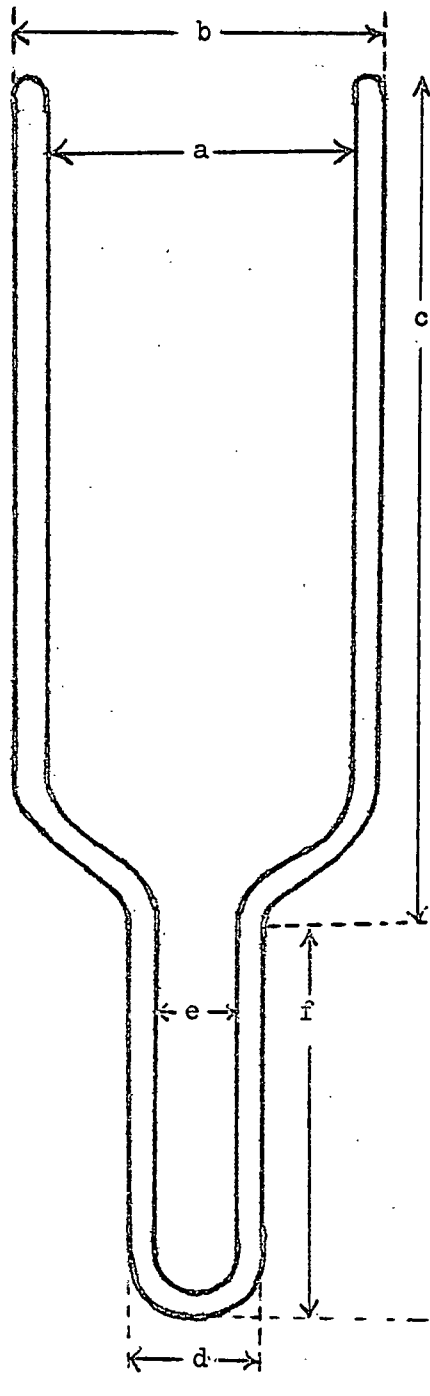


FIG. 4.9 Dewar Vessels

Table 4.1

Dewar	Dimension in cm					
	a	b	c	d	e	f
Helium	4.15	5.55	43.50	2.95	1.80	14.50
Nitrogen	9.3	11.5	30.0	4.80	2.2	16.0

with an external Scalamp galvanometer.

The thermocouple was in contact with the powder sample, in the NMR spin echo measurements, and the temperature runs were performed while the sample was warming up.

In ESR measurements the resonance cavity is evacuated and filled with helium gas. The cavity is placed in a glass dewar and cooled by contact with a series of different melting-point mixtures. The materials and their relevant temperatures are listed in table (4.2). These mixtures were prepared by emulsifying with liquid nitrogen until equilibrium was achieved at the required temperatures.

Table 4.2

<u>Material</u>	<u>Temperature</u>
250 K	Carbon Tetrachloride
223 K	Pinene
200 K	Co ₂
179 K	Methylalcohol
143.3K	n. Pentane

CHAPTER 5

EXPERIMENTAL RESULTS

5.1 Lattice Parameters

The measurements were made on the following compounds

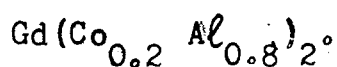
1. (a) $Gd_{1-x} Y_x Al_2$ ($x = 0.1$ to 0.9)
- (b) $Gd_{1-x} La_x Al_2$ ($x = 0.1$ to 0.4)
- (c) $Gd_{1-x} Dy_x Al_2$ ($x = 0.03, 0.05, 0.07, 0.1$)
- (d) $Gd (Co_{1-x} Al_x)_2$ ($x = 0.1$ to 1.0)

2. Rare earth Co_2

The compounds were prepared from 99.99% pure aluminium, 99.99% pure cobalt and 99.9% pure rare earth metals by arc and induction furnace melting (as explained in chapter 4, section 4.3). The ingots were annealed for about a week at $800^\circ C$. Powdered samples from the button specimens were examined by x-ray diffraction. The films so obtained were analysed in the usual way, the lattice parameter being derived from a Nelson Riley extrapolation (ref. 5.1) to eliminate systematic errors. A computer programme was written for analysing cubic powder diffraction patterns (ref. 5.2). All the compounds (except $Gd(Co_{1-x} Al_x)_2$) were single phase and shown to be cubic C15 ($MgCu_2$) structure. The lattice parameters of the first three compounds are given in tables (5.1, 5.2).

The lattice parameters of $Gd(Co_{1-x} Al_x)_2$ are summarized in table 5.3. The structure changes from C15 to C14 and then back to C15 occurs as follows:

- a) The cubic $MgCu_2$ (C15) type is stable from $GdAl_2$ to



b) The hexagonal MgZn_2 (C14) type is found from $\text{Gd}(\text{Co}_{0.3} \text{Al}_{0.7})_2$ to $\text{Gd}(\text{Co}_{0.7} \text{Al}_{0.3})_2$.

c) The cubic MgCu (C15) again is stable from $\text{Gd}(\text{Co}_{0.8} \text{Al}_{0.2})_2$ to GdCo_2 .

5.2 Curie temperature

The Curie temperatures of these compounds were determined by using an A.C. susceptibility technique (see chapter 4, section 4.4). For the compounds with Yttrium, Lanthanum and Dysprosium as diluting elements, the decrease of the Curie temperature proceeds linearly with the composition x , as shown in the figure (5.1). The $\text{Gd}(\text{Co}_{1-x} \text{Al}_x)_2$ samples show a complicated behaviour where the Curie temperature decreases linearly from pure GdAl_2 to $\text{Gd}(\text{Co}_{0.2} \text{Al}_{0.8})_2$ and from $\text{Gd}(\text{Co}_{0.8} \text{Al}_{0.2})_2$ to pure GdCo_2 , whereas for $\text{Gd}(\text{Co}_{0.6} \text{Al}_{0.4})_2$ and $\text{Gd}(\text{Co}_{0.7} \text{Al}_{0.3})_2$ there are two transition temperatures indicating the possibility of two phases (fig. 5.2) in the specimen.

5.3 Spin Echo observation

In the spin echo experiments (see chapter 3, and 4), the echo amplitude, obtained from the oscilloscope, is measured as a function of pulse separation and frequency, assuming that the other variables, e.g. pulse repetition frequency (PRF) and pulse width are fixed. The results are given for the following cases.

Table 5.1

Lattice Parameters of $Gd_{1-x}Al_x$, C15 Cubic Laves Phase

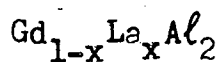
Composition x	Lattice Parameter in Å
0	7.900 ± 0.001
0.1	7.894 ± 0.001
0.2	7.889 ± 0.001
0.3	7.886 ± 0.001
0.4	7.884 ± 0.001
0.5	7.875 ± 0.001
0.7	7.849 ± 0.001
0.9	7.853 ± 0.001

Table 5.2

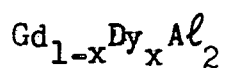
Lattice Parameters of $Gd_{1-x}La_xAl_2$ and $Gd_{1-x}Dy_xAl_2$

Cubic Laves Phase

Composition Lattice Parameter in
 x Å



0	7.900 ± 0.001
0.1	7.918 ± 0.001
0.2	7.930 ± 0.001
0.3	7.952 ± 0.001
0.4	7.964 ± 0.001



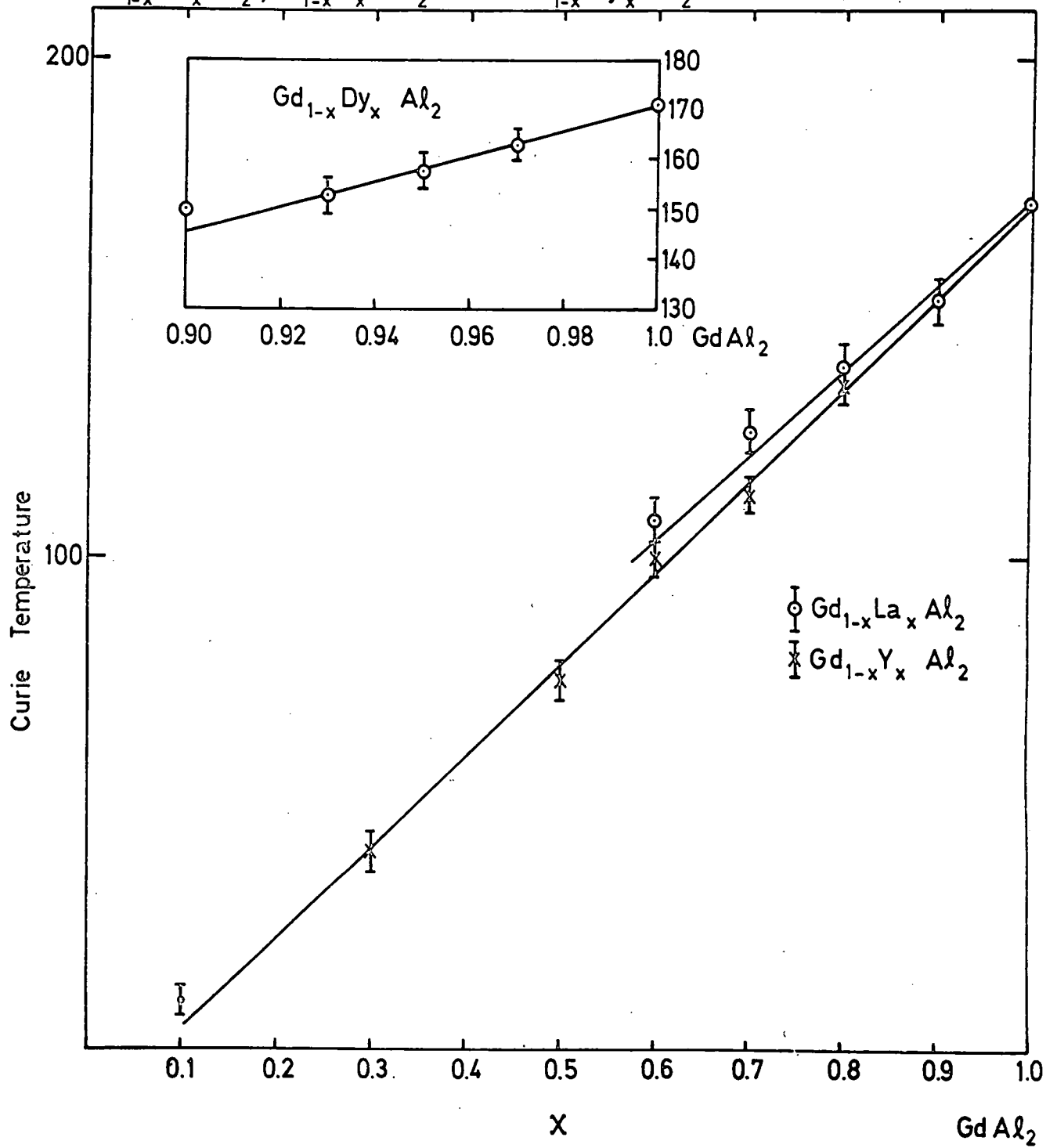
0.03	7.896 ± 0.001
0.05	7.893 ± 0.001
0.07	7.891 ± 0.001
0.10	7.890 ± 0.001

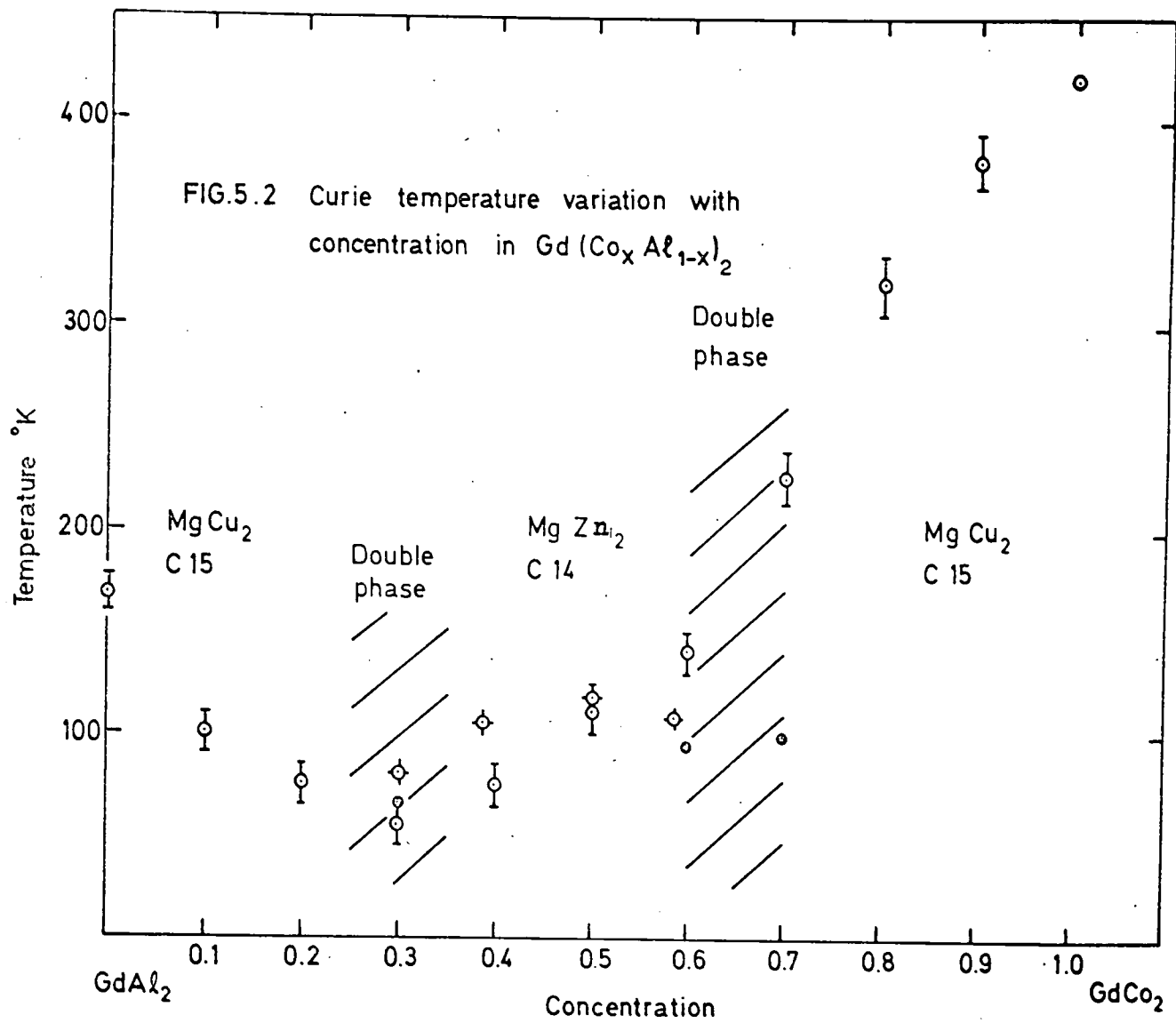
Table 5.3

Lattice parameters of $\text{Gd}(\text{Co}_x\text{Al}_{1-x})_2$

Composition	Structure	a (Å)	c (Å)	c/a
0	C15	7.900		
0.1	C15	7.850		
0.2	C15	7.780		
0.3	C14	5.460	8.740	1.582
0.4	C14	5.460	8.640	1.584
0.5	C14	5.40	8.520	1.578
0.6	C14	5.38	8.510	1.578
0.7	Not indexed			
0.8	C15	7.340		
0.9	C15	7.304		
1.0	C15	7.255		

Fig.5.1 The curie temperature variation with concentration for $Gd_{1-x}La_xAl_2$, $Gd_{1-x}Y_xAl_2$ and $Gd_{1-x}Dy_xAl_2$





5.3.2 Gd A' Al₂ (A' = Y, La, Dy)

In this case we are investigating the ²⁷Al resonance in Gd_{1-x}Y_xAl₂, Gd_{1-x}La_xAl₂ and Gd_{1-x}Dy_xAl₂. The rf field strength of the two pulses of 5 μS duration with 70 Hz P.R.F. was adjusted to maximum echo height. The echo amplitude for GdAl₂ oscillated as a function of the pulse spacing τ as shown in fig. (5.3). This oscillation vanishes at τ = 27 μS. For this reason the line shape measurements have been carried out where the separation between the pulses, was kept constant at about 30 μsec. (The line shapes of the resonances were determined by point-to-point plots of the echo amplitudes as the frequency of the rf was varied in 0.5MHz steps).

All measurements were performed at 4.2 K, except for GdAl₂ where the echo amplitude has been measured as a function of temperature up to 27 K where the echo disappeared into the receiver noise. Fig.(5.4) shows the reciprocal of the echo amplitude as a function of temperature. The measurements were made in zero external magnetic field. Prior to the measurements, however, the samples were magnetized after cooling down to 4.2 K in a field of 9kOe applied perpendicular to the rf field.

The observed echo amplitude as a function of frequency should be corrected to determine the true line shape along the wide range of frequency. Streever and Uriano (ref.5.3) found that the echo amplitude must be divided by square of the frequency at each point along the resonance line. This correction was proposed because the spin echo signal observed

Fig.5.3a Spin echo oscillation as a function of τ , the frequency is 61.5 MHz, for $GdAl_2$.

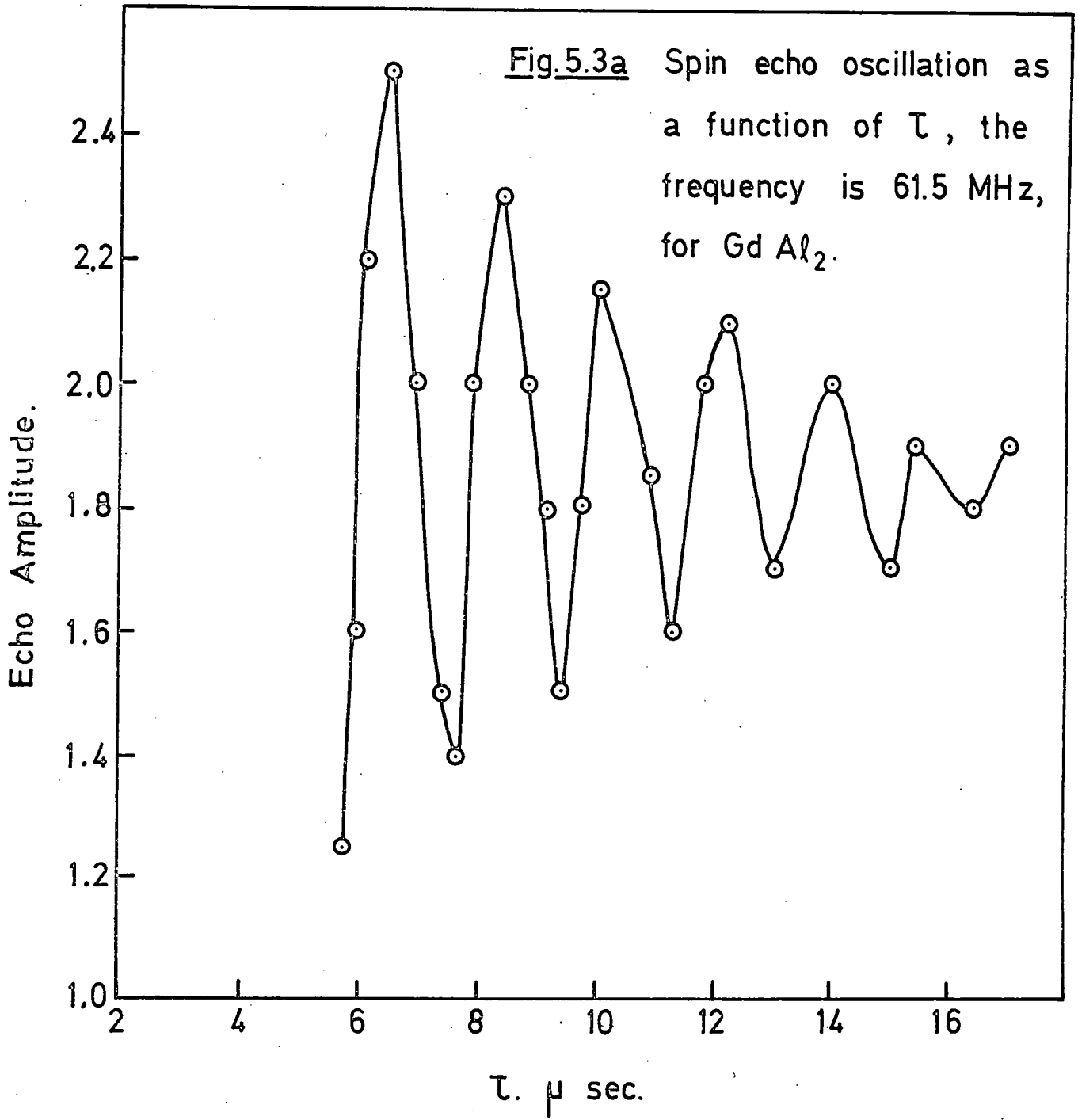


FIG. 5.3b Spin echo oscillation as a function of τ , the frequency is 49.5 MHz, for $GdAl_2$.

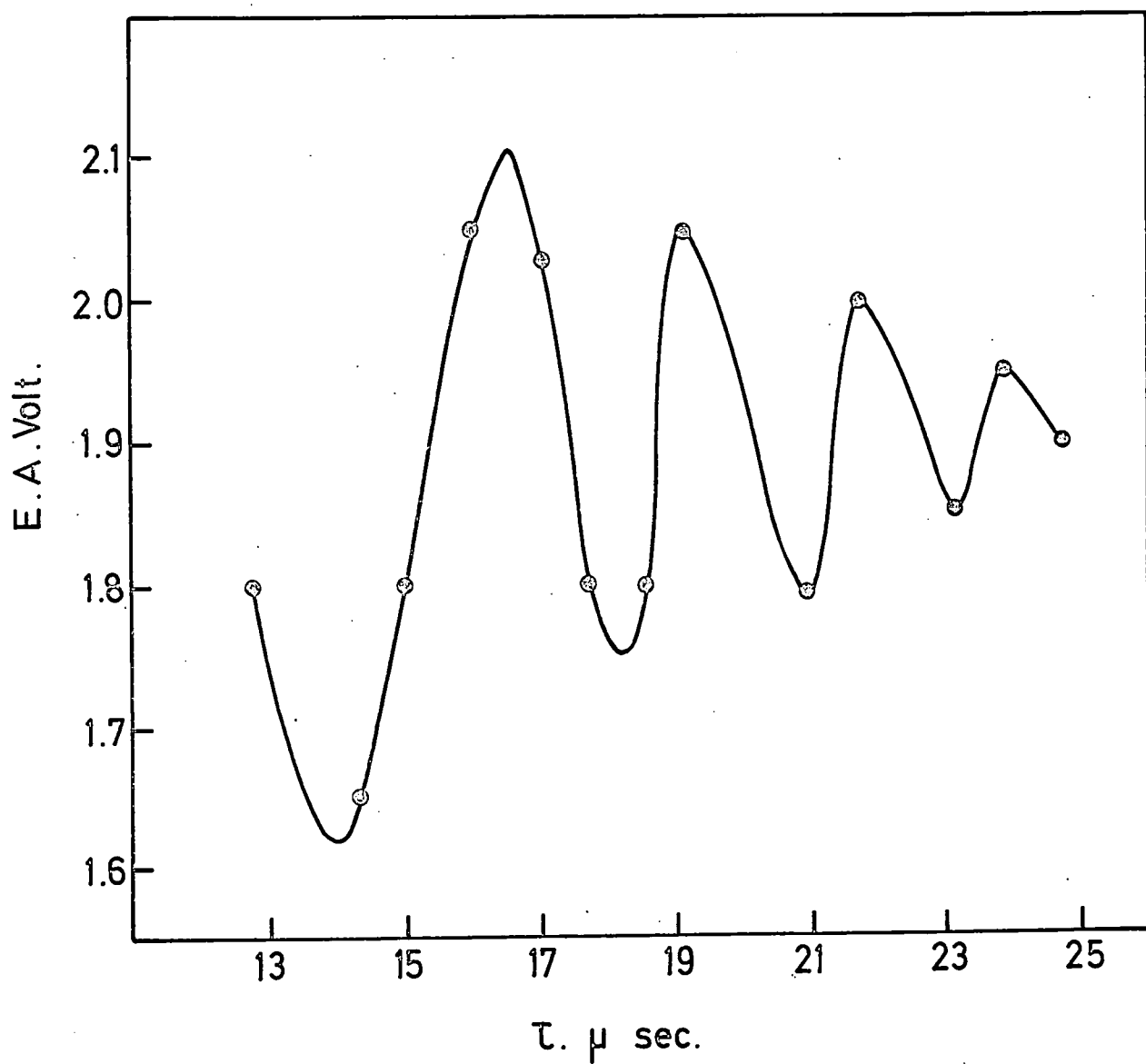
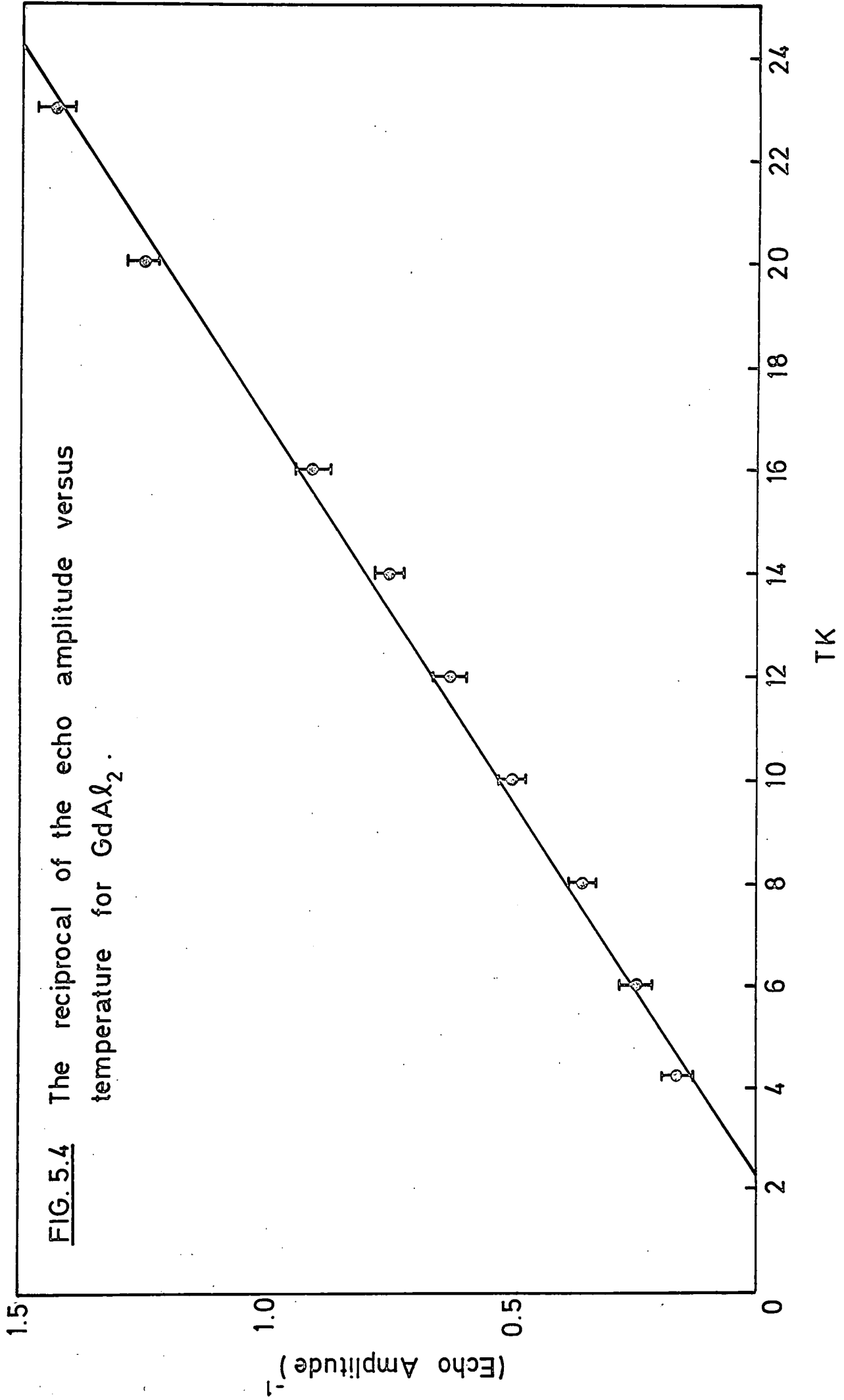


FIG. 5.4 The reciprocal of the echo amplitude versus temperature for $GdAl_2$.



in a free precession experiment is proportional to the macroscopic moment M . Thus the e.m.f. is proportional to ωM . Because M is proportional, in turn, to the microscopic moment multiplied by the nuclear polarization, the experimental echo intensity at each frequency is divided by the square of that frequency. Kobayashi (ref. 5.4) and Kubo (ref. 5.5) found that the observed distribution of the echo height against frequency was better corrected by a factor ω^3 .

In the present measurements we found that a better fit to experimental data was obtained by dividing the echo amplitude by ω^3 .

The observed echo amplitude, which is used to plot the resonance lineshape must, in theory, be corrected for signal reduction caused by relaxation effects. In other words the echo height at "zero time" must be calculated from an extrapolation of the relaxation-time graph to $2\tau = 0$. However, we have found that, in our samples, this correction does not alter the lineshapes significantly, so it has not been applied.

The spectra shown in figs. (5.5, 5.7) are corrected by ω^3 and smoothed twice according to

$$E^s(\nu) = \frac{1}{2} E(\nu) + \frac{1}{4} [E(\nu - 0.5) + E(\nu + 0.5)]$$

where 0.5MHz is the distance between the measuring points.

For $x = 0$, i.e., in pure $GdAl_2$ the ^{27}Al resonances (fig. 5.5) are found to be essentially in agreement with those reported by Shamir et al. (see chapter two). The two lines at about 49.5MHz, and 61.5MHz (half width = 2.2 MHz), with an intensity ratio of about 3 : 1, have been explained as being due to ^{27}Al nuclei at the two different sites in (111)

FIG. 5.5 $A\ell$ resonance in $Gd_{1-x}Y_xAl_2$; measured at 4.2K with $H_{ext}=0$, corrected and smoothed.

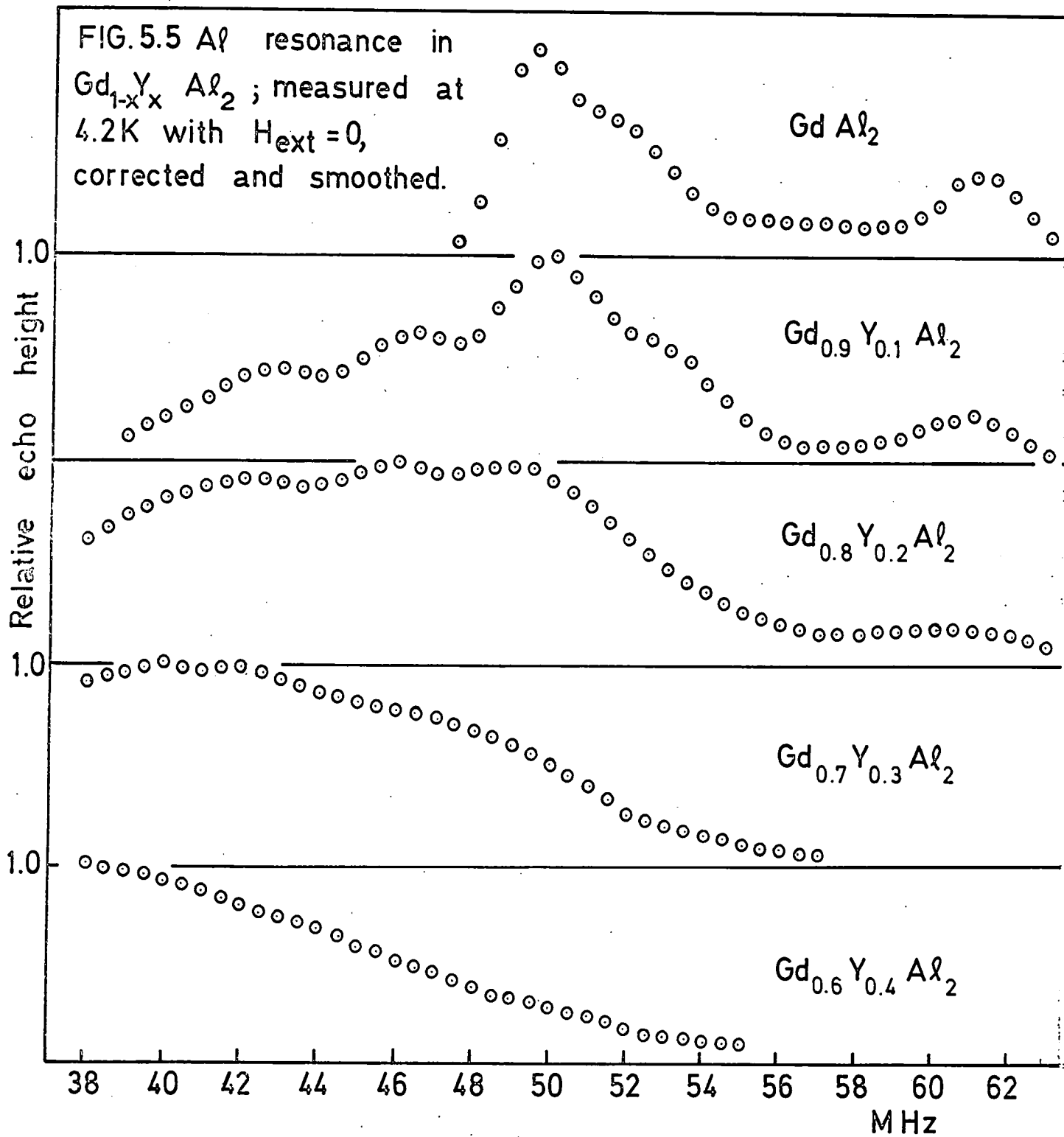


FIG. 5.6.A ρ resonance in $Gd_{1-x}La_xAl_2$ measured at 4.2K with $H_{ext} = 0$ corrected and smoothed.

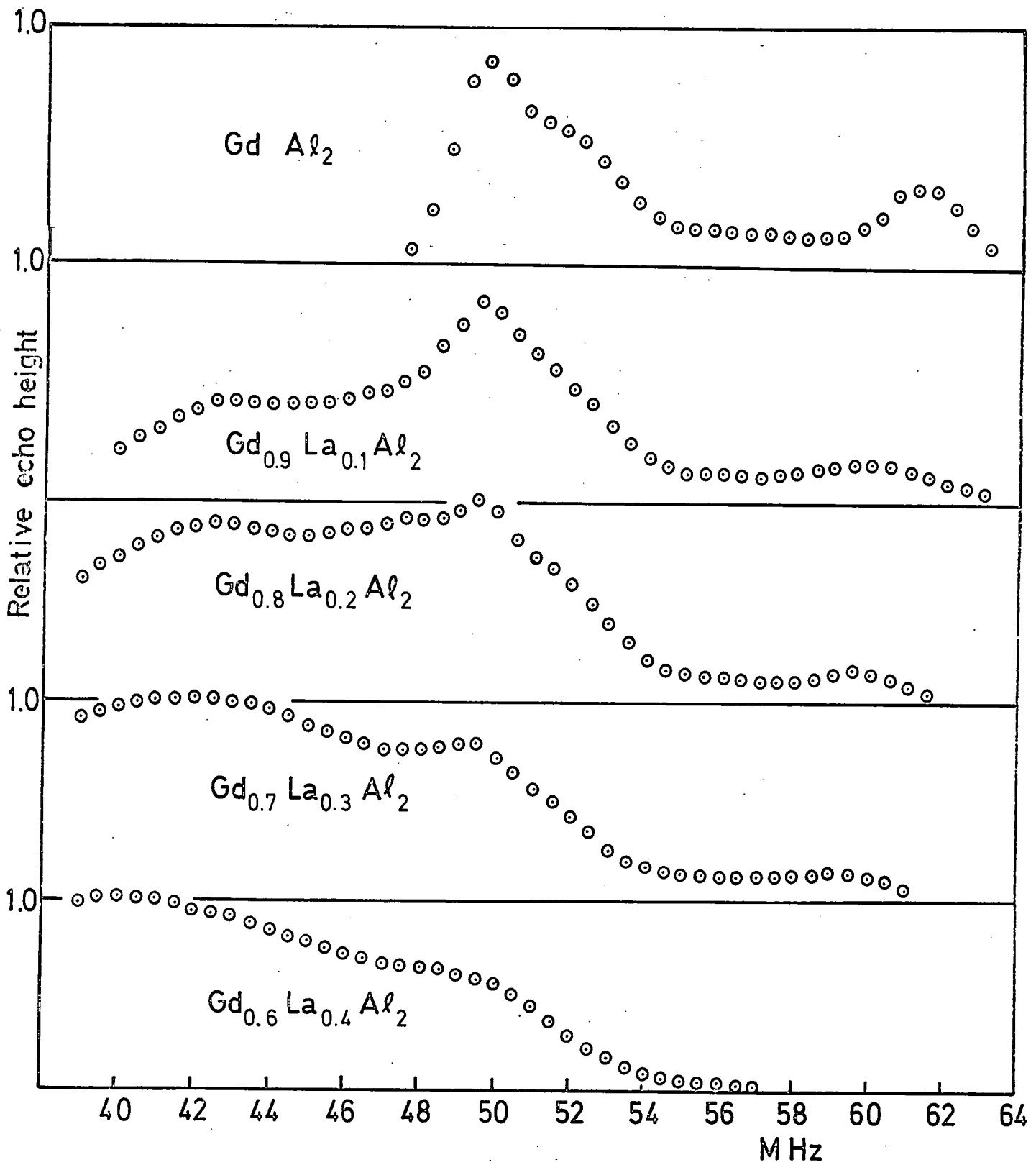
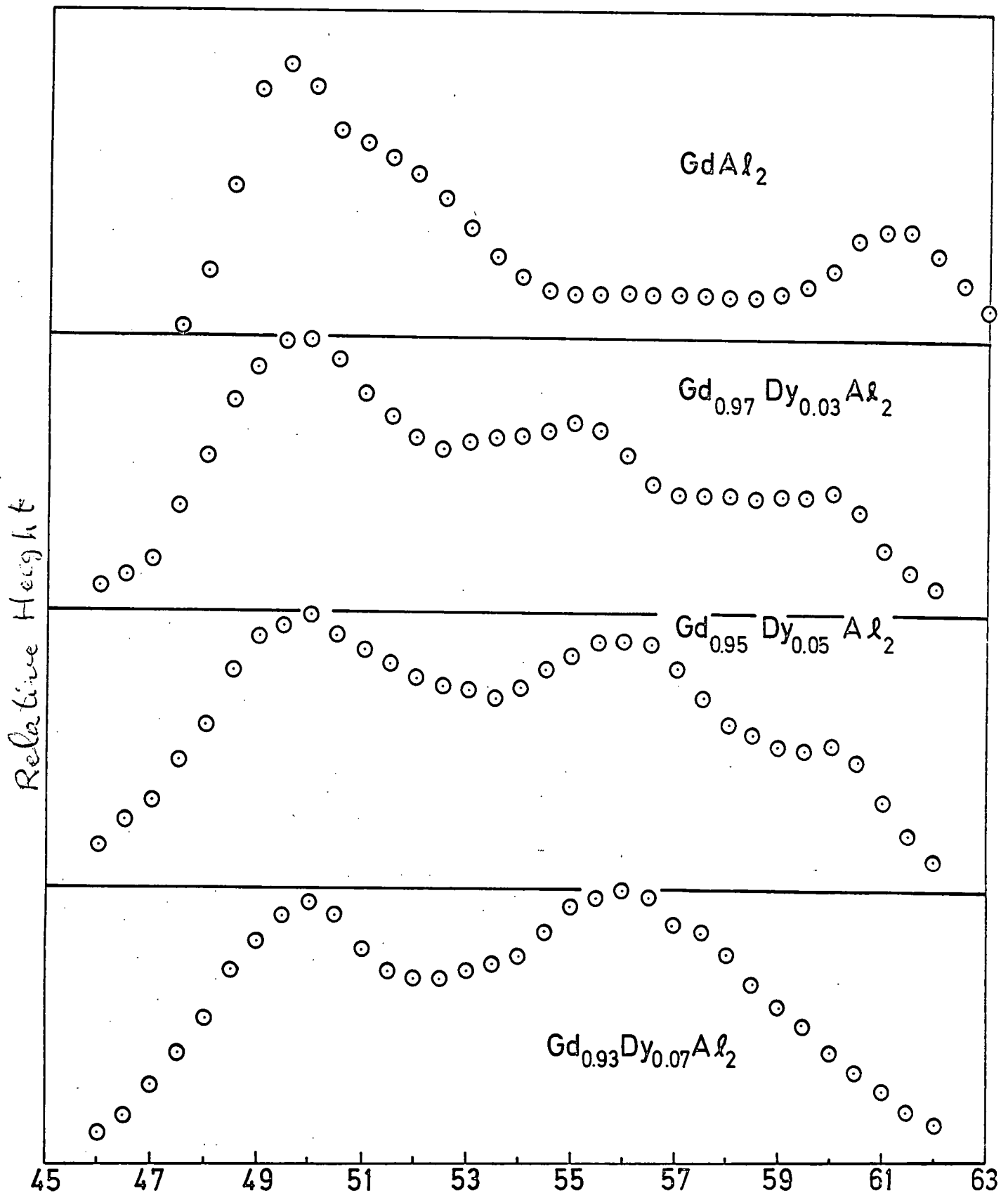


FIG.5.7 $A\ell$ resonance in $Gd_{1-x} Dy_x Al_2$ measured at 4.2 with $H_{ext} = 0$. Corrected and smoothed.



magnetized domains in $GdAl_2$. These two lines give a hyperfine field of about (47.2 ± 0.5) kOe (see chapter six). An additional line at about 52.2 MHz (≈ 47.1 kOe) with a half width of about 3.4 MHz and about 0.7 times as high as the lower line was observed. The Al resonances in $Gd_{1-x} Y_x Al_2$ are shown in fig. 5.5, and the corresponding spectra for $Gd_{1-x} La_x Al_2$ are given in fig. 5.6. In fig. 5.7 the Al resonance in $Gd_{1-x} Dy_x Al_2$ is presented. In the case of $Gd_{1-x} Y_x Al_2$ and $Gd_{1-x} La_x Al_2$ the higher Al resonance is smeared out, whereas the lower resonance lines obviously remain essentially unshifted and are supplemented by new resonances primarily at the low frequency side. At least two structure bumps can be seen at about 42-43 MHz and 45.5-46.5 MHz for small dilutions. This structure is more pronounced for the compounds with Yttrium. This may be due to the greater similarity between Gd and Y than between Gd and La.

It is clear from these results that the maximum of the Al resonance spectrum is not displaced linearly with x for low dilution in either the Y compounds or the La compounds. Nevertheless, the centre of gravity does follow a linear law i.e. $\nu_{cgr} = (1-x) \gamma H_{hf}(Al_2)$ within the experimental accuracy for the examples tested.

With small substitutions of dysprosium to the basic $GdAl_2$ compound, the echo amplitude was observed to decrease very rapidly and become unobservable for more than 7% Dy concentration. The Al resonance at 49.5 MHz is observable for all concentrations up to 7% Dy whereas the 61.5 MHz resonance has almost vanished at 5% Dy. An additional line is observed at

56.5 MHz as shown in fig. 5.7.

5.3.2 ACo₂

For the line shape measurements in these compounds we have used the same technique, with a pulse separation of about 10 μ S. No quadrupole oscillation was found in these compounds.

We have observed the signal from the Co nuclei in GdCo₂ as shown in fig. (5.8). The centre of the resonance is at about 61.3 MHz corresponding to the hyperfine field of 60.8 kOe. This result agreed with Taylor et al. (see chapter two). The result for HoCo₂ is shown in figure (5.9). In this case the spectrum shows two peaks, one at 51 MHz, and the other at 63.0 MHz. This spectrum is similar to that found in GdAl₂ and can be understood in term of two inequivalent cobalt sites in the unit cell. In TbCo₂ and NdCo₂ also, the centre of the resonance line is at 62.5 MHz, however the line intensities were too small to allow detailed observation. Other ACo₂ samples have been examined but no echoes have been found.

Measurements were also made on GdCo₂ as a function of temperature. The behaviour of the hyperfine field at the ⁵⁹Co nucleus as a function of temperature is shown in fig. (5.10). Over this temperature range the echo amplitude varies in an unexpected manner, decreasing rapidly from its value at 4.2 K before passing through a broad minimum at 40 K and a local (ref. 5.6) maximum at 79 K. Beyond this the amplitude falls monotonically. This variation of echo amplitude is shown in figure (5.11).

5.3.3 Gd(Co_{1-x} Al_x)₂ compounds

In this compound for $x = 0$ we can see the resonance of

FIG. 5.8 Co resonance in Gd Co₂ at 4.2 K. with H_{ext} = 0; corrected for sensitivity variation of spectrometer and smoothed.

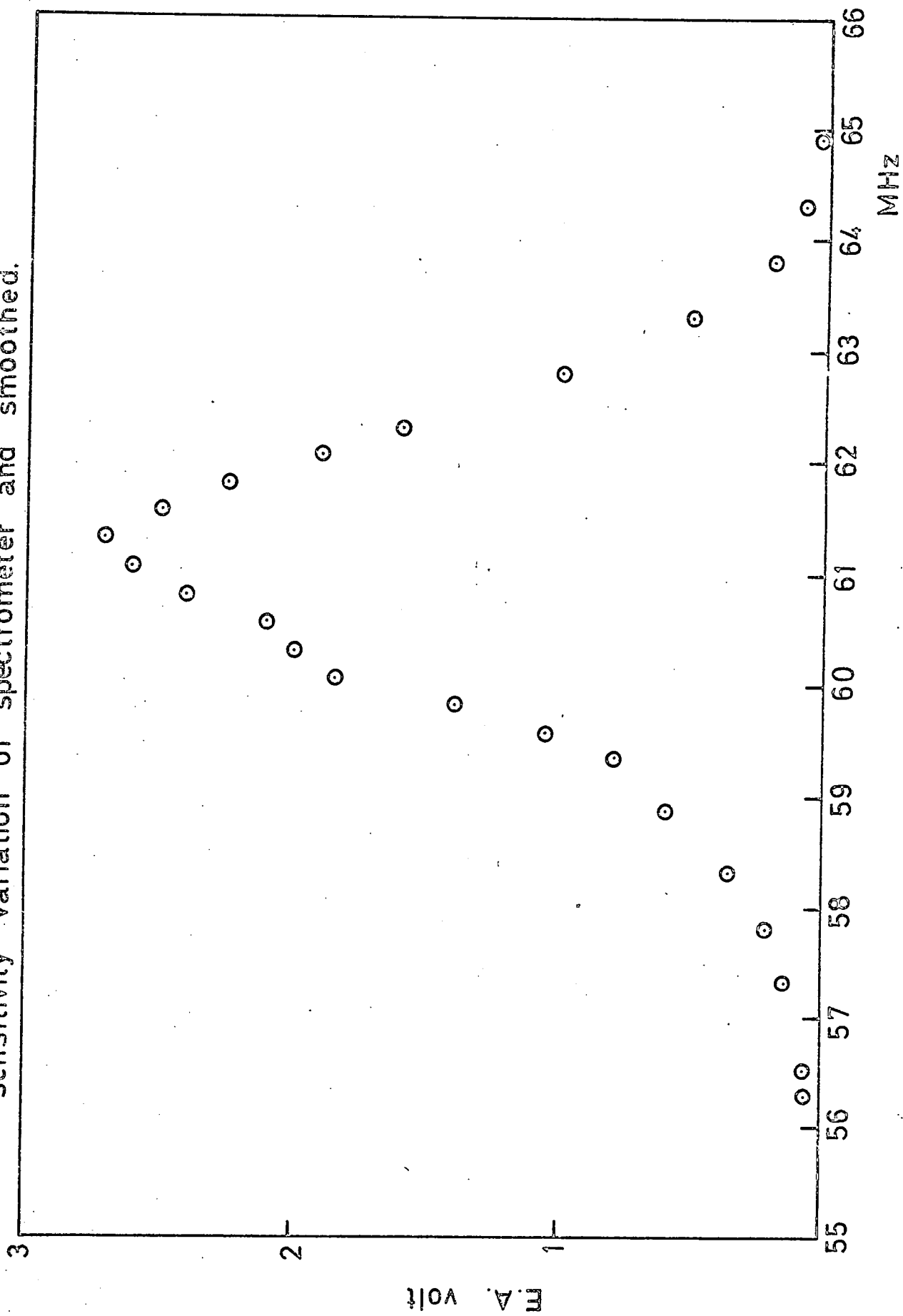


Fig. 5.9 Co resonance in HoCo_2 , TbCo_2 and NdCo_2 at 4.2°K and $H_{\text{ext}}=0$ corrected and smoothed.

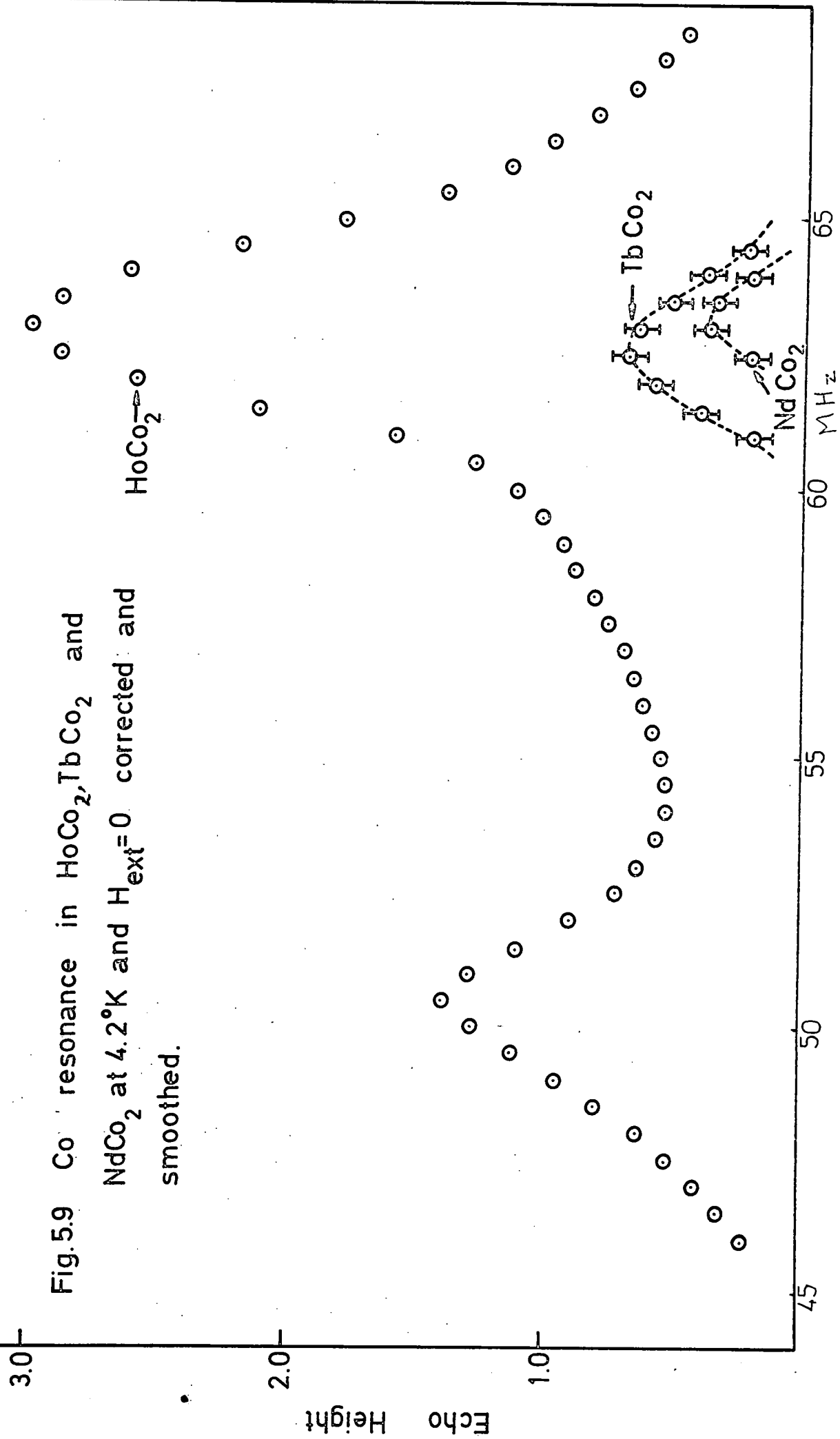
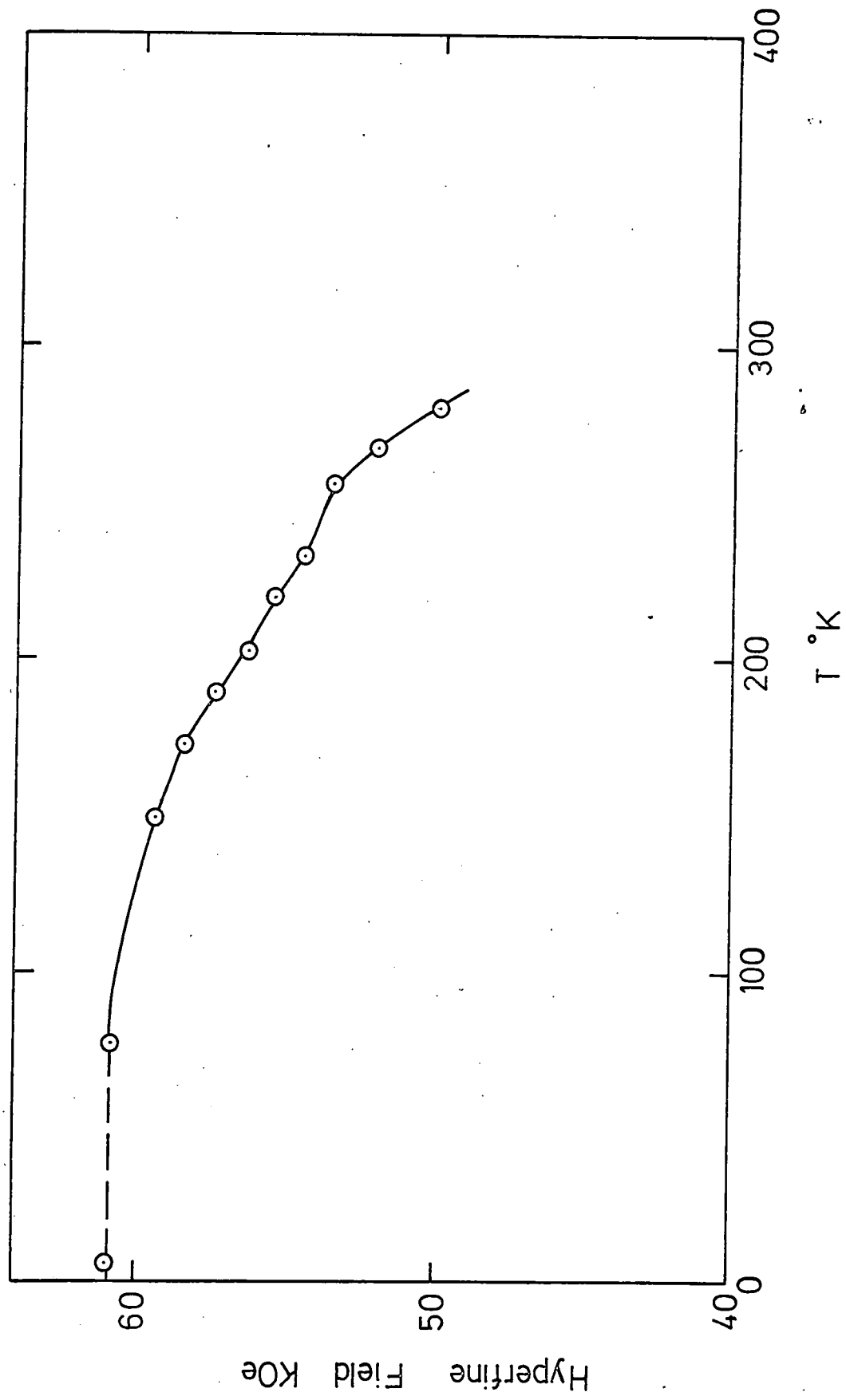


FIG. 5.10 OBSERVED HYPERFINE FIELD IN Gd CO₂ VS TEMPERATURE.



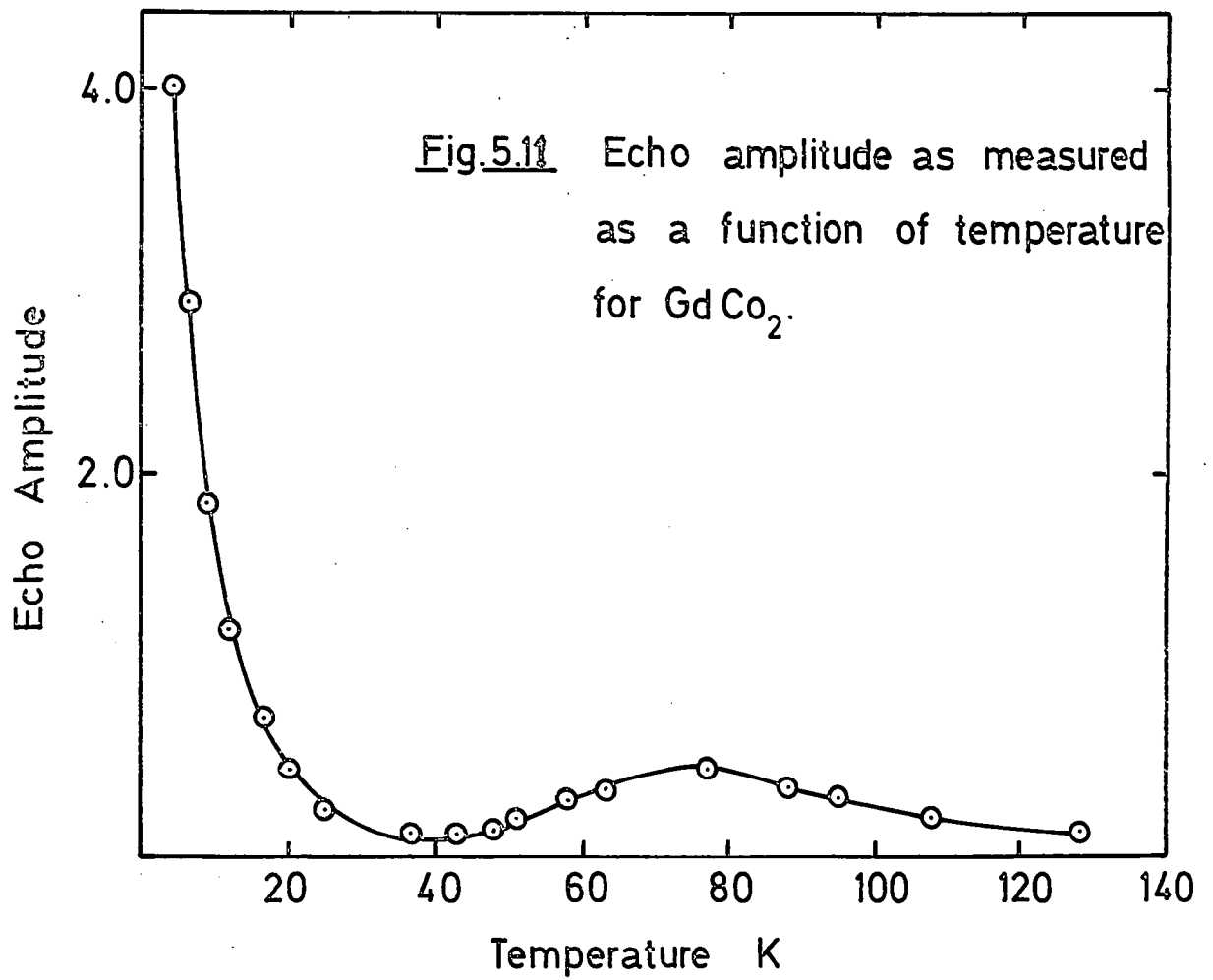


Table 5.4

Relaxation time T_2 and T_1

Compound	TK	Freq. MHz	T_2 μ sec.	T_1 μ sec.
GdAl ₂	4.2	49.5	450 \pm 40	2100 \pm 100
		61.3	520 \pm 40	2100 \pm 100
Gd _{0.9} Y _{0.1} Al ₂	4.2	49.5	420 \pm 40	1800 \pm 100
		61.3	300 \pm 40	
Gd _{0.8} Y _{0.2} Al ₂	4.2	49.5	400 \pm 40	1600 \pm 100
			150 \pm 40	
Gd _{0.7} Y _{0.3} Al ₂	4.2	49.5	400 \pm 40	1500 \pm 100
GdCo ₂	4.2	61.5	140 \pm 20	1800 \pm 100
	77	61.5	28	140 \pm 20

Co in GdCo_2 and for $x = 1$ the resonance of Al in GdAl_2 .

For $\text{Gd}(\text{Co}_{0.9}\text{Al}_{0.1})_2$, $\text{Gd}(\text{Co}_{0.8}\text{Al}_{0.2})_2$ and $\text{Gd}(\text{Co}_{0.7}\text{Al}_{0.3})_2$

the resonance is very broad with peaks centred at (42 - 43 MHz), (49.5 - 50.5 MHz), (55.5 - 56.5 MHz) and 61 MHz as shown in

fig. (5.12a). For $\text{Gd}(\text{Co}_{0.6}\text{Al}_{0.4})_2$, $\text{Gd}(\text{Co}_{0.5}\text{Al}_{0.5})_2$,

$\text{Gd}(\text{Co}_{0.4}\text{Al}_{0.6})_2$ and $\text{Gd}(\text{Co}_{0.3}\text{Al}_{0.7})_2$, we observed only one line the centre of which is at 38 MHz fig. (5.12b). Some

structure was observable in this line in the $\text{Gd}(\text{Co}_{0.5}\text{Al}_{0.5})_2$

specimen but disappeared with Al addition. For $\text{Gd}(\text{Co}_{0.2}\text{Al}_{0.8})_2$

and $\text{Gd}(\text{Co}_{0.1}\text{Al}_{0.9})_2$ the spectrum is similar to $\text{Gd}_{1-x}\text{Y}_x\text{Al}_2$ where

the structure at about (42 - 43 MHz) and (45.5 - 46.5 MHz) are observable in addition to another resonance at 56 MHz.

fig. (5.12c).

5.3.4 GdFe₂

An attempt has been made to observe the Gd resonance in previous compounds but without success. For GdAl_2 the frequencies of the Gd resonances have been found to be at 22 and 28 MHz (ref. 1.89) which is out of the range of our system.

For GdFe_2 we have observed the Gd resonance at 56.5 MHz (fig. 5.13). This frequency represents the ^{155}Gd hyperfine field of 470.8 MHz. The other resonance for the other ^{157}Gd isotope has not been seen.

5.4 Relaxation Measurements

The measurement of the spin-spin relaxation time, T_2 , was done for some of the compounds as given in table (5.4).

FIG. (5.12a)

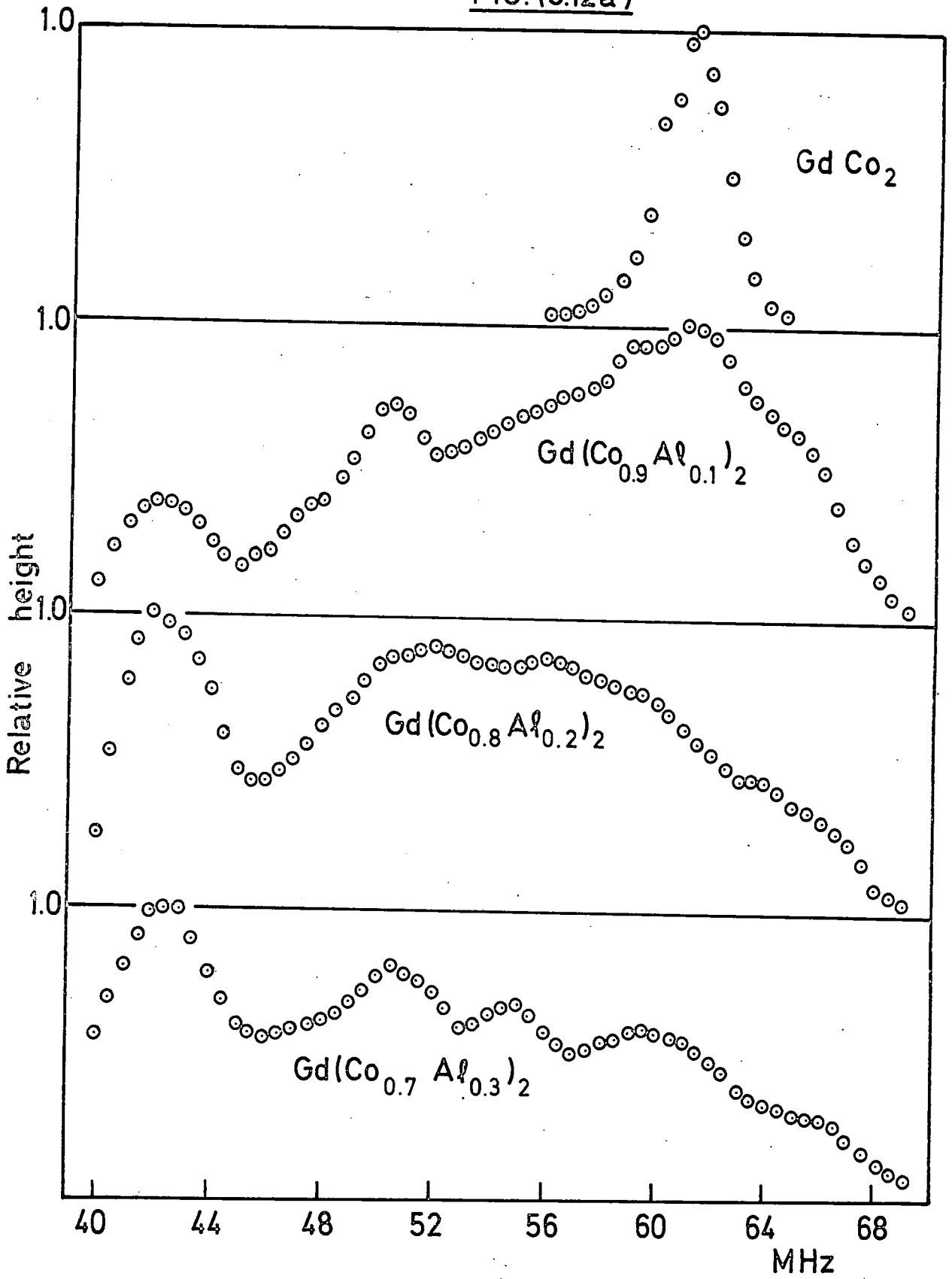


FIG. (512b)

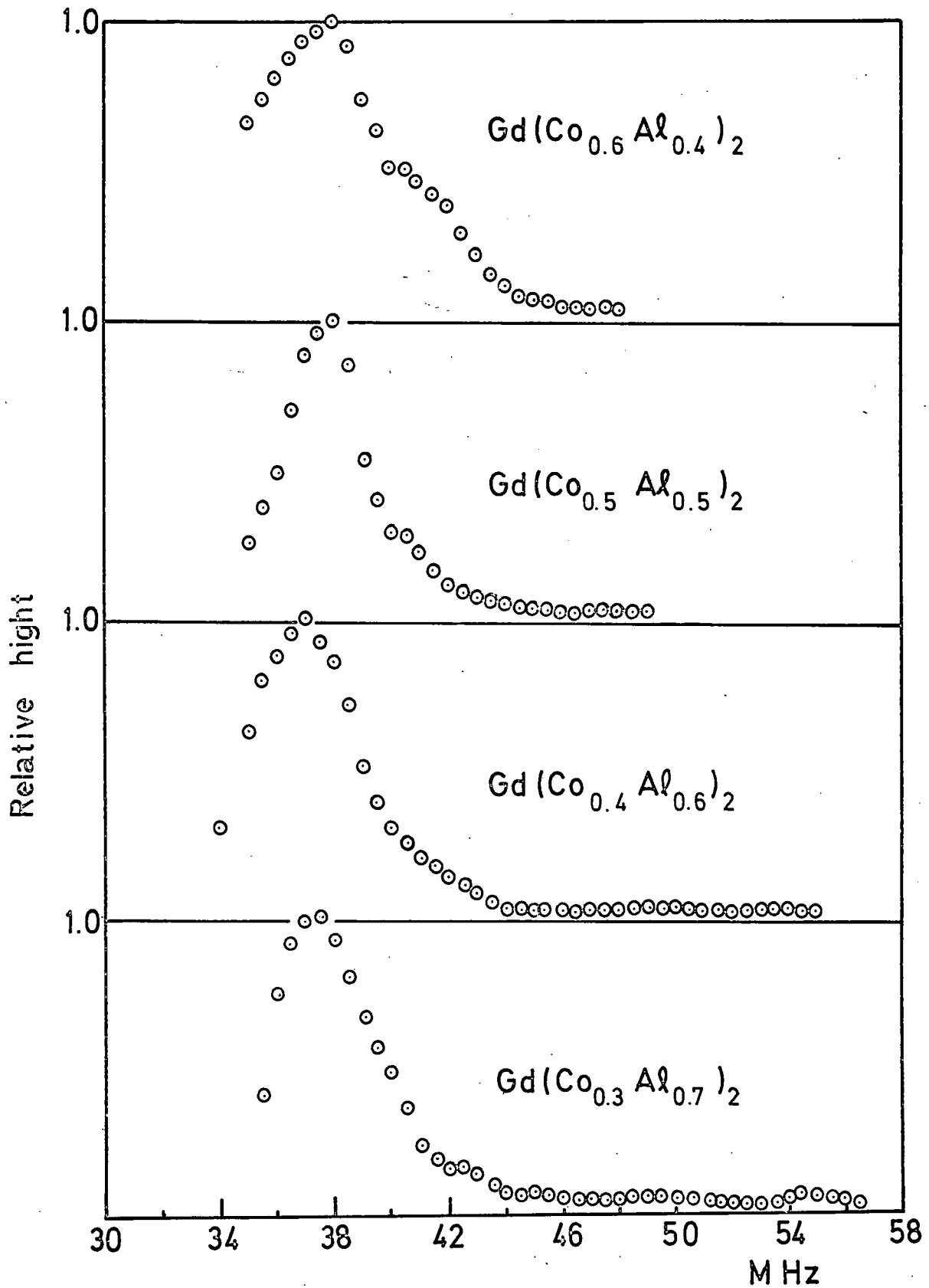


FIG. (5.12c)

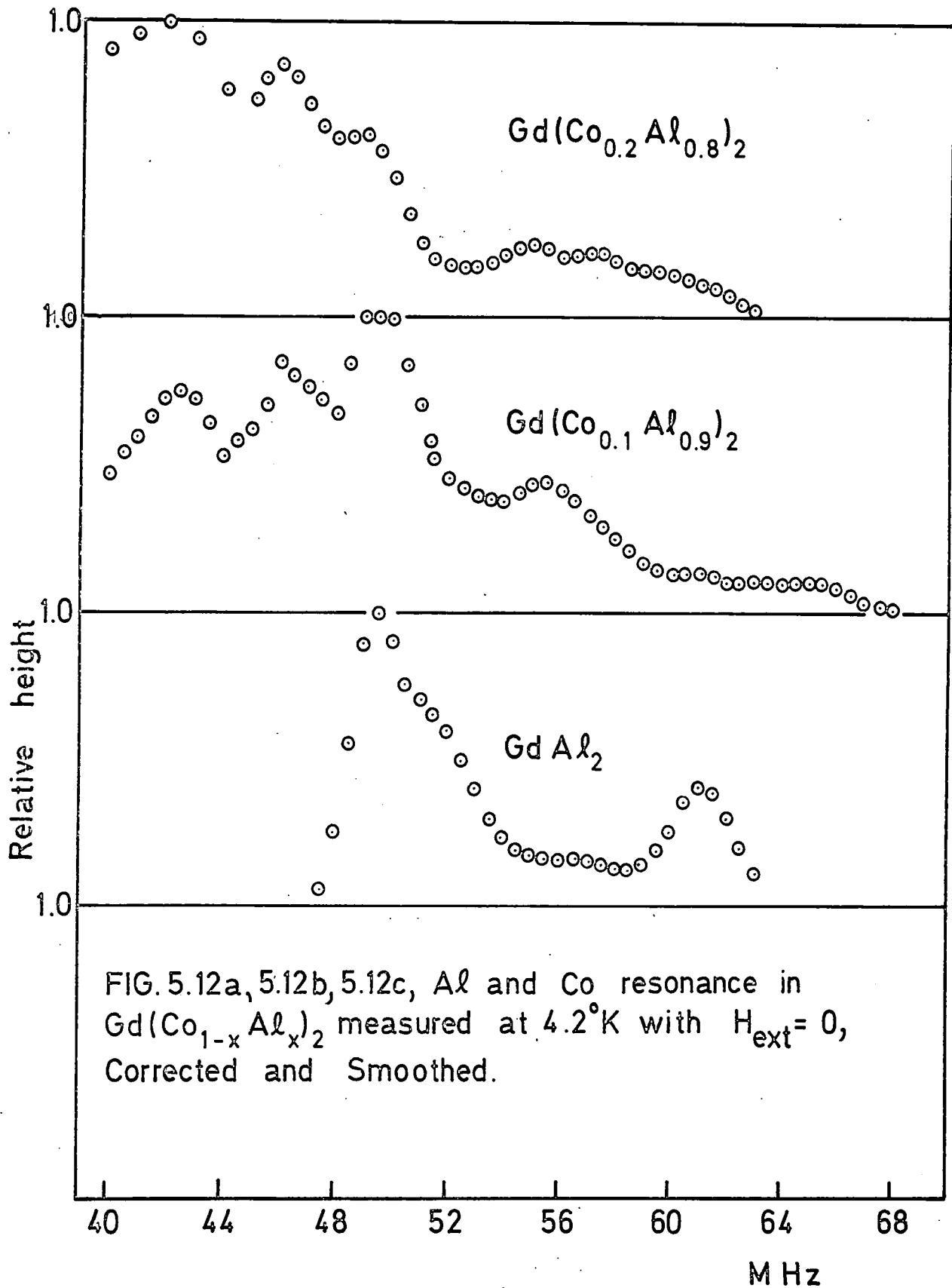
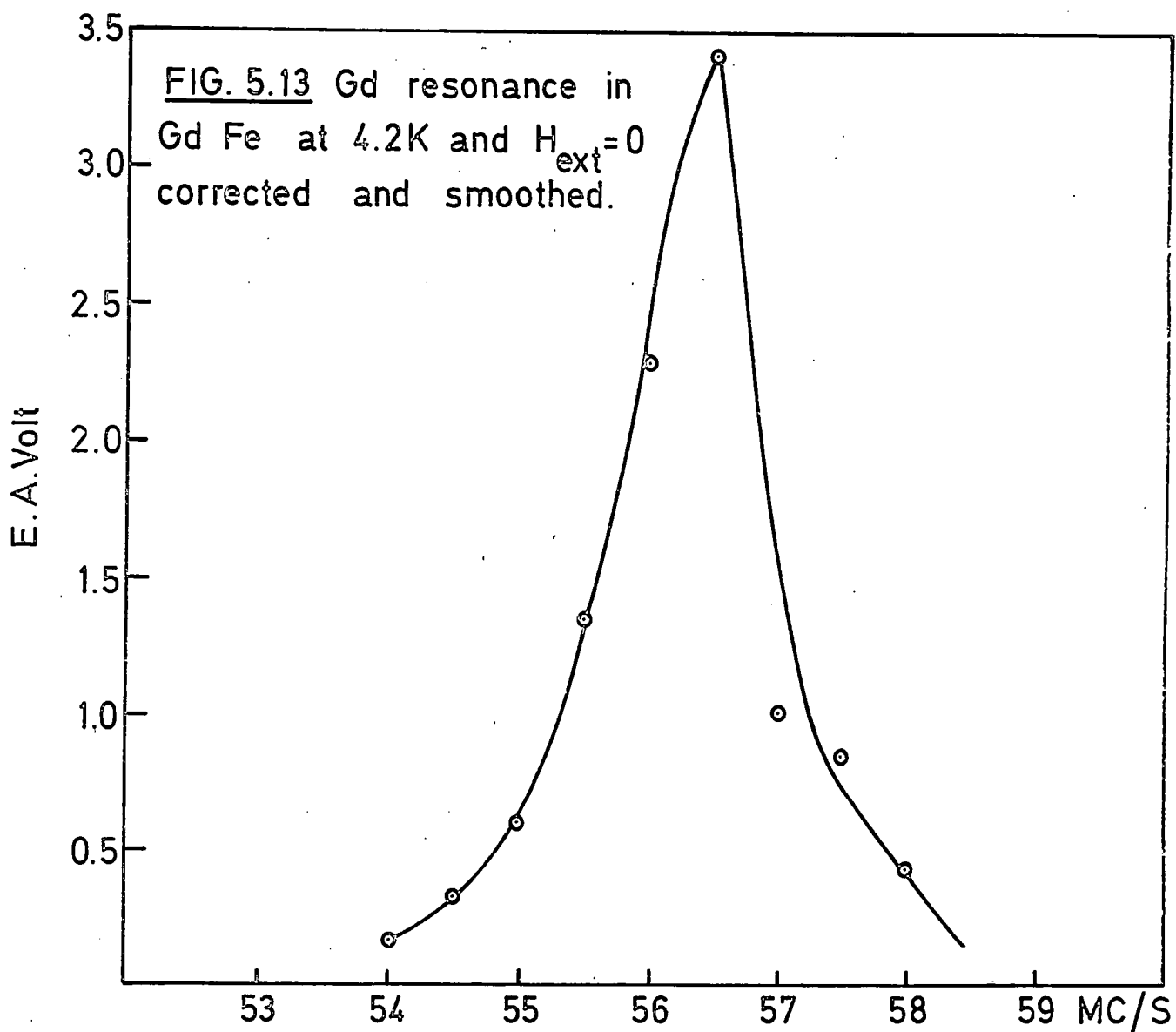


FIG. 5.12a, 5.12b, 5.12c, Al and Co resonance in $Gd(Co_{1-x}Al_x)_2$ measured at $4.2^\circ K$ with $H_{ext} = 0$, Corrected and Smoothed.



The height of the spin echo signal was measured by varying the time interval between the two pulses necessary to produce the echo, and the logarithm of the decay of the echo height was plotted against twice this time interval. It was found that the spin-spin relaxation follows a simple exponential function and T_2 is determined as the decay time of this exponential function, $\exp(-2\tau/T_2)$ (see chapter 3, eqn. 3.18). Figure (5.14) shows the logarithm of the echo amplitude versus 2τ which is a straight line, and the slope of this line gives the spin-spin relaxation time T_2 .

For $GdCo_2$, the variation of T_2 with temperature is shown in fig. (5.15). As can be seen, the form of this dependence is very similar to that of the echo amplitude fig. (5.11).

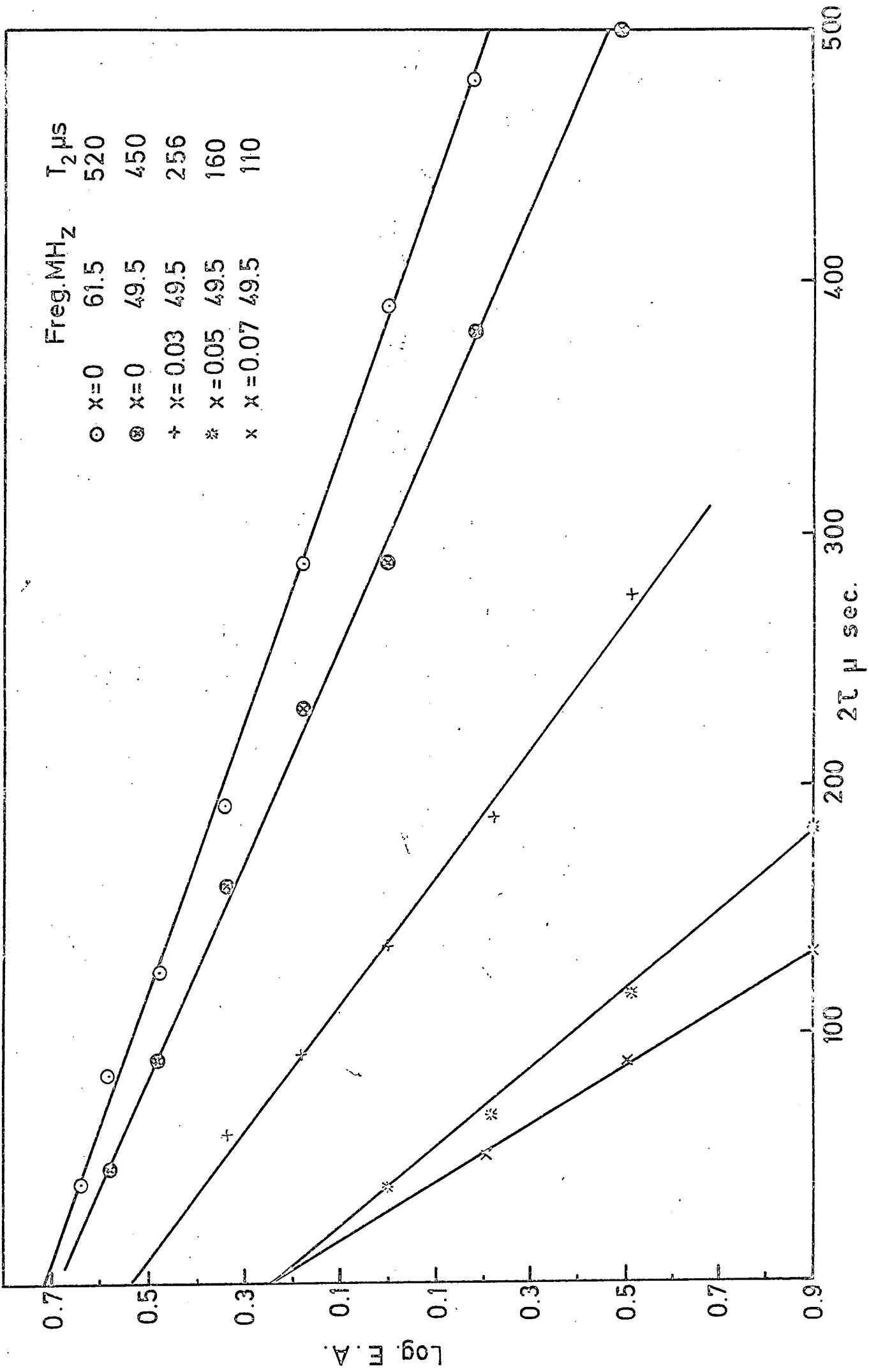
The spin-lattice relaxation time T_1 was measured by the stimulated echo method (see chapter 3, section 3.3.2), the separation between the first and second pulses was kept constant, while the delay of third pulse was varied. Fig. (5.16) shows the logarithmic decay curves of the stimulated echo amplitudes for the two resonance of ^{27}Al in ferromagnetic $GdAl_2$ compounds plotted against the time interval between the first and third pulses at 4.2 K.

The decay curves shown in fig. (5.16) are not simply exponential as predicted from the equation

$$V(SE) = V_0(SE)e^{-T/T_1}$$

so it is difficult to determine the spin-lattice relaxation time. The longest time-constant of such a graph is taken to be T_1 .

FIG. 5.14. Spin spin relaxation time measurements for $Gd_{1-x} Dy_x Al_2$



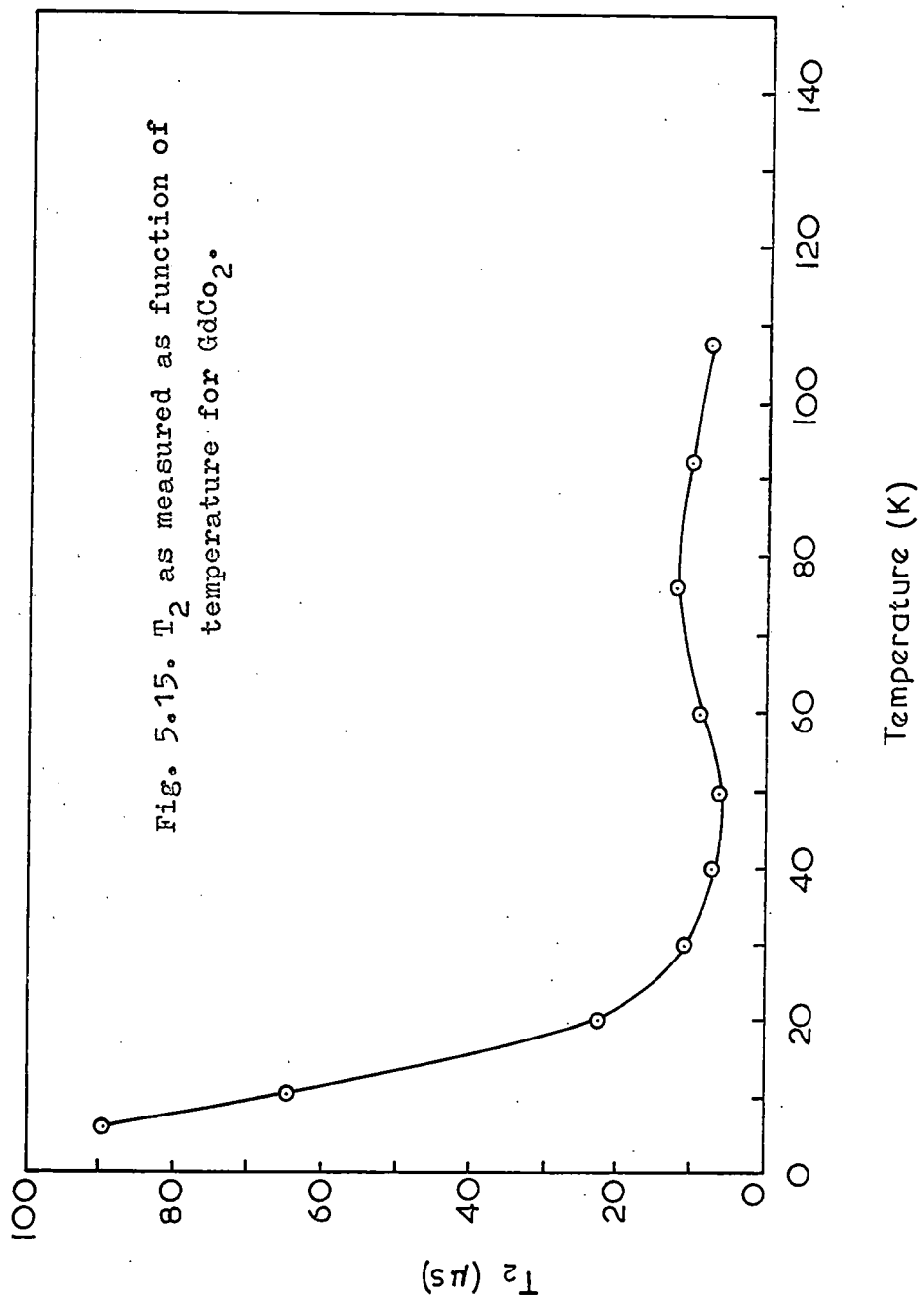
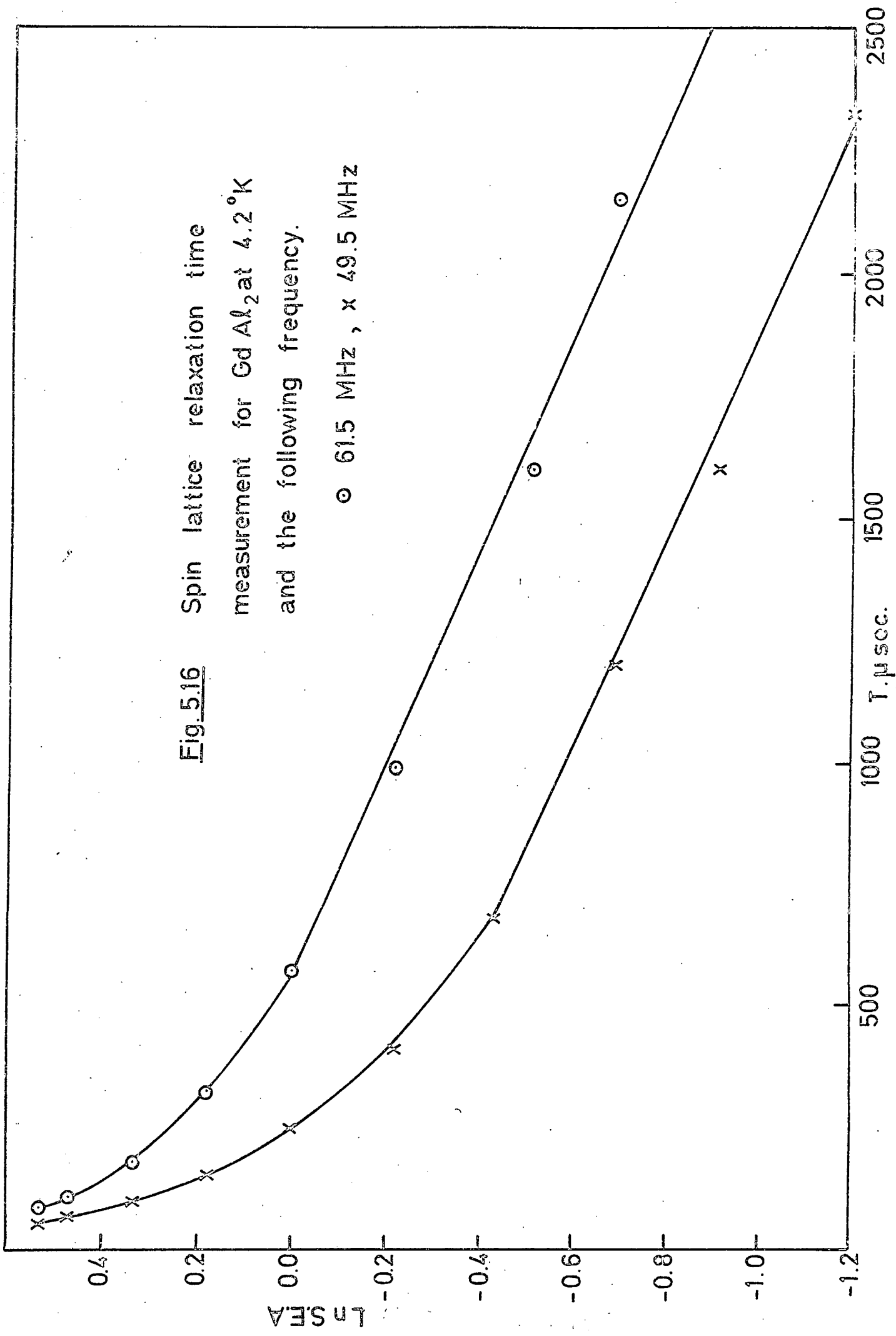


Fig. 5.16 Spin lattice relaxation time measurement for $GdAl_2$ at $4.2^\circ K$ and the following frequency.

○ 61.5 MHz, x 49.5 MHz



5.5 E.S.R. results

Electron spin resonance measurements have been performed to determine the line width and g-shift for $Gd_{1-x}Y_xAl_2$ using the system which is described in chapter 4. The magnetic field was calibrated with a D.P.P.H. sample. A typical spectrum for $GdAl_2$ is shown in fig. (5.17). In these compounds the power absorbed from an rf field is, to first order, proportional to a linear combination of the real and imaginary components of the susceptibility, i.e. $b\chi' + \chi''$. Both components involve line shape functions, which in this case are Lorentzian (see chapter 3, eqn. 3.28).

The derivative response is readily found to be of the form

$$\frac{dP}{dx} = K \left[\frac{b-2x-bx}{(1+x^2)^2} \right] + m(H-H_0) \quad (5.1)$$

where $x = (H-H_0)/\Delta H$, H_0 is the resonant field, ΔH is the half-power, half-line width. The $m(H-H_0)$ term is included to allow for any drift in the receiver during the resonance scan.

Analysis of the E.S.R. data makes use of a computer fitting program (Durham NUMAC Computer Library programme TPT9 : Lib) to plot directly onto the experimental data. It proved possible to adjust the parameters K , ΔH , b , H_0 and m to fit to the experimental curves. The results are shown in figs. (5.18, 5.19). In fig. (5.18) we present the temperature dependence of the line width in the paramagnetic region for different concentrations whereas in fig. (5.19) we present the temperature dependence of the line width as well as the g values for $Gd_{0.9}Y_{0.1}Al_2$ in the paramagnetic and in the ferromagnetic state.

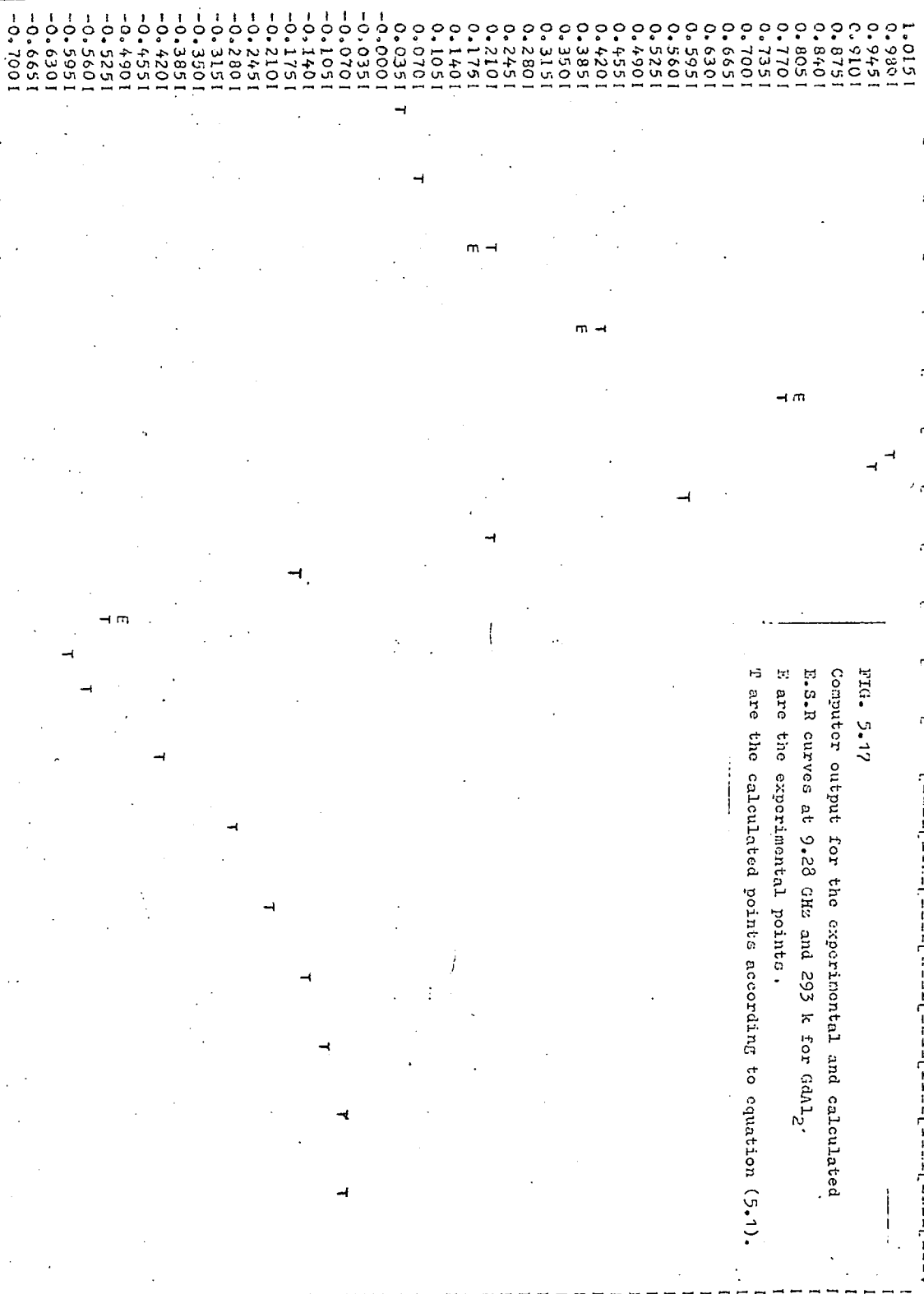


FIG. 5.17

Computer output for the experimental and calculated ESR curves at 9.28 GHz and 293 K for $GdAl_2$. E are the experimental points, T are the calculated points according to equation (5.1).

2360.5000 2660.5000 2960.5000 3260.5000 3560.5000 3860.5000 4160.5000 4460.5000 4760.5000 5060.5000

FIG. 5.18 The temperature dependence of the line width for different concentration as the following.

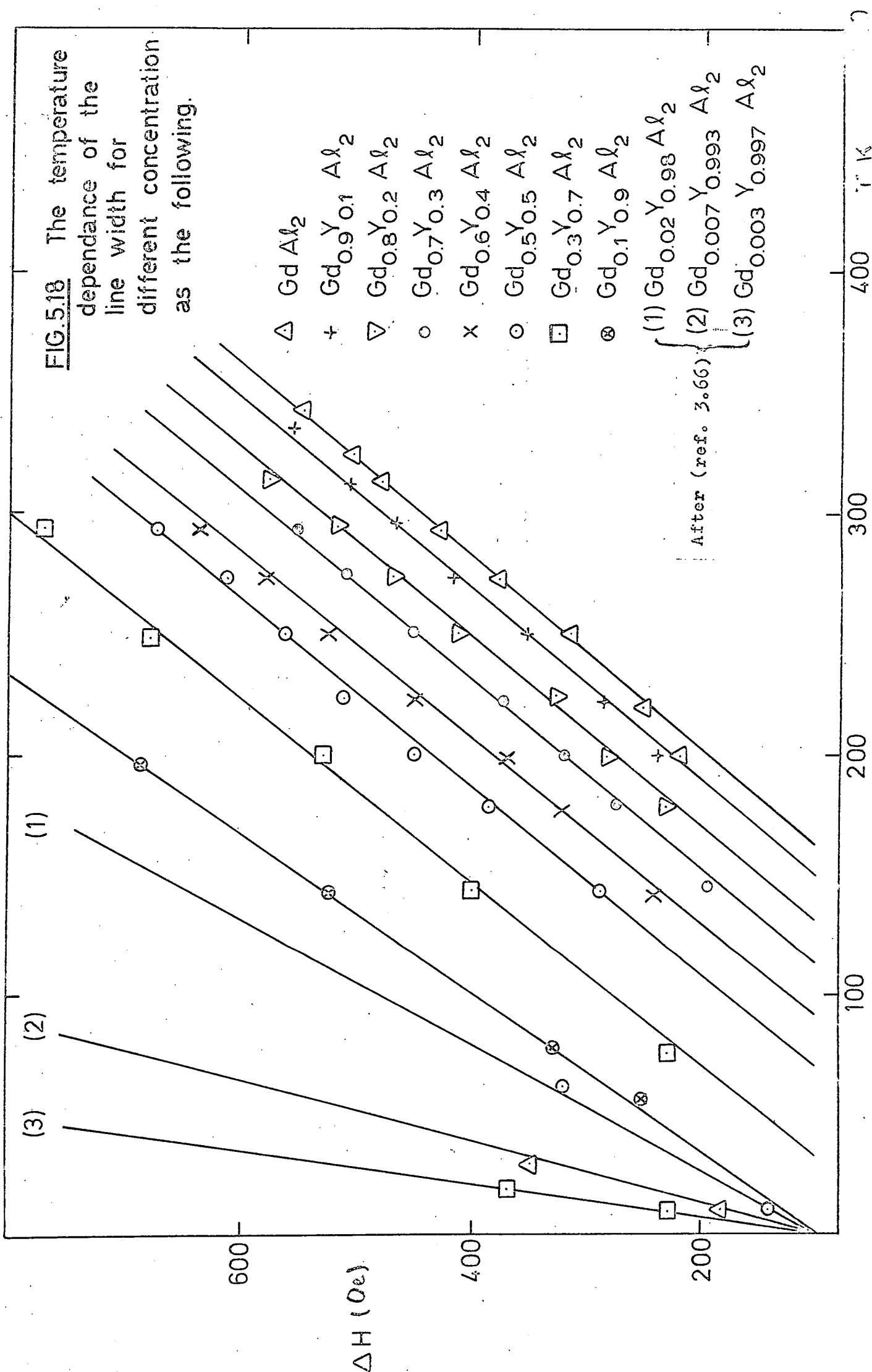
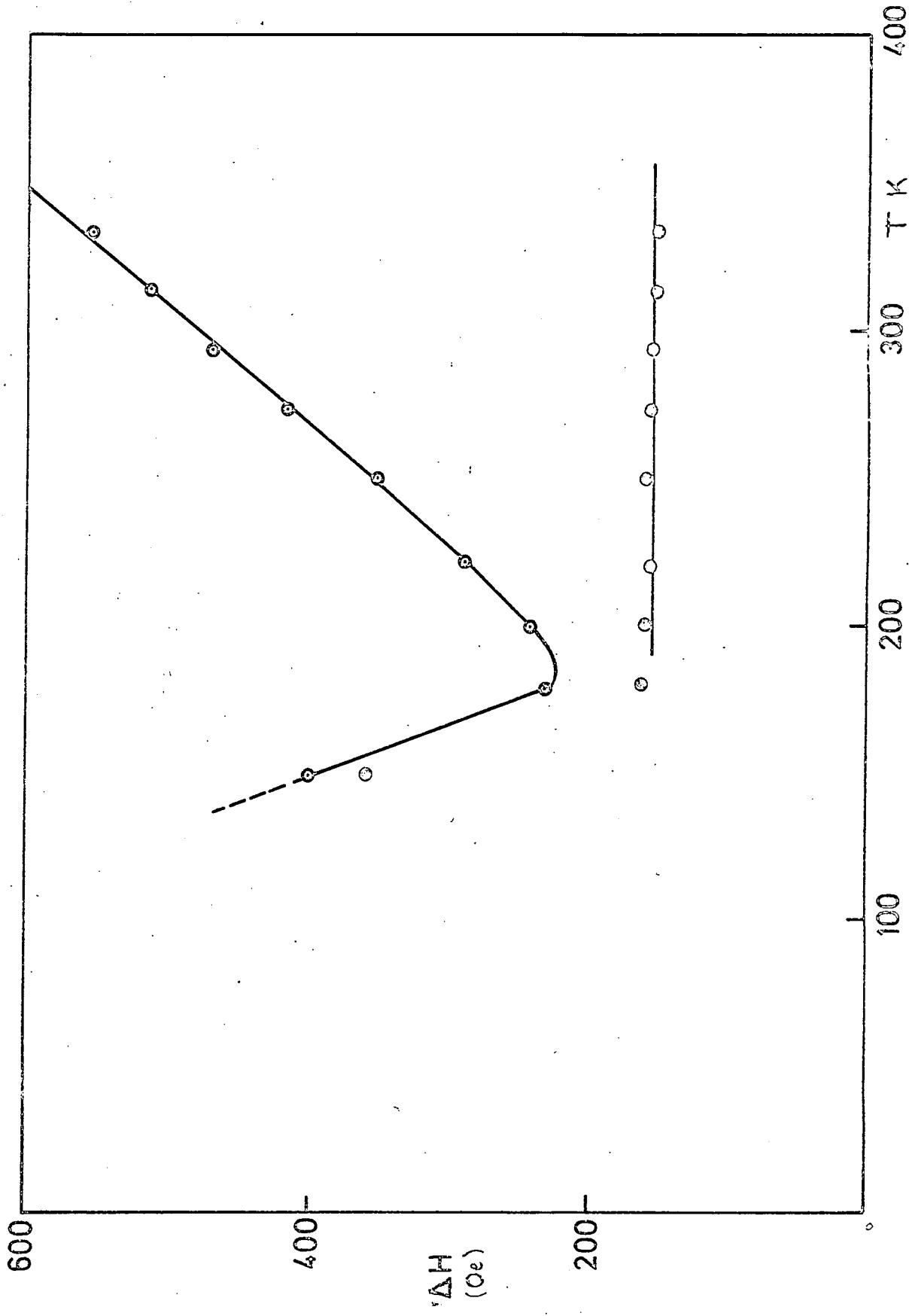


FIG. 5.19. The temperature dependence of the line width and g-values for $Gd_{0.9}Y_{0.1}Al_2$



CHAPTER 6

DISCUSSION OF RESULTS

On the basis of the information given in chapters 1, 2 and 3, we shall discuss in detail the results given in chapter 5.

6.1 $Gd_{1-x} Y_x Al_2$ and $Gd_{1-x} La_x Al_2$ Compounds.

6.1.1 The Lattice Parameter and the Curie Temperature.

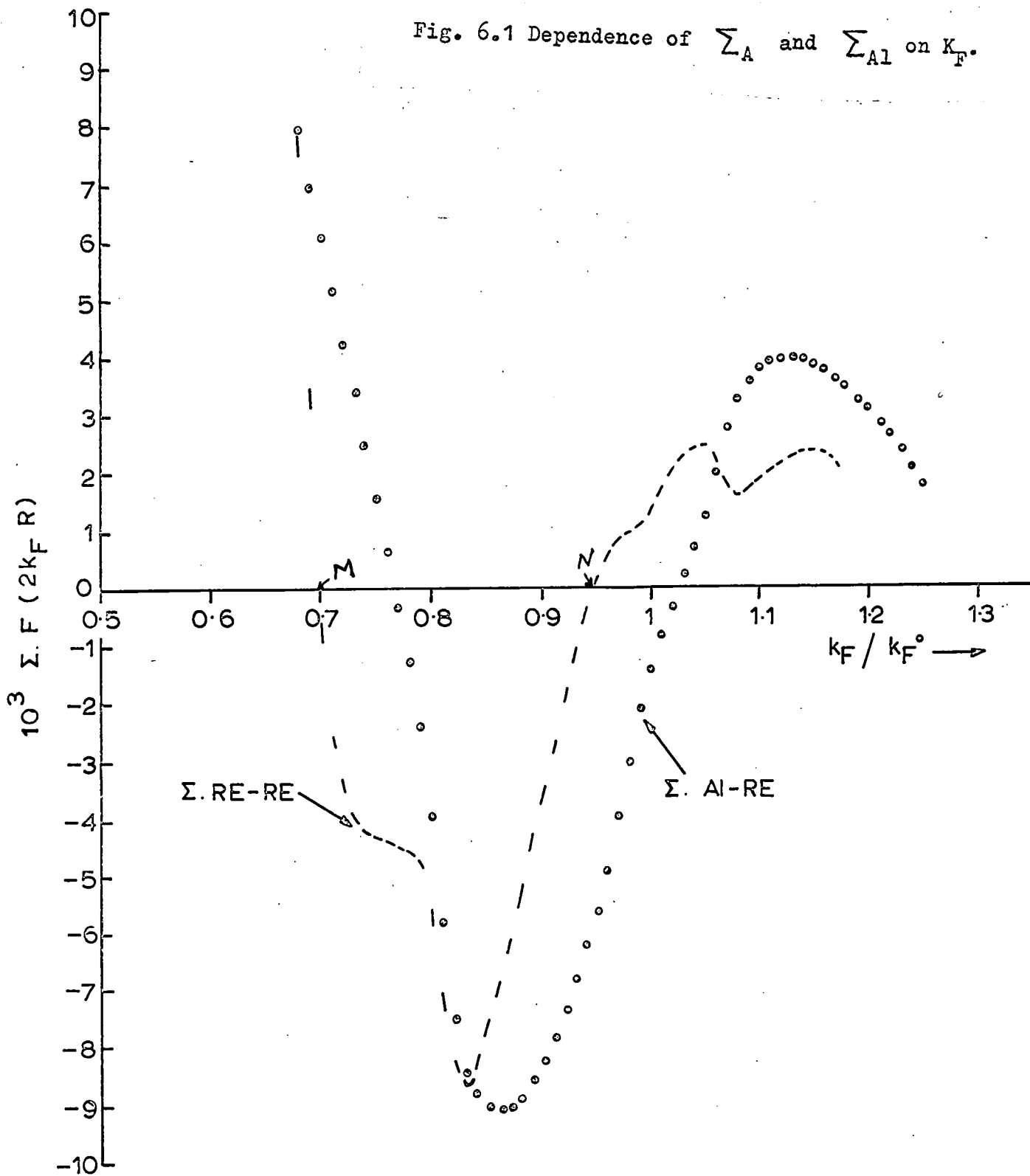
The variation of the lattice parameter in these compounds, given in tables (5.1, 5.2), follows Vegards law approximately, showing a dependence of the lattice parameter on the concentration. This variation suggests that there is substitutional replacement of Gd by Y or La in these compounds.

The Curie temperature as a function of composition is shown in fig. (5.1). It is seen in this figure that the decrease of the Curie temperature proceeds linearly with concentration x. This variation is in excellent agreement with the value obtained by Buschow et al. (ref. 2.21), their results having been shown in fig. (2.2), chapter two. The dependence of Curie temperature on the Y or La concentration can be understood in terms of the RKKY theory (chapter two) in which the Curie temperature is simply proportional to the average interaction of one rare earth ion with all other rare - earth ions and is given by

$$\Theta_p = - \frac{3\pi Z^2 \Gamma^2}{4K_B E_F} (g_j - 1)^2 J(J+1) \sum F(2K_F R_{nm}) \quad (6.1)$$

where the $\sum F(x)$ is defined in equation 2.2. The Fermi momentum is denoted by K_F and the summation is performed over all rare -

Fig. 6.1 Dependence of Σ_A and Σ_{A1} on K_F .



earth atoms n around a reference rare earth atom m . E_F is the Fermi energy. For the simplest Fermi surface model (the free electron gas) this energy is given by.

$$E_F = \frac{\hbar^2}{2m} K_f^2 \quad (6.2)$$

and the free-electron value of K_f is given by the expression $K_f^0 = (3\pi^2 N)^{1/3}$ where N is the number of conduction electron per unit volume Z/V . For $GdAl_2$, N is obtained under the assumption that each rare earth and each Al atom contributes three electrons to the conduction band and using the lattice constant $a = 7.900 \text{ \AA}$ then $K_f^0 = 1.63 \times 10^8 \text{ cm}^{-1}$. By assuming the wave vector K_f is given by $K_f^0 \times K_f'$, the summation $F(2K_f R_{nm})$ was computed as a function of K_f' (fig. 6.1) taking into account all rare earth atoms within a radius of 75 \AA . From the definition of K_f and the shell radius R_{nm} , $K_f \propto \frac{1}{a}$ and $R_{nm} \propto a$. The lattice parameter a does not affect, the $\sum F(2K_f R_{nm})$, since R_{nm} occurs only in the product $K_f \times R_{nm}$. From the relation (6.1), it can be seen that the sign of θ is independent of the sign of Γ , but depends on the sign of $\sum F(2K_f R_{nm})$. A positive value of θ indicates that this summation must be negative in these compounds. However, since $\sum F(2K_f R)$ must be negative to give a positive θ , it is obvious that the value of K_f must lie between the points M and N in fig. (6.1).

A numerical estimation of K_f and Γ in $GdAl_2$ has been found by several authors using different techniques, by solving the equations which are related to the techniques that have been used (chapter 2, section 2.2).

Returning to the dilution experiment in the $Gd_{1-x}Y_xAl_2$ and

$Gd_{1-x}La_xAl_2$, the addition of Y and La decreases the number of Gd atoms and hence the results could adequately be described by replacing the function $\sum F(2K_f R_{nm})$ in equation (6.1) by $(1-x) \sum F(2K_f R_{nm})$. In other words, the Curie temperature decreases from the value observed for $x = 0$, down to zero for $x = 1.0$. Experimentally this is the case for $Gd_{1-x}La_xAl_2$ and is a good approximation also for $Gd_{1-x}Y_xAl_2$.

6.1.2 N.M.R. Line Shapes

In chapter one we have discussed the magnetic hyperfine field in general and have defined the hyperfine field due to the conduction electron polarization given by equation (2.11) according to the RKKY theory. In this section, we will discuss the hyperfine field at the ^{27}Al nucleus in $Gd_{1-x}Y_xAl_2$ and $Gd_{1-x}La_xAl_2$ for $x = 0.1, 0.2, 0.3, 0.4$. The experimental results for these compounds are shown in figs. (5.5, 5.6) chapter 5. A simple physical model can account phenomenologically for the profiles in these figures. In this model the effective field at the aluminium nucleus can be represented by the equation.

$$H_{eff} = H_{hf} + H_d + H_{loc} \quad (6.3)$$

The first term H_{hf} arises from the contact interaction between the s-f exchange-polarized conduction electrons and the ^{27}Al nucleus. This equation has been given in chapter one to be

$$H_{hf} = \frac{9\pi Z A(0)}{4E_F g_I \mu_I} \langle S \rangle \sum F(2K_f R_{nm}) \quad (6.4)$$

The second term in equation (6.3) is the dipolar field and may be given by.

$$H_d = \sum_K \frac{(3\mu_K \cdot r_K)r_{iK}}{r_K^5} - \frac{\mu_{iK}}{r_K^3} \quad (6.5)$$

where r_K is the distance vector from the site considered to the Kth Gd site; μ_K is the magnetic moment associated with the Kth lattice site.

The third term in equation (6.3) represents the correction term for nonspherical domains. We shall assume spherical domains in order to make this term zero.

In chapter two we have discussed the easy direction of magnetization in the cubic Laves phase compounds $AA\ell_2$ and AFe_2 and also we have seen that in $AA\ell_2$ the easy direction can be determined directly from the experimental spin echo work by considering the number of lines in the spectrum and the intensity ratio of these lines.

In fact in the cubic Laves phase (fig. 1.6), when the magnetization M is pointing in an arbitrary direction, each of the four $A\ell$ sites in the tetrahedron, such as sites a, b_1, b_2, b_3 is subjected to a different magnetic dipolar field H_d . Thus, there are, in the general case, four magnetically inequivalent $A\ell$ sites. The number of inequivalent sites is reduced when the magnetization M is directed along one of (111), (110), and (100) directions as shown in fig. (2.3).

A computer program has been written to calculate the dipolar magnetic field for the cubic Laves phase using equation (6.5) for the three easy directions knowing the magnetic moment and the lattice parameter. This is demonstrated in table (6.1) where H_d is calculated with $\mu = 7\mu_B$ and the lattice parameter a ($GdAl_2$) = 7.90 Å. This calculation was achieved by extending

the summation in equation (6.5) over 75 \AA radius, including approximately 10.6×10^4 rare earth atoms.

Returning to the GdAl_2 experimental results, the spectrum consists of two peaks at 49.5 and 61.5 MHz and the ratio of the intensities of the two peaks is approximately 3:1. From this result and the above discussion, the easy direction of magnetization in GdAl_2 is (111) the low frequency peak being associated with the (b) sites and the high frequency peak with the (a) site. These two lines give the hyperfine field by solving the effective field ($H_{\text{eff}} = \nu/\gamma$ where ν is the frequency and $\gamma = 1.1094$) and using H_d values from table (6.1), where $H_d = 4.129 \text{ kOe}$ for the b atom and 7.074 kOe for the a atom, and using the following relation ref. (2.9).

$$H_{\text{eff}}(a) = H_{\text{hf}}(a) + H_d(a) \quad (6.6a)$$

$$H_{\text{eff}}^2(b) = H_{\text{hf}}^2(b) + H_d^2(b) - 2H_{\text{hf}}(b) H_d(b) \cos(H_{\text{hf}}(b), H_d(b)) \quad (6.6b)$$

We then find

$$H_{\text{hf}}(a) = 47.9 \pm 0.5$$

$$H_{\text{hf}}(b) = 47.0 \pm 0.5$$

These results reveal that the hyperfine field at both sites is essentially the same and thus the difference between the total effective fields must be caused by the difference in the dipolar fields. However, a more physical approach would be to solve equations (6.6a) and (6.6b) simultaneously for H_d and H_{hf} . Such a solution is possible if we assume $H_{\text{hf}}(a) = H_{\text{hf}}(b)$, because there is a simple relation between the dipole field at (a) and (b),

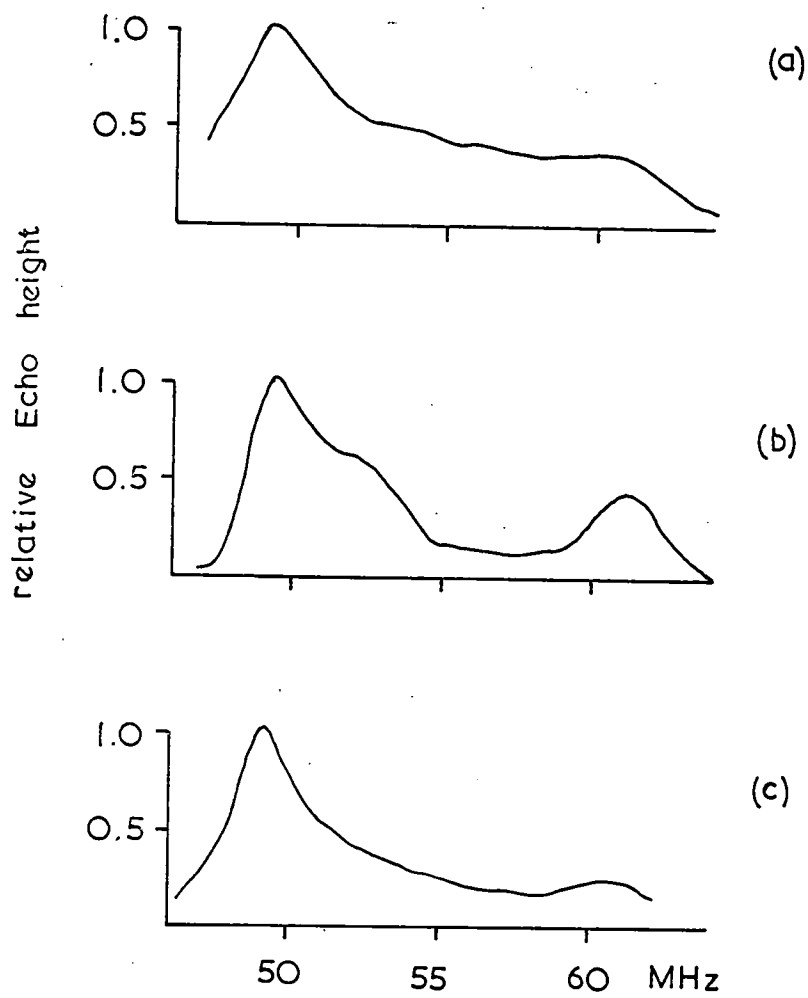


Fig. 6-2. ^{27}Al resonance in GdAl_2 at 4.2°K with $H_{\text{ext}} = 0$ for different grain sizes. (ref. 2.10); (a) $< 50\ \mu\text{m}$, (b) $\sim 60\ \mu\text{m}$, (c) $90\text{-}120\ \mu\text{m}$.

independent of the size of μ and given by

$$H_d(a) = \sqrt{3} H_d(b)$$

From these assumptions we get

$$H_d^{\text{Exp.}}(a) = 8.02 \text{ kOe}$$

$$H_d^{\text{Exp.}}(b) = 4.63 \text{ kOe}$$

$$H_{hf} = 47.38 \text{ kOe}$$

This value of H_{hf} is the same as the above value within $\pm 2\%$. The experimentally - measured values of $H_d(a)$ and $H_d(b)$ are, however, some 13% greater than the calculated values shown in table (6.1).

Before turning to the diluent compounds a final note is necessary concerning the line shape in GdAl_2 . As seen in fig. (6.2), ref. (2.10), the ^{27}Al lineshape depends on sample grain size. In fig. 6.2c a stronger decrease of signal height with frequency is observed, probably due to a mean particle radius exceeding the skin depth. Relatively long grinding treatments result in a finer powder (fig. 6.2a) which is found to cause line broadening and increase the back ground level. For these specimens the spectrum contains signals other than the pure (111) domain resonances. With increasing deformation of the powder particles the line due to the a sites (61.15 MHz) can be found to shift to frequencies below 60 MHz. Apart from a background intensity of about 10% between the two (111) domain nuclei resonances, we have observed (with 60 μm particles) an additional line at about 52.2 MHz ($\approx 47 \text{ kOe}$) with a half width of about 3.4 MHz and about 0.7 times as intense as the b line

Table 6.1 Computed values of the dipolar field at $A\ell$ sites in $GdAl_2$ (in kOe)

Direction	site	$H_d(x)$	$H_d(y)$	$H_d(z)$	Hd	$\cos(H_d, H_{hf})$
(1,1,1)	(5,5,5)	-4.084	-4.084	-4.084	7.074	1
	(5,7,7)	4.129	0.019	0.019	4.129	$-1/\sqrt{3}$
	(7,5,7)	0.019	4.129	0.019	4.129	$-1/\sqrt{3}$
	(7,7,5)	0.019	0.019	4.129	4.129	$-1/\sqrt{3}$
(110)	(5,5,5)	-2.506	-2.506	-5.004	6.132	$1/\sqrt{3}$
	(5,7,7)	2.535	2.515	0.030	3.571	-1
	(7,5,7)	2.515	2.535	0.030	3.571	-1
	(7,7,5)	-2.499	-2.499	5.040	6.156	$1/\sqrt{3}$
(100)	(5,5,5)	-0.000	-3.538	-3.538	5.004	0
	(5,7,7)	0.019	3.567	3.567	5.044	0
	(7,5,7)	-0.009	3.567	-3.517	5.009	0
	(7,7,5)	-0.009	-3.517	3.567	5.009	0

(fig. 6.2b). The line position corresponds to the resonance field of domain nuclei with no dipolar shift and could be due to ^{27}Al nuclei in (100) domains for which the dipolar field (≈ 5.0 kOe, table (6.1)) is perpendicular to the hyperfine field (≈ 47.2) kOe) and therefore induces only a very small difference between the absolute values of H_{eff} and H_{hf} . As we have seen in chapter two the (100) domains are observed in several of the other AAAl_2 compounds and may be present in GdAl_2 as closure domains or in distorted regions.

From the above discussion the hyperfine field at ^{27}Al in GdAl_2 is 47.2 kOe for the three peaks which may be described by rewriting equation (6.4) as follows:

$$H_{\text{hf}}(\text{RKKY}, x = 0) = C \langle S \rangle \sum F(2K_{\text{f}}R_{\text{nm}}) = -47.2 \text{ kOe} \quad (6.7)$$

where $C = 9\pi Z^2 \Gamma A(0) / 4 E_{\text{F}} g_{\text{I}} \mu_{\text{I}}$

The summation in this equation is different from that in equation (6.1). In this equation R_{nm} represents the distance between a rare earth ion and an aluminium site. We have calculated this summation in a similar way to the other summation as a function of the wave vector K_{f} as shown in fig. (6.1).

The average hyperfine field for the magnetically diluted samples ($x \neq 0$) will then be given by

$$H_{\text{hf}}(\text{RKKY}, x \neq 0) = (1-x) C \sum F(2K_{\text{f}}R_{\text{nm}}) \langle S \rangle \quad (6.8)$$

provided that Z , E_{F} , and $A(0)$ do not depend on x . This is true within the free electron model as Gd, La, Y and Al all supply three conduction electrons but it is at best a crude approximation in the real system.

In order to obtain expressions for the concentration dependence of the hyperfine fields, we must take account of the

different configurations arising from the variety of possible occupations of the Gd neighbour shells and the corresponding statistical weights. The numbers of Gd sites in the nearest Gd shells around the Al atoms in $GdAl_2$ are

$$Z_1 = 6 \quad R_1 = \frac{1}{8} \sqrt{11} a, \quad Z_2 = 8 \quad R_2 = \frac{1}{8} \sqrt{27} a$$

$$Z_3 = 6 \quad R_3 = \frac{1}{8} \sqrt{43} a \quad Z_4 = 18 \quad R_4 = \frac{1}{8} \sqrt{59} a \dots \text{see}$$

appendix 1.

Since a gadolinium atom situated in a shell outside the third nearest neighbour shell contributes less than 1% to the sum in equation (6.7), we took as a first approximation.

$$H_{hf}(RKKY, x, n_1, n_2, n_3) = C \langle S_Z \rangle \left(n_1 F(2K_f R_1) + n_2 F(2K_f R_2) \right. \\ \left. + n_3 F(2K_f R_3) + (1-x) \sum_{\substack{l > 4 \\ l < 25}} N_l F(2K_f R_l) \right) \quad (6.9)$$

The relative amplitude of each configuration was assumed to be given by the binomial distribution, because of the randomness of the impurities; that is:

$$P(x, n) = \binom{N}{n} x^n (1-x)^{N-n} \quad ; \quad \binom{N}{n} = \frac{N!}{n!(N-n)!}$$

is the probability for an Al atom to be surrounded by n Gd neighbours, x is the concentration, N is the total number of Gd sites in the shells being considered (N=20 for three shells) and $\binom{N}{n}$ is the binomial coefficient. If there are N atomic sites available in i shell (i = 1, 2, 3, ..., n), and if there are n atoms (n ≤ N) to occupy them, then the probability that the ith shell contains ni atoms is:

The Probability

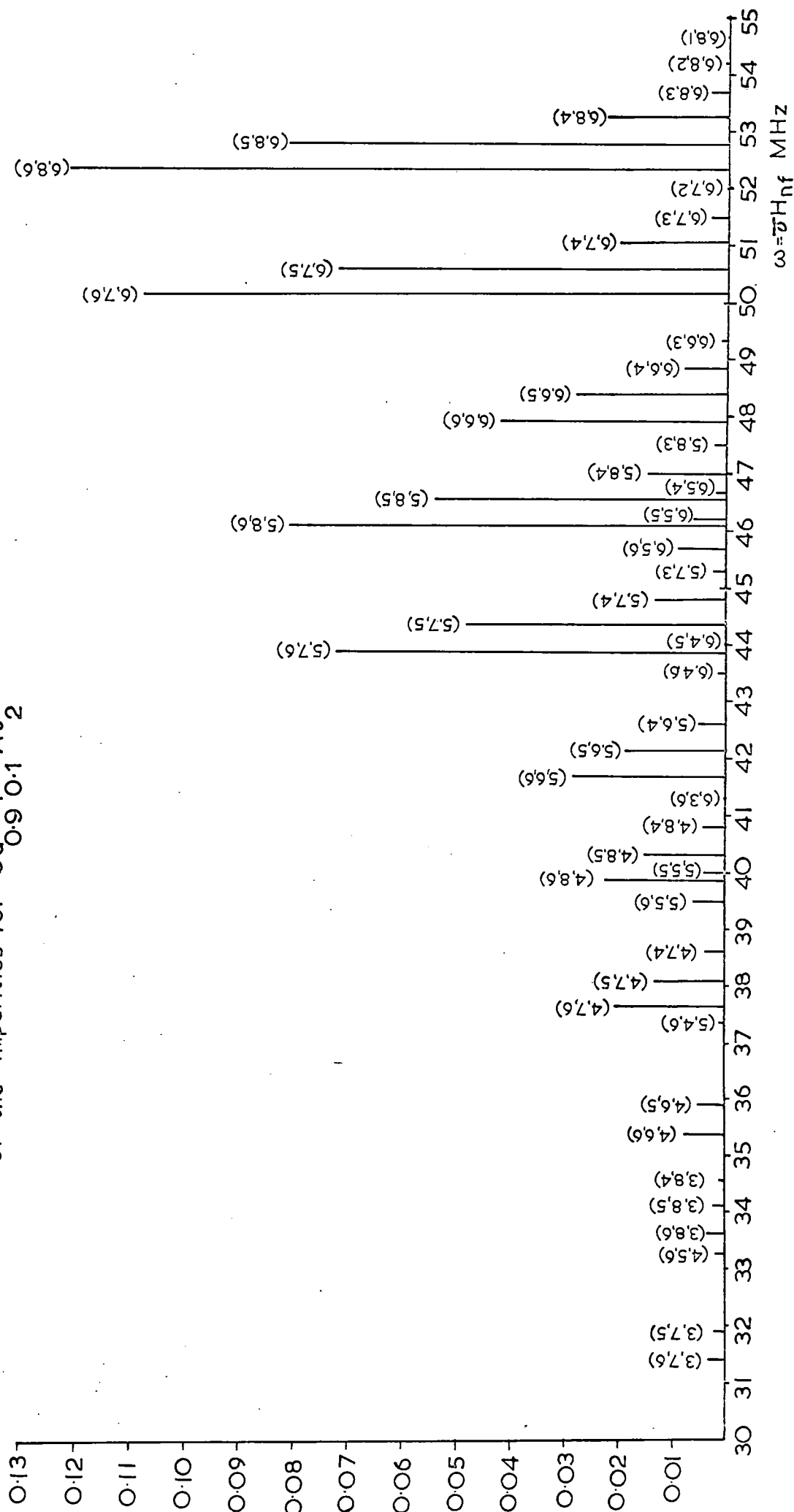


Fig. 6-3. Schematic diagram showing the effect of RKKY function on nuclear magnetic resonance of the impurities for $Gd_{0.9}Y_{0.1}Al_2$

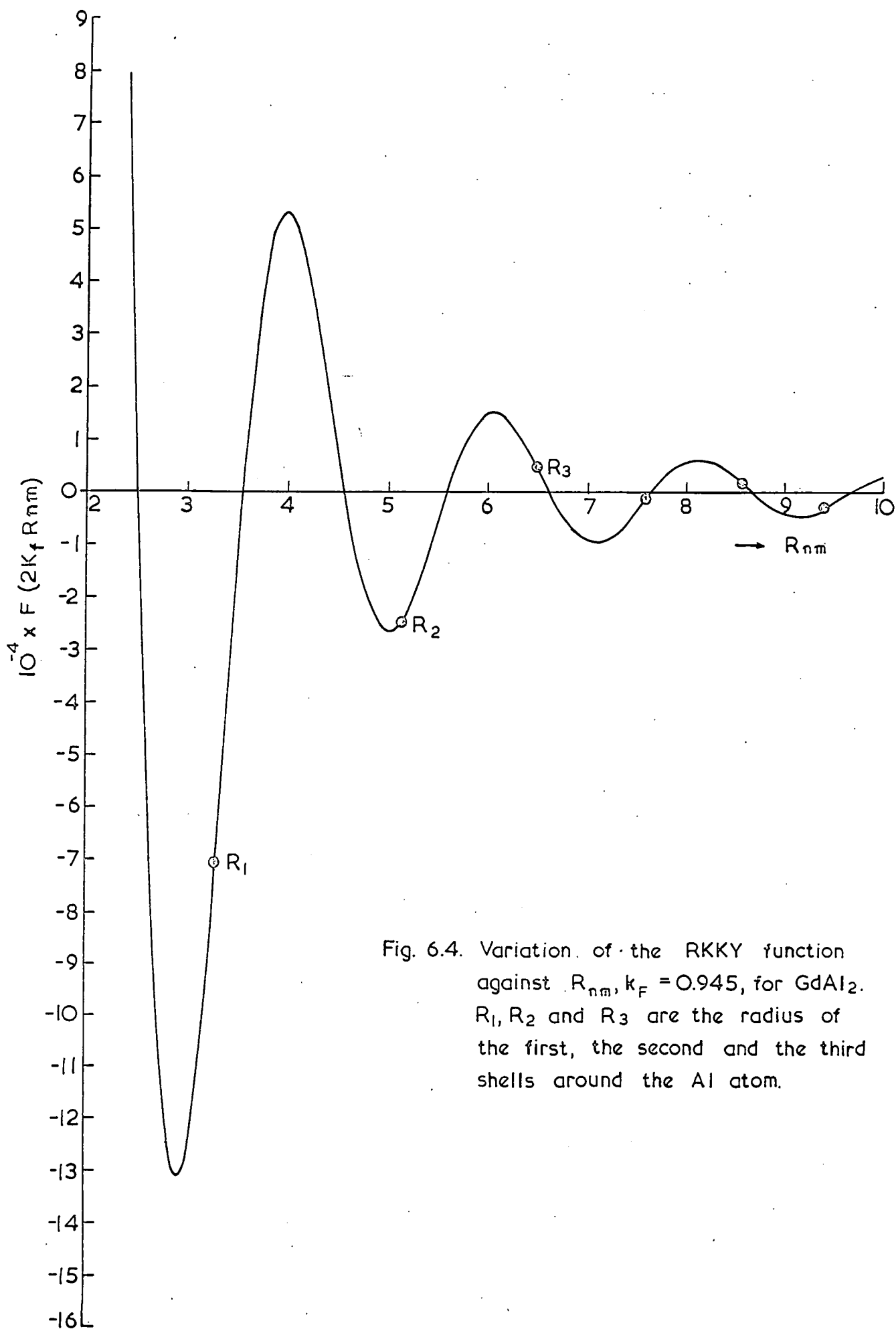


Fig. 6.4. Variation of the RKKY function against R_{nm} , $k_F = 0.945$, for $GdAl_2$. R_1 , R_2 and R_3 are the radius of the first, the second and the third shells around the Al atom.

$$P(Z_i, n_i) = \binom{Z_1}{n_1} \binom{Z_2}{n_2} \dots \binom{Z_i}{n_i} \frac{1}{n} \binom{N}{n}$$

where $N = Z_1 + Z_2 + Z_3 + \dots + Z_i$

and $n = n_1 + n_2 + n_3 + \dots + n_i$

The required probability of having n_1, n_2, n_3 Gd atoms in three shells for an impurity concentration is

$$P(x, n_1, n_2, n_3) = \binom{6}{n_1} \binom{8}{n_2} \binom{6}{n_3} \times \binom{n_i}{20} \times P(x, n) \quad (6.10)$$

where $n_1 = 0, 1, 2, 3, \dots, 6$, $n_2 = 0, 1, 2, 3, \dots, 8$ and $n_3 = 0, 1, 2, 3, \dots, 6$.

The consequences of the RKKY interactions and the corresponding probabilities (The probability represents the centre of the absorption line for each contribution) equations (6.9, 6.10) are shown schematically for $x = 0.1$ in fig. (6.3). It can be seen from this figure that the principal resonance is due to an aluminium nucleus surrounded by 20 gadolinium atoms. Substitution of 1 atom of Y or La into the first shell moves this resonance about 6 MHz lower in frequency. Subsequent substitutions into this shell will move the resonance to lower frequencies in increments of about 6 MHz. Substituting Y or La into the second shell moves the resonance again to lower frequencies, but this time in increments of about 2.25 MHz/atom. When substitution occurs into the third shell, the resonant frequency is increased by increments of about 0.5 MHz/atom. This change in sign of the frequency shift can be understood by referring to the polarization oscillation shown in fig. (6.4). The radii of the first two shells have negative values of $F(2k_f R_{nm})$ while the third shell radius has a positive value. It is worth

nothing that the amplitude of each of the resonances in fig.6.3 is directly proportional to the probability of occupation of a given shell. Hence, the amplitudes produced by the configurations (5, 8, 6), and (6, 8, 5) are identical; however, although sequential substitution into the first and into the third shell produce similar diminutions in amplitude, the effective amplitude decay with frequency is much greater in the case of the third shell than in the case of the first shell. This is a direct result of the frequency increment for the first shell being -6 MHz, whereas that for the third shell is + 0.5 MHz.

a. Calculations neglecting second-order dipolar contribution.

In order to calculate the NMR-line profile, dipolar contributions and line-widths have also to be considered. Exact calculation of the dipolar contributions for the diluted samples is complicated by two problems. First there is a computational difficulty since it is not now possible to collect the Gd atoms in shells of equal A^2 distance because their contribution to the total field differs in value and/or direction from one atom to another. Therefore each Gd position must be treated independently, increasing the computational time (e.g. for $x = 0.1$ and taking into account the minimal probability of value 2% of the maximum value, 9933 instead of 120 configurations have been taken into account). The second problem is physical and more severe, since the mixture of (111) domain lines and other lines in pure $GdAl_2$ depends on sample preparation, it is not certain that the ratio of (111) - to "(100)" - and another line is constant for Y or La dilution, even if all the samples had been subjected to the same treatment. Also

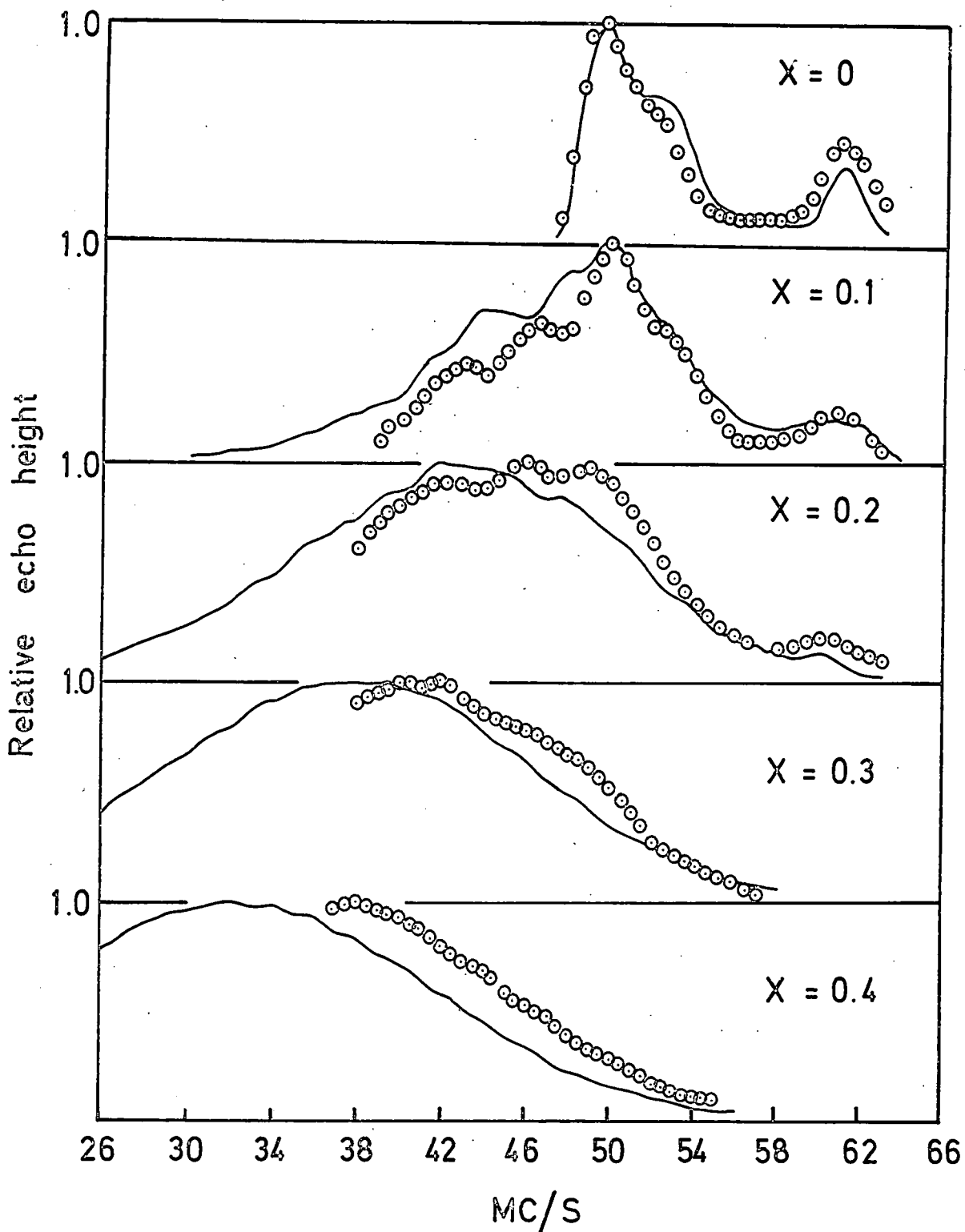
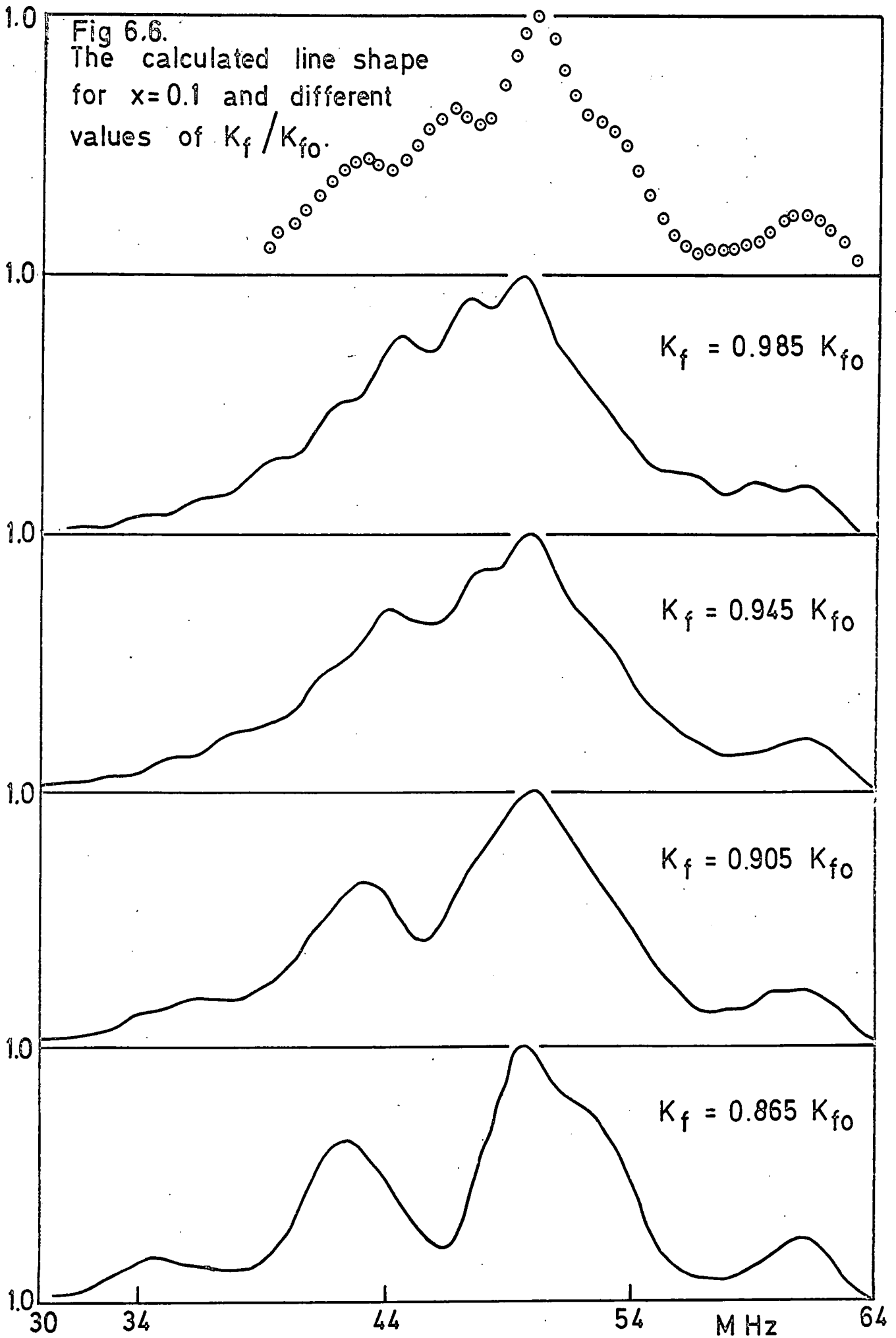


FIG.6.5. Calculated and experimental Al line profiles for different concentration x , — calculated with line area normalized to experimental value;
 ○ Curve Observed line for $\text{Gd}_{1-x}\text{Y}_x\text{Al}_2$



in diluted samples it is not known whether the (111) -domains are preferred as they are in GdAl_2 .

From the above difficulties, these second-order dipolar contributions were neglected from the profile calculations of figs. (6.5, 6.6). The calculations were performed by considering the experimentally-observed three-line spectrum for pure GdAl_2 . The centre of gravity of the two lines a and b (111) and the 52.2 MHz line (100) are both found to occur at the same hyperfine field position. We now assumed the following for the calculation.

- 1) The 52.2 MHz line can be calculated from equation (6.9) as shown in fig. (6.3).
- 2) From experiment we know that the separation of the a-line from the centre of gravity is ≈ 9 MHz and that the separation of the b-line from the C of G is ≈ -2.7 MHz. Using the data illustrated in fig. 6.3, we shall assume in all cases that the a-line for a particular configuration is 9 MHz above the frequency shown in the figure for that configuration. Similarly the b-line will be assumed to be 2.7 MHz below the frequency in the figure.
- 3) The line shape for each line was assumed to be Gaussian. The experimental line widths have been used which are 2.2 MHz for a and b and 3.4 MHz for the 52.2 MHz line.
- 4) The amplitudes of the three lines are given by the product of the experimentally-determined intensity ratio and the probability.
- 5) It was assumed that the contributions of the different shells are additive and independent of their relative positions.

Fig. (6.5) shows the model calculation line profiles for

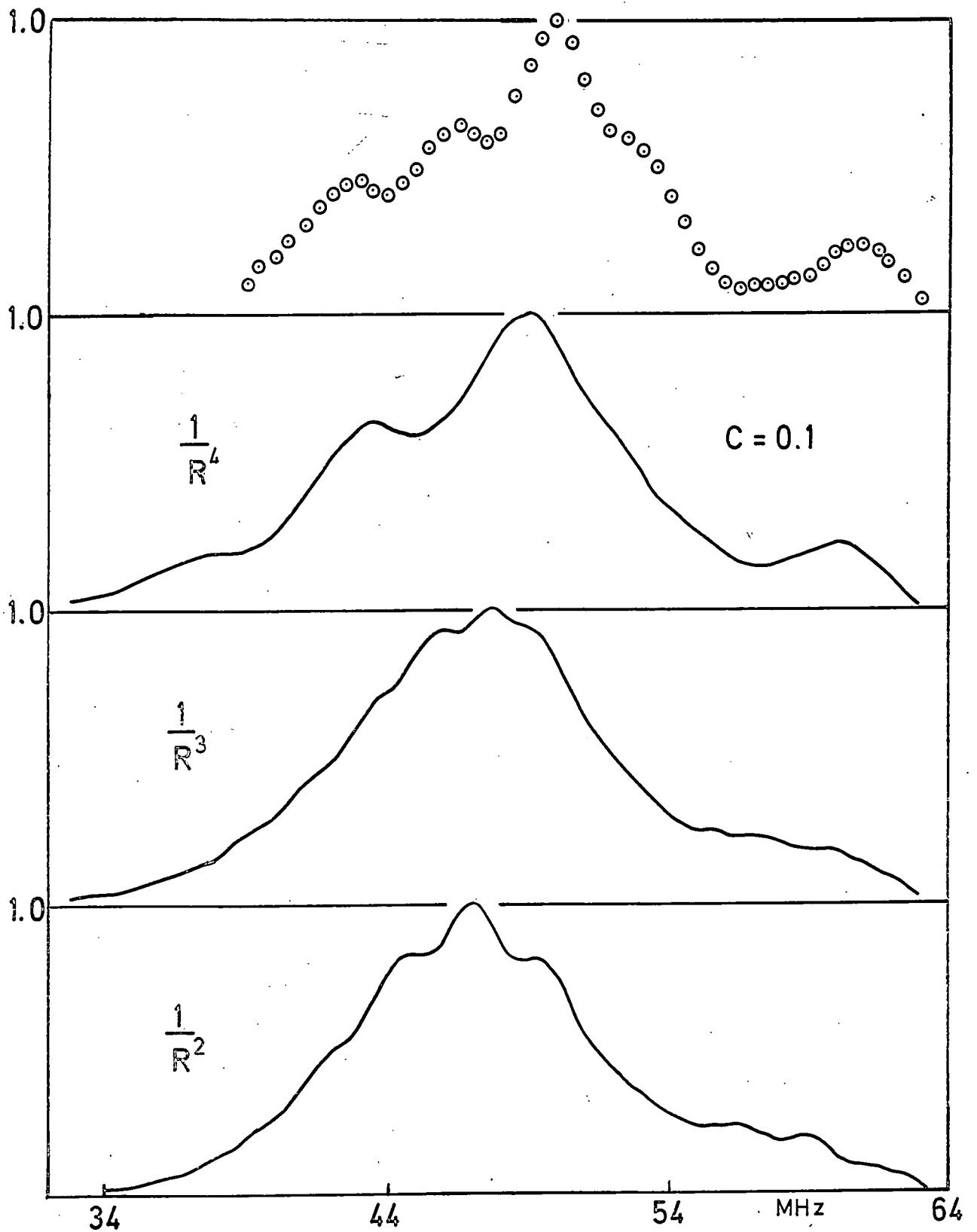


FIG.6.7. The calculated line shape with R^{-2} , R^{-3} and R^{-4} dependence of the conduction electron polarization for $x=0.1$

$x = 0.1$ for different values of K_f . By comparison with the experimental result, a K_f/K_f^0 - value near to 0.940 appears to give satisfactory line fitting.

Fig. (6.6) shows the series $x = 0.0$ to 0.40 for $K_f/K_f^0 = 0.945$. The calculated and measured spectra agree reasonably well.

In order to establish whether instead of the oscillatory RKKY function, the observed line profiles can be equally well described by a different R - dependence of the conduction electron polarization which is uniform in space, we attempted to fit the line profiles with a simple, non-oscillatory R -dependence under the same conditions and assumptions. We replaced $F(2K_f R_{nm})$ of equation (6.9) arbitrarily by the functions C'/R^2 , C'/R^3 , or C'/R^4 but did not consider higher powers of $1/R$ because this would imply that the exchange interaction in $Gd_{1-x}Y_xAl_2$ and $Gd_{1-x}Lu_xAl_2$ is essentially a short range interaction in contradiction (ref. 6.1) to the observed linear decrease of the Curie temperature with increasing x up to $x = 0.98$ (ref. 6.2). As an example, the results for $x = 0.1$ are shown in fig. (6.7) for the R^{-2} and R^{-3} and it is clearly seen that a slowly decreasing nonoscillatory function cannot explain the observed structure. In contrast to the experimental observations it is seen that in this case the maximum amplitude position is shifted to lower frequency. The R^{-4} dependence also does not give a good fit because the 46.5 MHz line is missing. However, the overall agreement is better in the case of R^{-4} . From these calculations, it can be concluded that an oscillatory conduction electron polarization is necessary to account for the line-shape in $GdAl_2$.

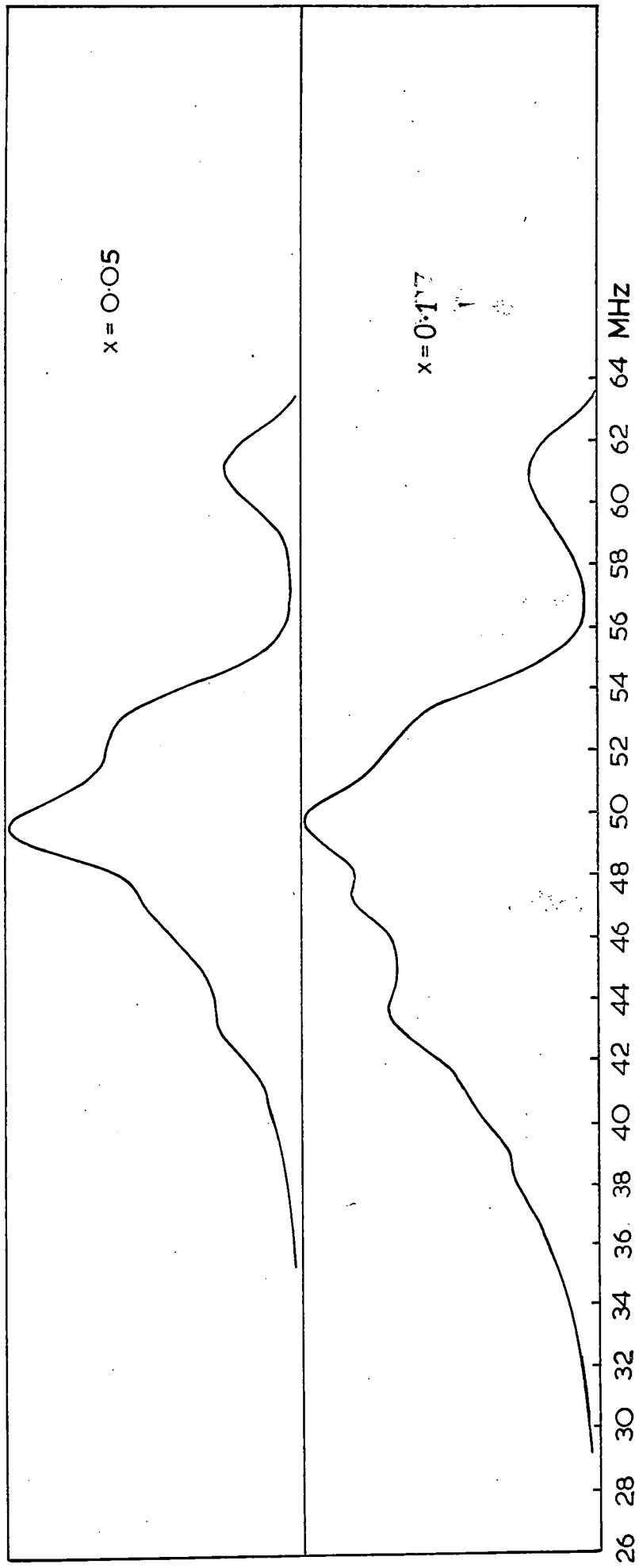
b. Calculation including the second-order dipolar contributions

To examine the validity of the assumption made in the previous section, we calculated some line-shapes allowing for the second-order dipolar field contributions. So as to limit computational time to a reasonable value, only the concentrations $x = 0.05$ and 0.10 were investigated. The ^{27}Al line-shape is considered to be composed of (111) and (100) domain signals although the (100) signals may be taken as representative of all the lines which are centred around the pure hyperfine field position. In this case we will assume that the (100) line can be calculated from the equation (6.9) whereas the (111) lines arise from equation (6.6). In this case we have to consider the dipolar field for each atom, for each configuration, for example in the case of 19 atoms we have the following configurations

$$\begin{array}{l} 19 \quad 6 \quad 8 \quad 5 \quad (1,1,1,1,1,0) \\ \quad \quad \quad \quad \quad (1,1,1,1,0,1) \\ \quad \quad \quad \quad \quad (1,1,1,0,1,1) \\ \quad \quad \quad \quad \quad (1,1,0,1,1,1) \\ \quad \quad \quad \quad \quad (1,0,1,1,1,1) \\ \quad \quad \quad \quad \quad (0,1,1,1,1,1) \end{array} \quad (6.11)$$

and the same thing for (6, 7, 6) and (5, 8, 6). For the configurations (6.11), the hyperfine field calculated for the (100) domains is the same, but the fields from the a and b sites are different, because the dipolar field for each case is different. However, because the Gd sites in the third shell are symmetrically disposed the dipolar contributions from diametrically-opposite sites are equal. This reduces

Fig. 6-8. Calculated Al line profiles for small x and $k_F = 0.945 k_F^0$ with the second-order dipolar contributions taken into account.



the effective number of calculations by half.

The probability equation (6.10) in this case is:

$$P(x, n_1, n_2 \dots n_{10}) = \binom{Z_1}{n_1} \binom{Z_2}{n_2} \dots \binom{Z_9}{n_9} \binom{Z_{10}}{n_{10}} \binom{N}{n} P(x, n)$$

The other assumptions in the last section have been used in this calculation. The result is shown in fig. (6.8), and is reasonably similar to the previous calculation.

The results from the above model can be summarized as follows.

1. The observed line-shapes can not be fitted with a nonoscillating polarization function as shown in fig. (6.7).
2. Using the RKKY polarization function with large values of K_f/K_f^0 (eg. 0.985) there are too many lines as shown in fig. (6.5) while for small K_f/K_f^0 (eg. ≤ 0.905) there are not enough lines predicted for diluted $GdAl_2$ in the frequency range of interest. Only for an intermediate K_f/K_f^0 value (eg. 0.945) is the number of lines given correctly with reasonable fitting between the measured and calculated line profiles for the different concentrations as shown in fig. (6.6).
3. The positions of the two observed lines at about 42.5 MHz and 46.5 MHz can not be described exactly by the RKKY polarization function, for $K_f/K_f^0 = 0.945$, they are calculated to occur at about 43.8 and 47.6 MHz. Even allowing for a concentration dependence of the relative weights of the (111) and (100) signals and a deviation of K_f/K_f^0 from 0.946, it was not possible to fit both peaks.

These two peaks correspond essentially to Al atoms for which one nearest (42.5 MHz) and one next nearest (46.5 MHz) Gd neighbour is replaced by nonmagnetic Y or La. In the

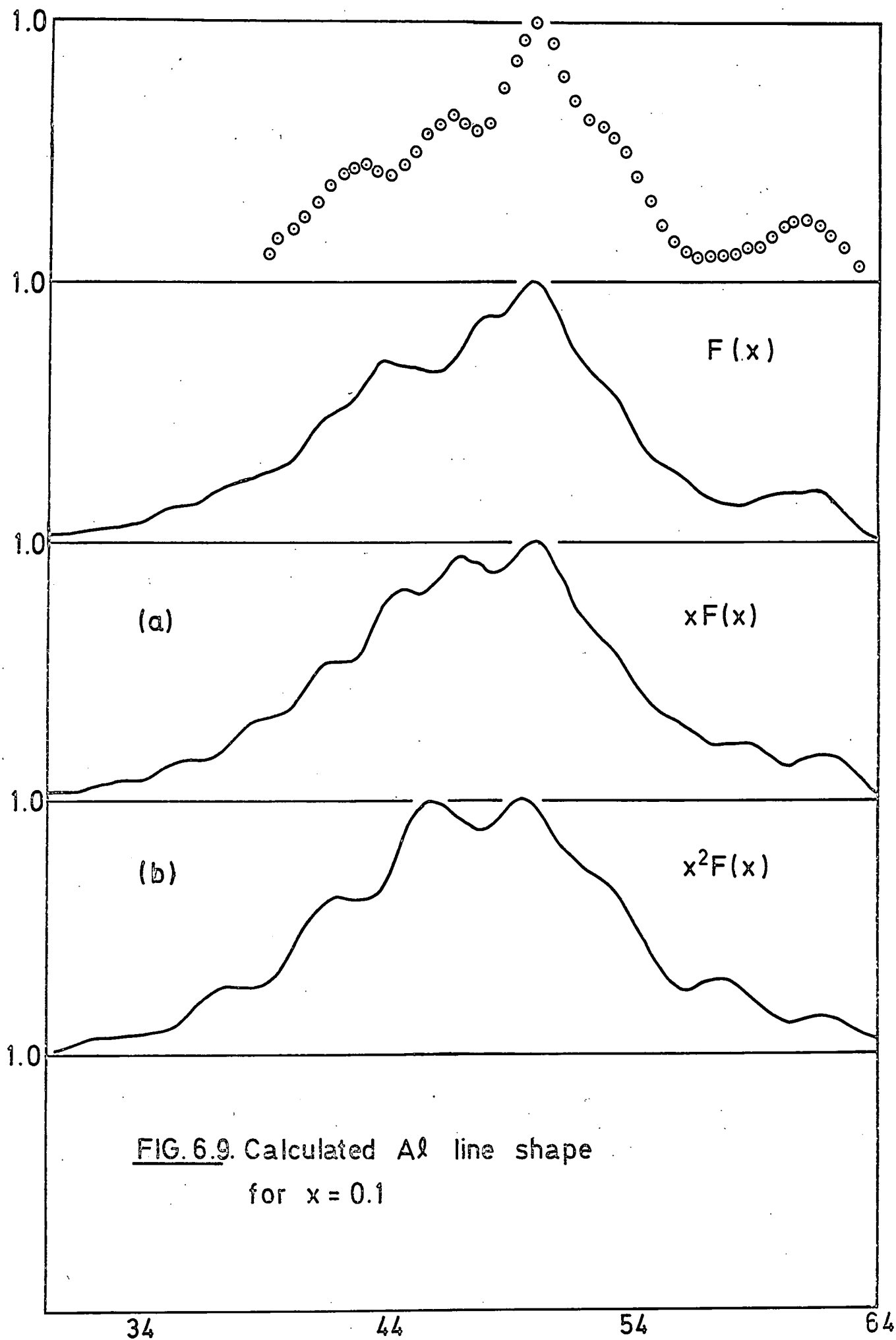
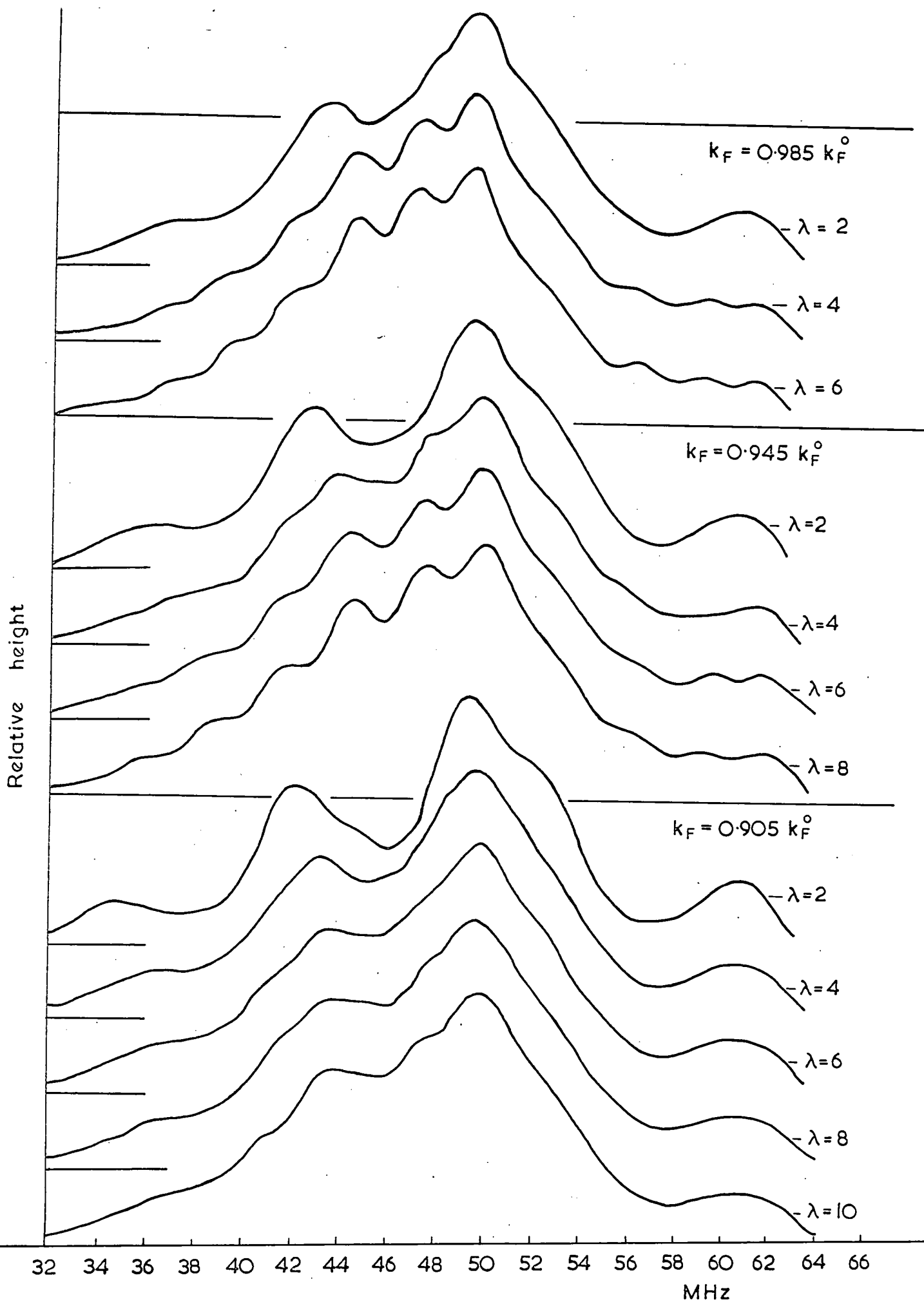


Fig 6.10. The calculated line shape for $x=0.1$ for different values of k_F/k_F^0 and the mean free path.



K_f range of interest both of these neighbours give a negative RKKY contribution to the hyperfine field, whereas the third nearest neighbours contribute positively see fig. (6.4) (which is important in order to prohibit the shift of 49.5 MHz line). Investigation of the K_f dependence of these contributions, and the lineshape, showed that an exact fit of the peak position can only be given if there is a considerable positive (ferromagnetic) direct contribution superposed on the negative RKKY contribution of the nearest neighbours or if the polarization decreases less strongly with distance than in the RKKY model (with $J(q) = \Gamma =$ constant, chapter one). Since a positive direct contribution is not likely (ref. 6.3) for the large Gd-Al distance (3.276°A), the second possibility seems more realistic. As we have seen in chapter one, Yosida (ref. 6.4) calculated the spin polarization introducing a cut off $q = 2K_f$ to the product $J(q) f(q)$ such that $J(q) f(q) = 2J(0)$ for $q \leq 2K_f$ and $J(q) f(q) = 0$ for $q > 2K_f$ (fig. 1.8). In this case, the usual RKKY function $F(2K_f R_{nm})$ should be replaced by $2K_f R_{nm} F(2K_f R_{nm})$. Using this function, with the same assumptions as were used for the calculation of fig. (6.6), the results are shown in fig. (6.9a), which shows too many lines in disagreement with the experimental results. Buschow et al. (ref. 6.5) discussed Yosidas assumption and took into consideration the effect of the mean free path of the conduction electrons by using the Yosida function multiplied by $e^{-R_{nm}/\lambda}$ (λ is the mean free path). We have calculated the line shape for several values of λ and at different values of K_f as shown in fig. (6.10). Notice that the amplitude of the oscillation decreases as the mean free path decreases. In this case and for a given K_f the influence of the mean free path on the line

shape is similar to the effect of the K_f by using the ordinary RKKY function. For a particular line shape the value of the mean free path λ increases as the wave vector K_f decreases. As can be seen from the figs. (6.9a and 6.10) these modifications have not altered the positions of the component lines as predicted from the usual RKKY function. Only the intensities of the component lines have changed. Finally fig. 6.9b shows the calculated line shape in which we considered the nonspherical Fermi surface where the $F(2K_f R_{nm})$ falls off as R^{-1} (see chapter 1). In other words we replaced the usual RKKY function $F(2K_f R_{nm})$ by $(2K_f R_{nm})^2 F(2K_f R_{nm})$. In this case the two peaks at 42.5 MHz and 46.5 MHz agreed well with the experimental results but the amplitude fitting is obviously poorer.

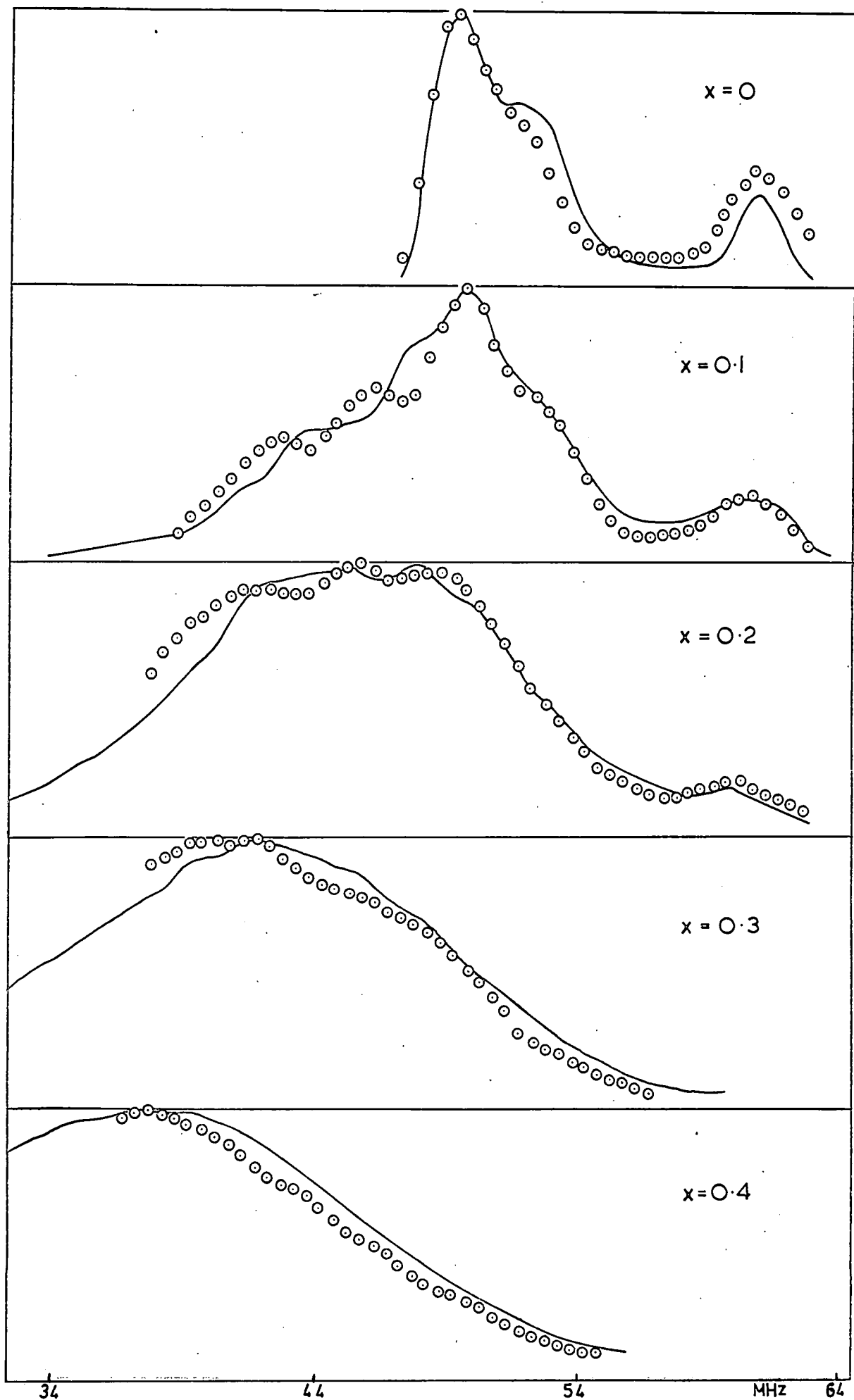
The above attempts have been made to modify the RKKY function to get a better fit to the experimental results. This modification is performed by changing the position of the components of each configuration which make up the hyperfine field spectrum.

From the Mossbauer effect studies of the hyperfine field at $^{57}\text{Fe-Co}$ alloys, Wertheim et al. (refs. 6.6, 6.7) analysed the results in terms of the occupancy of the coordination shells around an iron atom. The relative amplitude of the spectrum was assumed to be given by the following binomial distribution.

$$P = \frac{P(x, n_1, n_2)}{1 + (E - \alpha n_1 - \beta n_2)^2}$$

incorporating a least-squares fit with E_2 , α and β as the free parameters. $P(x, n_1, n_2)$ defined as the equation (6.10), E is related to the line width, α , β measure the difference in the absorption due to a nn and nnn impurity.

Fig. 6-11. Calculated and experimental Al line profiles for different x , after using the value of α, β, τ and E .



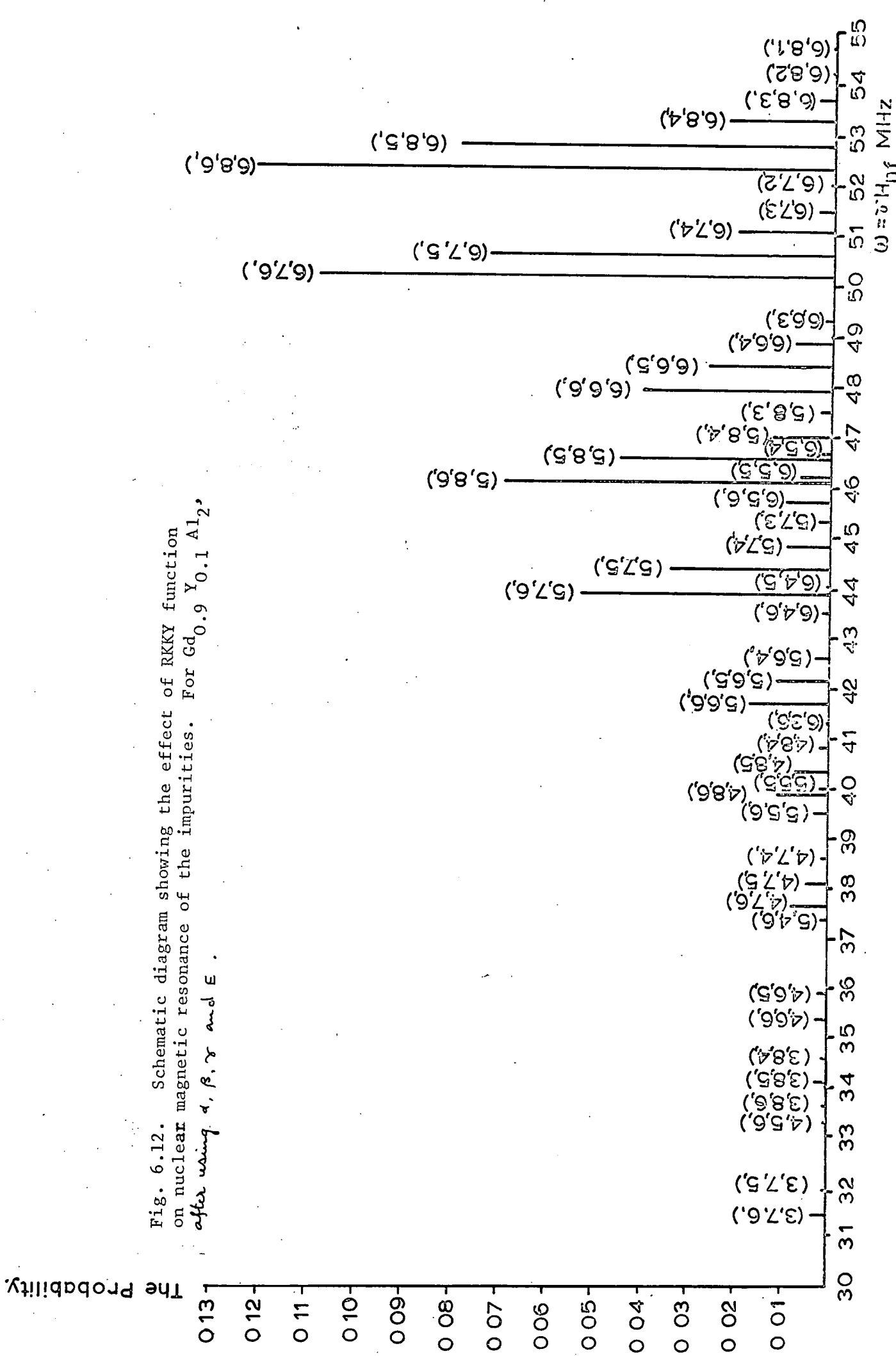


Fig. 6.12. Schematic diagram showing the effect of RKKY function on nuclear magnetic resonance of the impurities. For $Gd_{0.9}Y_{0.1}Al_2$, after using ρ, β, γ and E .

Following the above assumption, we have divided the probability equation (6.10) by $(1 + (E - \alpha n_1 - \beta n_2 - \gamma n_3)^2)$ to accommodate three shells, and we have used the fitting program to get the values of E, α, β, γ by comparison with the experimental result. We found the values of E, α, β and γ as 5.3, 0.6, 0.2 and 0.05 which give a better fit than the previous calculation as shown in fig. (6.11). In fact the effect of E, α, β and γ is to change the value of the probability (which represents the line amplitude) from its original value as shown in figs. (6.3, 6.12).

6.1.3 E.S.R. of $Gd_{1-x}Y_xAl_2$

The electron spin resonance of Gd in $Gd_{1-x}Y_xAl_2$ was measured in the concentration range for $x = 0.1$ to $x = 1$. For all concentrations the g-value was found to be 1.985 ± 0.005 independent of temperature and this is in fair agreement with the value obtained by Peter et al. (ref. 3.26) of 1.982 for $GdAl_2$ and with Hacker et al. (ref. 3.59) who quoted a room temperature g-value of 1.984 and with recent work by Taylor (ref. 6.8) of 1.989 ± 0.005 .

The line width ΔH , i.e. the half power-half width of the absorption part of the resonance line, is given in fig. (5.18). There one sees that ΔH increases linearly with temperature, and the increase of the line width with temperature $d(\Delta H)/dT$ is small for higher Gd concentration as shown in fig. (6.13). For $GdAl_2$ the line width has a slope of 2.52 Oe/K. This is in good agreement with the value obtained by Taylor (ref. 6.8) of 2.1 Oe/K.

The decrease of the slope $d(\Delta H)/dT$ with increasing Gd concentration and the constancy of the g-value for all concentrations

indicates that the relaxation is bottlenecked (chapter 3, section 3.4.3). In this case the line width and g-shift may be given by Hasegawa's equations (3.47) which are:

$$\tau \Delta H = \frac{x}{1+x} \delta_{ie} \quad (6.12a)$$

$$\Delta g = \left(\frac{x}{1-x} \right)^2 \Delta g_0 \quad (6.12b)$$

where

$$x = \frac{\delta_{el}}{\delta_{ei}} \quad (6.13a)$$

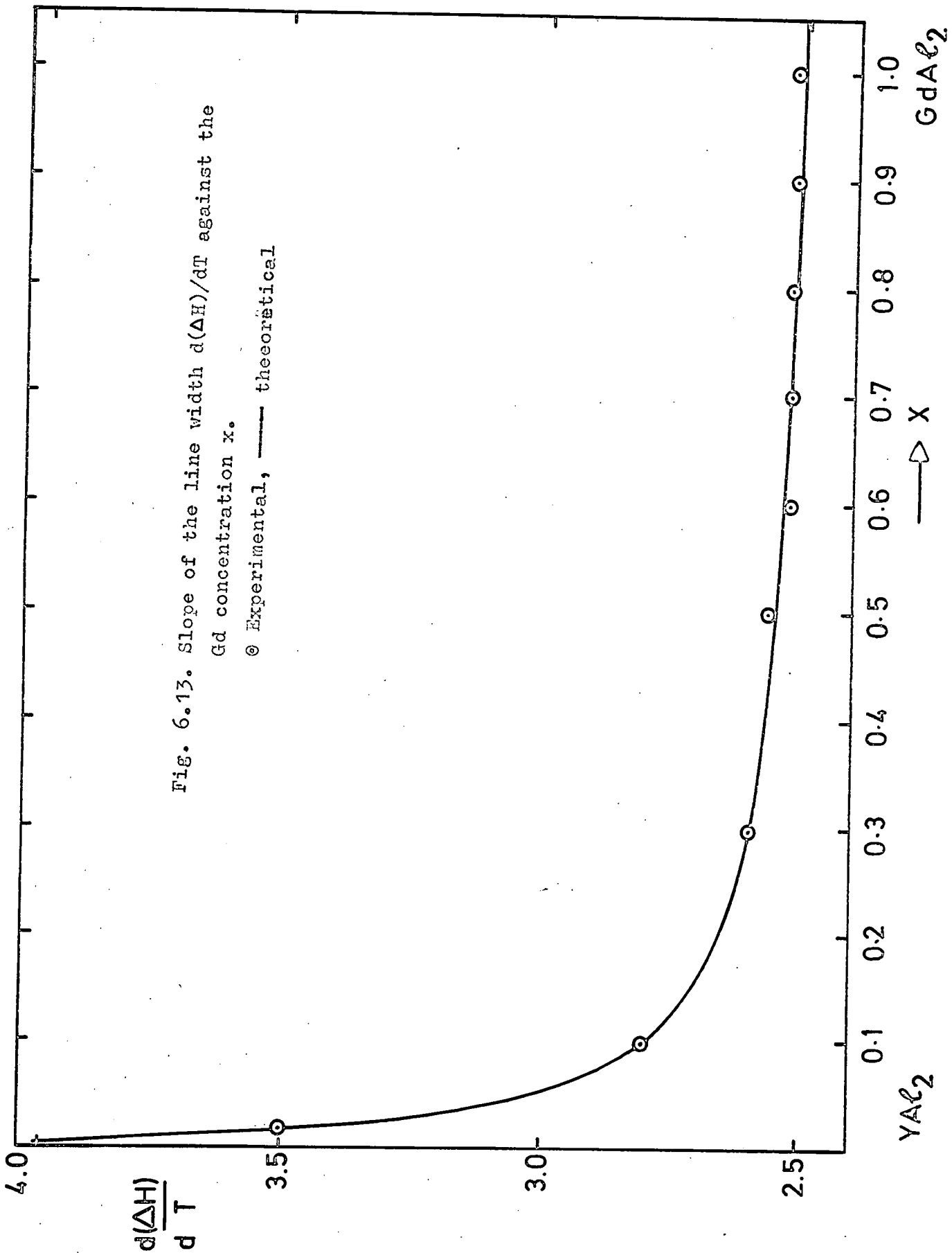
$$g_0 = \frac{3 J n}{2 g_e E_F n_0} \quad (6.13b)$$

$$\delta_{ei} = \left(\frac{2}{3\hbar} N(E_F) J^2 S(S+1) \text{conc.} \right) \quad (6.13c)$$

$$\delta_{ie} = \left(\frac{\pi}{\hbar} \right) N(E_F)^2 J^2 K T \quad (6.13d)$$

$$\delta_{el} = \delta_{el}^0 + \frac{d(\delta_{el})}{d(\text{conc.})} \quad (6.13e)$$

An attempt has been made to evaluate ΔH from equation (6.12a) by using a computer fitting program. By substituting δ_{ei} , δ_{ie} and δ_{el} (δ_{ei} and δ_{ie} are the relaxation times from the conduction electrons to the local ions and vice versa and δ_{el} is the relaxation time from electron to the lattice) into equation (6.12a) and assuming J , δ_{el}^0 and $\frac{d(\delta_{el})}{d(\text{conc.})}$ as free parameters



and using $N(E_F)$ to be 0.91 eV (ref. 3.66), the agreement between the theoretical and experimental curves is good as shown in fig. (6.13). From this fitting we obtained the following values.

$$J = + 0.091 \text{ eV}^{\frac{1}{2}}$$

$$\delta_{ie} = 2.83 \times 10^9 \text{ T sec}^{-1}$$

$$\delta_{ei} = 3.79 \times 10^{14} \times \text{conc.} \text{ sec}^{-1}$$

$$\delta_{el}^0 = 8.3 \times 10^{10} \text{ sec}^{-1}$$

$$\frac{d(\delta_{el})}{d(\text{conc.})} = 5.9 \times 10^{12} \text{ sec}^{-1}/\text{conc.}$$

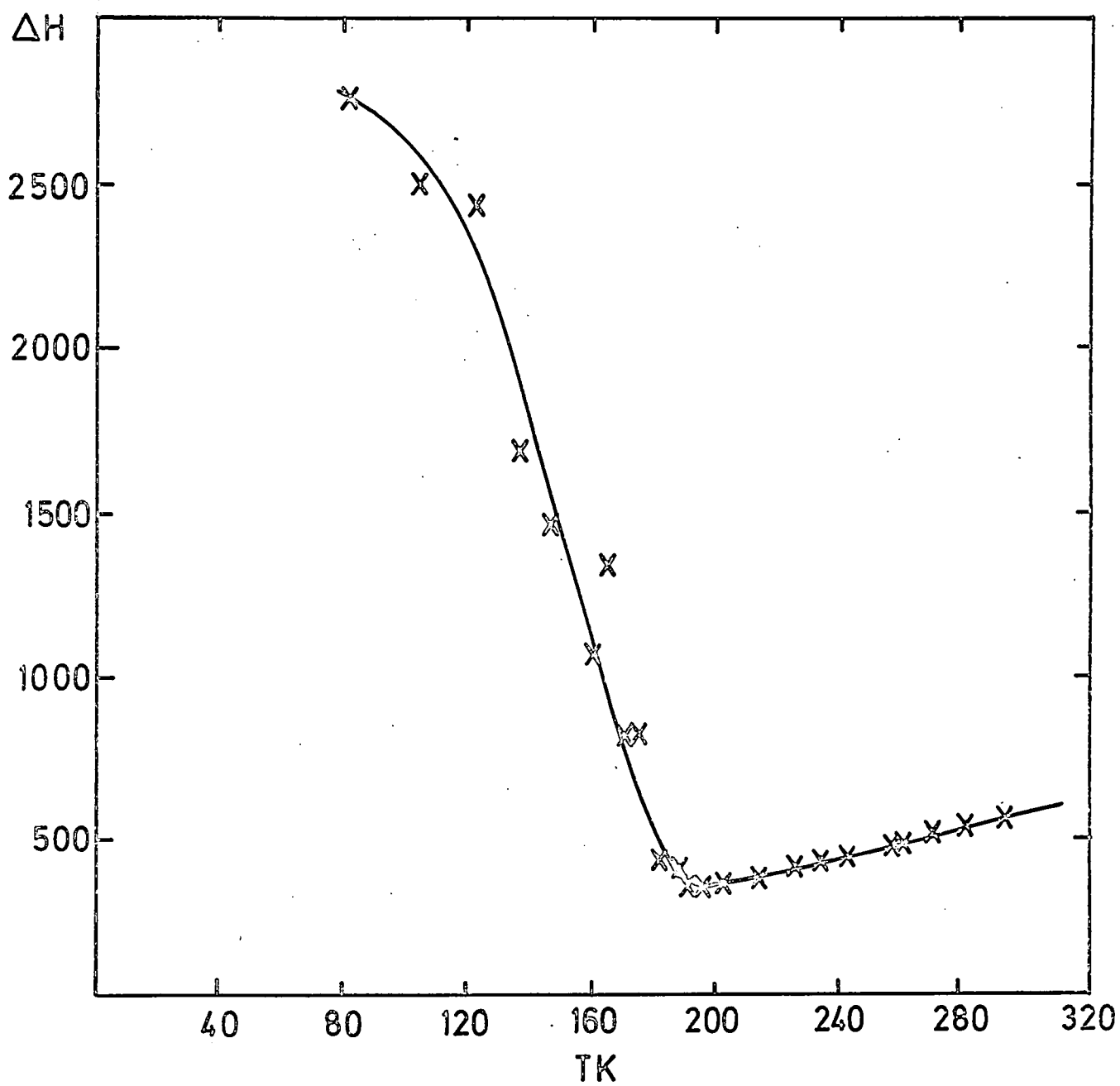
This solution has not solved the following experimental results.

1. The residual line width for each concentration.
2. The behaviour of the line width below the Curie temperature.

For the first problem, ΔH in the paramagnetic region decreases linearly with temperature for all compounds. However, the extrapolated plot of line width versus temperature to OK is not zero but has values which are both positive and negative depending on the compounds studied. A non zero intercept has also been noted by several authors (ref. 3.48, 3.66). This problem has been solved by considering the effect of the relaxation path δ_{il} from the local moments to the lattice which represents the residual line width. In this case the line

X This value of J is obtained by assuming the exchange Hamiltonian is defined by $-J sS$ ($J \equiv \sqrt{\quad}$).

Fig. 6.14. The temperature dependence of the line width for $GdAl_2$ (ref. 6.8)



width, equation 6.12a, becomes:

$$\Delta H = \frac{x}{1+x} \Delta H_K + \Delta H_{res} \quad (6.14)$$

In our results ΔH_{res} has values within the range -300 ± 10 to 100 ± 10 Oe.

The solution to the second problem is still obscure. In fact it was found that the line width ΔH became narrower as the temperature was reduced consistent with a linear temperature dependence due to spin lattice relaxation. Eventually a minimum in the line width occurred followed by a rapid broadening of the line below this point. This broadening may be attributed to ferromagnetic ordering and therefore it would seem justifiable to refer to the minimum of the ΔH against temperature graph as a measure of the Curie temperature. This is shown in fig. (6.14) for $GdAl_2$ (ref. 6.8) and in fig. (5.19) for $Gd_{0.9}Y_{0.1}Al_2$.

Now the line width may be represented by the following empirical equation

$$\Delta H = a (T - T_C) + b \quad (6.15)$$

where T_C is Curie temperature and a is the slope $d(\Delta H)/dT$ and b is the residual line width for $T = T_C$. b has a value of 100 ± 10 Oe for all the concentrations. By fitting this equation to the experimental result we found that the value of the Curie temperature is the same as the result obtained from A.C. susceptibility measurements (section 6.1.1).

The g -shift is negative as compared with the g value characteristic of the Gd ion ($g = 1.992$). Use of a free

electron picture gives $E_F = 5.1$ eV for $GdAl_2$, assuming three conduction electrons per lattice site, and leads, using the measured g-shift and equation 6.13b to a value $J = -0.032 \pm 0.02$ eV. This value is smaller than the values above which was obtained from the line width calculation (eqn. 6.12a). The negative sign can be attributed to the effect of the interband mixing as explained in chapters 1 and 2.

A final point which needs mentioning is the discrepancy between our value for J and those extracted from Knight shift measurements for $GdAl_2$. The latter requires $J = 0.91$ eV which is to be compared with that which we have obtained i.e. 0.091 eV. This discrepancy is huge, and may be due to the effect of neglecting the interelectron correlation which enhances the Pauli spin susceptibility or due to the premises used in the traditional RKKY theory.

6.2 N.M.R. of GdDyAl₂

The substitution of Dy for Gd results in the rapid disappearance of the ^{27}Al resonance line, the resonance being only observable to approximately 7% Dy substitution. The very short relaxation times may have led to this disappearance. Recently, the resonance of ^{27}Al in DyAl_2 was found to be 29.8 MHz (ref. 2.9) and the easy direction of magnetization is (100). Since we know that the easy direction of pure GdAl_2 is (111) then the peak which appears at 56.5 MHz may be due to the change of the easy direction from (100) to (111). A third possibility is that the resonance frequency in GdAl_2 moves outside the working range of the spectrometer as the Dy concentration is increased.

6.3 N.M.R. of ACo₂ (A is a rare earth)

The magnetic properties of these compounds have been discussed by several authors as we have seen in chapter 2. In this section we will discuss the hyperfine field at the ^{59}Co nucleus in some of these compounds. The experimental spectra of GdCo_2 , HoCo_2 , TbCo_2 and NdCo_2 are shown in figs. (5.8, 5.9). These measurements show that the resonance frequency of the cobalt nucleus remains essentially the same at about 61.5 kOe.

The hyperfine field of metallic Co has been reported to be 216.5 kOe (ref. 6.9) and - 215 kOe (ref. 6.10). This field was originally assumed to be positive, i.e. parallel to the ionic magnetization, however, subsequent work by Hanna et al. (ref. 6.11) on the sign of the field at the ^{57}Fe nucleus in iron metal showed that in this case the sign was negative and

these authors suggested that the same would apply to cobalt metal.

The NMR of ^{59}Co in hcp cobalt has been observed as a function of temperature from 4.2 K to 730 K by Kawakami et al. (ref.6.12). They found that the hyperfine field at 0 K is - 223 kOe which is larger by ~ 8 kOe than in the fcc phase. The difference between the two hyperfine fields comes from the anisotropy in the orbital field and partly from that in the dipolar field. The negative sign is known to be due to the Fermi contact field due to the inner core electrons, this field is negative and dominant.

Returning to the rare earth - Co_2 , the large decrease of the hyperfine field of the ^{59}Co nucleus from the value in pure metals (217 kOe) to the value in ACo_2 (60 kOe) may be ascribed to two general sources (ref. 6.13) namely:

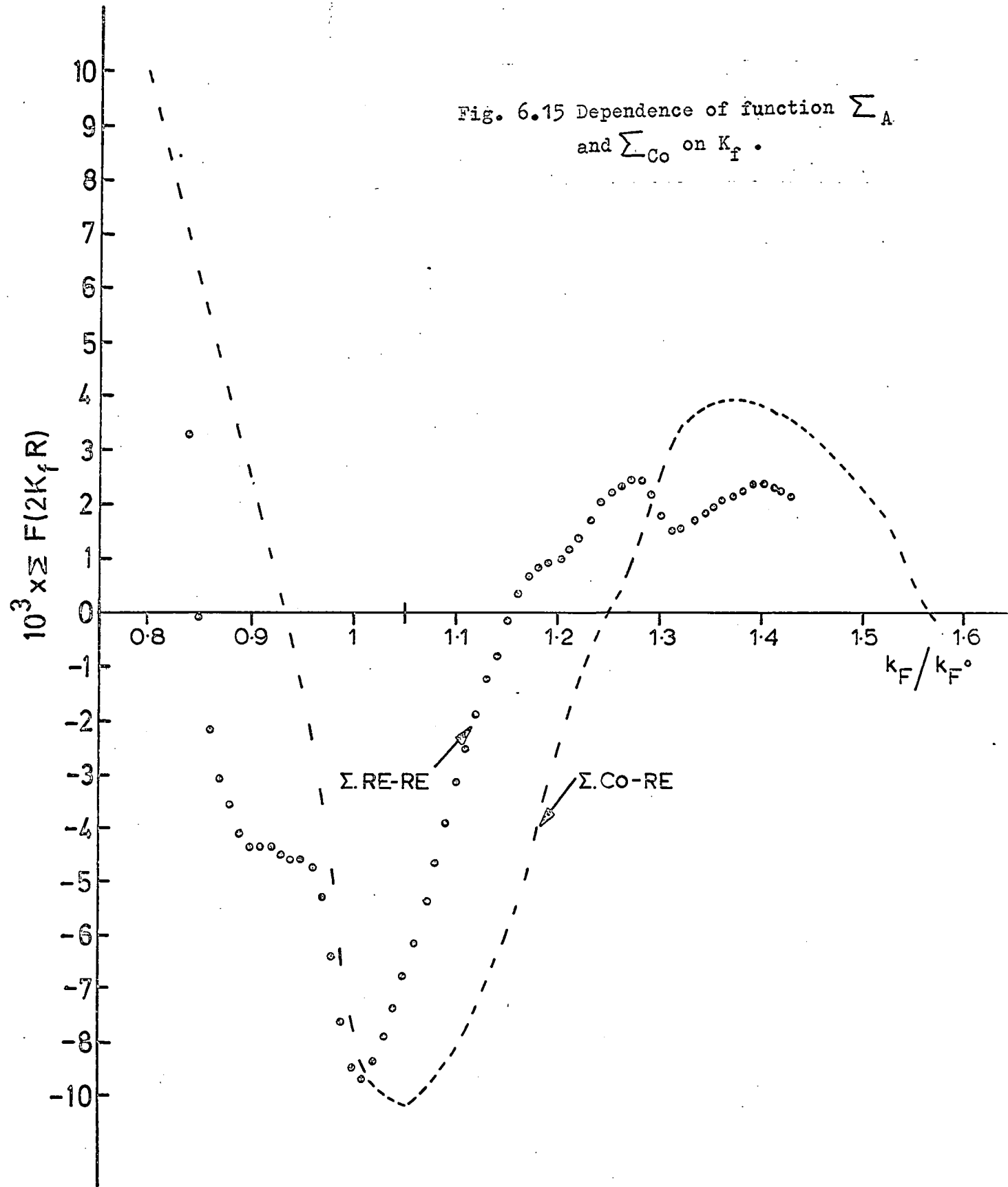
1. The field due to the cobalt ions which includes a contribution from the ions "own" moment and a contribution from the neighbouring cobalt ions.
2. The field due to the conduction electron polarization by the neighbouring rare earth ions.

From the first term, the decrease of the cobalt moment from $1.7\mu_B$ in pure cobalt to about $1.0\mu_B$ in ACo_2 should consequently result in a decrease in the magnitude of the hyperfine field from 217 kOe to 135 kOe. This term may be given by.

$$H_{\text{Co}} = \frac{217 \times \mu_{\text{Co}}}{1.7} \quad (6.16)$$

From the second term, the observed field of 60 kOe results then from an opposing contribution from the conduction electron polarization by the rare earth sublattice, this term is given by equation (6.4) to be

Fig. 6.15 Dependence of function Σ_A
and Σ_{Co} on K_f .



$$H_{ce} = C A(0) \sqrt{\langle S \rangle} \sum F(x)$$

The summation $\sum F(x)$ for ACo_2 compounds was computed as a function of K_f Fig. (6.15) as for $GdAl_2$. K_f^0 was taken to be $K_f^0 = 1.461 \times 10^8 \text{ cm}^{-1}$ by assuming that the number of the conduction electrons per unit volume for the rare earth and the cobalt contribute three and one electrons respectively to the conduction band.

The $GdCo_2$ and $HoCo_2$ spectra show two peaks. For $GdCo_2$ one peak is at 60 MHz and the other at 61.5 MHz and for $HoCo_2$ one is at 51 MHz and the other at 63 MHz. The intensity ratio for the two peaks are 1:3. This line shape represents the resonances caused by the hyperfine field at the two inequivalent Co sites, (a) and (b) and is similar to the line shape observed in $GdFe_2$ and $GdAl_2$. From this result the easy direction of magnetization in $HoCo_2$ and $GdCo_2$ is (111) the low frequency peak being associated with the (a) site and the high frequency peak with (b) sites. This behaviour is similar to the $GdFe_2$ (ref. 6.14) but opposite to that of $GdAl_2$, where the low frequency peak arises from the (b) sites and the high frequency peak from the (a) site.

The only contribution which can produce systematic differences between inequivalent lattice sites is the dipolar field. Assuming that the rare earth and Co moments are localized, the dipolar field can be obtained in terms of lattice sums for each site, performed over the A and the Co atoms. We have calculated the dipolar field for the two cases by using equation (6.5) in a similar way to the calculation of the $GdAl_2$ dipolar field. The magnetic moments of the tripositive lanthanides were taken

as equal to $g_J J$, and the Co moment as $1.0 \mu_B$. The lattice parameter for $GdCo_2$ is 7.242 \AA whereas for $HoCo_2$ is 7.134 \AA . The results are given in table (6.2). The total dipolar field can be given by,

$$H_d = H_d^{Co-Co} + H_d^{Co-A} \quad (6.17)$$

and the total hyperfine field can be given by.

$$H_{hf} = H_{ce-re} + H_{Co} \mu_{Co} \quad (6.18)$$

From the equation, since the Co and rare earth (Gd, Ho) moments are coupled antiparallel the two dipoles will be antiparallel and will be in the direction of magnetization. In $GdAl_2$ H_d represents the magnetic field induced at the Al site by the localized magnetic moments residing at the rare earth sites, and we found this field to be antiparallel to the magnetization. This case should be the same for H_d^{Co-A} . We can write equation as

$$H_d = H_d^{Co-Co} - H_d^{Co-A} \quad (6.19)$$

Since H_d^{Co-A} is a dominant term then H_d becomes negative, i.e. in the opposite direction to the magnetization. Because of the negative g-shift in $GdCo_2$ (ref. 3.62) the conduction electron polarization is negative (equation 6.4). Therefore the sign of the hyperfine field due to the Gd contribution should be negative while the distribution due to the cobalt moment should be positive. The equation may be written as, eqn. (6.18)

$$H_{hf} = -H_{ce-re} + H_{Co} \mu_{Co} \quad (6.20)$$

Returning to the two Co sites a and b, by analogy with the calculation for $GdAl_2$ we can write the two effective fields

Table 6.2 Computed values of the dipolar field at Co sites in $GdCo_2$ and $HoCo_2$ (in kOe).

Direction	site	$H_d(x)$	$H_d(y)$	$H_d(z)$	H_d^*	\mathbf{x}
(111)	(5,5,5)	1.635	1.635	1.635	2.832	Co - Co
		-5.304	-5.304	-5.304	9.186	Co - Gd
	(5,7,7)	-1.631	0.003	0.003	1.631	Co - Co
		5.357	0.025	0.025	5.357	Co - Gd
$HoCo_2$						
(111)	(5,5,5)	1.693	1.693	1.693	2.932	Co - Co
		-7.849	-7.848	-7.848	13.594	Co - Ho
	(5,7,7)	-1.689	0.003	0.003	1.689	Co - Co
		7.920	0.038	0.038	7.920	Co - Ho

as:

$$H_{\text{eff}}(a) = H_{\text{hf}}(a) + H_d(a)$$

$$H_{\text{eff}}(b)^2 = H_{\text{hf}}(b)^2 + H_d^2(b) - 2H_d(b)H_{\text{hf}}(b) \quad (6.21a)$$

$$\cos(H_d(b)H_{\text{hf}}(b)) \quad (6.21b)$$

By solving these two equations simultaneously for H_d and H_{hf} , by assuming $H_{\text{hf}}(a) = H_{\text{hf}}(b)$, and $H_d(a) = \sqrt{3}H_d(b)$, we found for HoCo_2 that:

$$H_d^{\text{Exp}}(b) = -5.28 \text{ kOe}$$

$$H_d^{\text{Exp}}(a) = -9.15 \text{ kOe}$$

whereas the values calculated from equation (6.19) and table (6.2) are:

$$H_d^{\text{Cal}}(b) = -6.23 \text{ kOe}$$

$$H_d^{\text{Cal}}(a) = -10.61 \text{ kOe}$$

The hyperfine field associated with H_d^{Exp} is found to be 58.64 kOe and with H_d^{Cal} to be 60.0 kOe which are the same within the experimental errors of 2.3%. The errors between the two dipoles are 14%. For GdCo_2 the experimental and calculated magnetic dipoles are

$$H_d^{\text{exp}}(b) = -0.64 \text{ kOe}$$

$$H_d^{\text{exp}}(a) = -1.11 \text{ kOe}$$

$$H_d^{\text{Cal}} (b) = - 3.73 \text{ kOe}$$

$$H_d^{\text{Cal}} (a) = - 6.2K \text{ kOe}$$

As we can see the agreement between the values is very poor. A possible cause of this is that, unlike the case of HoCo_2 , the lines corresponding to the a - and b - sites in GdCo_2 are not fully resolved. The situations for TbCo_2 and for NdCo_2 cannot at present be fully investigated because their spin echo signal are very small as shown in fig. (6.9).

From the above discussion, it appears the ACo_2 compounds have an essentially constant ^{59}Co hyperfine field. If we assume that μ_{Co} (second term in equation) is constant across the series, then H_{Co} is apparently constant. Since H_{hf} is constant then H_{ce} must also be constant. However, in equation (6.4) S_z is given by $(g-1) J$ and we can expect H_{ce} to decrease linearly for the series, provided $A(0)$, Γ and K_f are constant. Consequently, since $H_{\text{ce re}}$ is known to be constant, one or more of these terms must change. Unfortunately, no experimental information is available about the values of Γ , $A(0)$ and K_f and the reasons for the constant value of H_{ce} must await further experimental investigations.

The experimental results of ACo_2 are similar to the results obtained for the ^{57}Fe hyperfine field in AFe_2 compounds.

In these iron compounds, the field at the iron nucleus has been shown by Wertheim and Wernick (ref. 6.15) to remain constant at approximately 230 kOe independent of the rare earth with which it is associated in the compound. These authors used this constant field value to argue that the iron atomic

configuration, and the conduction electron polarization, were also independent of the rare earth involved in the compound. However as Piercy and Taylor (ref. 6.16) have shown the iron moment is not the same in all of these compounds but varies in a range from $1.5\mu_B$ to $2.2\mu_B$. Consequently, it would appear that in these compounds, the various contributions to the hyperfine field adjust as the rare earth sublattice is changed, so as to leave the magnitude of the field almost constant.

This can occur either by the contributions from the moment of the iron ions just cancelling the rare earth moment or, alternatively, the change in the rare earth contribution is compensated by the change in the iron ion contribution.

6.3.1 The temperature dependent hyperfine fields in GdCo₂

The temperature dependence of the hyperfine field in rare earth intermetallic DyFe₂ has been studied by Bowden et al. (ref. 6.19) using Mossbauer techniques. The ⁵⁹Co hyperfine field with temperature has been studied using n.m.r. and the results are shown in fig. (6.16) (ref. 6.12), whereas the variation of the Gd hyperfine field with temperature is shown in fig. (6.17) (ref. 6.17). In our measurement we have studied the hyperfine field of ⁵⁹Co in GdCo₂ as shown in fig. (5.10). Taylor et al. (ref. 6.18) have studied the magnetic properties of GdCo₂, and the magnetization-temperature curve for this compound is shown in fig. (6.18).

In interpreting the shape of the magnetization data and of the hyperfine field data, it is desirable to have a model for the phenomenon of spontaneous magnetization. We have

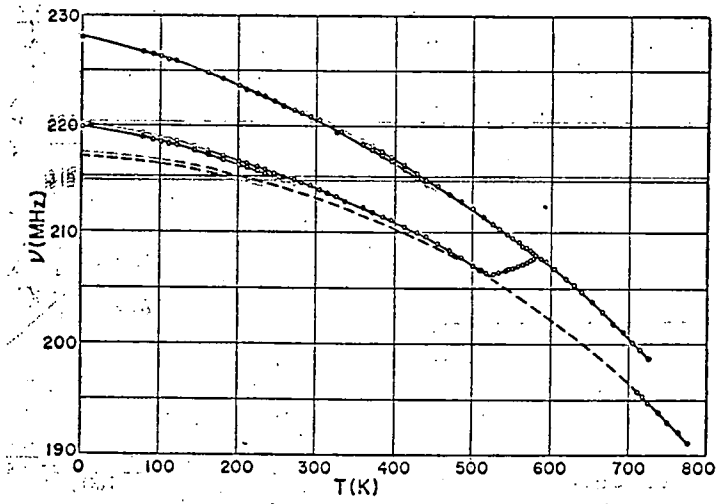


Fig. 6.16. Temperature dependence of ^{59}Co NMR frequencies in hcp cobalt. The dashed curve represents the data in the fcc phase (ref. 6112)

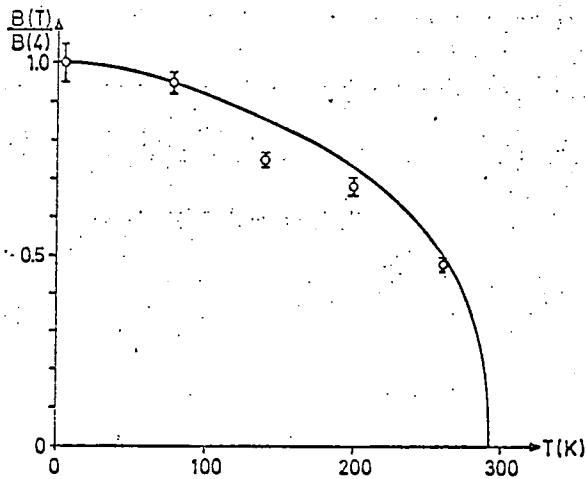
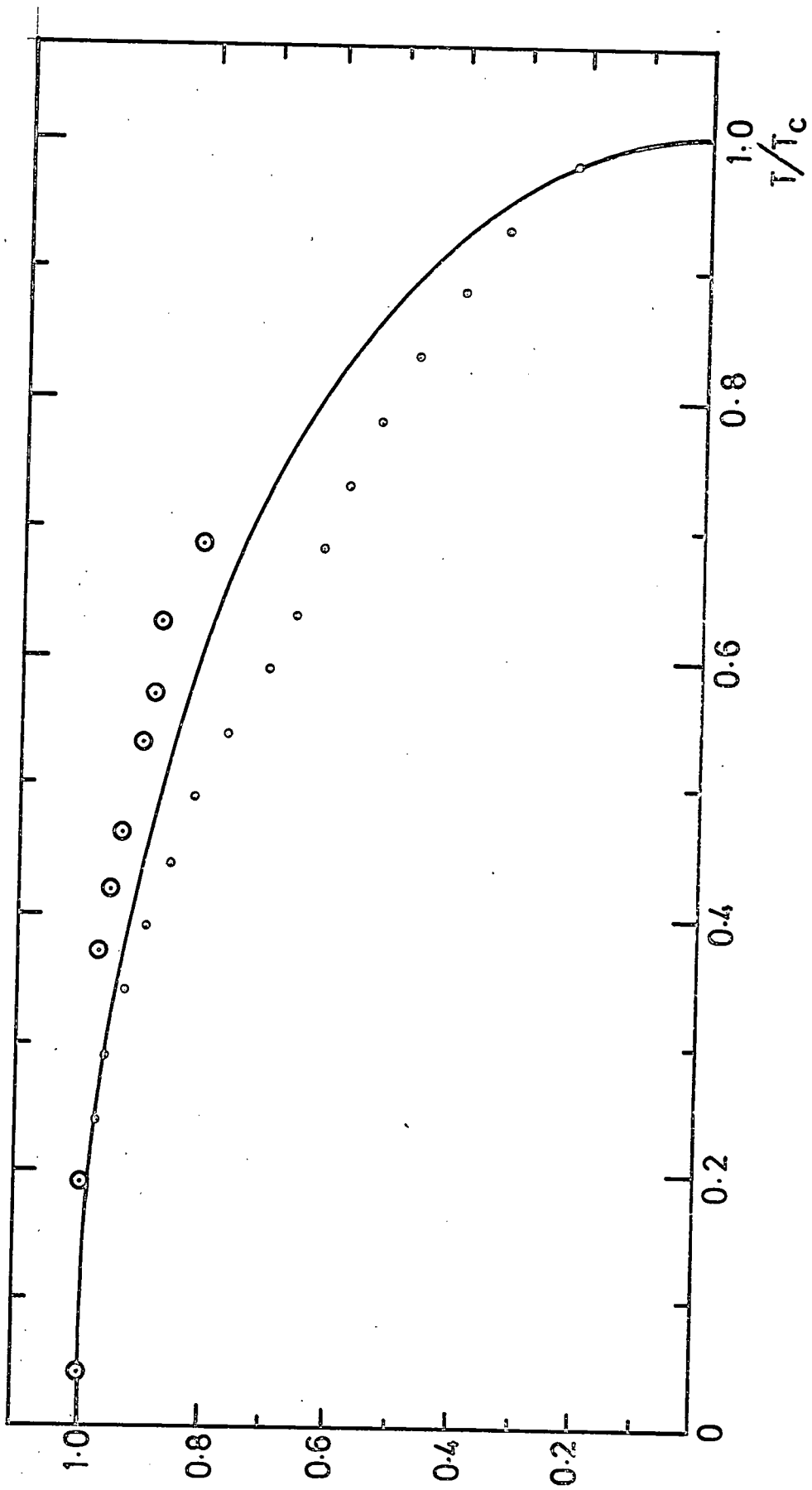


Fig. 6.17. The reduced magnetic hyperfine field at Gd in gadolinium metal. The full line is the magnetization curve for Gd. (ref. 6.17)

Fig. 6.18 Experimental obtained hyperfine fields at Co nuclei in GdCo_2 compared to molecular field calculation for $J=7/2$ — and to measured magnetization . . .



chosen to discuss our results in terms of the molecular field model. In applying the results of this model to the hyperfine fields we make the assumption that the hyperfine field is proportional to the bulk sample magnetization. That is, we assume $H_{hf}(T)/H_{hf}(0) = M(T)/M(0)$. For a spin J associated with Gd, and a Curie temperature T_C , the molecular field model yields.

$$\frac{H_{hf}(T)}{H_{hf}(0)} = \frac{M(T)}{M(0)} = B_J \left\{ \frac{3J}{J+1} \frac{T_C}{T} \frac{M(T)}{M(0)} \right\}$$

The Brillouin function of argument x for spin J is $B_J(x)$. We have computed this function for $J = 7/2$ and the results are shown in fig. (6.18). From fig. (6.18) the hyperfine field at ^{59}Co in GdCo_2 can be seen to decrease with temperature in nearly the same manner as does the magnetization.

In the last three figures, a slight dip can be seen in the experimental curves at around $T/T_C = 0.5$ to 0.6 with the notable exception of Co metal. Thus, although the dip is seen in the hyperfine field of the ^{59}Co nucleus in GdCo_2 , and in the magnetization of the compound itself, it is reasonable to assume that this arises from the Gd nucleus and not from the Co nucleus. Referring to equation (6.20) and to fig. (6.15) it can be seen that, because the experimental results show H_{hf} to have a dip in its temperature variation, and because the temperature variation of $H_{\text{Co}} \mu_{\text{Co}}$ has no such dip, the dip itself must come from the $-H_{\text{ce-re}}$ term.

6.4 N.M.R. of $Gd(Co_{1-x}Al_x)_2$

The pseudobinaries $Gd(Co, Al)_2$ present a more difficult problem of interpretation of the observed resonance spectra than the other materials discussed previously and as yet they are not understood. As we have seen, the series divides into three composition ranges with structural changes from $MgCu_2$ (C15) to $MgZn_2$ (C14) to $MgCu_2$ in going from $GdCo_2$ to $GdAl_2$. In both the C15 regions the resonance spectrum is very complex, and consists of many overlapping components giving a total line with of more than 30 MHz.

In both the terminal cubic compounds $GdCo_2$ and $GdAl_2$ the hyperfine field at the Co or Al site has been shown to be in the (111) direction and there seems to be no reason to assume that this is not also the case in the C15 pseudobinary compositions. In the frequency range in which we have observed the resonances (35 - 70 MHz) for these materials we can anticipate that both ^{59}Co and ^{27}Al will be detectable. The gadolinium resonance is known to be out of this range in $GdAl_2$ but Budnick (1970) ref. (6.20) has suggested that in $GdCo_2$ one of the gadolinium isotope resonances may coincide with the ^{59}Co resonance at 61 MHz. This of course could account for the unusual temperature dependence of the ^{59}Co resonance with temperature in $GdCo_2$. Consequently over the pseudobinary range we may expect to observe resonances from all three constituent elements. Since the gadolinium signals are always very much weaker than the aluminium and cobalt signals however, it seems safe to assume that the gadolinium nuclei do not contribute directly to the observed signals.

Fig. 6.19
 Hyperfine field contributions for
 ^{59}Co and ^{27}Al nuclei as estimated
 for $\text{Gd}(\text{Co}_{1-x}\text{Al}_x)_2$.

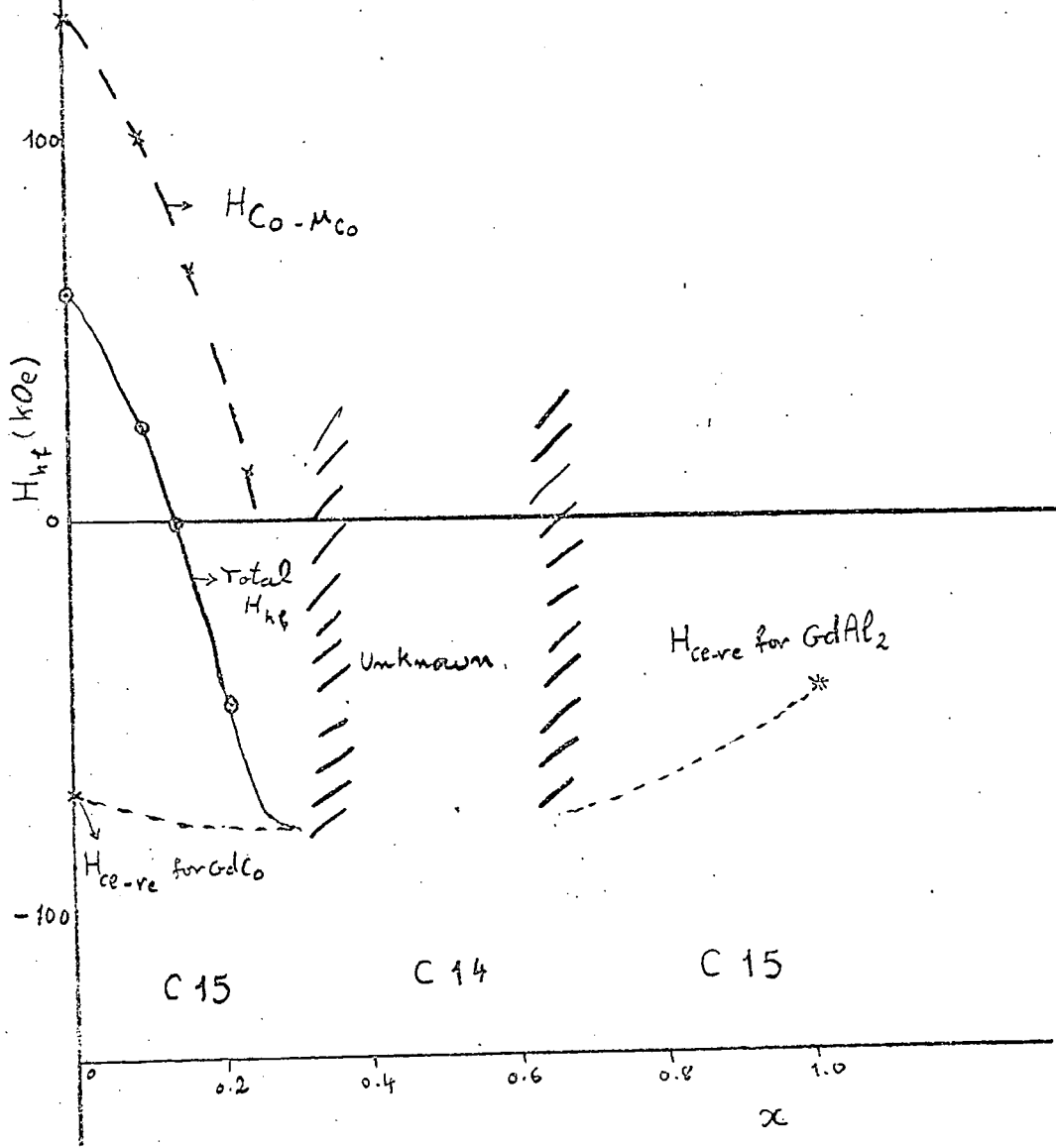
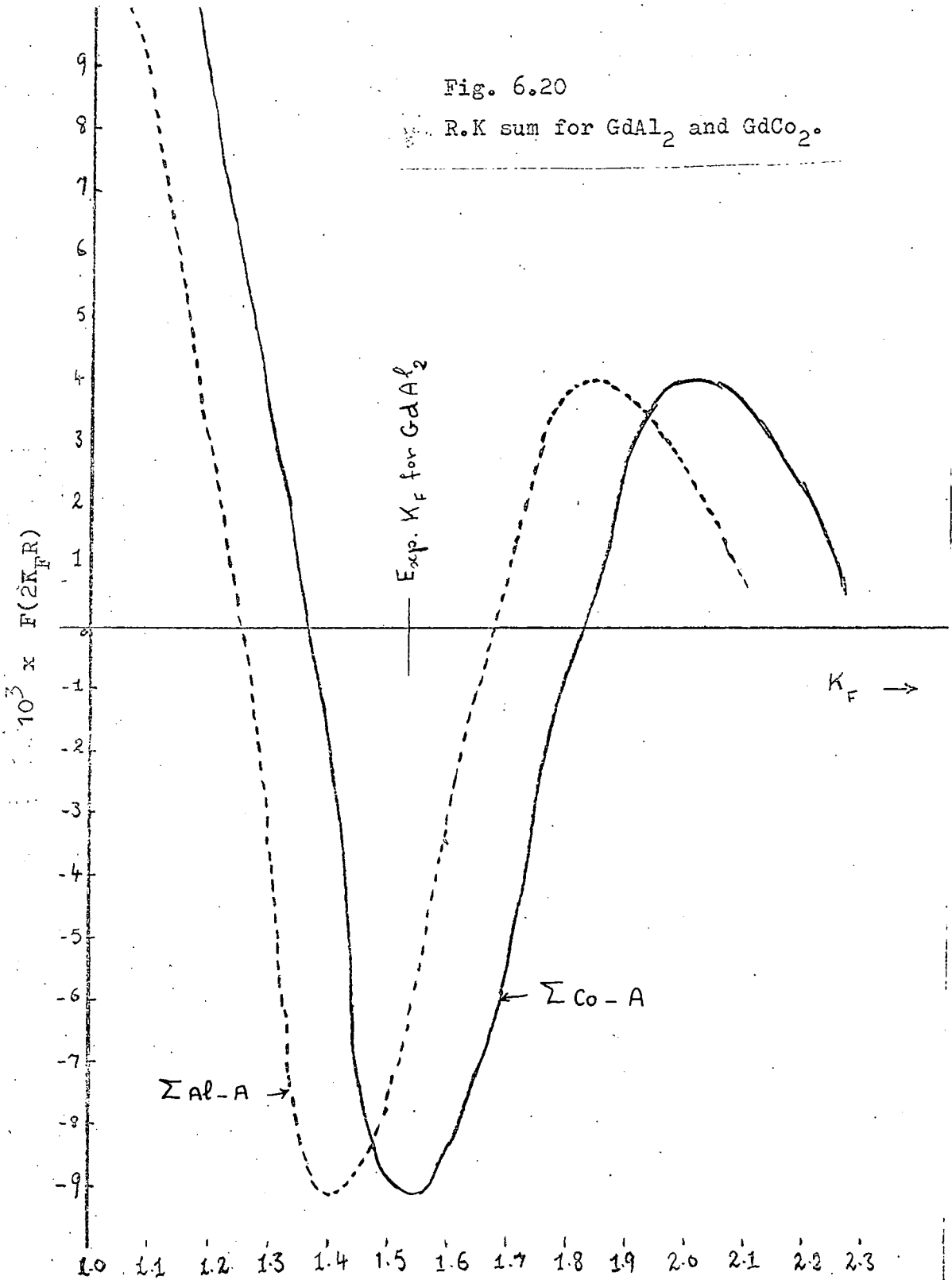


Fig. 6.20

R.K sum for $GdAl_2$ and $GdCo_2$.



The magnetic studies show that with increasing aluminium substitution in GdCo_2 , the moment associated with the cobalt ions decreases rapidly, becoming zero at about 25% Al. Since a large contribution to the ^{59}Co field strength in GdCo_2 arises from the cobalt sublattice this may be expected to decrease with the cobalt moment. Using the same value of the ^{59}Co hyperfine field / Co moment ratio, the cobalt contribution will vary as shown in fig. (6.19). The gadolinium contribution to the ^{59}Co field is opposed to the cobalt contribution as we have seen, consequently it can be anticipated that the total ^{59}Co field will fall to zero at some composition. The Al concentration at which this occurs however, will depend upon the detailed behaviour of the gadolinium contribution with increasing aluminium content. Since aluminium substitution leads to an increase in the valence electron concentration, the corresponding change in the Fermi vector will be reflected directly into a field contribution to the total field through equation (6.4). Wallace and Craig (1967) (ref. 6.21) have shown that the electron concentration increases from about 1.0 in GdCo_2 to 3.0 in GdAl_2 , hence from the value of $K_f = 1.53 \text{ A}^{-1}$ for GdAl_2 , we can obtain a value in GdCo_2 of $K_f = 1.41 \text{ A}^{-1}$. Fig. (6.20) shows the Ruderman-Kittel sum for both these compounds, using the appropriate lattice parameters, and it is evident that in going from GdCo_2 to GdAl_2 the sum, and hence the gadolinium field contribution must pass through a maximum. Since the magnitudes of the parameters in equation (6.4) are largely unknown in the pseudobinary region the magnitude of the increase can not be established with certainty and only a crude estimate is given in fig. (6.19). From this figure then it is evident that

the ^{59}Co field should become zero in the composition range near to 15% Al. This should then result in the cobalt resonance being out of the range of investigation for all but the 30% Al concentration in the cobalt rich C15 compositions. On this basis the observed spectra for $x = 0.1$ and 0.2 must arise from the ^{27}Al nuclei and since the gadolinium contribution to the total field at the Al site increases only slightly over this range, the detailed changes in the spectrum shape must occur through the effects of changing the cobalt neighbour distribution about the aluminium ions. This would then suggest that the signal maxima at 42 and 50 MHz should be treated as satellites of the main line at 61.5 MHz arising from n, nn and nnn neighbour contributions to the field as is usual in the analysis of nmr data of cobalt alloys (ref. 6.22). A considerable contribution to the overall broadening of the spectrum can be expected to arise from the changing cobalt dipole contribution to the total field caused by the aluminium substitution. Unfortunately, within this framework the $x = 0.3$ specimen should represent only the gadolinium contribution to the hyperfine field since here $\mu_{\text{Co}} = 0$. This is clearly not the case when viewed in the simplest way, as there is still a great deal of structure remaining in the observed spectrum, although there is some evidence of the resonances at 50 MHz and 61 MHz observed in pure GdAl_2 . The cause of the structure is a source of considerable conjecture in this sample, and it is likely that more basic magnetic data is required before any further conclusions can be made about its origin.

In the C15 pseudobinaries at the aluminium-rich end of the series, the limited magnetic measurements indicate a

molecular moment in excess of the gadolinium ionic gJ value. This may be due to a positive conduction electron polarization contribution to the total moment or alternatively to a finite cobalt moment aligned parallel to the gadolinium moments. This latter possibility appears unlikely however, since it is generally accepted that the addition of electrons in crossing the compound series results in the filling of the cobalt 3d states. This occurs at about 30% Al (i.e. when $\mu_{Co} = 0$). Consequently we can assume that only the conduction electron polarization contribution to the total field is present in these compounds. In the absence of other effects the ^{27}Al field should then be constant and independent of cobalt concentration. This is not the case however, as is readily obvious from fig. (5.12) and the origin of the detailed structure in the resonances from these materials must originate from some other contribution (compare the $x = 0.3$ sample). The only suggestion which one can readily make is that in fact the cobalt sublattice magnetization is not zero at all points in the sample, and consequently gives rise to an inhomogeneous contribution to the aluminium resonance. Before this can be fully established, more detailed investigations of the magnetic properties of these pseudobinaries are necessary, preferably using neutron diffraction techniques to establish the cobalt sublattice magnetization directly.

In the Cl4 phase, the spectrum is very much simpler than the cases discussed above, its overall shape being essentially constant. For the $x = 0.4$ sample the resonance line is clearly resolvable into two components at 38 and 42 MHz.

With increasing x (i.e. decreasing cobalt concentrations) the smaller resonance line at 42 MHz falls relative to the 38 MHz line. Since in this composition region the total hyperfine field again arises from the conduction electron polarization caused by the gadolinium ions, the fields at both nuclei should be constant and equal. While it is tempting to associate the high frequency peak with the cobalt nuclei because of its behaviour on dilution, the differences in the γ values for the Al and Co nuclei would result in a difference in the fields at the two nuclei of about 20%.

6.5 Conclusion

From the measurements on $Gd_{1-x}Y_xAl_2$ and $Gd_{1-x}La_xAl_2$, the line profile analysis shows that the experimentally observed Al spectra in Y or La diluted $GdAl_2$ can be predicted roughly by the RKKY theory, if instead of the free electron value K_f^0 the reduced value $K_f = 0.945 K_f^0 = 1.53 \text{ \AA}^{-1}$ is taken. Line structures obviously represent a sensitive means of testing the choice of the K_f value and give the possibility of evaluating K_f independently of the other parameters entering the calculation, for example the constant C of equation (6.7) and the analysis of the magnetic data.

In the present calculations, in order to get the analytical expressions of equations (6.1, 6.4) the q dependence of the exchange integral $J(q)$ was abandoned. The values of C and K_f therefore represent averages over the q dependence. The sampling involved in the Gd neighbour configurations is certainly different and more anisotropic than the sampling involved for undiluted $GdAl_2$. For these reasons it is grat-

ifying that the value for K_f derived above and the value obtained with $GdAl_2$ from measurement in the paramagnetic region are essentially the same. This seems to indicate that in these compounds a spherical approximation for the Fermi surface is not too bad.

In the line fitting procedure a number of drastic approximations have been made and it is at present unclear which of these is most responsible for the discrepancies between the experimental and theoretical line shape. It is difficult to arrive at a clear cut conclusion even in the case of $GdAl_2$ since it is necessary to allow for the dipolar contributions to the line shape. Nevertheless the results do show that the observed ^{27}Al line profiles of the compounds studied can be understood in terms of an RKKY like oscillatory conduction electron polarization.

In e.s.r. measurement, for $Gd_{1-x}Y_xAl_2$, the constancy of g value ($g = 1.985 \pm 0.005$) for all the concentration and the variation of $d(\Delta H)/dt$ with composition indicate that the relaxation is bottlenecked. The behaviour of the line width with temperature in the paramagnetic and ferromagnetic regions makes it possible to find the Curie temperature.

The hyperfine fields at the ^{59}Co nucleus have been observed in $GdCo_2$, $HoCo_2$, $TbCo_2$ and $NdCo_2$. The field strength to be essentially constant at about 60.7 kOe. The two-line spectrum is attributed to two inequivalent Co sites and can be interpreted in terms of the different magnetic dipoles at the two sites. The easy direction of the magnetization is (111) for $HoCo_2$ and for $GdCo_2$.

The hyperfine field is composed of two main contributions

(1) the field due to the cobalt which includes a contribution from the ions "own" moment and a contribution from the neighbouring cobalt ions.

(2) the field due to the conduction electron polarization by the neighbouring rare earth ions.

The first one contributes approximately + 135 kOe while the second contributes - 70.8 kOe. Since the hyperfine field represents the total of these contributions, it can be seen that the sign is positive i.e. parallel to the magnetization.

In conclusion for $Gd(Co, Al)_2$ compounds the interpretation is severely limited by the large number of variables involved in a complex magnetic system about which there is insufficient reliable magnetic data, and as suggested above any understanding of these spectra must wait for a better understanding of the magnetostatic properties, in particular the behaviour of the cobalt ions in such materials.

REFERENCES

CHAPTER 1

- 1.1 K.N.R. Taylor & M.I. Darby, "Phys. of Rare Earth Solids" Chapman and Hall Ltd. 1972.
- 1.2 R.J. Elliott, Ed. "Magnetic Properties of Rare Earth Metals" Plenum Press. 1972.
- 1.3 K.N.R. Taylor, Contemp. Phys. 2,423 (1970).
- 1.4 T. Kasuya, in "Magnetism" Vol. 2B, G.T. Rado & H. Suhl, Eds. Academic Press, 1965 Ch.3.
- 1.5 R.J. Elliot, in "Magnetism" Vol.2A, Academic Press, 1965 Ch.7.
- 1.6 B.R. Cooper, in "Solid State Physics" 21, F. Seitz, D. Turnbull & H. Ehrenreich, Eds. Academic Press 1968.
- 1.7 K.N.R. Taylor, Advances in Physics 20, 551 (1971).
- 1.8 J.J. Rhyne & T.R. McGuire, IEEE Transactions on Magnetics, Mag. 8, 105 (1972).
- 1.9 J.W. Cable & E.O. Wollan, Phys. Rev. 165, 733 (1968)
- 1.10 G. Will, R. Nathan & H.A. Alperin, J. Appl. Phys. 35, 1045 (1964).
- 1.11 V.M. Kuchin, V.A. Semerkov, S.Sh.Shilshtein, Soviet Phys. J. ETP, 28, 649 (1969).
- 1.12 W.D. Corner, W. Roe & K.N.R. Taylor, Prog. Phys. Soc. 80, 927 (1962).
- 1.13 D.R. Behrendt, S. Legvold & F.H. Spedding, Phys. Rev. 109, 1544 (1958).
- 1.14 W.C. Koehler, J.W. Cable, M.K. Wilkinson & E.O. Wollan, Phys. Rev. 151, 414 (1966).
- 1.15 J.W. Cable, E.O. Wollan, W.C. Kochler & M.K. Wilkinson, J. Appl. Phys. 32, 495 (1961).
- 1.16 D.B. Richards & S. Legvold, Phys. Rev. 186, 508, (1968).
- 1.17 W.C. Thoburn, S. Legvold & F.H. Spedding Phys. Rev. 110, 1298 (1958).
- 1.18 H.R. Child & J.W. Cable, J. Appl. Phys. 40, 1003 (1969).

- 1.19 S. Weintein, R.S. Craig & W.E. Wallace, J. Appl. Phys. 34, 1354 (1963).
- 1.20 S. Weintein, R.S. Craig & W.E. Wallace, J. Chem. Phys. 39, 1449 (1967).
- 1.21 H.R. Child, W.C. Koehler, E.O. Wollan & J.W. Cable, Phys. Rev. 138A, 1655 (1965).
- 1.22 F. Laves, & H. Wilte, Metallwirtschaft 14, 645 (1935).
- 1.23 F. Laves, Naturwiss, 27, 65 (1939).
- 1.24 V.M. Goldschmidt, Z. Metallik, 13, 449 (1921).
- 1.25 A.E. Dwight, Trans. ASM, 53, 479 (1961).
- 1.26 I.R. Harris, R.C. Mansey & G.V. Raynon, J. Less-common metals 9, 270 (1965).
- 1.27 J.H. Wernick & S. Geller, Trans. AIME 218, 866 (1960).
- 1.28 R.E. Hungsberg, & K.A. Gschneidner, Tr. J. Phys. Chem, Solids 33, 401 (1972).
- 1.29 R.C. Mansey, G.V. Rayner & I.R. Harris, J. Less-common metals 14, 329 (1968).
- 1.30 J. Farrell, & W.E. Wallace, J. Inorg. Chem. 5, 105 (1966).
- 1.31 E. Burzo, J. Less-Common Metals 23, 123 (1971).
- 1.32 H. Oesterreicher and W.E. Wallace, J. Less-Common Metals 13, 19 (1967).
- 1.33 H. Oesterreicher & W.E. Wallace, J. Less-Common Metals 13, 475 (1967).
- 1.34 H. Oesterreicher, J. Appl. Phys. 42, 5137 (1971).
- 1.35 M.A. Ruderman & C. Kittel Phys. Rev. 96, 99 (1954).
- 1.36 T. Kasuya, Progr. Theoret. Phys. (Japan) 16, 45 (1956).
- 1.37 K. Yosida, Phys. Rev. 106, 893 (1957).
- 1.38 R.J. Elliott, in "Magnetism", G.T. Rado & H. Suhl eds. Academic Press, New York Vol. IIA. 385 (1965).
- 1.39 T. Kasuya, in "Magnetism" op.cit. (1966) Vol.IIB.
- 1.40 J. Kondo, Prog. Theoret. Phys. (Kyoto) 32, 37 (1964).
- 1.41 M. Bailyn, Adv. Phys. 15, 179 (1966).
- 1.42 Y. Rocher, Adv. Phys. 11, 233 (1962).
- 1.43 J. Friedel, Adv. Phys. 3, 446 (1954).

- 1.44 J. Kondo, in "Solid State Physics", F. Seitz, D. Turnbull, & H. Ehrenreich, eds) Academic Press New York 23, 183 (1969).
- 1.45 J.H. Van Vleck, Rev. Mod. Phys. 34, 681 (1963).
- 1.46 S.H. Liu, Phys. Rev. 121, 451 (1961).
- 1.47 R.E. Watson & A.J. Freeman, Phys. Rev. 152, 566 (1966).
- 1.48 R.E. Watson & A.J. Freeman, Phys. Rev. Letters 14, 695 (1969).
- 1.49 R.E. Watson & A.J. Freeman, Phys. Rev. 178, 725 (1969).
- 1.50 C. Kittel, in "Solid State Phys." 22, 1 (1968).
- 1.51 K.H.J. Buschow, A. Oppelt & E. Dormann, Phys. Stat. Sol. (b) 50, 647 (1972).
- 1.52 P.G. DeGennes, J. Phys. Radium 23, 630 (1962).
- 1.53 D. Shaltiel, J.H. Wermick, H.J. Williams & M. Peter, Phys. Rev. 28, 271 (1967).
- 1.54 I.A. Campbell, J. Phys. F. Metal Phys. 2, 147 (1972).
- 1.55 P.A. Wolff, Phys. Rev. 120, 814 (1960) and 129, 84 (1963).
- 1.56 A.W. Overhauser, J. Appl. Phys. 34, 1019 (1963).
- 1.57 C. Herring, in "Magnetism", G.T. Rado & H. Suhl eds. Academic Press, Vol. IV (1966).
- 1.58 B. Giovannini, M. Peter & J. Schrieffer, Phys. rev. letters, 12, 736 (1964).
- 1.59 L. Roth, H.J. Zeiger & T.A. Kaplan, Phys. Rev. 149, 519, (1966).
- 1.60 P.R.P. Silva, Phys. Rev. 166, 679 (1968).
- 1.61 A. Blandin, J. Phys. Chem. Solids 22, 507 (1961).
- 1.62 F. Gautier, J. Phys. Chem. Solids 24, 387 (1963).
- 1.63 I. Nowic, in "Mossbauer Effect Methodology" Vol.2 (Ed. I.J. Gruverman), Plenum Press, New York (1966).
- 1.64 A. Abragam & B. Bleaney "Electron Paramagnetic Resonance of Transition ions", Clarendon Press, Oxford (1970).
- 1.65 R.J. Elliot, K.W.H. Stevens, Proc. Roy. Soc. (London) A.218, 553 (1953).

- 1.66 A.J. Freeman & R.E. Watson, Phys. Rev. 123, 2027 (1961).
- 1.67 A.J. Freeman, R.B. Frankel, "Hyperfine interactions" Academic Press (1967).
- 1.68 E. Matthias, D.A. Shirley "Hyperfine Structure and Nuclear Radiations" North Holland Publishing Company, Amsterdam (1968).
- 1.69 B. Bleaney, J. Appl. Phys. 34, 1024 (1963).
- 1.70 S. Ofer, I. Nowic & S.G. Cohen, "Chemical Applications of Mossbauer Spectroscopy (Eds. V.I. Goldanski & R.H. Harber) Academic Press (1968).
- 1.71 F. Dintalman, E. Dorman & Oppelt, Sol. Stat. Comm. 8, 1257 (1970).
- 1.72 S. Kobayashi, N. Sano, J. Itoh, J. Phys. Soc. (Japan) 21, 1456 (1966).
- 1.73 S. Kobayashi, N. Sano, J. Itoh, J. Phys. Soc. (Japan) 23, 474 (1967).
- 1.74 S. Hufner & J.H. Wernick, Phys. Rev. 173, 448 (1968).
- 1.75 H. Zmora, M. Blau & S. Ofer, Phys. Letters 28A, 668 (1969).
- 1.76 S. Hufner, Phys. Letters 19, 1034 (1967).
- 1.77 I. Itoh, S. Kobayashi & N. Sano, J. Appl. Phys. 39, 1325 (1968).
- 1.78 B. Bleaney, "Magnetic Properties of Rare Earth Metals" Plenum Press 383 (1972).
- 1.79 A.P. Guimaraes and A.A. Gomes, Phys. Stat. Sol. (b) 55, 361 (1973).
- 1.80 S.G. Bailey, Ph.D. Thesis, Manchester (1972).
- 1.81 S. Ofer, I. Nowic, Nucl. Phys. A 93, 689 (1967).
- 1.82 U. Antzmony, E.R. Bouminger & S. Ofer, Nucl. Phys. 89, 433 (1966).
- 1.83 S. Ofer, M. Rakary, E. Segal, B. Khurgin, Phys. Rev. 138, A 241 (1965).
- 1.84 R.L. Cohen, Phys. Rev. 134, A 94 (1964).
- 1.85 J.I. Budnick & S. Skaliski "Hyperfine Interaction" 724 (1968).
- 1.86 Guimaraes, Ph.D Thesis, Manchester (1971).

- 1.87 R.E. Gegenworth, J.I. Budnick & Skalski, Phys. Rev. Letters 18, 9 (1967).
- 1.88 I.S. Mächenzie, M.A.H. Macausland, A.R. Wagge, A.P. Giumaraes, E. Holden, S. Baily, "Proc. XVI colloque Ampere" Bucharest (1970).
- 1.89 F. Dintelmann & H.J. Buschow, Z. Angew Phys. Bd. 31, 181 (1971).
- 1.90 U. Antzmony, E.R. Bauminger, D. Lebenbaum, A. Mustache, S. Ofer, & J.H. Wernick, Phys. Rev. 163, 314 (1967).
- 1.91 A. Henberger, F. Pobell, P. Kienle, Z. Phys. 205, 503 (1967).
- 1.92 Y. Seiwa, T. Tsuda, A. Hiral & C.W. Searle, Phys. Letters 43 A 23, (1973).
- 1.93 D. Bloch, J. Varron, A. Berton & J. Chaussy, Sol. Stat. Comm. 12, 685 (1973).

REFERENCES

CHAPTER 2

2. 1 P.G. de Gennes, J. Phys. Radium 23, 510 (1962).
2. 2 Y.A. Rocher, Adv. Phys. 11, 233 (1962).
2. 3 E.D. Jones, Phys. Rev. 180, 455 (1969).
2. 4 B. Bleany, in Hyperfine Interaction, Academic Press, Chapter one (1967).
2. 5 V. Jaccarino, B.T. Mathias, M. Peter, H. Suhl & J.H. Wernick, Phys. Rev. Letters 5, 251 (1960).
2. 6 V. Jaccarino, J. Appl. Phys. 32, 1025 (1961).
2. 7 K. Yosida, Phys. Rev. 106, 893 (1957).
2. 8 A.J. Dekker, J. Appl. Phys. 36, 906 (1965).
2. 9 N. Kaplan, E. Dormann, K.H.J. Buschow, D. Lebenbann, Phys. Rev. B 7, 40 (1973).
- 2.10 E. Dormann, K.H.J. Buschow, K.N.R. Taylor, G. Brown, M.A.A. Issa, J. Phys. F. Metal Phys. 3, 220 (1973).
- 2.11 S. Koide & M. Peter, Rev. Mod. Phys. 36, 160 (1964).
- 2.12 E.D. Jones & J.I. Budnick, J. Appl. Phys. 37, 1250 (1966).
- 2.13 R.G. Barnes & E.D. Jones, Sol. Stat. Comm. 5, 285 (1967).
- 2.14 W.H. Jones, T.P. Graham & R.G. Barnes, Phys. Rev. 132, 1898 (1963).
- 2.15 K.H.J. Bushow, A.M. Van Diepen & H.W. de Wijn, Phys. Letters 24A, 536 (1967).
- 2.16 H.J. Williams, J.H. Wernick, E.A. Nesbit & R.C. Sherwood, J. Phys. Soc. Japan 17, suppl. B.I, 91 (1962).
- 2.17 R.W. Hill & J.M. Machado Clasilva, Phys. Letters 30A, 13, (1969).
- 2.18 H.G. Purwius, Z. Physik, 233, 27 (1970).
- 2.19 N. Nereson, C. Olsen & G. Arnol, J. Appl. Phys. 39, 4605 (1968).

- 2.20 N. Nereson, C. Olsen & G. Arnol, J. Appl. Phys. 37, 4575 (1966).
- 2.21 K.H.J. Burshow, J.F. Fast, A.M. Van Diepen & H.W. de Wijn, Phys. Status Solidi 24, 715 (1967).
- 2.22 V. Niculescu, I. Pop & M. Rosenberg, Phys. Status Solidi, 53, 701 (1972).
- 2.23 H.J. Van Daal & K.H.J. Buschow, Solid State Comm. 7, 217 (1969).
- 2.24 F. Dentilmann, E. Dormann & K.H.J. Burshow, Sol. Stat. Comm. 7, 217 (1969).
- 2.25 N. Shamir, N. Kaplan & J.H. Wernick, J. Phys. Paris 32, C1 - 9P2 (1971).
- 2.26 F. Dentilmann & K.H.J. Buschow, Z. Angew. Phys. 31, 181 (1971).
- 2.27 W.H. Swift & W.E. Wallace, J. Phys. Chem. Sol. 29, 2053 (1968).
- 2.28 K.H. Mader & W.E. Wallace, J. Chem. Phys. 49, 1521 (1968).
- 2.29 B. Stalinski & S. Polrzywnicki, Phys. Stat. Solidi 14, K157 (1966).
- 2.30 H. Hacker, R. Gupta, M.L. Shephard, Phys. Stat. Solidi (a) 9, 601 (1972).
- 2.31 C. Deenadas, A.W. Thompson, R.S. Craig & W.E. Wallace, J. Phys. Chem. Sol. 32, 1853 (1972).
- 2.32 J.A. Mydosh, M.P. Kawatra & J.I. Budnick, Phys. Letters 24A, 421 (1967).
- 2.33 M.P. Kawatra & J.A. Mydosh, Phys. Letters 28A, 182 (1968).
- 2.34 B.R. Coles, D. Griffiths, R.J. Lown & R.H. Taylor, J. Phys. 3, L12 (1970).
- 2.35 M.B. Maple, Sol. Stat. Comm. 8, 1915 (1970).
- 2.36 R.E. Watson, S. Koide, M. Peter & A.J. Freeman, Phys. Rev. 139, A167 (1965).
- 2.37 H.W. de Wijn, K.H.J. Buschow & A.M. Van Diepen, Phys. Stat. Sol. 30, 759 (1968).
- 2.38 J.I. Budnick, R.E. Gegenworth & J.H. Wernick, Bull. Am. Phys. Soc. 10, 317 (1965).
- 2.39 G.K. Wertheim, V. Jaccarino, J.H. Wernick, Phys. Rev. A 135, 151 (1964).

- 2.40 M.V. Nivitt, C.W. Kimball & R.S. Preston, 1964, Proc. Int. Conf. Magnetism, Nottingham.
- 2.41 G.J. Bowden, Ph.D Thesis, Manchester. (1967).
- 2.42 J. Farrell & W.E. Wallace, J. Inorg. Chem. 5, 105 (1966).
- 2.43 E. Burzo & J. Laforest, Intern. J. Magnetism 3, 171 (1972).
- 2.44 G.P. Felcher, L.M. Corliss & J.M. Hastings, J. Appl. Phys. 36, 1001 (1965).
- 2.45 B. Bleany, Proc. R. Soc. A, 276, 28 (1963).
- 2.46 W.E. Wallace & E.A. Skrabek, Rare Earth Research II, ex. by Vorres (Gordon & Breach) p. 431 (1964).
- 2.47 J. Crangle & J.W. Ross, Proc. Int. Conf. on Magnetism Nottingham p.240 (1964).
- 2.48 R.M. Moon, W.C. Koehler & J. Farrell, J. Appl. Phys. 36, 978 (1965).
- 2.49 D. Bloch, F. Chaisse, F. Givord, J. Voiron & E.B. Burzo, J. Physique 32, C1 - 659 (1970).
- 2.50 D. Block & R. Lemaire, Phys. Rev. B2, 2648 (1970).
- 2.51 E. Burzo, Intern. J. Magnetism, 3, 161 (1972).
- 2.52 K.H.J. Buschow, R.P. Van Stepele, J. Appl. Phys. 41, 4066 (1970).
- 2.53 R.C. Mansey, R.C. Raynor, G.V. and I.R. Harris, J. Less, Common Metals 14, 329 (1968).
- 2.54 K.H.J. Buschow, Phys. Stat. Sol. (a) 7, 199 (1971).
- 2.55 G. Primavesi Ph.D. Thesis, Durham University (1972).
- 2.56 J.M. Moreau, C. Michel, M. Simons, T.J. O'Keefe & W. J. Janes, J. Physique 32, C1 - 670 (1970).
- 2.57 E. Burzo, Zeit f. Angrew Phys. 32, 127 (1971).
- 2.58 E.A. Skrabec & W.E. Wallace, J. Apply. Phys. 34, 1356 (1963).
- 2.59 M. Mansmann & W.E. Wallace, J. Chem. Phys. 40, 1167 (1963).
- 2.60 A.R. Piercy & K.N.R. Taylor, J. Appl. Phys. 39, 1096 (1968).
- 2.61 K.N.R. Taylor, Phys. Letters 29A, 372 (1969).

- 2.62 A.R. Piercy & K.N.R. Taylor, J. Phys. C. 2, 1112 (1968).
- 2.63 M. Slanicka, G.J. Primavesi & K.N.R. Taylor, J. Phys. F. 1, 5 (1971).
- 2.64 G.K. Wertheim & J.H. Wernick, Phys. Rev. 125 (1937) (1962).
- 2.65 G.J. Bowden, D. St. P. Bunbury, A.P. Guimaraes & R.E. Snyder, J. Phys. C1, 1376, (1968)
- 2.66 G.J. Bowden, D. St. P. Bunbury, A.P. Guimaraes and R.E. Snyder, J. Appl. Phys. 39, 1323 (1968).
- 2.67 R.L. Cohen & J.H. Wernick, Phys. Rev. 134, B 503 (1964).
- 2.68 R.L. Cohen, Phys. Rev. 134, A94 (1964).
- 2.69 A.P. Guimaraes, Ph.D. Thesis, Manchester 1971.
- 2.70 A.J. Freeman & R.E. Watson, Magnetism IIA, ed. by Rado & Suhl (Academic Press) p.167 (1965).
- 2.71 K.N.R. Taylor, & J.T. Christopher, J. Phys. C. (Sol. Stat. Phys.), 2, 2237 (1969).
- 2.72 A.P. Guimaraes & D. St. P. Bunbury, J. Phys. F. Metal Phys. 3, 885 (1973).

REFERENCES

CHAPTER 3

3. 1 I.I. Rabi, N.F. Ramsy & J. Schwinger, Rev. Mod. Phys. 26, 167 (1954).
3. 2 A. Abragam & B. Bleany, "Electron Paramagnetic Resonance of Transition Ions" Oxford (Clarendon Press) 1970.
3. 3 A. Abragam, "The Principles of Nuclear Magnetism" Oxford (Clarendon Press) 1961.
3. 4 C.P. Slichter, "Principles of Magnetic Resonance" (Harper and Row) 1963.
3. 5 F. Bloch, Phys. Rev. 70, 460 (1946).
3. 6 F. Bloch, W.W. Hnsen & M. Packard, Phys. Rev. 70, 474 (1946).
3. 7 A.N. Daniel, Appl., Spect. 26, 430 (1972).
3. 8 E.L..Hahn, Phys. Rev. 80, 580 (1950).
3. 9 H.Y. Carr & E.M. Purcell, Phys. Rev. 94, 630 (1954).
- 3.10 S. Meiboom & D. Gill, Rev. Sci. Insti. 29, 688 (1958).
- 3.11 "Pulsed N.M.R. Spectrometers" and "Digital Pulse Program Generator" Bruker Scientific Inc.
- 3.12 T.C. Farral & E.D. Becker, "Pulse and Fourier Transform N.M.R." (Academic Press) 1971.
- 3.13 T.P. Das & A.K. Saha, Phys. Rev. 93, 749 (1954).
- 3.14 E.T. Jaynes, Phys. Rev. 98, 1099 (1955).
- 3.15 A.L. Bloom, Phys. Rev. 98, 1105 (1955).
- 3.16 J.S. Mackenzie, Thesis, Manchester (1969).
- 3.17 H. Abe, H. Yasuoka & A. Hirai, J. Phys. Soc. Japan 21, 77 (1966).
- 3.18 P.C. Reidi & R.G. Scurlock, Phys. Letters. 24A, 42 (1967).
- 3.19 N. Shamir, N. Kaplan, & J.H. Wernick, J. Phys. (Paris) 32, C1-902 (1971).

- 3.20 N. Kaplan, E. Dormann, K.H.J. Buschow & D. Lebenbaum
Phys. Rev. B7, 40 (1973).
- 3.21 J. Degani & N. Kaplan, 7, 2132 (1973).
- 3.22 G.F. Hermann, D.E. Kaplan & R.M. Hill, Phys. Rev.
181, 829 (1958).
- 3.23 M. Peter, D. Shaltiel, J.H. Wernick, H.J. Williams,
J.B. Mock & R.C. Herwood, Phys. Rev. 126, 1395 (1962).
- 3.24 F.J. Dyson, Phys. Rev. 98, 349 (1955).
- 3.25 G. Feher & A. Kip, Phys. Rev. 98, 337 (1955).
- 3.26 M. Peters, J. Durpraz & H. Cottet, Helv. Acta 40, 301
(1967).
- 3.27 P.A. Wolff, Phys. Rev. 120, 814 (1960).
- 3.28 P.A. Wolff, Phys. Rev. 129, 84 (1963).
- 3.29 A. Narath, in "Hyperfine Field Interaction" Ch.7.
- 3.30 J. Korringa, Physica 16, 601 (1950).
- 3.31 J. Kondo, Solid State Phys., 183 (1968).
- 3.32 J. Butterworth, Phys. Rev. Letters 5, 370 (1960).
- 3.33 A. Narath, "CRC, Critical reviews in Solid State
Science" , 1 (1972).
- 3.34 M. Bose, "Nuclear Magnetic Resonance Spectroscopy"
ed. by J.W. Emsby et al. Ch. 5, 335 (1968).
- 3.35 T. Moriya, J. Phys. Soc. Japan, 18, 516 (1965).
- 3.36 A. Narath & H.T. Weaver, Phys. Rev. 175, 373 (1968).
- 3.37 R.W. Shaw & W.W. Warren, Phys. Rev. 175, 373 (1968).
- 3.38 H. Hasegawa, Progr. Theoret. Phys. (Kyoto) 21, 483 (1959).
- 3.39 A. Overhauser, Phys. Rev. 89, 689 (1953).
- 3.40 H.K. Schmidh, Z. Naturforsch, 27, 19 (1972).
- 3.41 A.C. Gossard, A.J. Heeger & J.H. Wernick, J. Appl.
Phys. 38, 1251 (1967).
- 3.42 N. Nakamura & N. Kinokhita, J. Phys. Soc. (Japan)
22, 335 (1967) and 23, 449 (1967).
- 3.43 N. Nakamura & N. Kinokhita, J. Phys. Soc. (Japan)
26, 48 (1969).

- 3.44 A.C. Gossard, K.Y. Komatani & J.H. Wernick, J. Appl. Phys. 39, 849 (1968).
- 3.45 Y. Oda, & K. Asayama, J. Phys. Soc. (Japan) 29, 869 (1970).
- 3.46 G. Koopmann, V. Engel, K. Baberschke & S. Hufner, Sol. State Com. 11, 1197 (1970).
- 3.47 C. Rettori, D. Davidov, R. Orbach & E.P. Chock and B. Ricks Phys. Rev. 7, 1 (1973).
- 3.48 W. Schafer, H.K. Schmidt & B. Elschner, Z. Phys. 254, 1 (1972).
- 3.49 G. Weimann & B. Elschner & K.H. Buschow & R.P. Van Staple, Sol. State Com. 77, 871 (1972).
- 3.50 H. Cottett, P. Donze, J. Dupraz, B. Giovannini, M. Peter, Z. Angew. Phys. 24, 249 (1968) and Helv. Acta Phys. 40, 357 (1967).
- 3.51 D. Davidov & D. Shaltiel, Phys. Rev. Letters 21, 1752 (1968).
- 3.52 S. Schultz, M.R. Shanabarger & P.M. Platzman, Phys. Rev. Letters, 19, 749 (1967).
- 3.53 S. Schultz, G. Dunifer & C. Latham, Phys. Letters 23, 192 (1966).
- 3.54 B. Giovannini, Phys. Letters 26 A, 8 (1967).
- 3.55 V. Jaccarino, B.T. Mathias, M. Peter, H. Suhl & J.H. Wernick, Phys. Rev. Letters 5, 252 (1960).
- 3.56 D. Shaltiel, J.H. Wernick, H.J. Williams, M. Peter, Phys. Rev. 135, 1346 (1964).
- 3.57 J.H. Wernick, H.J. Williams & A.C. Gossard, J. Phys. Chem. Sol. 28, 271 (1967).
- 3.58 D. Davidov & D. Shaltiel, Phys. Rev. 169, 329 (1968).
- 3.59 H. Hacker, R. Gupta & M.L. Sheppard, Phys. Stat. Sol. 9, 601 (1972).
- 3.60 R.H. Taylor, Thesis, Imperial College London, (1972).
- 3.61 I. Ursu & E. Burzo, J. Magnetic Resonance 8, 1 (1972).
- 3.62 E. Burzo, Inter. J. Phys. 3, 161 (1972).
- 3.63 D. Davidov & D. Shaltiel, Phys. Rev. Letters 21, 1752 (1968).
- 3.64 D. Davidov & G. Dublon & D. Shaltiel, Phys. Rev. B3, 3651 (1971).

- 3.65 D. Debray & E. Ryba, J. Phys. (Paris) 32, C1, 1130 (1971).
- 3.66 D. Davidov, A. Chelkowski, G. Retton, R. Orbach and M.B. Maple, Phys. Rev. B, 7, 1029 (1973).

REFERENCES

CHAPTER 4

- 4.1 W.G. Clark, Rev. Sci. Inst. 35,316(1964).
- 4.2 Services 'Text Book of Radio' , vol 5, p=220 ; HMSO (1958)
- 5.3 R.P. Hunt, Ph. D thesis (to be published) Durham university.
- 5.4 C.A. Poldy, Ph.D thesis, Durham university (1972)

REFERENCES

CHAPTER 5

- 5.1 J.B. Nelson & D.P. Riley, Proc. Phys. Soc. 57, 160 (1945).
- 5.2 G.J. Primavesi, Ph.D Thesis, Durham University, 1972.
- 5.3 R.L. Streever & G.A. Urian, Phys. Rev. 139, A135 (1965).
- 5.4 S. Kobayashi, K. Asayama & J. Itoh, J. Phys. Soc. Japan 21, 65 (1966).
- 5.5 H. Kubo, M. Kontani & J. Itoh, J. Phys. Soc. Japan 22, 929 (1967).
- 5.6 G. Brown, M.A.A. Issa, K.N.R. Taylor, J. Phys. F. Metal Phys. 1, L10 (1971).

REFERENCES

CHAPTER 6

6. 1 D.J. Morgan & Rushbrooke, Mol. Phys. 1, 291 (1961).
6. 2 M.B. Maple, Thesis, University of California, 1969.
6. 3 R.E. Watson, A.J. Freeman, Phys. Rev. Letters. 6, 277 (1961).
6. 4 K. Yosida, Phys. Rev. 106, 893 (1957).
6. 5 K.H.J. Buschow, A. Oppelt & E. Dormann, Phys. Stat. Sol. (b) 50, 647 (1972).
6. 6 G.K. Wertheim, V. Jaccarino, J. H. Wernick and D.N.E. Buchanan, Phys. Rev. Lett. 12, 24 (1964).
6. 7 G.K. Wertheim, D.N.E. Buchanan, and J.H. Wernick, J Appl. Phys. 42, 1602 (1971).
6. 8 R.H. Taylor, Thesis, Imperial College London. (1972)
6. 9 A.M. Portis & A.C. Gossard, J. Appl. Phys. 31, 2055 (1960).
- 6.10 N. Veno, H. Nagai, J. Phys. Soc. Japan 31, 1275 (1971).
- 6.11 S.S. Hanna, J. Heberle, C. Littlejohn, G.H. Perlow, R.S. Preston, & D.H. Vincent, Phys. Rev. Letters 4, 177 (1960) and Phys. Rev. Letters 4, 513 (1960).
- 6.12 M. Kawakami, T. Hihara & Y. Koi, J. Phys. Soc. Japan 33, 1591 (1972).
- 6.13 K.N.R. Taylor & J.T. Christopher, J. Phys. C. 2, 2237 (1969).
- 6.14 R.E. Gegenworth, J.I. Budnick & S. Skalski, J. Appl. Phys. 37, 1244 (1966).
- 6.15 G.K. Wertheim & J.H. Wernick, Phys. Rev. 125, 1937 (1962).
- 6.16 A.R. Piercy, K.N.R. Taylor, J. Appl. Phys. 39, 1096 (1968).
- 6.17 L. Bostrom, B. Jonsson, G. Carlsson & E. Karlsson, Phys. Scripta, 3, 183 (1971).
- 6.18 K.N.R. Taylor, H.D. Ellis & M.I. Darby, Phys. Letters, 20, 327 (1966).

- 6.19 G.J. Bowdon, Thesis, Manchester (1967).
- 6.20 J.I. Budnick, Private Communication.
- 6.21 W.E. Wallace and R.S. Craig in "Phase stability in metals and alloys" P.S. Rudrman (ed) McGraw Hill N.Y. (1967).
- 6.22 S. Kobayashi, K. Asayam and J. Itoh
J. phys. soc. Japan, 21, 65 (1966).

APPENDIX 1

MgCu₂: Structure

$$R_n = \frac{a}{8} \sqrt{x}$$

where R_n is the distance between any two of the atoms in this structure, n is the number of the shell and a is the lattice parameter.

Mg - Cu		
no. of the shell	no. of Cu in each shell	x
1	12	11
2	16	27
3	12	43
4	36	59
5	28	75
6	24	91
7	36	107
8	24	123
9	36	139
10	48	155
11	60	171
12	24	187
13	48	203
14	48	219
15	24	235
16	84	251
17	24	267
18	36	283
19	96	299

Cu - Cu		
no. of the shell	no. of Cu in each shell	x
1	6	8
2	12	24
3	12	32
4	12	40
5	24	56
6	6	64
7	18	72
8	12	88
9	24	96
10	36	104
11	24	120
12	12	128
13	24	136
14	36	152
15	24	160
16	24	168
17	24	184
18	8	192
19	42	200

20	72	315
21	36	331
22	60	347
23	52	363
24	36	379
25	96	395
26	72	411
27	24	427
28	60	443
29	86	459
30	60	475
31	108	491
32	52	507
33	60	523
34	108	539
35	48	555
36	60	571
37	84	587
38	60	603
39	60	619
40	120	635

20	48	216
21	48	224
22	12	232
23	48	248
24	6	256
25	48	264
26	24	280
27	36	288
28	60	296
29	24	312
30	24	320
31	24	328
32	60	344
33	24	352
34	60	360
35	48	376
36	24	384
37	54	392
38	24	408
39	72	416
40	36	424

Mg - Mg		
no. of the shell	no. of Mg in each shell	x
1	4	12
2	12	32
3	12	44
4	6	64

Cu - Mg		
no. of the shell	no. of Mg in each shell	x
1	6	11
2	8	27
3	6	43
4	18	59

5	12	76	5	14	75
6	24	96	6	12	91
7	16	108	7	18	107
8	12	128	8	12	123
9	24	140	9	18	139
10	24	160	10	24	155
11	12	172	11	30	171
12	8	192	12	12	187
13	24	204	13	24	203
14	48	224	14	24	219
15	36	236	15	12	235
16	6	256	16	42	251
17	12	268	17	12	267
18	36	288	18	18	283
19	28	300	19	48	299
20	24	320	20	36	315
21	36	332	21	18	331
22	24	352	22	30	347
23	24	364	23	26	363
24	24	384	24	18	379
25	36	396	25	48	395
26	72	416	26	36	411
27	36	428	27	12	427
28	24	460	28	30	443
29	48	480	29	48	459
30	24	492	30	30	475
31	12	512	31	54	491
32	60	524	32	26	507
33	48	544	33	30	523
34	36	556	34	54	539

35	30	576	35	24	555
36	28	588	36	30	571
37	72	608	37	42	587
38	48	620	38	30	603
39	24	640	39	30	619
40	12	652	40	60	635



A study of the lineshape of the NMR spin echo spectra of the compounds $Gd_{1-x}Y_xAl_2$ and $Gd_{1-x}La_xAl_2$

E Dormann†, K H J Buschow‡, K N R Taylor§,
G Brown§ and M A A Issa§

† Experimental Physik II, Technische Hochschule, Darmstadt, Germany

‡ Phillips Research Laboratories, Eindhoven, Holland

§ Physics Department, University of Durham, Durham, UK

MS received 8 June 1972

Abstract. NMR spin echo spectra of $Gd_{1-x}Y_xAl_2$ and $Gd_{1-x}La_xAl_2$ ($0 \leq x \leq 0.30$) were studied in the ferromagnetically ordered state at 4.2 K. The Al resonance line profiles were analysed under the assumption of various models for the spatial extent of the conduction electron polarization and general confirmation of a RKKY like oscillatory polarization was found. Slowly decreasing nonoscillatory polarization functions are shown to be unable to explain the observed spectra. The line shape is shown to depend rather critically on the value of the Fermi wavevector k_F . The polarization seems to decrease less strongly with distance than might be expected from the RKKY function.

1. Introduction

In several recent investigations the Ruderman–Kittel–Kasuya–Yosida theory (Ruderman and Kittel 1954, Kasuya 1956 and Yosida 1957) has been used to discuss and/or describe the results of the measurements of bulk magnetic properties (Buschow *et al* 1967, Leon *et al* 1971, Swift and Wallace 1971) Knight shift (Jaccarino 1961) and hyperfine field (Dintelmann and Buschow 1971) of the compound $GdAl_2$ and the corresponding pseudobinary compound $Gd_{1-x}RE_xAl_2$ ($RE = La, Y, Th$). To compare experiments with theory, the following expressions have been used (Yosida 1957, de Gennes 1962):

$$\theta_p = -\frac{3}{4}\pi \left(\frac{Z^2 \Gamma^2}{k_B E_F} \right) (g-1)^2 J(J+1) \sum_{n \neq m} F(2k_F R_{nm}) \quad (1)$$

$$\mathcal{H}_{sf} = -6\pi Z \Gamma \sum_n F(2k_F R_{nm}) \quad (2)$$

$$H_{hf} = +\frac{9}{4}\pi \left(\frac{Z^2}{E_F} \right) \frac{A(0)}{g_I \mu_I} \Gamma \langle S_z \rangle \sum_{n \neq m} F(2k_F R_{nm}) \quad (3)$$

$$F(x) = (x \cos x - \sin x)/x^4.$$

The quantity Γ has the form of an effective exchange integral between the rare earth spin S and the conduction electron spin s and is defined by the Hamiltonian $\mathcal{H} = -\Gamma \mathbf{s} \cdot \mathbf{S}$. Z represents the average number of conduction electrons. In equation (1) the summation is over all the Gd sites of the lattice with a Gd site at the origin. In equation

(2) the summation is also over all Gd sites with an Al atom at the origin but in equation (3) the choice of the origin depends on whether the hyperfine field refers to Gd or Al nuclei. The experimental parameters θ_p , \mathcal{J}_{sf} and H_{hf} represent respectively the asymptotic Curie temperature (obtained from the temperature dependence of the magnetic susceptibility), the s-f coupling constant (obtained from the slope of the Al Knight shift against susceptibility), and the hyperfine field (obtained from spin echo measurements in ferromagnetically ordered Gd_{1-x}RE_xAl₂). In Buschow *et al* (1967) the experimental values for θ_p and \mathcal{J}_{sf} have been used to solve equation (1) and (2) for k_F and Γ with the result $\Gamma = -0.91$ eV, $k_F = 0.94 k_F^0 = 1.53 \text{ \AA}^{-1}$. The 6% deviation of k_F from the free electron value $k_F^0 = (3\pi^2 Z/V)^{1/3} = 1.63 \text{ \AA}^{-1}$ was shown to be in close agreement with the rapid decrease of θ_p in the series Gd_{1-x}Th_xAl₂. Two more values for k_F have been proposed: from the results of bulk magnetic measurements on GdAl_{2-x}Ni_x compounds and by application of equation (1) Leon *et al* (1971) conclude that $k_F = 0.86 k_F^0 = 1.4 \text{ \AA}^{-1}$ for GdAl₂ whereas Swift and Wallace (1971) from a similar investigation of the compounds Gd_{1-x}Eu_xAl₂ arrive at the value $k_F = 0.95 k_F^0 = 1.54 \text{ \AA}^{-1}$. Dintelmann *et al* (1971) used equation (3) to compare the neighbour contribution to the Gd and Al hyperfine fields in ferromagnetically ordered Gd_{1-x}Y_xAl₂ with the predictions of the RKKY approach (Yosida 1957) and find at least a qualitative agreement with experimental data using the values for Γ and k_F reported by Buschow *et al* (1967). In all these cases, in order to obtain agreement with experiment the value of the Fermi wavevector k_F was allowed to depart slightly from the free electron value k_F^0 . This means that the assumption made in the RKKY approach of free s-like conduction electrons is abandoned. As a first approximation for the solution of the real q dependent averaging problems $\sum_{m,q} |J(q)|^2 f(q) \exp(iq \cdot R_{mn})$ in equation (1) and $\sum_{m,q} A(q) J(q) f(q) \exp(iq \cdot R_{mn})$ in equations (2) and (3), the same values of Γ , the usual RKKY function and one equally reduced parameter k_F is used in equation (1) as in equations (2) and (3). The validity of this procedure is not at all selfevident (Oppelt *et al* 1972) but it is of common use and easiest to perform. Further, it seems to be more reliable, if the deviation of k_F from k_F^0 is kept small.

All the investigations cited above consider only summations in the RKKY expressions (equations (1)–(3)) in which the R dependence remains fixed by the crystal structure requirements and in which only k_F was allowed to vary. So the bulk magnetic properties reported by Buschow *et al* (1967) for the compounds Gd_{1-x}RE_xAl₂ could adequately be described by replacing the function $\sum_{n \neq m} F(2k_F R_{nm})$ in equation (1) by $(1-x) \sum_{n \neq m} F(2k_F R_{nm})$. In the present investigation an attempt will be made to obtain a more direct test of the R dependence of the oscillatory RKKY function by considering the statistically weighted contributions of the different configurations due to the various possible Gd neighbour shell occupations in the magnetically dilute compounds. By means of a line shape analysis of the NMR spectra obtained for the compounds Gd_{1-x}La_xAl₂ and Gd_{1-x}Y_xAl₂ for small values of x we hope to demonstrate whether a spatially nonuniform conduction electron polarization such as implied in the derivation of equations (1)–(3) is essential or not. It will furthermore be shown that the line shape depends rather critically on the value of the k_F parameter and its value can be determined rather accurately independent of the previous results.

2. Experimental procedure

The samples used were prepared from 99.99% pure aluminium and 99.9% pure rare

earths by arc melting. Most ingots were annealed for about 45 h at 900°C, some La diluted samples for a week at 850°C; quenching or longer annealing periods did not change the NMR spectra significantly. The homogeneity of the pulverized samples (about 60 μm in diameter) was checked by x ray analysis. Spin echo spectra of $\text{Gd}_{1-x}\text{Y}_x\text{Al}_2$ and $\text{Gd}_{1-x}\text{La}_x\text{Al}_2$ (with $x = 0, 0.05$ up to 0.30) were taken in Darmstadt with the aid of a Bruker B-KR 322s spectrometer utilizing phase sensitive detection and a boxcar integrator†. The rf field strength of two pulses of 1 μs duration, separated by 30 μs , with 100 μs repetition rate, was adjusted to maximum echo height.

Maximum height was chosen as the optimum echo criterion rather than constant echo shape (as specified by Dean and Urwin (1970) for domain wall resonances) as we believe the present measurements are associated with the bulk material and are not resonances in domain walls. This conclusion is supported by our own observations and those of Kaplan (1971) in which the modulation of the echo height by the quadrupolar and dipolar fields are clearly visible.

All measurements were performed at 4.2 K in zero external field; (prior to the measurements, the samples were magnetized after cooling down to 4.2 K in fields up to 11 kG perpendicular to the rf field). The variation of the spectrometer sensitivity was controlled with the help of a Rohde and Schwarz Polyskop. By comparison with proton FID, the phase sensitive detected signals had to be divided, in the range of interest of this investigation, by about the third power of the frequency, in order to obtain the resonance field distribution. The spectra shown in this paper (figures 1–4) are corrected in this way and smoothed twice according to

$$E'(v) = \frac{1}{2} E(v) + \frac{1}{4} \{ (E(v) - 0.2) + (E(v) + 0.2) \} \quad (4)$$

where 0.2 MHz is the distance between the measuring points.

3. Experimental results

3.1. Gd resonances

Before the observed gadolinium spectra are markedly broadened or superposed by the much stronger Al^{27} resonance in $\text{Gd}_{1-x}\text{Y}_x\text{Al}_2$ a shift of the Gd^{155} and Gd^{157} resonances to lower frequencies is observed (Dintelmann and Buschow 1971, Dintelmann *et al* 1970). Corresponding shifts could not be detected in $\text{Gd}_{1-x}\text{La}_x\text{Al}_2$. In this case, the Gd resonances are broadened before any definite shift could be discerned (at $x = 0$: halfwidth $\simeq 1 - 1.4$ MHz; whereas at $x = 0.10$: halfwidth $\simeq 2 - 2.4$ MHz). This is probably due to the fact that lanthanum distorts the GdAl_2 lattice more severely than yttrium (lattice constants: $a(\text{YAl}_2) = 7.858 \text{ \AA}$, $a(\text{GdAl}_2) = 7.900 \text{ \AA}$, $a(\text{LaAl}_2) = 8.147 \text{ \AA}$).

3.2. Al resonances in GdAl_2

For $x = 0$, that is pure GdAl_2 , the Al^{27} resonances (figure 1) are found to be essentially in agreement with those reported by Shamir *et al* (1971). The two lines at about 49.45 MHz and 61.15 MHz in figure 1(b) (halfwidths $\simeq 2.2$ MHz), with an intensity ratio of about 3:1, have been explained as being due to Al^{27} nuclei at the $b(\times 3)$ and $a(\times 1)$ sites.

† Measurements were also carried out simultaneously in Durham using a conventional spin-echo system. The two sets of results were essentially identical and only the Darmstadt data is given in the following.

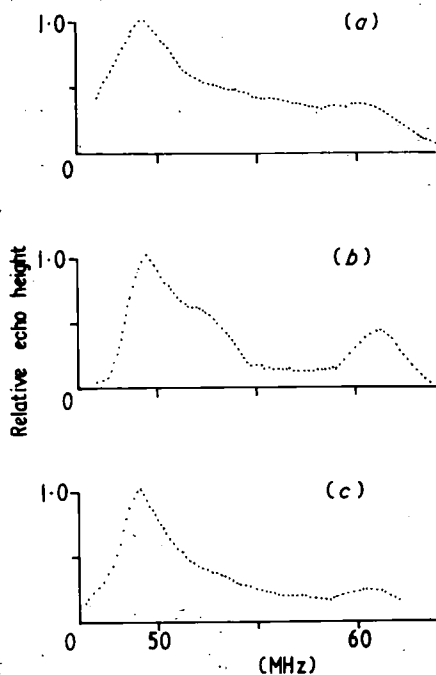


Figure 1. Al^{27} resonance in $GdAl_2$ at 4.2 K with $H_{ext} = 0$ for different grain sizes. The spectra are corrected for sensitivity variation of the spectrometer and smoothed twice; (a) $< 50 \mu m$, (b) $\sim 60 \mu m$, (c) $90-120 \mu m$.

respectively in (111) magnetized domains of $GdAl_2$. The differences in these resonance fields have been ascribed to different dipolar contributions in the expression $H_{res} = H_{dip} + H_{hf}$. From the two lines we derive, with $\gamma = 1.1094 \text{ MHz kG}^{-1}$ that $|H_{hf}| = (47.2 \pm 0.8) \text{ kG}$ (the sign of the field was shown to be negative by Shamir *et al* (1971)) and the dipolar field values $H_{dip}(a/b) = 8.0/4.6 \text{ kG}$ correspond, to within 15%, with the point dipole sum taken in a sphere of 20 \AA radius (assuming $7.0 \mu_B$ per Gd ion in the (111) direction). Due to the quadrupolar interactions which are small compared with the linewidth for the directions of H_{res} , echo oscillations are observed for the a and b line (Shamir *et al* 1971).

As can be seen by a comparison of the spectra given as examples in figures 1(a)–1(c), the details of the Al^{27} lineshape depend on sample preparation and grain size. In figure 1(c) a stronger decrease of signal height with frequency is observed, probably due to a mean particle radius exceeding the skin depth. Relatively long grinding treatments result in a finer powder (figure 1(a)) which is found to cause line broadening and increase the background. For these specimens the spectrum contains signals other than the pure (111) domain resonances. With increasing deformation of the powder particles the line due to the a sites (61.15 MHz) can be found to shift to frequencies below 60 MHz . Apart from a background intensity of about 10% between the two (111) domain nuclei resonances, we observe with our $60 \mu m$ sample (figure 1(b)) an additional line at about 52 MHz ($\approx 47.0 \text{ kG}$) with a halfwidth of about 3.4 MHz and about 0.75 times as intense as the b line. A study of the magnetic field dependence of the signal intensity proved that this line is also caused by nuclei in domains. The line position corresponds to the resonance field of domain nuclei without any essential dipolar shift and could be due to

Al^{27} nuclei in (100) domains for which the dipolar field (~ 4.9 kG, calculated within 20 \AA radius) is perpendicular to the hyperfine field and therefore induces only a small difference between the absolute values of H_{res} and H_{hf} . The (100) domains are observed in several of the other REAl_2 compounds and may be present in GdAl_2 as closure domains or in distorted regions. No separate Al^{27} resonances due to nuclei in domain walls could be discerned in the spectrum of figure 1(b) in contrast to earlier interpretations. The absence of Al^{27} wall lines can be explained by a smearing out of the corresponding resonance line as a result of the anisotropic dipolar contribution to the resonance field. The centre of gravity of the Al^{27} resonance spectrum of GdAl_2 (figure 1(b)) lies at about 52.7 MHz, that is 47.5 kG. This is close to the pure hyperfine field position.

3.3. Al resonances in yttrium and lanthanum diluted GdAl_2

Since the samples with a particle size of about $60 \mu\text{m}$ gave the 'purest' Al spectrum in the previous section (figure 1(b)), the dilution experiments were performed with samples prepared in a similar way. The upper part of the Al resonances in $\text{Gd}_{1-x}\text{Y}_x\text{Al}_2$ is shown in figure 2; the corresponding spectra for $\text{Gd}_{1-x}\text{La}_x\text{Al}_2$ are given in figure 3. Figure 4 shows the spectrum for a $\text{Gd}_{0.75}\text{La}_{0.25}\text{Al}_2$ sample over a wider frequency range. The accuracy in this case is reduced due to the fact that additional probe coils were necessary to span the wider frequency range.

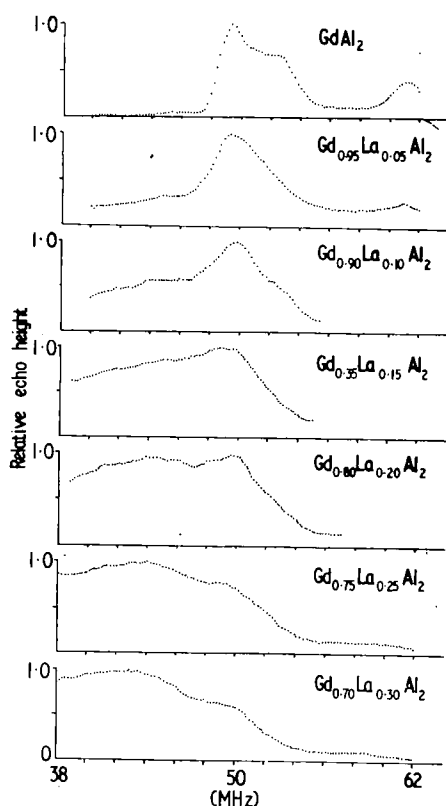


Figure 2. Upper frequency range of the Al^{27} resonance in $\text{Gd}_{1-x}\text{Y}_x\text{Al}_2$; measured at 4.2 K with $H_{\text{ext}} = 0$; corrected and smoothed as in figure 1.

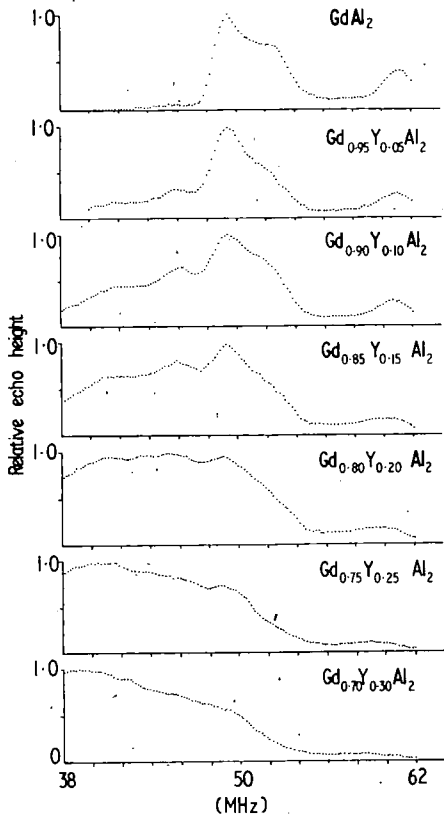


Figure 3. Upper frequency range of the Al^{27} resonance in $Gd_{1-x}La_xAl_2$; measured at 4.2 K with $H_{ext} = 0$; corrected and smoothed as in figure 1.

In the diluted samples the higher Al resonance is smeared out, whereas the lower resonance lines obviously remain essentially unshifted and are supplemented by new resonance lines primarily at the low frequency side. Some structure can be seen, at least two bumps at about 41–42 MHz and 45–46 MHz for small dilutions x . This structure is more pronounced for the compounds with yttrium. This again may be due to the greater similarity between Gd and Y than Gd and La. It is clear from these results that the maximum of the Al resonance spectrum is not displaced linearly with x for low dilution in either $Gd_{1-x}Y_xAl_2$ or $Gd_{1-x}La_xAl_2$. Nevertheless, the centre of gravity follows a linear law that is $\nu_{cgr} = (1-x)\gamma H_{hf}(GdAl_2)$ within the experimental accuracy for the examples tested.

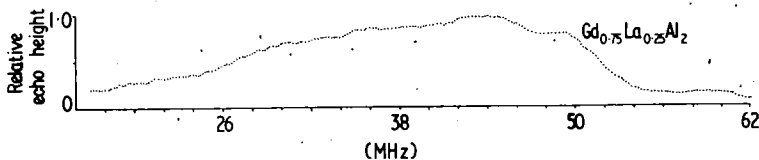


Figure 4. The Al^{27} resonance in $Gd_{0.75}La_{0.25}Al_2$ (after 10 days annealing at 850°C) measured at 4.2 K with $H_{ext} = 0$, corrected and smoothed as in figure 1.

4. Line profile analysis

Dintelmann and Buschow (1971) showed that because of the negligible contributions of the conduction electrons to the magnetic moment in the ordered state of GdAl_2 , the RKKY theory could qualitatively describe the spin echo results obtained for the ferromagnetic state of this system†. In the following the value of $C = 9\pi Z^2 \Gamma A(0)/4E_F g \mu_B$ appearing in equation (3) will be chosen so as to match the observed hyperfine field at the Al nuclei in GdAl_2 :

$$H_{\text{hf}}(\text{RKKY}, x = 0) = C \sum_{m \neq n} F(2k_F R_{nm}) \langle S_z \rangle_m = -47.2 \text{ kG}. \quad (4)$$

The average hyperfine field for the magnetically diluted samples ($x \neq 0$) will then be given by

$$\overline{H_{\text{hf}}(\text{RKKY}, x \neq 0)} = (1 - x) C \sum_{m \neq n} F(2k_F R_{nm}) \langle S_z \rangle_m \quad (5)$$

provided that $(k_F a)$, Z , E_F , Γ and $A(0)$ do not depend on x . This is true within the free electron model as Gd, La, Y and Al all supply three conduction electrons but it is at best a crude approximation in the real system. The breakdown of the free electron model is shown for example by the difference of the Pauli susceptibilities: $\chi_p(\text{LaAl}_2) = 3.16 \times 10^{-6}$ and $\chi_p(\text{YAl}_2) = 4.83 \times 10^{-6}$. Nevertheless, the almost linear dependence of the asymptotic Curie temperatures θ_p on dilution by La or Y observed over the whole range $0 \leq x \leq 1$ by Buschow *et al* (1967) indicates that the approximation of a constant value for C and $(k_F a)$ which will be assumed for the smaller range $x = 0-0.30$ is not too unrealistic.

In order to obtain expressions for the concentration x dependence of the hyperfine fields, we took account of the different configurations arising from the variety of possible occupations of the Gd neighbour shells and the corresponding statistical weights. The numbers of Gd sites in the nearest Gd shells around the Al atoms in GdAl_2 are:

$$\begin{aligned} N_1 &= 6 & R_1 &= \frac{1}{8}\sqrt{11}a & N_2 &= 8 & R_2 &= \frac{1}{8}\sqrt{27}a \\ N_3 &= 6 & R_3 &= \frac{1}{8}\sqrt{43}a & N_4 &= 18 & R_4 &= \frac{1}{8}\sqrt{59}a \dots \end{aligned}$$

Since a gadolinium atom situated in a shell outside the third nearest neighbour shell contributes less than 1% to the sum in equation (4) in the k_F range of interest we took as a first approximation

$$\begin{aligned} H_{\text{hf}}(\text{RKKY}, x, n_1, n_2, n_3) &= C \langle S_z \rangle \{n_1 F(2k_F R_1) + n_2 F(2k_F R_2) + n_3 F(2k_F R_3) \\ &+ (1 - x) \sum_{\substack{l > 4 \\ l < 25}} N_l F(2k_F R_l)\} \end{aligned} \quad (6)$$

with the statistical weights

$$W(x, n_1, n_2, n_3) = w(x, n_1)w(x, n_2)w(x, n_3) \quad (7)$$

where

$$w(x, n_i) = \frac{N_i!}{(N_i - n_i)!n_i!} x^{(N_i - n_i)}(1 - x)^{n_i}.$$

† In Dintelmann and Buschow (1971) a value for $H_{\text{hf}}(\text{Al}, \text{RKKY})$ of -27 kG was calculated, compared with the observed value of -47.2 kG .

Here n_i, N_i are the numbers of actual and maximal rare earth sites occupied by Gd atoms within the i th shell. All configurations were considered for which $W(x, n_1, n_2, n_3)$ was at least of the order of 2% compared with $W(x, n_1, n_2, n_3)_{\max}$, for example, 164 configurations for $x = 0.30$.

4.1. Calculations neglecting dipolar contributions

In order to calculate the NMR line profiles dipolar contributions and linewidths have also to be considered. Exact calculation of the dipolar contributions for the diluted samples is complicated by two problems. First there is a computational difficulty since it is not now possible to collect the RKKY equivalent Gd atoms in shells of equal Al distance because their dipolar contribution to the total field differs in value and/or direction from one atom to another. Therefore each Gd position must be treated independently, increasing the computational time (eg for $x = 0.05$, 2150 instead of 15 configurations have to be taken into account for the (111) lines). The second problem is physical and more severe; since the mixture of (111) domain lines and other lines in pure $GdAl_2$ depends on sample preparation, it is not certain that the ratio of (111) to (100) and other lines is constant for Y or La dilution even if all the samples had been subjected to the same treatment. Also, in diluted samples it is not known whether the (111) domains are preferred as they are in $GdAl_2$.

In the Al^{27} spectrum of pure $GdAl_2$ shown in figure 1(b) in spite of dipolar contributions, the centre of gravity and the 52 MHz line ((100) line) are both found to occur at about the bare hyperfine field position. The centres of gravity of the calculated (111), (100) or (110) domain line splittings (intensities 3:1, 1, 2:2 respectively) also lie within 0.3 MHz of the hyperfine field frequency. Since all the average values of dipolar splitting can be supposed to decrease with decreasing sample magnetization (and therefore with increasing x), the dipolar contributions were neglected for the profile calculations of figures 5-7.

For the calculation of figure 5 we have used the experimentally observed (figure 1(b)) three line spectrum along with the corresponding x dependent weighting factor to

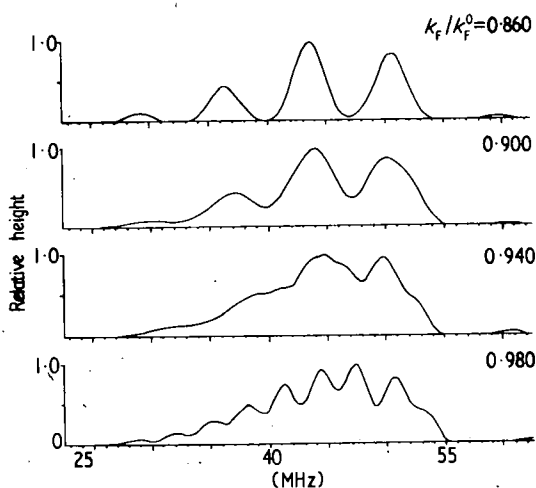


Figure 5. Calculated Al line profiles for $x = 0.15$ and different values of k_f/k_f^0 .

represent only those lines corresponding to H_{hf} (RKKY, x , 6, 8, 6) in equation (6). For all the other lines we took the same form function, namely approximately the a and b line profile of pure GdAl_2 , with 2.2 MHz halfwidth and zero intensity for $\Delta\nu > 2$ MHz. These lines are centred around the undisturbed hyperfine field positions determined by the various values that can be estimated from the quantity H_{hf} (RKKY, x , n_1 , n_2 , n_3) occurring in equation (6) and have the corresponding x dependent weighting factors. The 10% background intensity is neglected. Figure 5 shows the model calculation line profiles for $x = 0.15$ and different values of k_F . It can be seen that the lineshape is quite sensitive to k_F . By comparison with figure 2, a k_F/k_F^0 value near to 0.940 appears to give satisfactory line fitting.

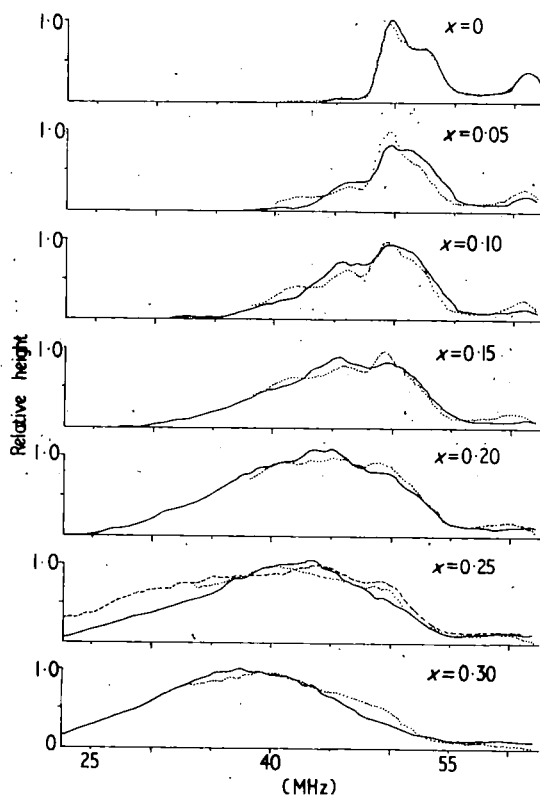


Figure 6. Calculated and experimental Al line profiles for different concentrations x . Full curve, calculated with line area normalized to the experimental value; dotted curve, observed line for $\text{Gd}_{1-x}\text{Y}_x\text{Al}_2$; broken curve for $\text{Gd}_{0.75}\text{La}_{0.25}\text{Al}_2$.

Figure 6 shows the series $x = 0.0$ to 0.30 for the value $k_F/k_F^0 = 0.945$. In this case the experimentally observed background intensity for the $x = 0$ sample between 43 and 62 MHz (with maximum value of about 10%) is taken into account disregarding the x value. Also a broader line form is assumed, corresponding to the shape of the GdAl_2 -52 MHz line which has a halfwidth of 3.4 MHz and zero intensity for $\Delta\nu > 4$ MHz. The calculated and measured spectra agree reasonably well under this assumption. For differences in k_F/k_F^0 of more than ± 0.015 , the agreement is obviously poorer.

In order to establish whether, instead of the oscillatory RKKY function (equation (3)) the observed line profiles can be equally well described by a different R dependence of the conduction electron polarization which is uniform in space we attempted to fit the line profiles with simple, nonoscillatory R dependences under the same conditions and assumptions as for figure 5. We replaced $F(2k_F R)$ of equation (3) arbitrarily by the functions c'/R^2 , c'/R^3 or c'/R^4 but did not consider higher powers of $1/R$ because this would imply that the exchange interaction in $Gd_{1-x}Y_xAl_2$ and $Gd_{1-x}La_xAl_2$ is

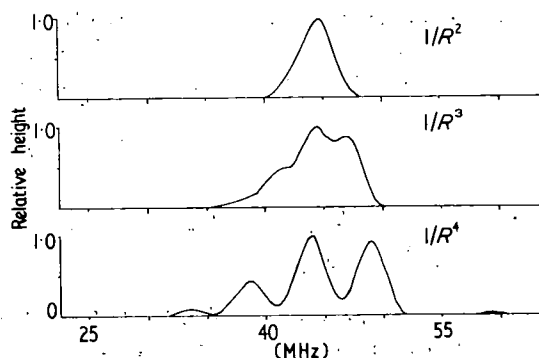


Figure 7. The calculated line profiles with R^{-2} , R^{-3} and R^{-4} dependence of the conduction electron polarization for $x = 0.15$.

essentially a short range interaction in contradiction (Morgan and Rushbrooke 1961) to the observed linear decrease of the Curie temperature with increasing x up to $x = 0.98$ (Maple 1969). As an example, the results for $x = 0.15$ are shown in figure 7 for the R^{-2} function and it is clearly seen that a slowly decreasing nonoscillatory function cannot explain the observed structure. In contrast to the experimental observations it is seen that in this case the maximum is shifted linearly with $(1 - x)$ and neither the width (even allowing for an additional dipolar contribution of the order of the $GdAl_2$ values, that is about 3 MHz at the low and 9 MHz at the high frequency side) nor the shape is represented in a proper way. The R^{-3} and R^{-4} dependences also do not give a fit with the observed line shape under the assumptions made in the calculation. Nevertheless, by using these more rapidly decreasing functions it is possible to obtain better agreement with the width (in the case of R^{-4}) or some qualitative peculiarities of the shape (in the case of R^{-3}) of the observed spectrum; at least in the special case of $x = 0.15$. However, for all these nonoscillating functions, the frequency of the maximum is essentially shifted linearly with $(1 - x)$ in contrast to the experimental result for small x . Since the dipolar contributions which has so far been neglected, will not induce a shift of the maximal peak to frequencies higher than the hyperfine field frequency it can be concluded from these calculations that an oscillatory conduction electron polarization is necessary to account for the line shape in $GdAl_2$.

4.2. Calculations including the dipolar contributions

So as to examine the validity of the assumption made in §4.1 above we calculated some lineshapes allowing for the dipolar field contributions. So as to limit computational

time to a reasonable value, only the concentrations $x = 0, 0.05$ and 0.10 were investigated. The Al lineshape is considered to be composed of (111) and (100) domain signals although the (100) signals may be taken as representative of all the lines which are centred around the pure hyperfine field position and for which the dipolar contribution only leads to a broadening comparable with the (100) case.

The component lines are centred around the different values which can be taken from

$$H_{\text{res}} = |H_{\text{hf}}(\text{RKKY}, x, n_1, n_2, n_3) + H_{\text{dip}}(x; r_{11}, \dots, r_{1n_1}; r_{21}, \dots, r_{2n_2}; r_{31}, \dots, r_{3n_3})| \quad (8)$$

where $H_{\text{hf}}(\text{RKKY}, x, n_1, n_2, n_3)$ is calculated using equation (6), the direction being opposite to that of the magnetization in the domains considered. For H_{dip} all the values of the sum over the anisotropic dipole-dipole interaction are used which arise from the possible distributions of the n_1, n_2 and n_3 Gd moments (pointing either along the (111) or the (100) direction) over the different sites in the first, second and third neighbour shell. The moments which are farther away give a contribution of less than 0.4 kG to the dipole sum and consequently are taken into account as an average only. This treatment then gives

$$H_{\text{dip}}(x; r_{11}, \dots, r_{1n_1}; r_{21}, \dots, r_{2n_2}; r_{31}, \dots, r_{3n_3}) = H_{\text{dip}}(r_{11}, \dots, r_{1n_1}; r_{21}, \dots, r_{2n_2}; r_{31}, \dots, r_{3n_3}) + (1-x)H_{\text{dip}}(4-20 \text{ shells in GdAl}_2). \quad (9)$$

As noticed previously in § 3.2, our calculated values of the dipole field had to be increased by 15% to fit the observed GdAl₂ splitting. For the lines centred around H_{res} , the experimentally observed GdAl₂ lineshapes (figure 1(b), halfwidths 2.2 MHz and 3.4 MHz) and the weights

$$W(x, n_1, n_2, n_3) = x^{20-(n_1+n_2+n_3)}(1-x)^{n_1+n_2+n_3} \quad (10)$$

are used.

The lineshape depends on the percentage of (111) and (100) domains. In order to obtain an estimate of the dipolar field influence, calculations were performed for pure (111) or (100) domains as well as for the experimentally observed mixture (GdAl₂, figure 1(b)). The results are as follows.

(i) The observed line shapes cannot be fitted with a nonoscillating polarization function as shown in figure 7, because for example the 49.5 MHz line is shifted to lower frequency for $x = 0.05$ and 0.10 in contrast to the experimental results (for the R^{-4} dependence by 0.7 and 1.4 MHz respectively).

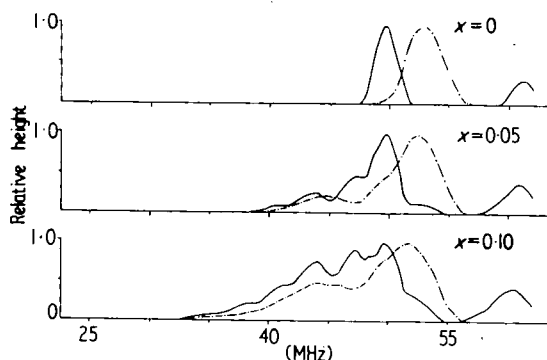


Figure 8. Calculated Al line profiles for small x and $k_F/k_F^0 = 0.945$ with the dipolar contributions taken into account. Full curve (111) domain nuclei; dotted and broken curves, (100) domain nuclei.

(ii) Using the RKKY polarization function with large values of k_F/k_F^0 (eg 0.980) there are too many lines as shown in figure 5 while for small k_F/k_F^0 (eg ≤ 0.900) there are not enough lines predicted for diluted $GdAl_2$ in the frequency range of interest. Only for an intermediate k_F/k_F^0 value (eg 0.945) is the number of lines given correctly. Also in agreement with experiment, essentially no shift of the 49.5 MHz line is found. Figure 8 shows the calculated line profiles of (111) and (100) domain nuclei signals for $k_F/k_F^0 = 0.945$.

(iii) The positions of the two observed peaks at about 42 and 46 MHz cannot be described exactly by the RKKY polarization function including a dipolar contribution; for $k_F/k_F^0 = 0.945$, they are calculated to occur at about 43.7 and 47.2 MHz. Even allowing for a concentration dependence of the relative weights of the (111) and (100) signals and a deviation of k_F/k_F^0 from 0.945, it was not possible to fit both peaks.

These two peaks correspond essentially to Al atoms for which one nearest (42 MHz) and one next nearest (46 MHz) Gd neighbour is replaced by nonmagnetic Y or La. In the k_F range of interest both of these neighbours give a negative RKKY contribution to the negative hyperfine field, whereas the third nearest neighbours contribute positively (which is important in order to prohibit the shift of the 49.5 MHz line). Investigation of the k_F dependence of these contributions and the lineshape showed that an exact fit of the peak positions can only be given if there is a considerable positive (ferromagnetic) direct contribution superposed on the negative RKKY contribution of the nearest neighbours or if the polarization decreases less strongly with distance than in the RKKY model (with $J(q) = \Gamma = \text{constant}$). Since a positive direct contribution is not likely (Watson and Freeman 1961) for the large Gd-Al distance (3.276 Å); the second possibility seems more realistic. Yosida (1957) showed that with the assumption $J(q)f(q) = 2J(0)$ for $q < 2k_F$ and $J(q)f(q) = 0$ for $q > 2k_F$ a polarization function is obtained, which varies with $k_F R F(k_F R)$ instead of with the usual RKKY function $F(k_F R)$. Using this function, with the same assumptions as were used for the calculation of figure 8 the observed peak positions can be fitted with k_F values of about $(0.935-0.955)k_F^0$.

5. Concluding remarks

The line profile analysis shows that the experimentally observed Al spectra in Y or La diluted $GdAl_2$ can be predicted roughly by the RKKY theory if instead of the free electron value k_F^0 the reduced value $k_F = 0.945 k_F^0 = 1.53 \text{ \AA}^{-1}$ is taken. Line structures obviously represent a quite sensitive means of testing the choice of the k_F value and give the possibility of evaluating k_F independently of the other parameters entering the calculation, for example the constant C of equation (4) and the analyses of the magnetic data.

In the present calculations, in order to get the analytical expressions of equations (1)–(3) the q dependence of the exchange integral $J(q)$ was abandoned. The values of Γ and k_F therefore represent averages over the q dependence. The sampling involved in the above mentioned Gd neighbour configurations is certainly different and more anisotropic than the sampling involved for undiluted $GdAl_2$. For these reasons it is gratifying that the value for k_F derived above and the value obtained with $GdAl_2$ from measurements in the paramagnetic region are essentially the same. This seems to indicate that in these compounds a spherical approximation for the Fermi surface is not too bad. A similar conclusion has been reached recently by Shamir *et al* (1971).

In the line fitting procedure a number of drastic approximations have been made and

it is at present unclear which of these is most responsible for the discrepancies between the experimental and theoretical line shape. It is difficult to arrive at a clear cut conclusion even in the case of GdAl_2 since it is necessary to allow for the dipolar contributions to the line shape. Nevertheless the results do show that the observed Al^{27} line profiles of the compounds studied can be understood in terms of an RKKY like oscillatory conduction electron polarization.

Acknowledgments

We wish to thank Professor Dr B Elschner for his interest in this work and the helpful discussions with Professor N Kaplan are acknowledged.

The Bruker NMR equipment was provided by the Bundesministerium für Bildung und Wissenschaft. Numerical calculations were performed at the Rechenzentrum der Technischen Hochschule, Darmstadt. The Durham spin-echo system was constructed under grants from the USAF and the SRC.

The work forms part of the special research project 'Festkörperspektroskopie Darmstadt/Frankfurt' and part of the 'Intermetallic Compound Research Project' supported in Durham by the SRC.

References

- Buschow K H J, Fast J F, van Diepen A M and de Wijn H W 1967 *Phys. Stat. Solidi* **24** 715-20
Dean R H and Urwin R J 1970 *J. Phys. C: Solid St. Phys.* **3** 1747-51
Dintelmann F, Buschow K H J 1971 *Z. angew. Phys.* **31** 181-4
Dintelmann F, Dormann E and Buschow K H J 1970 *Solid St. Commun.* **8** 1911-4
de Gennes P G 1962 *J. Phys. Radium* **23** 510-21
Jaccarino V 1961 *J. appl. Phys.* **32** S102-3
Kasuya T 1956 *Prog. theor. Phys.* **16** 45-57
Leon J B, Rao V U S and Wallace W E 1971 *J. Less Common Metals* **24** 247-51
Maple M B 1969 *PhD Thesis* University of California
Morgan D J and Rushbrooke G S 1961 *Mol. Phys.* **1** 291-303
Oppelt A, Dormann E and Buschow K H J 1972 *Phys. Stat. Solidi* (b) **51** at press
Ruderman M A and Kittel C 1954 *Phys. Rev.* **96** 99-102
Shamir N, Kaplan N and Wernick J H 1971 *J. Phys., Paris* **32** C1 902-4
Swift W M and Wallace W E 1971 *J. Solid St. Chem.* **3** 180-92
Watson R E, Freeman A J 1961 *Phys. Rev. Lett.* **6** 277-9, 388-90
Yosida K 1957 *Phys. Rev.* **106** 893-8

Letters to the Editor

Effects of pulsed field magnetization on the magnetic behaviour of R_3Co compounds

Abstract. Results are presented which indicate that the metamagnetic behaviour of the R_3Co compounds is probably the consequence of a time dependent behaviour of the magnetization at low temperatures. Magnetization curves obtained in pulsed fields, are appreciably different from those obtained in static fields, and in general, open hysteresis loops are observed, along with much higher values of the critical fields. It appears that the critical field values may depend upon the rate of field increase.

In a recent publication, Feron *et al.* (1970) reported on the magnetic properties of the intermetallic compounds R_3Co , where R is a rare earth element. In keeping with earlier work on the R_3Ni series (Feron *et al.* 1968) their results, obtained using the axial extraction technique, showed metamagnetic behaviour at 4.2 K for the compounds with R = Nd, Gd, Dy and Ho. A critical field was also observed at 4.2 K for Tb_3Co , but the initial magnetization of this compound was followed by an open hysteresis loop showing no evidence of a critical field.

In the course of an extensive series of measurements on these, and related compounds in our laboratory, we have examined the magnetic behaviour of the R_3Co systems both in pulsed (rise time = 0.2 ms) and static fields. It is the purpose of this note to indicate certain differences which exist between results obtained using these two techniques, and to point out the possible mis-classification which can occur when critical fields are observed in magnetization behaviour. The detailed results of our observations will be published elsewhere.

The experimental, pulsed field, magnetization curves for the compounds with Nd, Gd, Tb, Dy and Ho all show the existence of a critical field at 4.2 K, beyond which the observed magnetization increases quite rapidly with increasing field before approaching some saturation value. Only in the gadolinium compound does the increasing and decreasing field curve follow the same path, in the remainder the initial magnetization is followed by an open hysteresis loop which lies well to the left of the initial magnetization curve. In the earlier static field observations (Feron *et al.* 1970), a hysteresis loop was only observed in the case of Tb_3Co , and it was not clear where this lay with respect to the initial magnetization. Some evidence of the critical fields appears, however, in the pulsed field loops for the terbium and dysprosium compounds but not for Ho_3Co . The magnetization curves at 4.2 K for Gd_3Co and Dy_3Co are given in figure 1 along with those from Feron (1970). As may be seen, the details of these two sets of data are appreciably different, as is also the case for the remaining compounds, and we have indicated these differences in table 1. A

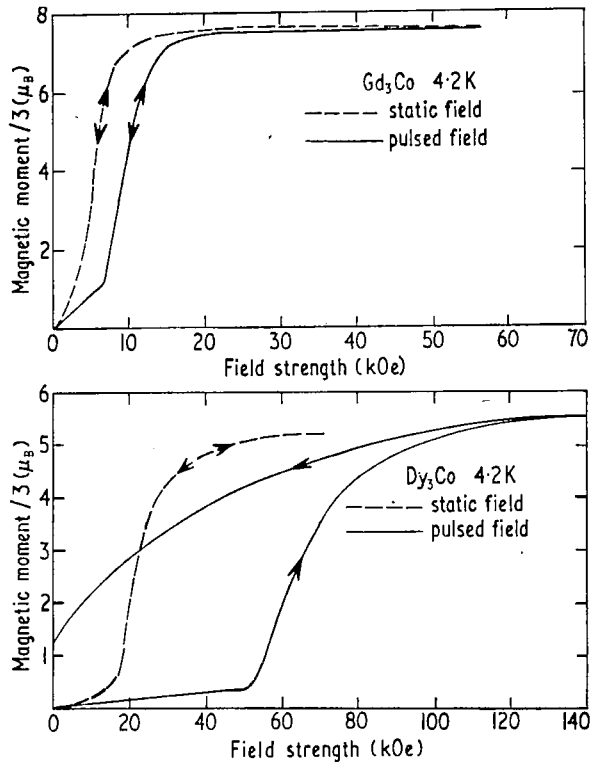


Figure 1. The magnetization-field curves for Gd_3Co and Dy_3Co at 4.2 K obtained using both pulsed and static field data are taken from Feron *et al.* (1970).

Table 1.

	Pulsed Fields			Static Fields		
	critical field (KOe)	$dM/dH(\mu_B/KOe)$ ($H=0$)	hysteresis loop	critical field (KOe)	dM/dH ($H=0$)	hysteresis loop
Gd_3Co	7 ± 1	0.18	No	3	0.3	No
Tb_3Co	65 ± 3	0.01	Yes	10	0.014	Yes
Dy_3Co	50 ± 2	0.007	Yes	16	0.014	No
Ho_3Co	2 ± 0.5	?	Slight	2	?	No

further discrepancy is also found in the Gd_3Co data, in that the critical field is still clearly visible (2 KOe) at 77 K using the pulse-field observations.

The observed behaviour of the magnetization in the pulsed fields is remarkably similar to that reported by ourselves for the $DyCo_2$ - $DyNi_2$ pseudobinaries (Slanicka *et al.* 1971) in which an extensive time dependence in the magnetization process at liquid helium temperatures was also discovered. It was possible to account for this behaviour in terms of the effects of high magnetocrystalline anisotropy on the thickness and mobility of the domain walls in the unmagnetized state. It is now reasonably well established that for suitable values of the exchange and anisotropy energies, the width of a domain wall may become comparable to the atomic spacing (Bulaevskii and Ginzburg 1964, Barbara *et al.* 1970) and that under these conditions the initial magnetization process will be one of magnetization rotation only, and take place for fields in excess of some critical coercive field (Barbara *et al.* 1970, Graham 1971). This has been called 'intrinsic pinning', in a qualitative description of the process by Zijlstra (1970). Since the rotation is limited by an

energy barrier associated with the magnetocrystalline anisotropy, the magnetization in an applied field can be expected to increase at a rate proportional to $\exp \{(-E_A + MH)/kT\}$ where E_A is the anisotropy energy and M the domain magnetization. At low temperatures, the time constant of this increase lies well within the range of measurement for values of the exchange and anisotropy constants which are not too restrictive. Once magnetized, the subsequent behaviour will be similar to that of a single domain particle and will be influenced by the demagnetizing field. As a result (i) the coercivity of the hysteresis loop will be less than that of the initial magnetization curve, and (ii) any time dependence of the magnetization on decreasing (and subsequently reversing) the field will be different from that of the initial magnetization.

In all low temperature measurements of this kind of material we are dealing with a nonequilibrium process. In the simplest case the magnetization may be written:

$$M(H, t) = M_s \{1 - \exp(-t/\tau)\}$$

with

$$1/\tau = A \exp \{ \{ < E_A + M_s H(t) \} / kT \}$$

and, for the pulsed field measurements,

$$H(t) = H_0 \sin \omega t = H_0 \sin \frac{2\pi}{\tau_1} t.$$

In the course of the measurement, sudden changes in $M(H, t)$ will only be observed when the time constant of the change τ becomes appreciably less than the time rate of field change. This latter term can be replaced by τ_1 for the pulsed field observations and by the measurement time in the case of static field measurements. Since there can be a difference of as much as 10^7 (10^{-4} s to 10^3 s) in the rate of field change, the value of the observed critical field may differ appreciably between the two extremes. It should also be pointed out that in the static field observations the form of the results will depend critically on the details of the experimental method. For example, in the extraction method, if the specimen is allowed to remain in the field for several time constants of the rate process then it may be assumed that the measurements will approach the equilibrium values, but for times shorter than this the results will characterise a somewhat nebulous intermediate state.

In cases such as the compounds under discussion, which on magnetizing show a critical field phenomena, the magnetic state will return to a multidomain configuration, over a finite time, on decreasing the applied field due to the effects of temperature and demagnetizing field. This will be assisted to some extent in polycrystalline materials by domain wall nucleation occurring at the grain boundaries (Zijlstra 1970). An apparently 'metamagnetic' behaviour can then be expected for static measurements, which will have a similar magnetic behaviour for both increasing and decreasing fields. For pulsed fields, however, the observed magnetization-field behaviour can either be similar to that in static fields, or show an open hysteresis loop, depending upon the relative values of the two time constants over the range of applied fields used.

In view of the above discussion we believe that most, if not all, of these compounds are ferromagnetic, but that their behaviour at low temperatures is severely affected by large values of the magnetocrystalline anisotropy. It is suggested that the previously reported metamagnetic behaviour arises as a consequence of the method of measurement rather than from a classical antiferromagnetic moment configuration. Similar conclusions have been reached from a different approach (Buschow 1969) for Dy_3Al_2 , which had previously been reported to be metamagnetic at low temperatures.

Physics Department,
University of Durham.

K. N. R. TAYLOR
G. J. PRIMAVESI
15th January 1971

- BARBARA, B., BECLE, C., LEMAIRE, R., and PACCARD, D. 1970, *C.R. Acad. Sci., Paris*, **271**, 880.
 BULAEVSKII, L. N., and GINZBURG, V. L. 1964, *Sov. Phys-JETP*, **18**, 530
 BUSCHOW, K. H. J. 1969, *Phys. Lett.*, **29A**, 12
 FERON, J. L., GIGNOUX, D., LEMAIRE, R., and PACCARD, D. 1970, *Les Elements des Terres Rares II CNRS*, 75.
 FERON, J. L., LEMAIRE, R., PACCARD, D., and PAUTHENET, R. 1968, *C.R. Acad. Sci., Paris*, **267B**, 371
 GRAHAM, C. D. 1970, *Magnetic Conference*, to appear in *J. Appl. Phys.*
 SLANICKA, M. I., TAYLOR, K. N. R., and PRIMAVASI, G. J., to be published.
 ZIJLSTA, H. 1970, *IEEE Trans. Mag.*, **6**, 179.

Anomalous nuclear resonance behaviour of ^{59}Co in GdCo_2

Abstract. Spin echo measurements of the ^{59}Co nuclear resonance in GdCo_2 have revealed a rapid decay of the spin-echo amplitude with temperature up to 40 K followed by a further growth up to 79 K and subsequent decay above this temperature.

In order to investigate the temperature dependence of the hyperfine field at the ^{59}Co nucleus in GdCo_2 , a spin-echo spectrometer was used, operating at frequencies near 60 MHz. Envelope demodulation was employed, following a conventional 32 MHz if amplifier, the echo being displayed on an oscilloscope. The resonance line shape is shown in figure 1. To minimise the effects of spin-spin relaxation on the primary echo (Hahn 1950)

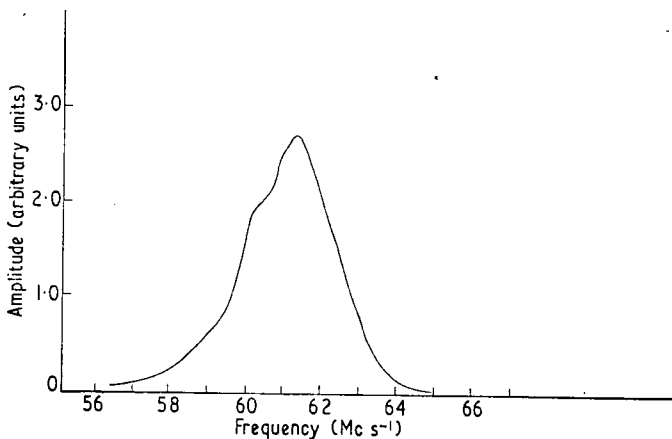


Figure 1. Line shape of the ^{59}Co nuclear resonance in CdCo_2 , obtained by spin echo measurement at 4.2 K.

the two, low-power, rf driving pulses were as closely spaced as would allow the echo to be produced clear of the receiver recovery curve. The pulse width used for this series of measurements was $0.5\ \mu\text{s}$, the pulse separation $6.5\ \mu\text{s}$ and the repetition frequency 100 Hz. In a similar investigation, Taylor and Christopher (1969) had been unable to make echo observations above 15 K because of the reduction in echo amplitude with increasing temperature. The present spectrometer was capable of producing a noise-free primary echo in

GdCo₂ at 77 K and hence no difficulties of measurement were anticipated below this temperature.

The hyperfine field strength observed at 4.2 K during these measurements is 60.8 kOe, in agreement with previous observations. With increasing temperature its magnitude decreases slightly (1%) between 4.2 K and 165 K, at which temperature the echo was no longer visible. Over this temperature range the echo amplitude varied in an unexpected manner, decreasing rapidly from its value at 4.2 K before passing through a broad minimum at

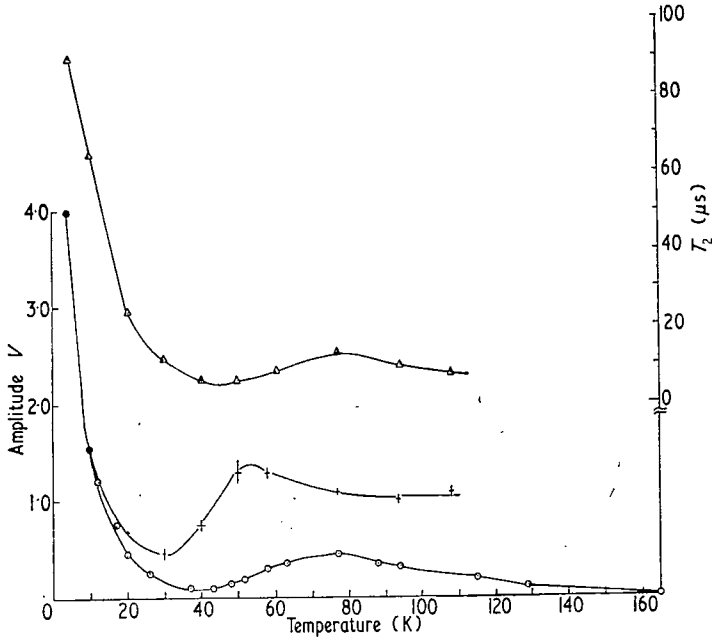


Figure 2. Echo amplitude, corrected amplitude and T_2 against temperature. The circles represent the observed amplitudes; the triangle represent the values of T_2 (right-hand ordinate); the crosses represent the corrected amplitudes (together with indications of the cumulative errors) which have been normalized to give the same amplitude at 4.2 K.

40 K and a local maximum at 79 K. Beyond this the amplitude falls monotonically and is unobservable above 165 K. This variation of echo amplitude is shown in figure 2.

In an attempt to understand the origin of these changes in the resonance amplitude, those parameters have been examined which are likely to affect its value directly, namely spin-spin and spin-lattice relaxation and the domain wall enhancement factor.

Values of the spin-spin relaxation time T_2 were obtained over the entire temperature range using the conventional two-pulse technique, the echo decay being a true exponential in each case. The variation of T_2 with temperature is shown in figure 2. As can be seen, the form of this dependence is very similar to that of the echo amplitude and must account, at least in part, for its anomalous behaviour. Measurements of the spin-lattice relaxation time T_1 using the three-pulse method, are severely limited at low driving-pulse power levels by the very small stimulated echo amplitudes above 4.2 K. As a result T_1 has been satisfactorily measured only at 4.2 K and 77 K. Separate measurements at higher driving-pulse power levels have indicated that T_1 also has a local maximum at 79 K.

With the observed values of T_2 , the echo formation time of 13 μ s leads to a 13% decrease from the zero-time echo amplitude at 4.2 K and an 89% decrease at 40 K. Consequently

the observed amplitudes have been corrected for the T_2 decay and are plotted in figure 2 for comparison. The basic features of the curve still exist, but are shifted to lower temperatures. This method of correction assumes that only a single-time-constant relaxation process is operative. Time constants very much less than $13 \mu\text{s}$ (the minimum echo formation time of this spectrometer) cannot be observed on this equipment. The corrected curve will therefore be subject to further modification if a very fast relaxation mechanism is found to be present.

Since many of the rare earth intermetallic compounds show evidence of the development of high magnetocrystalline anisotropy effects below 50 K, it is possible that such changes may occur in GdCo_2 and be reflected into the nuclear resonance through the domain wall enhancement factor η . However, measurements of η showed that it was essentially constant from 4.2 K to 165 K, in agreement with previously reported work (Dean *et al.* 1970) for other ferromagnetic materials.

Referring again to the corrected echo amplitudes of figure 2 it could appear that the basic variation is one involving a broad, deep minimum at 30 K. The existence of such a minimum would then arise only through a very fast relaxation process which is unobservable because of the spectrometer's minimum echo formation time as discussed above, or through a separate mechanism which decreases the number of excited nuclei. Examination of the data of figure 2 shows that between 4.2 K and 30 K the corrected echo amplitude is accurately proportional to (temperature) $^{-1}$. This is, of course, characteristic of normal behaviour (Dean *et al.* 1970) and it would perhaps indicate that the anomaly is not the amplitude minimum, but the local maximum at about 53 K. Unfortunately, the growth of a nuclear resonance with increasing temperature is not so readily interpreted as is a decay, especially in view of the constant enhancement factor. It is hoped that a more detailed observation of the effect can be made using a more sensitive spectrometer, presently under construction, to give a clearer insight into the mechanisms causing this apparent anomaly.

Department of Physics,
University of Durham,
South Road,
Durham.

G. BROWN
M. A. A. ISSA
K. N. R. TAYLOR
13 January 1971

DEANE, R. H., URWIN, R. J., and JAKINS, G. A., 1970, *Phys. Lett.* **33A**, 103-4.

HAHN, E. L., 1950, *Phys. Rev.*, **80**, 580-94.

TAYLOR, K. N. R., and CHRISTOPHER, J. T., 1969, *J. Phys. C: Solid St. Phys.*, **2**, 2237-45.